Titre: Title:	Airborne Transmission of Legionella from Cooling Towers : A Fluid Dynamics Approach
Auteur: Author:	Xavier Lefebvre
Date:	2024
Type:	Mémoire ou thèse / Dissertation or Thesis
Référence: Citation:	Lefebvre, X. (2024). Airborne Transmission of Legionella from Cooling Towers : A Fluid Dynamics Approach [Thèse de doctorat, Polytechnique Montréal]. PolyPublie. https://publications.polymtl.ca/61860/

URL de PolyPublie: PolyPublie URL:	https://publications.polymtl.ca/61860/
Directeurs de recherche: Advisors:	Étienne Robert, Émilie Bédard, & Michèle Prévost
Programme: Program:	Génie mécanique

POLYTECHNIQUE MONTRÉAL
affiliée à l'Université de Montréal

Airborne Transmission of *Legionella* from Cooling Towers: A Fluid Dynamics Approach

XAVIER LEFEBVRE
Département de génie mécanique

Thèse présentée en vue de l'obtention du diplôme de *Philosophiæ Doctor*
Génie mécanique

Décembre 2024

POLYTECHNIQUE MONTRÉAL
affiliée à l'Université de Montréal

Cette thèse intitulée :

Airborne Transmission of *Legionella* from Cooling Towers: A Fluid Dynamics Approach

présentée par **Xavier LEFEBVRE**
en vue de l'obtention du diplôme de *Philosophiæ Doctor*
a été dûment acceptée par le jury d'examen constitué de :

Stephane ETIENNE, président
Etienne ROBERT, membre et directeur de recherche
Emilie BEDARD, membre et codirectrice de recherche
Michèle PRÉVOST, membre et codirectrice de recherche
Caroline WAGNER, membre externe
Andreas NOCKER, membre externe

DEDICATION

À mes parents et ma soeur,
pour votre soutien indéfectible...

À Emma,
pour ton amour inconditionnel...

ACKNOWLEDGEMENTS

Cette thèse est le fruit d'une énorme collaboration scientifique, sociale et émotionelle.

Merci d'abord à tous ceux qui ont contribué à la rédaction de cette thèse. Merci Etienne, pour ton approche curieuse et contagieuse à la recherche. Tes exigences rigoureuses m'ont beaucoup appris et ont fait de moi un meilleur scientifique. Merci à Émilie pour ton support émotionel, ta superbe approche de gestion et ton dévouement à ton travail. Merci à Michèle pour ta contagieuse passion pour la science et ton désir expansif d'avoir un impact positif avec tes travaux. À vous trois, je ne pourrais assez vous remercier pour votre temps, vos judicieux conseils, votre confiance en mon travail et surtout, de m'avoir appris ce que c'est de la bonne science.

Un énorme merci à mes collègues de laboratoire LEMUR pour nos discussion saugrenues du midi, pour votre constante disposition à l'entraide et pour votre suport moral. Merci à ceux qui étaient là avant moi, Olivier, Mathieu, Elie, Antonella, Pablo, Tanja et Christian, qui m'ont mentoré et qui m'ont inspiré. Merci aussi à tous les collègues avec qui j'ai collaboré dans les 4 dernières années, de Polytechnique en génie mécanique, civil et chimique et de McGill en microbiologie et en microfluidique. Merci aussi à Julie, Jacynthe, Mélanie, Tetjana et Yves pour votre aide sur le terrain et au laboratoire, ainsi que pour votre support moral.

Merci à ma famille et mes amis pour leur support inconditionnel. Merci papa de m'avoir transmis ta pensée logique et surtout tes valeurs de travailler fort, tout en me rappelant de ne pas travailler trop fort! Merci maman de m'avoir appris à être organisé, discipliné et surtout ce que c'est que de tenir à quelque chose qui compte pour nous. Merci à vous deux de m'avoir aidé à m'émanciper dans ce qui me passionne, tout en gardant un bel équilibre de vie. Merci à Justine, tu seras toujours ma soeur préférée! Merci finalement à Emma, pour tes conseils lors de nos longues discussions, pour ta curiosité envers mon parcours en recherche, pour tout nos moments ensemble où je peux oublier la science et surtout pour ton amour inconditionnel. Merci aussi à tous ceux qui m'entourent au quotidien, je ne peux cependant pas vous promettre que je vais arrêter de parler de science!

Je tiens également à remercier les organismes qui ont financé ce travail : Hydro-Québec, le Conseil de recherches en sciences naturelles et en génie du Canada (CRSNG), et le Fonds de recherche du Québec - Nature et technologies (FRQNT).

RÉSUMÉ

En 2012, la deuxième plus importante éclosion de legionellose de l'histoire de l'Amérique du Nord a eu lieu à Québec, au Canada, entraînant 181 cas confirmés et 14 décès. La source de l'éclosion était une tour de refroidissement, un échangeur de chaleur qui fournit des conditions idéales pour la croissance de la bactérie responsable, *Legionella*, et qui génère de grandes quantités de d'aérosols capables de transporter ce pathogène. Malgré l'adoption de réglementations, les cas continuent d'augmenter partout dans le monde, atteignant en moyenne 1,9 à 2,4 cas pour 100 000 personnes annuellement en Amérique du Nord et en Europe en 2020. Les efforts de recherche ont été largement consacrés à la prévention de la croissance bactérienne. Cependant, comme cette maladie est transmise par l'inhalation d'aérosols contaminés en suspension dans l'air, une lacune majeure dans la caractérisation du processus d'infection réside dans la compréhension de la génération et du transport des aérosols. L'objectif principal de cette thèse est d'étudier ce problème en utilisant une approche de dynamique des fluides, intégrant également les aspects énergétiques des tours de refroidissement, pour améliorer l'évaluation du risque de transmission aérienne de *Legionella*. La recherche est divisée en 5 articles, chacun abordant un aspect spécifique du problème.

Le premier article est lié à la mesure des aérosols. En effet, l'évaluation précise des risques de contamination par *Legionella* à partir des tours de refroidissement nécessite une caractérisation précise des gouttelettes contaminées. Cependant, la performance des techniques de mesure bien établies dans le domaine de la science des aérosols est rarement évaluée pour les gouttelettes à base d'eau. Quatre instruments reposant sur des principes de fonctionnement différents pour fournir une distribution de taille des aérosols ont été comparés en utilisant des aérosols à base d'huile et d'eau. Des différences de mesures, causées par l'évaporation et le dépôt, ont été corrigées par des facteurs de correction empiriques, permettant une évaluation quantitative de la distribution de taille des aérosols à l'aide d'instruments abordables et accessibles. En mettant en oeuvre une technique de séchage proposée, les instruments peuvent fournir de manière fiable la distribution de taille à la source d'aérosols, une information critique pour l'évaluation du risque.

Le deuxième article explore l'évaluation du risque de *Legionella* provenant des tours de refroidissement par la caractérisation des gouttelettes d'aérosol générées et libérées par les systèmes en fonctionnement. L'évaluation quantitative des risques microbiens (EQRM), un modèle statistique couramment utilisé pour quantifier la charge associée aux maladies

d'origine hydrique, a été précédemment adaptée au contexte de la transmission de *Legionella* à partir des tours de refroidissement. Cependant, il repose sur des hypothèses dérivées d'études obsolètes, dont la validité est de plus en plus remise en question, ce qui pourrait avoir des implications significatives pour les résultats. Ainsi, une campagne d'échantillonnage *in situ* à grande échelle a été menée pour caractériser les aérosols rejetés par les tours de refroidissement afin d'améliorer ce modèle. Les résultats ont menés à la suggestion de stratégies pour mitiger les risques.

Le troisième article est dédié à la caractérisation de la dynamique d'évaporation des gouttelettes chargées de *Legionella*, un paramètre critique mais souvent négligé impliqué dans la transmission par voie aérosolisée. Diverses propriétés de l'eau, telles que la présence de solides non volatiles, la viscosité et la tension de surface, influencent l'évaporation. Les expériences ont montré qu'un tension de surface plus faible prolongeait l'évaporation jusqu'à 14%, tandis qu'une viscosité plus élevée retardait le début de l'évaporation. Les concentrations élevées de solides suspendus non volatiles ont presque doublé le temps d'évaporation. Ces résultats impactent les risques de contamination, soulignant la nécessité de modèles d'évaporation améliorés pour le développement de stratégies d'atténuation des risques efficaces.

Le quatrième article discute de l'effet de la densité en nombre d'aérosols sur leur dynamique d'évaporation. Une configuration expérimentale polyvalente a été développée en utilisant la tête d'impression à jet d'encre XAAR XJ128 pour générer des gouttelettes pour la caractérisation de l'évaporation dans un panache. Les mesures expérimentales ont été comparées à un modèle d'évaporation théorique pour une seule goutte d'eau pure dans de l'air à 30% d'humidité relative. Les résultats ont montré que la densité en nombre de gouttelettes influençait les taux d'évaporation, les gouttelettes s'évaporant à des taux comparables au modèle pour une humidité relative de 60 à 80% lorsque presque toutes les buses de la tête d'impression étaient utilisées.

Le cinquième article explore l'effet énergétique d'une stratégie émergente de réduction des risques impliquant la filtration de l'eau des tours de refroidissement. Bien que *Legionella* soit transmise par la voie aérienne, le contrôle de la croissance bactérienne dans l'eau de la tour de refroidissement est crucial. La filtration par micro-sable est efficace pour réduire *Legionella* et les risques de contamination, bien qu'elle ne soit pas largement adoptée. Pour inciter à son utilisation, l'impact sur l'efficacité énergétique de la tour de refroidissement a été évalué. Le coefficient de performance de la tour de refroidissement était, en moyenne, 18% plus élevé et s'est amélioré 63% du temps avec la filtration. La modélisation par apprentissage machine a estimé des économies d'énergie entre 5 et 13%, principalement en périodes de charges plus

élevées. Ainsi, l'intégration de la filtration augmente l'efficacité énergétique et le contrôle bactérien, favorisant la durabilité.

Une approche globale a été adoptée pour améliorer l'évaluation des risques de contamination par *Legionella* à partir des tours de refroidissement. En abordant la dynamique des fluides impliquée dans la mesure, le transport et l'évaporation des gouttelettes d'aérosol contaminées, ainsi que l'effet d'une stratégie émergente de réduction des risques sur l'efficacité énergétique d'un système de tour de refroidissement, cette recherche contribue au développement de stratégies d'atténuation efficaces.

ABSTRACT

In 2012, the second largest legionellosis outbreak in North America occurred in Quebec City, Canada, resulting in 181 confirmed cases and 14 deaths. The source of the outbreak was a cooling tower, a widely adopted heat exchanger which inherently provides ideal conditions for the growth of the *Legionella* bacteria responsible for the disease and that generates large quantities of aerosol droplets capable of transporting this pathogen. Despite new regulations, cases continue to rise worldwide, reaching 1.9 to 2.4 cases per 100,000 people annually in North America and Europe in 2020. Research efforts have been largely dedicated to preventing bacterial growth. As this disease is transmitted via the inhalation of airborne contaminated aerosol droplets, a major research gap lies in the understanding of the fluid dynamics of aerosol generation and transport. The main objective of this thesis is to investigate this problem using a fluid dynamics approach, also integrating the energetic aspects of cooling towers, to improve the risk assessment of airborne *Legionella* transmission. The research is divided into 5 articles, each addressing a specific aspect of the problem.

The first article is related to the measurement of aerosol droplets. Indeed, accurately assessing *Legionella* contamination risks from cooling towers requires precise characterization of contaminated aerosol droplets. However, the performance of measurement techniques well established in the field of aerosol science is seldom assessed for water-based droplets. Four instruments relying on different operating principles to provide aerosol size distribution were compared using oil and water-based aerosol droplets. While oil-based measurements were consistent, significant discrepancies arose for evaporating water-based particles. These differences, caused by evaporation and deposition, were addressed through empirical correction factors, enabling quantitative assessment of aerosol size distribution using affordable and accessible instruments. By implementing a proposed drying technique, sampling instruments can reliably provide size distribution at the aerosol source, critical information for airborne transmission risk assessment.

The second article explores the risk assessment of *Legionella* from cooling towers through the characterization of the aerosol droplets generated and released from operating systems. Quantitative microbial risks assessment (QMRA), a statistical model commonly employed to quantify the burden associated with waterborne diseases, was previously adapted to the context of *Legionella* transmission from cooling towers. However, it relies on hypotheses derived from outdated studies, the validity of which is increasingly questioned, potentially leading

to significant implications for the results. Thus, a large-scale *in situ* sampling campaign was conducted to characterize the aerosol released from cooling towers to improve this model. The improved QMRA emission model based on our measurements lead to the suggestion of strategies to mitigate risks.

The third article is dedicated to the characterization the evaporation dynamics of *Legionella*-laden droplets, a critical but often overlooked parameter involved in airborne transmission. Various water properties, such as non-volatile matter, viscosity, and surface tension, influence evaporation. Experiments showed that lower surface tension extended evaporation by up to 14%, while higher viscosity delayed evaporation onset. High non-volatile concentrations nearly doubled the evaporation time and increased droplet nuclei size, increasing contamination risks. Variability in droplet nuclei size and non-volatile concentration further impacts risks, highlighting the need for improved evaporation models for the development of effective mitigation strategies.

The fourth article discusses the effect of the number density of aerosol droplets on their evaporation dynamics. A versatile experimental setup was developed using the XAAR XJ128 inkjet printhead to generate droplets for evaporation characterization within a plume. Experimental measurements were compared to a theoretical evaporation model for a single droplet of pure water in quiescent air at 30% relative humidity. Results showed that the number density of droplets influenced evaporation rates, with droplets evaporating at rates comparable to the model for 60-80% relative humidity when nearly all printhead nozzles were employed.

The fifth article explored the energetic effect of an emerging risk mitigation strategy involving the filtration of cooling tower water. Although *Legionella* is transmitted via the airborne route, controlling bacterial growth in cooling tower water is crucial. Microsand filtration has proven effective in reducing *Legionella* and contamination risks, though it is not widely adopted. To incentivize its use, the impact on cooling tower energy efficiency was evaluated. The coefficient of performance of the cooling tower was, on average, 18% higher and improved 63% of the time with filtration. Machine learning modeling estimated between 5-13% energy savings, mainly in periods of higher loads. Thus, integrating filtration increases energy efficiency and bacterial control, promoting sustainability.

A comprehensive approach was adopted to improve the assessment of *Legionella* contamination risks from cooling towers. By addressing the fluid dynamics involved in the measurement, transport and evaporation of contaminated aerosol droplets, as well as the effect of an emerging microbial growth control strategy on the energy efficiency of a cooling tower system, this research contributes to the development of effective mitigation strategies.

TABLE OF CONTENTS

LIST OF TABLES

LIST OF FIGURES

LIST OF SYMBOLS AND ACRONYMS

Bm	Spalding number
C	Concentration
CDC	Centers for Disease Control and Prevention
c_p	Specific heat capacity
COP	Coefficient of Performance
CT	Cooling Tower
D	mass diffusivity
DALY	Disability-Adjusted Life Year
DEHS	Di-Ethyl-Hexyl-Sebacate
DOD	Droplet on Demand
D_p	Particle diameter
E	Energy
η	Capture efficiency
ΔG	Gibbs free energy
h	Heat transfer coefficient
HP	Horse Power
HVAC	Heating, Ventilation and Air Conditioning
I	Evaporation rate
L	Length
m or M	Mass
μ	Dynamic viscosity
μm	Micrometer
N	Number of particles
Nu	Nusselt number
OAS	Optical Aerosol Spectrometer
O_r	Cooling tower operating rate
p	Pressure
PBS	Phosphate-Buffered Saline
PDA	Phase Doppler Anemometry
PEG	Polyethylene Glycol
Pr	Prandtl number
Q	Heat flux
Q_{em}	Aerosol emission rate

QMRA	Quantitative Microbial Risk Assessment
R	Universal gas constant
r_d	Droplet radius
Re	Reynolds number
ρ_p	Particle density
S	Droplet Surface
Sc	Schmidt number
Sh	Sherwood number
SMPS	Scanning Mobility Particle Sizer
Stk	Stokes number
T	Atmospheric Temperature
T_d	Temperature on the surface of the droplet
TDS	Total Dissolved Solids
T_∞	Temperature of the surrounding air
T_{wb}	Wet-bulb temperature
t	Time
u	Flow Velocity
VBNC	Viable But Non-Culturable
VOAG	Variable Orifice Aerosol Generator
V	Droplet Volume
w	Drift eliminator channel width
WHO	World Health Organization

LIST OF APPENDICES

CHAPTER 1 INTRODUCTION

Si la nature n'était pas belle,
elle ne vaudrait pas la peine d'être connue
et la vie ne vaudrait pas la peine d'être vécue
- Poincaré (1908)

The transmission of infectious diseases is a major vulnerability of modern civilization, exacerbated by the growing population density. Indeed, the COVID-19 pandemic has detrimentally affected the world in drastic ways. In the midst of this global health crisis, death counts surged even with stringent regulations in place and the help of vaccines [1]. The economical repercussions are substantial and will be long-lasting [2]. It may have changed society as we know it, with pathogen transmission at the forefront of public awareness for the foreseeable future. Another environmental issue is rising antibiotic resistance, which further demonstrates that the way pathogens are dealt with can affect billions of people worldwide, sometimes in unintended ways [3]. However, the concept of a pandemic, and of infectious diseases in general, is not recent. Bacterial or virus-related outbreaks have tarnished history, yielding catastrophic effects. Indeed, the bacteria responsible for tuberculosis may have killed more people than any other microbial pathogen [4]. The black death is well known for wiping out half of Europe's population and the 1919 Spanish flu is still the deadliest pandemic in history, with a death count of 100 million [5]. Major health crises are often predicted by experts and yet, contamination dynamics are still misunderstood [6]. In order to help prevent history from repeating itself, a deeper understanding of the transmission routes of pathogens must be obtained.

The understanding of the airborne transmission of pathogens presents a complex challenge due to the intricate fluid dynamics involved in transporting pathogen-laden particles through the air [7]. A prime example is the bacteria *Legionella*, increasingly recognized as a significant cause of often underdiagnosed and sporadic community-acquired infections transmitted via the airborne route [8, 9]. The most frequent source of outbreaks for this pathogen is water from cooling towers, which are large heat exchangers widely installed on buildings using water as a heat transfer media to dissipate excess heat, and potentially pathogens, into the surrounding environment through an aerosol plume [10]. There are an estimated 2 million cooling towers installed in North America and *Legionella* accounts for approximately 1.9 yearly cases per 100 000 people [11]. Furthermore, the number of cases has been steadily

growing worldwide for the past 30 years [12]. With the temperature rise associated with climate change, the increasing energy demand for cooling towers is expected to exacerbate the risks of *Legionella* infections [13].

Historically, most of the scientific effort to limit the spread of pathogens from water sources has focused on water treatment and disinfection strategies [9]. As a result, the multiphase flow dynamics associated with the transport of *Legionella*-laden aerosol droplets from cooling towers remain poorly understood. Nonetheless, the emerging field of airborne disease transmission has been rapidly evolving in recent years, bridging the gaps between microbiology, aerosol science, and multiphase fluid dynamics. The airborne transmission of pathogens is now widely recognized as a critical research gap, but the complexity of the fluid dynamics involved in transporting pathogen-laden aerosol droplets leaves experts divided on the most effective mitigation strategies, as much remains unknown about how these pathogens spread through the air [3]. The following sections introduce the research gaps at the heart of these disagreements and leading to the scope of this project.

1.1 Airborne and droplet transmission

The World Health Organization (WHO) defines air pollution as the "Contamination of the indoor or outdoor environment by any chemical, physical or biological agent that modifies the natural characteristics of the atmosphere" [14]. As such, biological airborne particles can be considered as pollutants as they can cause detrimental respiratory diseases when inhaled. The transmission of pathogens via airborne aerosol droplets has long been recognized [15]. Yet, advancements on the characterization of the airborne transmission process of pathogens have been limited [3]. Current understanding largely centers on the following: The extent of pathogen survival and particulate transport behavior in the air is governed by the complex multiphasic dynamics between the pathogens, the aerosol droplets carrying them and the surrounding mixture of air and water vapor.

Two distinct transmission routes are described in the literature: droplet and airborne transmission. The World Health Organization (WHO) uses a threshold particle size of between 5 and 10 μm for the transition between the droplet and airborne transmission. However, the practical distinction between the transmission routes is disease-specific and dependent on environmental conditions [16]. Larger airborne particles behave differently than their smaller counterparts (Figure 1.1). Droplet transmission is characterized by relatively large particles with large settling velocities and limited effects from evaporation. For pathogen transmission to occur, the subject must be near the source to inhale the droplets or directly come in contact with them once they are deposited on surfaces (fomites). As for airborne transmis-

sion, smaller droplets settle slower and can remain airborne for longer as they reach a stable diameter through evaporation. The smaller the particles, the further they can travel in the airways and the lungs [17, 18]. However, small particles can only carry a limited number of pathogens [19].

This dichotomy between large and small droplets remains at the core of the mitigation strategies recommended by the World Health Organization (WHO) and The American Centers for Disease Control and Prevention (CDC) and is still debated today [20]. Nonetheless, potential outbreak sources such as cooling towers do not generate isolated pathogens, but rather a turbulent plume comprised of moist air and potentially contaminated particles. Seminal work by Bourouiba on anthropogenic airborne disease transmission identified that the transport mechanism of potentially contaminated particles is better represented by multiphase clouds flowing from a source point [21] (Figure 1.2). The effect of this updated model is that gas clouds extend the range of droplets of all sizes by trapping them and carrying them forward farther than they would reach had they been emitted as isolated droplets in a fluid at rest. Locally moist air can also protect droplets from evaporation. Therefore, contamination via aerosol is characterized by the dispersion of a particle-laden fluid into the environment, acting as a multiphase cloud, with both airborne and droplet transmission potentially contributing as transmission routes. The implications of the fluid dynamics governing pathogen-laden turbulent plume clouds are thus significant for the establishment of mitigation strategies for the airborne transmission of *Legionella* [3].

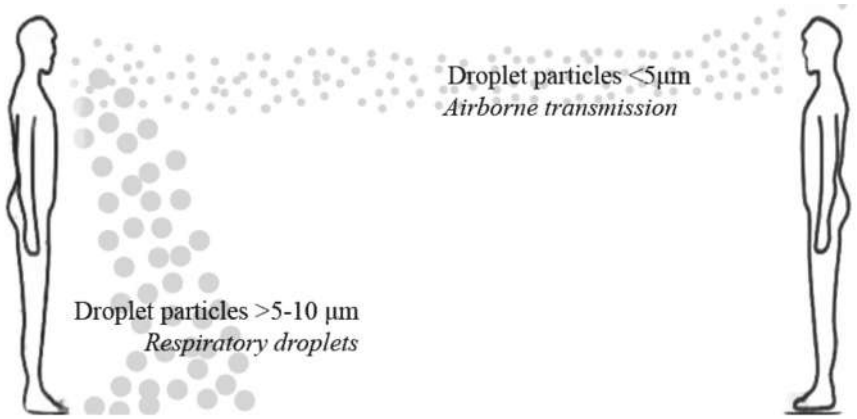

Figure 1.1 Illustration of the dichotomy between airborne and droplet transmission. Reprinted with written permission from CCA [22].

For convenience, and in accordance with the literature, *particle* and *droplets* will be used interchangeably to refer to individual finite pieces of the disperse phase suspended in air. *Aerosol* will refer to the entirety of the disperse phase within the surrounding continuous

Figure 1.2 Multiphase Turbulent Gas Cloud From a Human Sneeze. Reprinted with written permission from Cambridge University Press. [21, 23].

gas [24].

1.2 Water as a transmission vector

Airborne transmission does not only stem from anthropogenic aerosol droplets such as those produced by coughing, sneezing, talking or signing, but occurs from man-made engineered systems as well [3]. While the properties of the fluid carrying the pathogens diverge significantly between the two sources, the fundamental principle remains the same: Aerosol droplets containing pathogens are carried from the exposure source to the contamination site through a multiphase cloud.

Engineered systems offer the necessary nutrients and moisture for microbial growth, including biofilm accumulation (biofouling) driven by water stagnation in piping networks and suitable temperatures. They also facilitate aerosol generation and transport, allowing pathogens to spread. Among these pathogens, *Legionella* is particularly concerning due to its ubiquity in freshwater and its ability to thrive in systems such as cooling towers. Once contamination occurs, controlling the growth of *Legionella* becomes challenging [9]. Despite this, the significance of outbreaks and sporadic infections caused by *Legionella* is often underestimated [25]. As an airborne transmitted disease, the complexity of tracking its transport from unknown sources to inhalation sites adds to the difficulty of linking clinical cases to environmental

sources.

Potential infectious engineered sources involve aerosol generation as an unintended consequence of regular operation. Multiple aerosol generation mechanisms are reported in the literature and stem mostly from perturbations in a liquid-gas interface resulting in fluid fragmentation [26]. The end result is the creation of small water droplets containing biological matter. Bacteria and viruses trapped in these droplets are protected from the environment by an aqueous layer and can survive airborne for extended periods of time [27]. Once airborne, water from aerosol droplets evaporates partially leaving nuclei small enough to be inhaled. The size of water-based droplets evolves in accordance with environmental conditions such as temperature and relative humidity [28], which makes it challenging to accurately measure their size. Identifying the transmission routes of these pathogen-carrying particles involves a deep understanding of the fluid dynamics governing their evaporation and size distribution.

The advantage of studying engineered systems is that the aerosol generation is steady in time and the large volume of aerosol droplets generated makes their detection statistically easier. Toilets, whirlpools, spas, and even living (green) walls are considered potential sources of bacteria that can be transmitted via aerosol [29]. However, the most prominent source of *Legionella*-laden aerosol contamination remains cooling towers, illustrated in Figure 1.3, which generate and release large quantities of potentially contaminated droplets due to the direct contact between air and water inherent to their operation [30]. Aerosol generation, dispersion, and deposition within the cooling towers, as well as particle capture before they are released into the environment, are not sufficiently understood to enable the identification and prediction of the precise conditions leading to potential outbreaks.

1.3 Project scope

Regardless of the substantial efforts to reduce the risks associated with the airborne transmission of pathogens from engineered systems, such as cooling towers, sporadic cases and outbreaks still occur every year at an increasing rate worldwide. The lack of understanding of the fluid dynamics governing the transport of *Legionella*-laden aerosol droplets from cooling towers to inhalation sites is a critical gap in the current knowledge. This research therefore aims to shed light on the factors contributing to pathogen spread, with a focus on aerosol characterization, to inform more effective mitigation strategies.

In the following chapter, an extensive literature review is presented, covering the challenges associated with cooling towers and *Legionella*, the different aerosol size distribution measurement instruments available, as well as the water-based droplet evaporation mechanisms, to

(a) (b)

Figure 1.3 (a) Industrial cooling tower. (b) Aerosol plume generated from an industrial cooling tower and released into the ambient air [31].

identify the research needs of the project. After a critical assessment of the literature, the specific objectives of the project are discussed. The results are then discussed in the next 5 chapters in the form of 5 journal articles A general discussion of the impact of this work is presented in chapter 9. The thesis is finally summarized in chapter 10, also including limitations and recommendations for future work.

CHAPTER 2 LITERATURE REVIEW

I am an old man now, and when I die there are two matters on which I hope for enlightenment. One is quantum electrodynamics and the other is the turbulent motion of fluids. And about the former I am really rather optimistic.
- Horace Lamb (1932)

2.1 Challenges associated with cooling towers and *Legionella*

Cooling towers are an important part of typical Heating, Ventilation and Air Conditioning (HVAC) systems employed to evacuate excess heat from large buildings and industrial equipment. They are not only comprised of the tower itself but also include the plumbing system, pumps and chillers (Figure 2.1). The water for the heat exchange flows throughout this large surface area system, making it challenging to control the bacterial growth or to efficiently disinfect a highly contaminated cooling tower [32]. *Legionella* can develop anywhere in the network where it is wet, and then be transported toward the cooling towers where it can be aerosolized and discharged into the environment [33]. To fully grasp the issue of bacteria-laden aerosol dispersion from cooling towers, it is essential to understand the underlying fluid mechanisms at play. In this section, a detailed review of cooling towers and *Legionella* is presented, as well as the state of the art for regulations put in place and the current attempts to evaluate and reduce the contamination risks.

2.1.1 Water cooling towers

A cooling tower is a specialized heat exchanger that removes heat from process water through latent heat transfer between hot water and colder ambient air circulated inside the cooling tower [35] (Figure 2.2). As this occurs, a significant volume of water is evaporated and the excess heat of the building is discharged into the environment as a multiphase flow of vapor and aerosol droplets [36]. Despite the health risk associated with *Legionella* transmission, cooling towers remain widespread due to their relative affordability and efficiency [37].

Airflow dynamics

Cooling towers are typically divided into categories according to specific aspects of the system, the most interesting in the context of airborne transmission being airflow dynamics, impacting the aerosol generation and dispersion into the environment. The direction the air travels in cooling towers can either be considered a crossflow or a counterflow with respect

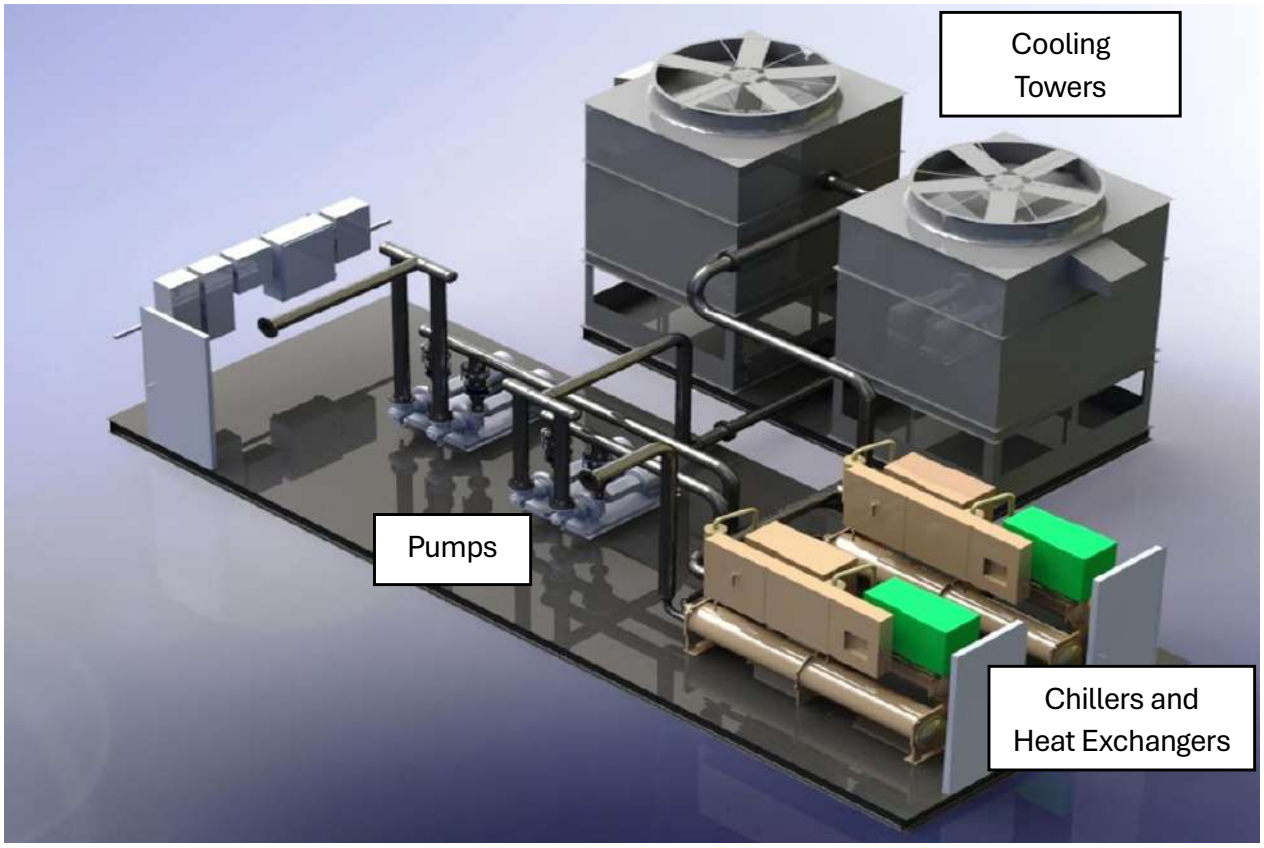

Figure 2.1 Cooling tower plumbing system, including pumps, chillers and heat exchangers. [34]

to the falling water (Figure 2.3) [39]. For crossflow cooling towers, water flows downwards vertically through the fill material, a medium used in cooling towers to increase the surface area available for heat transfer, while the air flows horizontally across the falling water. In counterflow cooling towers, the air enters an open area beneath the fill media and flows vertically upwards, against the flow of falling water sprayed from pressurized nozzles [40], generally making them approximately 25% more effective at heat transfer than crossflow cooling towers [41].

Another characteristic differentiating cooling towers is the way air is drawn into the system (Figure 2.4). It can affect performance, but also the aerosol generation and dispersion into the environment. Mechanical draft cooling towers use electric motor-driven fans to circulate the air through the tower. An axial fan is typically positioned on top of the cooling tower to pull the air through. It is the most common type of cooling tower and the most efficient [41]. In some systems, a blower-type centrifugal fan is placed at the air intake to force air into the cooling tower which creates high entering and low exiting air velocities. This is called a forced draft and it consumes more power than induced draft cooling towers [43].

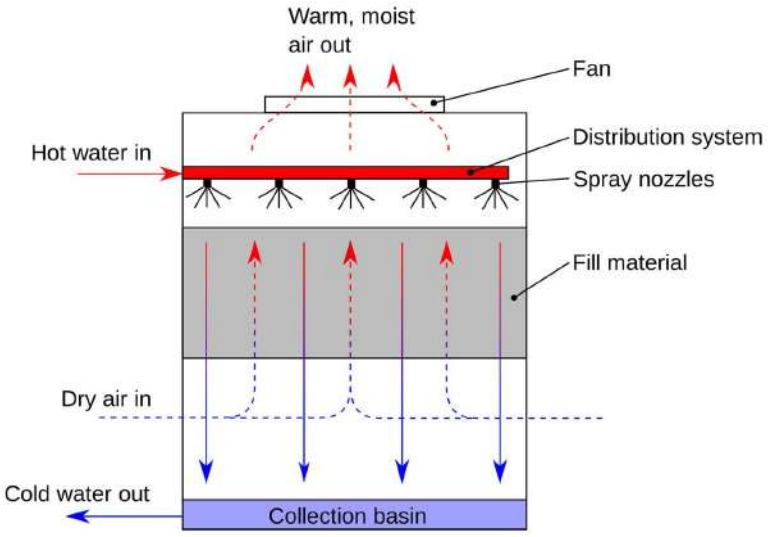

Figure 2.2 Cooling tower working principle [38].

Differences between cooling towers

Variations in the design of cooling towers, even among those of the same type, can significantly impact aerosol production and dispersion, particularly in terms of the positioning of spray nozzles relative to the fan [44]. Additionally, the fill material is prone to biofouling and bacterial growth, depending on the operational conditions [45] (Figure 2.5). These design variations create a diverse range of cooling tower configurations. Each system presents unique characteristics complicating the generalization of the fluid dynamics governing the airborne transmission of bacteria-laden aerosol droplets.

Aerosol generation

The aerosol generation processes inside cooling towers are not well characterized. However, the direct contact of water and air provides the right conditions for the generation of a large volume of aerosol droplets through multiple possible generation mechanisms. For bacteria-laden droplets, short-lived unsteady fluid fragmentation dominates the aerosol generation process, via coupled interfacial instabilities on the free surface [46]. One obvious way droplets are generated is through the spray nozzles of counterflow cooling towers which produce droplets expected to be within the 0.5 to 5 mm size range [47]. Smaller droplets evaporate when they come in contact with the air inside the cooling tower and the resulting small dried nuclei thus generated are expelled into the ambient air [48]. The inside of a counterflow cooling tower under the fill media looks similar to pouring rain (Figure 2.6). Therefore, droplets between 1 and 10 μm in diameter are likely also generated by the impact

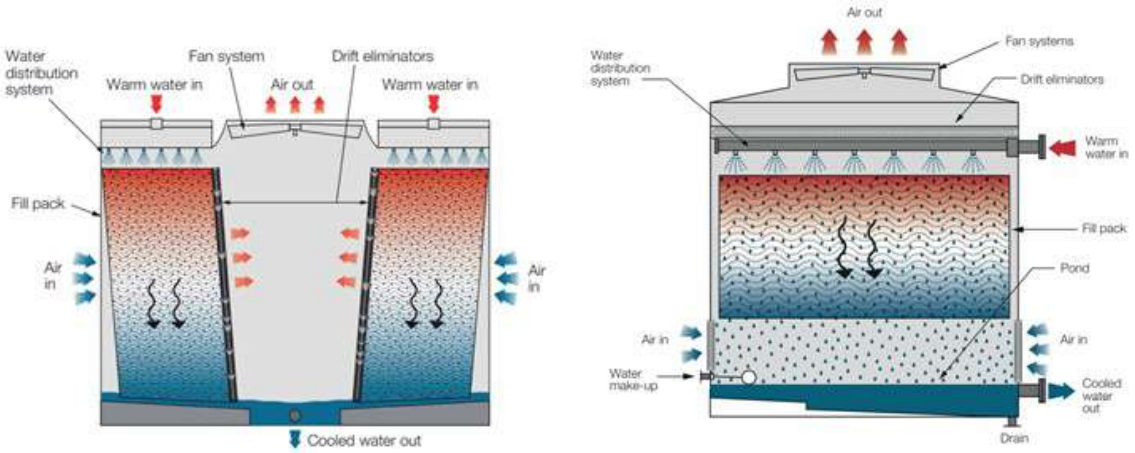

(a) (b)

Figure 2.3 a) Crossflow cooling tower. b) Counterflow cooling tower [42].

of larger water droplets in the shallow water basin [26]. Another known way to generate such particles is through the bursting of bubbles on the water film flowing on the walls of the fill media [49], from which droplets between 1 and 500 μm in diameter are expected to be generated [50]. Multiple other mechanisms could be involved in aerosol generation inside cooling towers, an overall inevitable phenomenon as the direct contact between water and air responsible for the aerosol generation also provides the heat exchange.

Each individual droplet size and trajectory, as well as its pathogen concentration and viability, are governed by the properties of both the droplet and the surrounding multiphase flow [51]. These characteristics and their evolution in time and space are critical to assessing the contamination risks and controlling the extent of an outbreak [24]. In the context of airborne transmission, the aerosol generation process provides the initial conditions of the individual pathogen-laden particles, but the transport through a turbulent plume in the environment determines their ultimate fate [21].

2.1.2 Drift eliminators

Once bacteria-laden aerosol droplets are discharged into the environment in a plume of air and water vapor from a cooling tower, airborne transmission and human contamination are governed by meteorology and are therefore disorderly and very difficult to manage. Thus, the contaminated droplets must ideally be captured at the outlet of cooling towers before they are released into the ambient air. Concurrently, a large volume of water is lost from cooling towers due to evaporation and aerosolization. Drift eliminators are used primarily

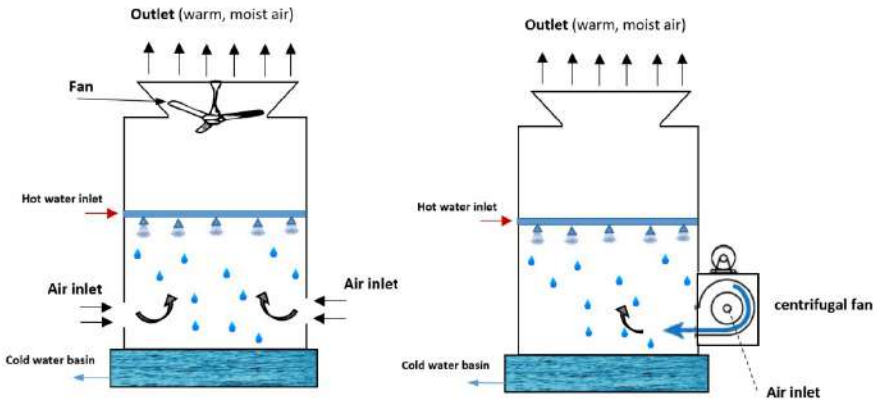

Figure 2.4 Left : Mechanical draft induced type cooling tower. Right : Mechanical draft forced type cooling tower. [39]

Figure 2.5 Biofouling in fill material

to limit these water losses to the unavoidable evaporative contribution, but they also lower aerosol dispersion [42]. Drift eliminators are cost-effective systems consisting of small channels imposing sharp bends to the airflow and covering the outlet of the exhaust air from the cooling tower (Figure 2.7). The design of drift eliminators strikes a balance between maximizing water capture efficiency and minimizing pressure losses, while minimizing material usage [52].

Types of drift eliminators

Different versions of drift eliminators are employed on cooling towers (Figure 2.8). A first type is the cellular drift eliminator, consisting of an alternating series of corrugated sheets assembled to form closed cells, which are designed specifically for particle removal efficiency. A second type is the blade-type drift eliminators, composed of thick blades that are held together with end caps. Cellular type drift eliminators provide more surface area to capture

Figure 2.6 Inside of an operating cooling tower

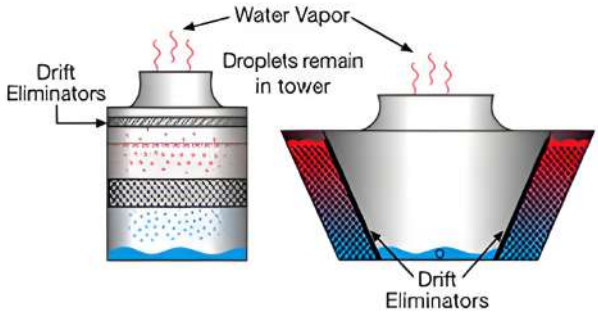

Figure 2.7 Location of drift eliminators on different types of cooling towers [42]

droplets and are thus the most efficient [39], but they are more costly [41].

Working principle

The mechanism behind particle capture in drift eliminators is described by aerodynamics (Figure 2.9). The channels of the drift eliminators first create a sudden change of direction in the air stream which separates denser droplets from the airflow. The separated droplets have too much inertia to abruptly change direction and impact the eliminator surface on which they lose their momentum and are drained back into the cooling tower [53].

Since the flow speed is small through drift eliminators, a two-dimensional incompressible flow can be assumed [55]. It is also assumed that the droplets are sufficiently small and light to have minimal effect on the airflow. The motion of the small droplets is essentially controlled by drag forces, not by gravity. Some large droplets escape collection because of

Figure 2.8 Blade type drift eliminator on the left and cellular type drift eliminator on the right [42]

air turbulence, and particle bounce can occur at liquid-air interface on the wet fill material under specific circumstances [53, 54, 56].

Drift eliminator efficiency at capturing aerosol droplets in a given size range is directly related to the infection risks associated with a specific system. The theoretical drift eliminator collection efficiency depends on the density of the particle ρ_p (kg/m^3), the particle diameter D_p (m), airflow velocity U_e (m/s), the viscosity of the gas μ (Pa $\cdot$ s), the width of the channels of the drift eliminator b (m) and the angle of the direction change of the drift eliminator θ ($^\circ$), and is given by the following equation [57]:

$$\eta = \frac{\rho_p (D_p)^2 U_e}{18 \mu b} \theta \tag{2.1}$$

As mentioned above, there is a compromise to be made between capture efficiency and energy consumption; a higher collection rate entails higher flow pressure drop which means higher energy consumption from the cooling tower. Essentially, in order to achieve the highest collection efficiency, drift eliminator geometry must be as complex as possible, increasing pressure drop [53]. Most cooling tower managers tend to value low energy consumption more than excessive water losses, simply because replacing the evaporated water is cheaper [58].

Multiple comparative studies on different types of drift eliminators have been conducted, either numerically or experimentally, typically in wind tunnels [59–63]. Most agree that

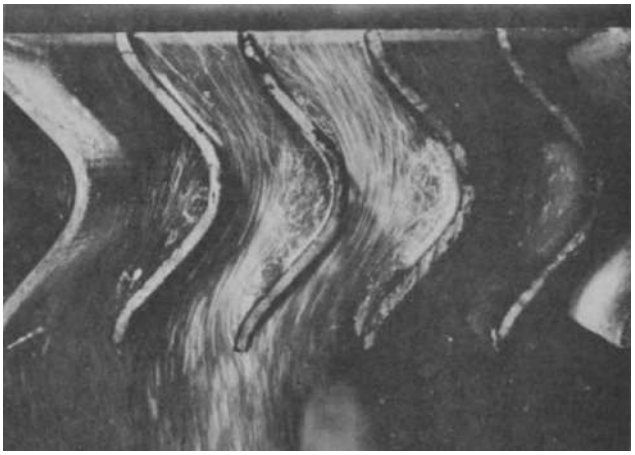

Figure 2.9 Droplet behavior and collection by drift eliminators, reprinted with written permission from Elsevier [54]

drift eliminator design can be further improved, especially towards the capture of smaller droplets [64]. Nevertheless, the drift eliminator efficiency at capturing droplets is dependent on the specific cooling tower characteristics [55] and the evaluation of drift eliminators needs to consider the entirety cooling system, as multiple factors can influence their efficiency [62], including the way the water is distributed in the cooling tower [64]. Furthermore, the optimal conditions for a specific drift eliminator are dynamic, depending among other things on the state of cleanliness of the cooling tower [65]. Even though each cooling tower system is unique, drift eliminators are mostly of the two types mentioned above and are not customized to the system. Even with the significant number of studies conducted on drift eliminators, knowledge is still limited on their capture efficiency in the context of airborne transmission.

2.1.3 *Legionella*

Measuring approximately 0.3-0.9 μm by 1.5-5 μm [66], *Legionella* is a Gram-negative bacillus, meaning that it is rod-shaped (Figure 2.10). The gram-negative characteristics provide the bacteria with a dual membrane structure that makes it highly resistant (50-100%) to commonly used antibiotics and chemical disinfectants [67]. *Legionella* is responsible for two pneumonia-like illnesses in humans, particularly affecting at-risk individuals: Legionnaires' disease, with a mortality rate of 10%, and Pontiac fever, an influenza-like, self-limited illness [10]. Legionellosis refers to both of these diseases. More than 95 % of cases are sporadic and the primary exposure source is rarely identified [68], which means that the total number of cases is most likely underestimated [69]. It is not typically transmitted anthropogenically because it is deposited too deep within the lungs to be ejected through a cough or a sneeze [70]. Thus, its preferred transmission media is water. *Legionella* is responsible for 402

M$ per year in health care cost in North America [11, 71, 72].

Legionella refers to the bacteria genus which is divided into multiple species. The most prevalent is the *Legionella pneumophila* species which is divided into 15 serogroups. The other species of *Legionella* are often grouped together and referred to as *Legionella spp.* In Europe, 90% of cases are caused by *Legionella pneumophila* and more than 85% are linked to serogroup 1 alone [73]. However, 24 of 58 known *Legionella* species have been implicated in human diseases [10].

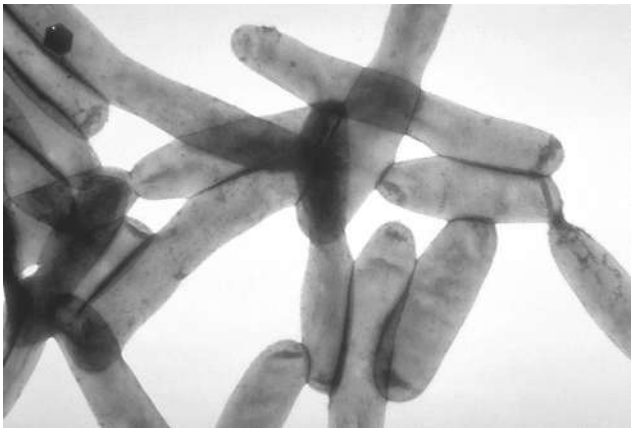

Figure 2.10 Scanning electron microscopy (SEM) impage of *Legionella pneumophila*

Legionella naturally exists in freshwater and quickly reproduces inside man-made engineering equipment that yields the right conditions for growth, such as intermittent stagnant water, temperature, hosts and biofilm. Aerobic biological systems provide the best environment for *Legionella* proliferation because of the temperature range, usually between 20 and 50 °C [74], and the presence of protozoa [75]. Indeed, *Legionella* grows inside protozoan hosts associated with biofilm and can be released into the water, assisted by the shear forces induced by turbulence in the flowing water [76].

Legionella **transmission**

Legionella is transmitted via inhalation of small airborne droplets from a contaminated water source that has allowed the organism to grow and spread (Figure 2.11). For example, whirlpools and flushing toilets generate aerosol droplets able to carry biological matter [77]. However, since most of these potential sources usually deal with small volumes of water and no significant forced airflow, the extent of the outbreak they can cause is limited. In contrast, cooling towers deal with large flow rates of air and potentially contaminated water. They are therefore the main source of *Legionella* outbreaks through the discharged aerosol

plume [78]. Contaminated cooling towers can even contribute to seeding other nearby cooling tower systems [79, 80].

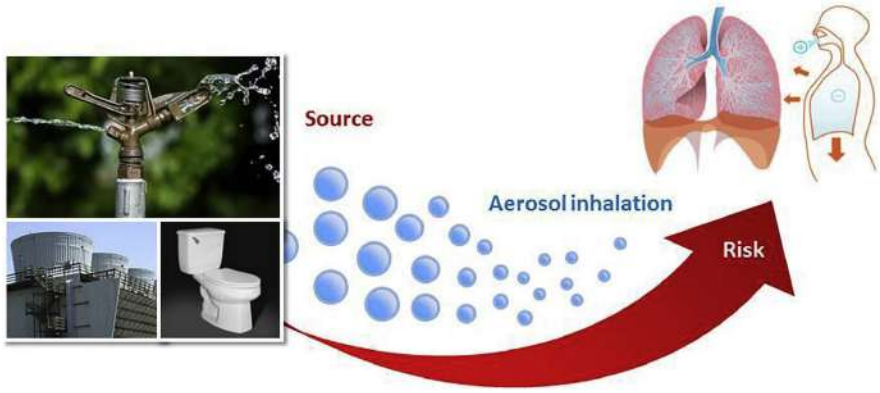

Figure 2.11 Transmission of *Legionella pneumophila*. Reprinted with written permission from Elsevier [81].

Effect of aerosolization on bacteria

The relationship between the concentration of bacteria inside the cooling tower water and the concentration of airborne bacteria discharged in the aerosol is of the utmost importance to accurately assess the risks associated with *Legionella* infections. This rate of bacteria transfer from water to aerosol is governed by the aerosolization mechanisms inside the cooling tower. Knowledge is limited on this relationship but a higher concentration of *Legionella* in water is not always linked with a higher concentration in aerosols [10]. The transfer rate of solids from a bulk liquid to the air has typically been considered very small, on the order of maximum 1% [82, 83], supposed from the working mechanisms of cooling towers [84–86]. However, in these studies, the bacteria concentrations were compared in different fluids (water vs. air). To adequately characterize the bacterial transfer from the bulk liquid to the generated droplets, the concentrations should be compared within the same media. In this case, the pathogen concentration in the cooling tower process water should be compared to the concentration inside the aerosolized water present in the air in the form of droplets. No basis for such a correlation was proposed, highlighting the pressing need to quantify it for an accurate assessment of the risks associated with *Legionella* infections.

The viability of pathogens being carried via the airborne route depends on multiple factors. A thorough review of these factors, from the generation of contaminated aerosol droplets to their inhalation and deposition in the respiratory tract, can be found in appendix A. Here, we will focus specifically on the survival of *Legionella* in aerosol droplets. *Legionella* thrives at 65% relative humidity and is significantly less active at 90% and 30% [87]. Solar

radiation has a lethal effect on airborne *Legionella* as well [10]. However, in the context of airborne transmission, the contamination through inhalation depends on the metabolic state of the bacteria. When the conditions are suboptimal, *Legionella* transitions into a viable but nonculturable (VBNC) state to enhance survivability. In that state, its only focus is to survive as it does not grow or reproduce until the ambient conditions become favorable again. This process can make *Legionella* detection harder, especially when airborne as it can be assumed that it enters the VBNC state when aerosolized [88]. In essence, the survival of bacteria in aerosol droplets depends on multiple environmental and metabolic factors, but it is typically in the range of hours [46, 89, 90].

Microbial growth control

The current most widespread method to control the growth of *Legionella* in a plumbing system is through chemical water treatment. Chemical compounds include chlorine, ozone and copper-silver ionization [91]. Continuous injection of biodispersive agents is typical as well to limit biofilm formation [92]. Cooling tower water disinfection and conditioning strategies for large units can cost from 50 000 to 300 000 USD annually [93]. These strategies are often damaging to the cooling tower system over time, inducing significant corrosion and scale formation, which can reduce the heat transfer efficiency by up to two orders of magnitude, and compromise cooling tower performance, potentially causing operational issues [40, 94].

In practice, every cooling tower system uses a specific treatment method which typically combines multiple chemical compounds used at different time intervals. *Legionella* can adapt to a wide variety of environments and often survives chlorine-based disinfection [10]. Therefore, chemical treatments are not always effective and important levels of contamination still occur, most often during the summer warm weather. As such, newer and older cooling tower systems are susceptible to *Legionella* contamination [95]. Sustainable physical treatments such as thermal inactivation and mechanical filtration of the process water have become more relevant in recent years [74, 96, 97]. Cross-flow microsand filtration effectively removes particulate matter and microorganisms larger than 1 μm from water. These systems are typically combined with a lower dosage of the chemical treatment. This approach not only enhances microbial control but also contributes to a reduction of corrosion and scale formation [98, 99], thereby improving the overall physical state of cooling tower systems. Nevertheless, cross-flow microsand filtration is not widely adopted [91].

2.1.4 Regulations

In 2012, between July 18th and October 8th, 181 cases of legionellosis were reported in the Quebec City area (QC, Canada), 14 of which were fatal. Cooling towers harboring the pathogenic strain and were held responsible for its dissemination [100]. This major outbreak led to the adoption of provincial regulations. Concentration of *Legionella* in water must not exceed 10^4 CFU/L, with regular monitoring and corrective actions required if this threshold is surpassed. If the concentration exceeds 10^6 CFU/L, the cooling tower must be shut down and disinfected. These thresholds are less stringent than those in Europe [101], and sporadic cases still occur every year throughout the province. Thus, updated regulations are needed [102].

Cases associated with *Legionella* remain largely underestimated in many countries worldwide. The United States has been known to have a reactionary mindset to outbreaks and be very late at establishing regulations for *Legionella* monitoring of cooling towers [103]. In contrast, the threshold for immediate action set by the European Working Group for Legionella Infections (EWGLI) is among the most rigorous in the world [104]. There is a clear dichotomy between Europe, which uses *Legionella spp.* as a benchmark for monitoring and regulation, and North America, where the focus is primarily on *Legionella pneumophila* as the key indicator for assessing health risks in water systems [104]. As *Legionella* infections have increased worldwide in the past few decades [8, 105, 106], it is often argued that standardized regulations are needed and that adequate training of cooling tower managers remains the best way to mitigate risks [95, 104].

There are currently no strict regulations regarding the discharge of aerosol particles from cooling towers into the environment in the province of Quebec. However, there are some guidelines from governments worldwide such as having a flow rate under 3 m/s, having airtight drift eliminators and protecting the humid surfaces from the sun to prevent temperature increases [107]. Guidelines are also provided on the total quantity of pollutants of all types that can be released into the environment from a stationary source, which should be lower than 15 μg/m^3 of air for particle matter smaller than 2.5 μm and lower than 45 μg/m^3 for particle matter smaller than 10 μm [14]. However, these guidelines cannot be easily applied to aerosol droplets because their mass changes constantly due to evaporation. Therefore, *Legionella* transport into the ambient air is technically governed by the WHO guidelines, but it is not adapted to address airborne transmission and also not enforced.

2.1.5 Risk assessment

The transmission of *Legionella* exhibits distinct seasonal patterns, with a higher incidence observed during warmer weather. Additionally, rainfall, elevated humidity, and low atmospheric

pressure have been linked to an increase in cases [10]. Assessing the risk of *Legionella* transmission is particularly complex due to the multitude of factors influencing droplet formation and their subsequent dispersion into the environment. Nonetheless, educated estimations can provide orders of magnitude for the risks.

In the realm of infectious disease control, particularly in the context of respiratory infections, Quantitative Microbial Risk Assessment (QMRA) provides a systematic framework to quantify the likelihood of exposure to airborne pathogens and assess the subsequent risk of infection. By integrating data on pathogen concentrations, aerosol dynamics, and human exposure factors, QMRA models the transmission dynamics, allowing for the identification of critical control points and the development of targeted intervention strategies. Hamilton et. al adapted the QMRA methodology to the airborne transmission of *Legionella pneumophila* from cooling towers [81,108]. It assumes that *Legionella pneumophila* exposure risks are based on the combination of multiple models: the emission of potentially contaminated aerosol droplets from a cooling tower, their atmospheric dispersion, the inhalation and deposition of the particles depending on their size, and finally the pathogenic dose-response specific to each individual.

Emission model

According to the QMRA methodology developed by Hamilton et. al, the emission rate of *Legionella pneumophila* into the environment Q_{em} (particles/s) can be calculated, with knowledge of the pathogen concentration per volume of water C_w (particles/$\mathrm{L_w}$) as well as the volumetric flow rate released from the cooling tower $\dot{V}_{air}$ ($\mathrm{L_{air}}$/s), the drift eliminator capture efficiency η (-), the ratio of bacteria transferred from the water to the airborne aerosol droplets R_{wa} (-), the volume of water aerosolized V_w ($\mathrm{L_w}$), the volume of air sampled by the OAS V_{air} ($\mathrm{L_{air}}$) and the ratio of accuracy for the detection method R_m (-):

$$Q_{em} = \frac{C_w \dot{V}_{air} V_w R_{wa} \eta}{V_{air} R_m} \tag{2.2}$$

The model considers the emission rate for droplets in the 1-10 μm size range. This emission model estimates the concentration of viable pathogens released from the cooling tower based on their water concentration. However, it lacks crucial data linking the concentration of *Legionella pneumophila* in the cooling water to that in the discharged aerosol droplets. Without this key information, the accuracy of the model is limited.

Atmospheric dispersion model

The atmospheric dispersion model allows to estimate the *Legionella pneumophila* concentration downstream from a cooling tower. Hamilton used a Gaussian atmospheric model which considers a point source for the emission [81, 108] (Figure 2.12). The average *Legionella pneumophila* concentration emitted by a cooling tower can be determined at any point in space according to the following equation :

$$C_{air}(x,y,z) = \frac{Q_{em}}{2\pi\mu\sigma_y\sigma_z}\exp[-\frac{y^2}{2\sigma_y^2}](\exp[-\frac{(z-H_e)^2}{2\sigma_z^2}] + \alpha\exp[-\frac{(z+H_e)^2}{2\sigma_z^2}])\exp[-\lambda\frac{x}{\mu}] \quad (2.3)$$

Where C_{air} (particle/m^3) is the average airborne *Legionella pneumophila* concentration, Q_{em} (particle/s) represents the emission rate of *Legionella pneumophila*, and μ is the average wind speed in the x direction (m/s). The terms σ_y and σ_z (m) denote the standard deviations of the concentration distribution in the y and z axes, respectively. The variables x, y, and z (m) represent the longitudinal, lateral, and vertical distances from the point source, while H_e (m) refers to the height of the point source relative to the ground. The reflection coefficient on the ground is denoted by α, and λ (s^{-1}) signifies the inactivation rate of *Legionella pneumophila*.

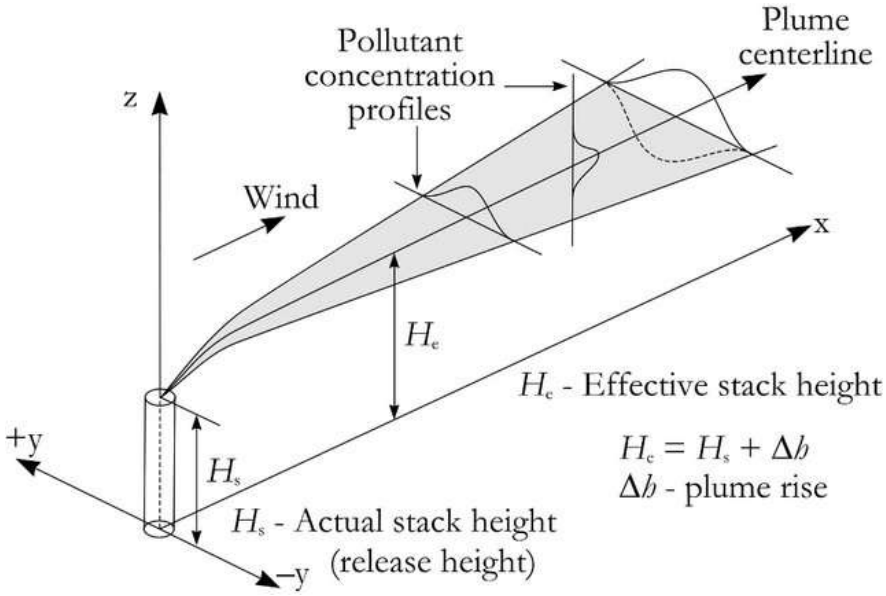

Figure 2.12 Gaussian distribution of the concentration within the plume of an atmospheric pollutant, reprinted with written permission from CCA [109]

The values of σ_y and σ_z can be obtained from the following semi-empirical equations :

$$\sigma_y = R_y x^{r_y} \tag{2.4}$$

$$\sigma_z = R_z x^{r_z} \tag{2.5}$$

Where x is the longitudinal distance from the emission source and R_y, R_z, r_y and r_z are determined from the atmospheric Pasquil-Gifford stability classes [110].

Inhalation and deposition model

The inhalation model defines the dose of *Legionella pneumophila* that is inhaled and deposited within the respiratory tract of an exposed subject. It can be calculated with the following equation, assuming a constant deposition rate of 25% in the respiratory tract [81, 108] :

$$D = C_{air} I t \sum_{i}^{n} F_i DE_i \tag{2.6}$$

Where D (particle) is the dose of *Legionella pneumophila* deposited in the respiratory tract of the exposed subject, C_{air} (particle/m^3) is the average airborne *Legionella pneumophila* concentration, and I (m^3/min) is the inhalation rate of the subject. The term T (min) represents the length of exposure. F_i (-) denotes the fraction of *Legionella pneumophila* aerosolized into droplets of size 1 to 10 µm, while DE_i (-) is the average probability that an aerosol of diameter i is deposited.

Dose-response model

Two dose-response models for *Legionella pneumophila* were developed by Armstrong and Haas [111] based on experimental data quantifying the probability of response (fever or mortality) in guinea pigs following inhalation of aerosols contaminated with *Legionella pneumophila* serogroup 1 [112]. The dose-response model provides the best fits to the data from these experimental animal studies. It can be expressed by the following equation:

$$P_{\text{inf}} = 1 - \exp(-rD) \tag{2.7}$$

Where P_{inf} (-) is the probability of infection, r (-) is the median probability that a *Legionella pneumophila* bacterium initiates infection.

This dose-response model has been used in QMRA studies to predict subclinical severity infection in humans [81, 108]. Clinical severity was defined as an infection requiring medical attention or the seeking of healthcare services. The epidemiological validation of these dose-response models was studied by Armstrong and Haas [113] based on data obtained during three outbreaks of legionellosis associated with public spas in Japan and the Netherlands. The authors found good agreement (generally less than one order of magnitude difference) between reported subclinical and clinical infections and the infection risks calculated by QMRA based on estimated exposures.

The dose-response models for *Legionella pneumophila* allow for estimating the probability of infection associated with a single exposure. To account for multiple exposure events over an extended period, the individual probability of infection can be combined according to the following equation:

$$P_{\text{inf, annual}} = 1 - \prod_{i=1}^{N}(1 - P_{\text{inf, }i}) \tag{2.8}$$

Where $P_{\text{inf, annual}}$ (-) is the probability of one or more infections over a total of N exposure events, and $P_{\text{inf, }i}$ (-) is the probability of infection per exposure event. If we assume that the probability of infection per event is constant, the probability of infection can be simplified to the following form:

$$P_{\text{inf, annual}} = 1 - (1 - P_{\text{inf}})^N \tag{2.9}$$

The health impact of a clinically severe infection is often assessed using the disability-adjusted life years (DALY) factor calculated by van Lier et al. based on surveillance data for Legionnaires' disease in the Netherlands [114], according to the following equation:

$$DALY = F_{DALY} \times P_{\text{inf}} \tag{2.10}$$

Where F_{DALY} (-) is the disability-adjusted life years factor for Legionnaires' disease, which accounts for the severity of the disease and the duration of the infection.

2.1.6 Experimental characterization of the aerosol droplets from cooling towers

Few experimental characterizations of aerosol droplets discharged from cooling towers have been conducted. One of the most pressing research gaps related to the contamination risks is the quantity of viable *Legionella* that are transferred from the bulk water to the aerosol droplets [108]. A key challenge in addressing this question is the ability to sample pathogens while maintaining their viability. Nocker et al. proposed a methodology using a liquid impinger to sample aerosol droplets, which was tested on four operational cooling towers. This approach enabled flow cytometry analysis of the collected samples, providing valuable insights into the viability of airborne pathogens [115].

One aspect of the aerosol discharged from cooling towers that remains elusive is the size distribution of potentially contaminated droplets. Ruiz et al. developed a methodology using an impactor combined with image processing to measure the size distribution of aerosol droplets from cooling towers. However, their technique lacked the resolution needed for accurate risk assessment [116]. As a result, current risk assessment models often rely on size distributions measured from aerosols generated in laboratory settings, which may not fully represent real-world conditions [66, 81]. The precise size distribution of aerosol droplets emitted from cooling towers therefore remains poorly characterized.

2.2 Considerations on energy

The evaporative cooling efficiency, or performance of a cooling tower in terms of heat transfer is affected by multiple parameters. A critical one is the wet-bulb temperature, the lowest temperature that can be reached under current ambient conditions only by the evaporation of water, which depends on the atmospheric temperature and the relative humidity. The heating or cooling load, which is the amount of thermal energy that a building needs to exchange with its environment in order to maintain the indoor temperature at established levels [117], as well as the flow rate of air and of circulating water [118] can also affect the performance of a cooling tower system. Additionally, heat inertia, a measure of heat gradually stored and released in a building, also plays a significant role in determining operational efficiency [119]. The evaporative cooling efficiency can be defined as the ratio of the energy to be evacuated by the tower (thermal load) to the energy required to operate the system [120]. This metric is called the coefficient of performance (COP) and is a measure of the effectiveness of transferring heat between two fluids [121].

Biofilm accumulation can also influence the performance of a cooling tower system. Biofilm can act as an insulating layer, decreasing the heat transfer rate by up to three orders of magnitude [122]. Biofilms can also reduce the effective diameter of pipes, impeding the flow of water and reducing the heat transfer efficiency as less water is exposed to the surrounding air [123]. Cross-flow microsand filtration can effectively remove biofilm and other particulate matter from the process water, thereby potentially improving the heat transfer efficiency of cooling tower systems [124–126].

One key characteristic influenced by the wet-bulb temperature, the load, the heat inertia and even biofilm accumulation is the operating rate, a ratio reflecting the working intensity of the cooling tower, according to the operation of the fan and the water pumps. It is calculated by averaging the ratios of the current operation over the maximal operation for the fan speed and the water pump [127]. However, although a consistently high operating rate is indicative of a low coefficient of performance, the operating rate of a cooling tower is not an indication of its efficiency [128]. Despite technical advancements in cooling tower design, most systems still operate below their optimal efficiency levels [129], resulting in increased energy consumption, higher operating costs, and potentially negative environmental impacts [130–132]. As such, there is a strong need to address these inefficiencies through the integration of innovative technologies.

2.3 Aerosol size distribution

As the fate of pathogen-laden aerosol droplets depends, among other factors, on their size, the infection risks cannot be assessed without proper physical characterization. The size distribution of aerosol droplets helps in understanding their physical properties as well as evaluating the infection probability. The number concentration for specific sizes can provide valuable information on the associated risks and guide the adoption of mitigation measures.

The number size distribution of particles dispersed in a fluid is represented by a list of values that defines the relative number of particles present according to their size [133], and is divided into small size classes called *bins*. In aerosol sizing instruments, the number of size bins is finite. When comparing aerosol size distributions measured by instruments with varying resolutions, the resulting plots of concentration versus particle diameter will differ due to discrepancies in the size binning of each measurement. To account for the fact that the number of size bins is not the same for every instrument, and that the bins are unequal in width, the y-axis on size distribution plots is normalized by dividing the number concentration (dN) of each bin by the logarithm of the bin width ($dlogD_p$) [134]. This results in a log-normal distribution that is independent of the bin width. Generally, log-normal distributions tend to be the best fit for single-source aerosol droplets. Some instruments already provide a normalized size distribution measurement, but for other instruments, the concentration must be normalized through data post-treatment to allow comparison with other instruments.

2.3.1 Sampling considerations

The ability of particles to follow streamlines is characterized by the Stokes number, a dimensionless parameter that describes the behavior of a particle in a flow. It is defined as:

$$\mathrm{St} = \frac{\rho_p \cdot d_p^2 \cdot g}{18 \cdot \mu \cdot v} \tag{2.11}$$

where St (-) is the Stokes number, ρ_p (kg/m^3) is the particle density, d_p (m) is the particle diameter, g (m/s^2) is the acceleration due to gravity, μ is the dynamic viscosity of the fluid (Pa $\cdot$ s), and v is the flow velocity (m/s). When the Stokes number is significantly less than one, particles can easily follow the airstream, resulting in lower capture efficiency. Conversely, particles with a Stokes number greater than one tend to deviate from the airstream, leading to effective impaction on the collection surfaces.

Some measurement instruments require the flow to be sampled. These instruments typically have an inlet where the flow is drawn in with a pump and then measured. A sampling tube

can also be added to the inlet of these instrument to add range to the instrument and reach in deeper areas [135, 136]. For instruments requiring sampling for measurement, the inlet flow rate must be controlled to ensure that the sample is representative of the flow. One of the ways to do this is through isokinetic sampling, where the flow rate of the sample being drawn in form the instrument is adjusted to match the flow rate of the source [137] (Figure 2.13). Isokinetic conditions are achieved when the velocity of the air entering the sampling probe matches the velocity of the surrounding flow, while sub-isokinetic and super-isokinetic conditions occur when the probe velocity is lower or higher, respectively. Under sub-isokinetic conditions, large particles, tend to bypass the probe due to their inertia, leading to under-sampling, whereas super-isokinetic conditions cause over-sampling as the probe pulls in more large particles than are representative of the flow. Smaller particles are less affected by non-isokinetic sampling because their low inertia allows them to follow the air streamlines into the probe more uniformly [137]. Isokinetic sampling has the advantage of providing a representative sample of the flow, but it can be difficult to achieve in practice due to the complexity of the flow and the need for a precise flow rate control.

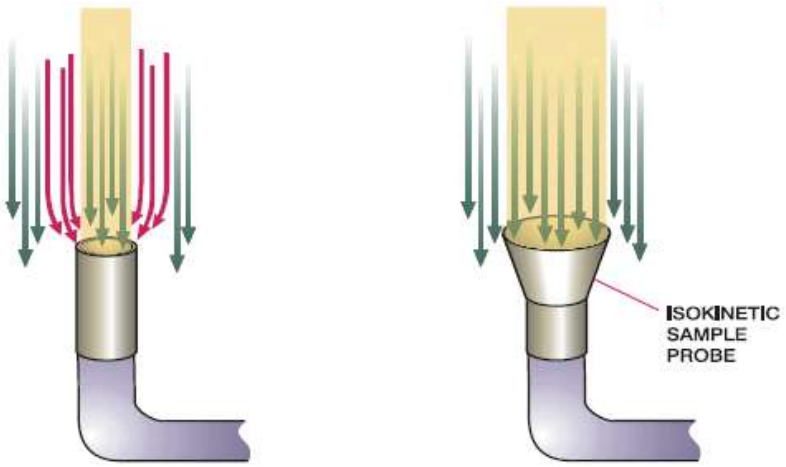

Figure 2.13 Schematic representation of isokinetic sampling.

2.4 Size distribution measurement instruments

Suspended particles can be characterized through different types of measurement depending on the instrument used. The most prominent are the aerodynamic diameter, the electrical mobility diameter, laser diffraction measurements and optical size measurements. The aerosol size covered by currently available measurement technologies ranges from 0.002 μm to several

millimeters between all types of instruments [138].

2.4.1 Impactors

Cascade impactors are perhaps the most widely used instruments for measuring fine particle size distribution. These devices work by utilizing a series of stages, each equipped with a collection surface, where particles are separated based on their aerodynamic behavior. As the sample aerosol flows through the impactor, larger particles, which cannot follow the streamline due to their inertia, impact the collection surfaces and are captured (Figure 2.14). The size associated to each stage is a D50 value, meaning that particles with a given threshold size are collected with 50% efficiency. Number size distribution can then be derived from the mass of particles collected on each stage, assuming sphericity and constant density [139]. The measured size range can be quite wide, from approximately 0.10 μm to 10 μm and the number of stages generally spans from 3 to 13, which yield a low resolution for this instrument. However, microbial detection and characterization can be conducted on the different stages and as such, the cascade impactor is the only approach that can provide size-resolved microbiological data [140, 141].

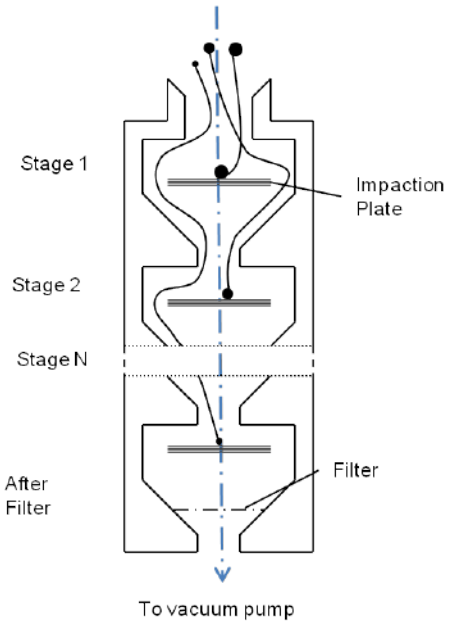

Figure 2.14 Measurement principle of the cascade impactor, reprinted with written permission from CCA [139].

2.4.2 Aerosol spectrometers

Optical aerosol spectrometers (OAS) are sampling instruments that measure the light scattered from single particles with a diode laser to obtain their size distribution (Figure 2.15

a). Laser diffraction measures the angular variation and intensity of light scattered as a laser beam passes around a suspended particle (Figure 2.15 b). Although OAS are typically employed for measurements of particle matter, they can theoretically be used to measure any flow of particles including water-based aerosol droplets.

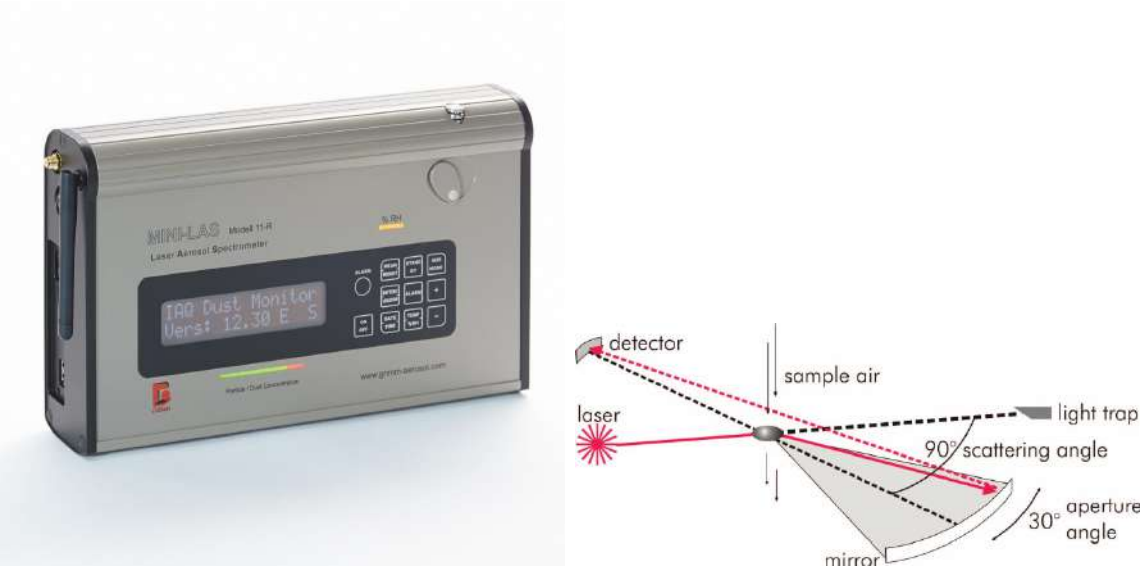

(a) (b)

Figure 2.15 a) Optical Aerosol Spectrometer (MiniLAS model 11-R, GRIMM Aerosol Technik Ainring GmbH & Co, Ainring, Germany). b) Measurement principle of the optical aerosol spectrometer, reprinted with written permission from Taylor & Francis [142].

2.4.3 Scanning Mobility Particle Sizers

The Scanning Mobility Particle Sizer (SMPS) is a commonly used instrument for measuring the size distribution and concentration of submicron particles, whether solid or liquid, in the range of 1 nm to 1000 nm. Upon entering the system, particles are electrically neutralized using either a radioactive source or soft x-rays. These neutralized particles then pass through a Differential Mobility Analyzer (DMA), which classifies them based on their electrical mobility. Electrical mobility refers to the ability of a particle to move in an electric field, with smaller particles having higher mobility due to their lower resistance to movement. Particles are thus subjected to an electrostatic force allowing a segregation according to their size [143]. As a result, smaller particles with higher mobility exit the DMA first, followed by larger particles with lower mobility. These particles then proceed to a Condensation Particle Counter (CPC), where the concentration of particles of a given size is measured [144]. A schematic representation of the SMPS mode of operation is illustrated in Figure 2.16.

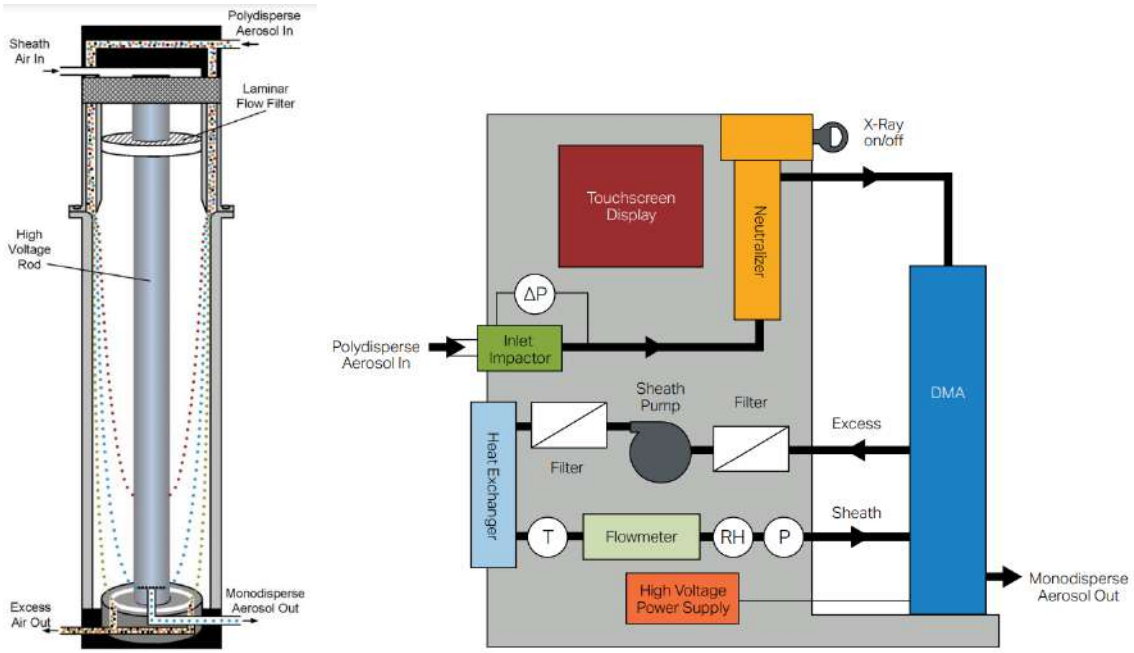

(a) (b)

Figure 2.16 a) DMA flow schematics. b) SMPS schematics. Reprinted with written permission from Taylor & Francis [144].

2.4.4 Phase Doppler Anemometry

Phase doppler anemometry is based on light-scattering interferometry where the measurement volume is defined by the intersection of two pairs of laser beams, each forming interference fringes. The measurements are performed on single particles as they move through this volume. Particles scatter light from both interference patterns. Receiving optics placed at a specific location projects a portion of the scattered light onto multiple detectors. Using three detectors provides both a large measurable size range and a high measurement resolution. Each detector converts the optical signal into a doppler burst containing information on the particle size and velocity [145]. The particle velocity is obtained from the doppler shift of the interference fringes, its size can be acquired from the phase shift. Phase doppler anemometry offers great potential for aerosol size distribution measurement. First, it exhibits a large dynamic range, detecting particles from 0,5 μm to 8000 μm, while simultaneously measuring velocity. Then, it is very precise and no experiment-specific calibration procedure is necessary. Moreover, it is very robust against optical distortions and movement of the measurement point allows the mapping of entire flow fields with an excellent spatial resolution (sub-mm). An overview of its working mechanism is illustrated in Figure 2.17.

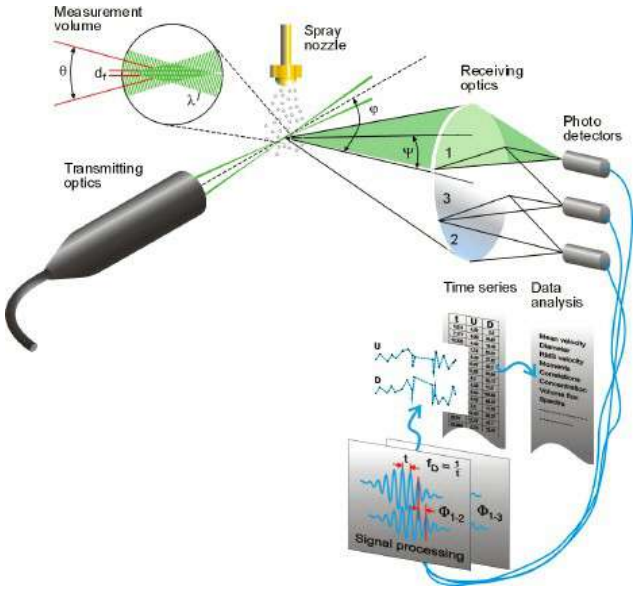

Figure 2.17 Measurement principle of phase doppler anemometry [145].

2.4.5 Instrument Comparison

An extensive amount of laboratory and field studies comparing different aerosol characterization techniques are available in the literature, but critical aspects inherent to water-based contaminated aerosol droplets remain poorly documented. The SMPS being the gold standard for sub-micron particle size distribution measurements, it is often used as a comparison basis for other instruments [146]. Sousan et al. [134] compared the SMPS with an OAS for particle matter and found that the OAS overestimated the concentration of particles smaller than 0.5 μm, but the instruments provided similar concentrations for larger particles. Mass concentrations were more similar but cannot be applied to water-based aerosol droplets because of evaporation [147]. Moore et. al compared different spectrometers against a reference SMPS and suggested that disparities between optical instruments could be due to the different optical properties of particles [148]. Since the size of water-based droplets can change rapidly, optical properties could also vary across the size range of interest, especially with the presence of non-volatile matter in the droplets. Also, the PDA system was found to accurately measure particles changing size when it was compared to image analysis for spray particles, despite a tendency to underestimate the size of particles [149], thus revealing good potential for aerosol evaporation experiments. Dodge [150] compared multiple instruments for sprayed droplets, including a PDA system. His general conclusion is that only instruments using the same measuring principles yield matching results and differences in average size distribution for instruments using different working mechanisms can be as high as a factor of 5. Finally, Vo et. al [151] compared different portable optical size spectrometers, reveal-

ing that portable instruments are as precise as their larger counterparts while providing the advantage of being sturdier and easier to transport.

2.5 Evaporation of contaminated airborne water-based droplets

Investigations on aerosol evaporation from as early as 1934 have demonstrated that water-based droplets quickly decrease in size in ambient air as they lose their water content through evaporation. This process leaves behind a small nucleus that contains some water and the solid parts of the initial particle content, including potentially viable pathogens [152]. The ability of the airborne pathogens to remain infectious under the conditions of the dried-up nuclei determines if it can be transmitted over a long distance via the aerosol route. As the fate of an aerosol droplet is thus dependent mostly on its size, evaporation plays a critical role in airborne transmission [3]. In this section, an exhaustive review of the fluid dynamics related to droplet evaporation in the context of airborne transmission is presented.

2.5.1 Evaporation mechanism of an aerosol

The configuration typically associated with aerosol droplets dispersed within moist air is that of a spherical droplet having no velocity relative to its surrounding gas (Figure 2.18) [153]. Indeed, aerosol droplets below 100 μm in diameter generally follow the streamlines of the airflow due to their low inertia [23].

The evaporation of aerosol droplets in humid air is fundamentally governed by the diffusion of water vapor through the surrounding air. This process is driven by the gradient in water vapor concentration between the surface of the droplet and the atmosphere [153]. According to Fick's law of diffusion, the mass flux of water vapor, J (kg/(m$^2 \cdot$ s)), from the surface of a droplet is proportional to the concentration gradient of water vapor, which can be expressed as [154]:

$$J = -D\frac{\partial C}{\partial r_d} = -D\frac{C_s - C_\infty}{r_{\text{final}} - r_{\text{initial}}}$$

where D (m^2/s) is the diffusion coefficient of water vapor in air, A (m^2) is the surface area of the droplet, C (kg/m^3) is the concentration of water vapor. C_s is the molar concentration of the vapor at liquid–vapor equilibrium near the droplet surface, and C_∞ is the molar concentration of the vapor at a large distance from the droplet. r_d is the radial distance from the droplet surface.

As water evaporates from the droplet, a higher concentration of water vapor at the surface

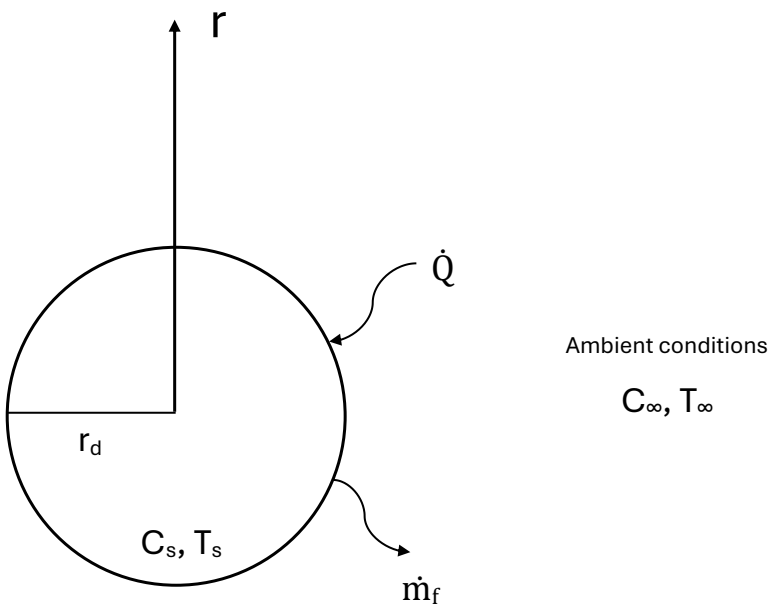

Figure 2.18 Airborne droplet evaporation process. $\dot{m}_f$ is the mass flow rate of water vapor, $\dot{Q}$ is the heat transfer rate, T_s is the surface temperature of the droplet, T_∞ is the temperature of the surrounding gas, C_s is the molar concentration of the vapor at liquid–vapor equilibrium near the droplet surface, C_∞ is the molar concentration of the vapor at a large distance from the droplet, D is the molecular diffusion coefficient of the vapor in the gas phase, r_d is the current radius of the droplet, A is the surface area of the droplet.

of the droplet compared to the surrounding air creates a concentration gradient that drives the diffusion of vapor away from the droplet. This concentration difference sustains the evaporation process, provided that the vapor pressure at the droplet surface exceeds that of the surrounding air. As evaporation progresses, the droplet will shrink and the process will continue as long as the local vapor concentration remains below the equilibrium vapor pressure at the surface ($C_s > C_\infty$) [24, 153, 154].

The mass flow rate of water vapor, $\dot{m}_f$ (kg/s), released from the droplet through evaporation can be calculated by multiplying the mass flux by the surface area of the droplet. Maxwell described the stationary evaporation of a droplet by assuming that the rate of evaporation is entirely determined by the rate of vapor diffusion in the surrounding gas, and that the vapor concentration near the droplet surface is equal to the vapor concentration at liquid–vapor equilibrium. As a result, Maxwell obtained the following equation for the rate of droplet evaporation [154, 155]:

$$\dot{m}_f = 4\pi r_d D(C_s - C_\infty), \tag{2.12}$$

The evaporation of water droplets is also significantly influenced by heat transfer, which is primarily driven by the temperature difference between the droplet and the surrounding gas [24, 153]. This thermal gradient creates a convective heat flux towards the droplet, facilitating the phase change from liquid to vapor. For simplicity, we neglect the contributions of conduction and radiation in our analysis, focusing on convective heat transfer, as these contributions are typically small compared to convective heat transfer in the context of airborne transmission [3]. According to the principle of energy conservation, the rate of heat transfer $\dot{Q}$ (W) from the droplet surface to the surrounding gas can be expressed as [24]:

$$\dot{Q} = h \cdot A \cdot (T_s - T_\infty)$$

where h (W/m^{2}K) is the convective heat transfer coefficient, A (m^2) is the surface area of the droplet, T_s (K) is the surface temperature of the droplet, and T_∞ (K) is the temperature of the surrounding gas.

Evaporation is a coupled process of diffusion and heat transfer [24, 153, 154]. Thus, the flow in this configuration is solved using the mass and energy conservation equations at the interface of the liquid and gas phases. Multiple models have been developed to describe the evaporation of droplets considering both mass and energy conservation equations. We will focus on two of the most prominent in the context of airborne transmission.

2.5.2 Models of droplet evaporation

The Balachandar et. al model was developed for the evaporation of droplets in the context of anthropogenic airborne transmission [20]. Assuming that the droplet is spherical, the rate at which a small sphere loses mass through evaporation is influenced by the diffusion of the vapor layer away from the surface of the droplet. The rate of evaporation is given by the following equation [156, 157]:

$$-\frac{dm}{dt} = \pi d D \rho_p Nu \ln(1 + B_m) \tag{2.13}$$

Here, m (kg) is the mass of a droplet with diameter d (m), D (m^2/s) is the diffusion coefficient of the vapor in the surrounding air, and ρ_p (kg/m^3) is the density of the surrounding air. The

dimensionless Spalding mass number B_m (-) is given by $B_m = \frac{Y_d - Y_p}{1 - Y_s}$, where Y_d (-) is the mass fraction of water vapor at the droplet surface, and Y_p (-) is the mass fraction of water vapor in the surrounding air. Nu (-) is the dimensionless Nusselt number, calculated according to the Froessling equation from the Reynolds number, Re, and the Prandtl number, Pr, knowing the velocity and viscosity of the surrounding air v (m/s) and μ ($\mathrm{N \cdot s/m^2}$) respectively, according to the following equations:

$$Nu = 2 + 0.4 Re^{1/2} Pr^{1/3} \tag{2.14}$$

$$Re = \frac{d \rho_p v}{\mu} \tag{2.15}$$

$$Pr = \frac{\mu}{\rho_p D} \tag{2.16}$$

Assuming that Nu and B_m remain nearly constant for small droplets, equation 2 can be integrated to derive the following relationship for the evolution of the droplet, defined as the squared law of evaporation [158]:

$$d(t) = \sqrt{d_e^2 - k' t} \tag{2.17}$$

Where

$$k' = 4 D Nu \ln(1 + B_m) \tag{2.18}$$

In these equations, d_e (m) is the initial diameter of the droplet, and k' represents an effective evaporative diffusivity with units of $\mathrm{m^2/s}$.

The Pruppacher-Klett model is more complex, considering the effect of Stefan flow and the temperature dependence of diffusion coefficients [159, 160]. The evaporation rate $\frac{dm}{dt}$(kg/s) is given by:

$$-\frac{dm}{dt} = \frac{2\pi d M_w D C_T p \mathrm{Sh}}{R T_\infty} \ln\left(\frac{p_s - p}{p_{sat} - p}\right)$$

Where

$$C_T = \frac{T_\infty - T_p}{T_\infty - 1.6} \left(\frac{2 - k}{T_\infty^{2-k} - T_p^{2-k}}\right) \tag{2.19}$$

In the previous equations, M_w (kg/mol) is the molecular weight of water and p (kg/m $\cdot$ s^2) is the atmospheric pressure of air. C_T (-) is a correction factor accounting for the temperature dependence of the diffusion coefficient, with k (-) being a constant between 1.6 and 2. The partial pressure of vapor on the droplet surface is given by p_s and p_{sat} (kg/m $\cdot$ s^2) is the saturation vapor pressure. T_∞ (K) is the temperature far from the droplets, Sh is the dimensionless Sherwood number, calculated according to the Froessling equation from the Reynolds number, Re, and the Schmidt number, Sc, which are given by the following equations:

$$Sh = 2 + 0.6\mathrm{Re}^{1/2}\mathrm{Sc}^{1/3} \tag{2.20}$$

$$Sc = \frac{\mu}{\rho_p D} \tag{2.21}$$

p_s can be calculated from the following equation:

$$\ln \frac{p_s}{p_{sat}} = \frac{4M_w \sigma_{LV} q_w}{RT_1 \rho_w d_e} \tag{2.22}$$

Where σ_{LV} (kg/s^2) is the surface tension of the droplet, q_w (-) is the mass fraction of water in the droplet and R (J/(mol $\cdot$ K)) is the universal gas constant.

Another important aspect of evaporation in the context of airborne transmission is the nuclei size of the aerosol droplet. The nuclei size is reached when the vapor pressure at the surface of the droplet is in equilibrium with the vapor pressure of the atmosphere, meaning the rates of evaporation and condensation are equal [161]. This final size of the droplet nuclei d_{dr} (m) is given by the following equation and is equivalent for both models. It is a function of ψ (-), the volume fraction of non-volatile solids suspended initially in the droplet [20, 159]:

$$d_{dr} = d_e \psi^{1/3} \tag{2.23}$$

Regardless of the model employed, the timescales for aerosol droplet evaporation are on the order of a few seconds for initial droplet sizes of several hundred microns, considering both mass and energy balances at the droplet surface [3]. Evaporation can be categorized into three distinct regimes based on droplet size: the diffusion regime for larger droplets, the diffusion-kinetic regime for intermediate sizes, and the kinetic regime for smaller droplets [162]. In

the case of aerosol droplets in the range of 100 μm generated within cooling towers, evaporation typically begins with diffusion and transitions to kinetic-driven processes as droplet size decreases [163]. This trend indicates that evaporation rates increase as droplet size decreases, following the well-known d^2 law [24, 153, 154]. According to this law, the square of the droplet diameter decreases linearly with time during the evaporation process, particularly in the diffusion regime. This relationship provides a simplified method for predicting evaporation times for droplets of varying sizes. However, the evaporation process is inherently complex and remains partially understood, especially regarding airborne transmission involving aerosol droplets with non-volatile matter and organic suspended solids [3].

2.5.3 Effect of non-volatile matter

The presence of a significant concentration of non-volatile matter in the bulk solution during the aerosolization process implies that a fraction of that non-volatile matter can be trapped inside the droplets upon their generation, and influence the subsequent evaporation process. The size distribution of the aerosol droplets is not uniform, inducing variability in the quantity of non-volatile matter aerosolized. As moisture evaporates, the solute concentration per unit of bulk liquid increases inside the droplet [164]. The non-volatile matter trapped inside droplets can slow the evaporation process down [165] and as the solute concentration increases with diminishing droplet diameter, the evaporation process is slowed down exponentially, leading asymptotically to the final droplet nuclei size. These solids also move inside the droplet during the evaporation process [166], but this motion does not appear to significantly affect the evaporation rate [167]. Nevertheless, the extent of the influence of non-volatile matter on evaporation dynamics is still not well-documented [20, 168].

The bulk media properties such as viscosity, a measure of the cohesive forces of the molecules forming the liquid, and surface tension, a measure of the tension per unit length at the free surface of the liquid, also play a significant role in the evaporation process. As viscosity increases, the evaporation rate decreases because of a reduction in the mass transfer rate between the core and the outer layer within the droplet [169]. Therefore, for equivalent conditions, water evaporates much quicker than oil because the molecular interactions are much stronger in oil than in water. Viscosity is different for water from different sources, which may extend the airborne droplet lifetime depending on the bulk media properties [170]. Cooling tower water, especially after a stagnation period, contains a large volume of dissolved solid particles compared to the normal drinking water used for the makeup of evaporated water, and is therefore significantly more viscous.

The addition of biodispersive agents (surfactants) in cooling towers reduces the surface ten-

sion. A lower surface tension is typically associated with a longer evaporation rate [171]. This occurs due to the dual interfacial properties of surfactants. Most surfactants have a hydrophilic head and a hydrophobic tail [172]. Consequently, once the droplet is generated, a surfactant lipid layer gradually forms on its surface, reducing surface tension [171] and impeding the diffusion of water molecules from the surface into the surrounding air, thereby decreasing the evaporation rate [156]. Essentially, the aerosol droplets generated from different bulk media will have different evaporation rates. Consequently, there is a strong research need to quantify the effect of surface tension and viscosity on the evaporation dynamics of airborne aerosol droplets.

In cooling towers, water properties such as viscosity and surface tension differ markedly from other water systems, potentially influencing evaporation. Viscosity can increase with the presence of biofilm, reaching up to 1.25 $\mathrm{mPa \cdot s}$ compared to 1 $\mathrm{mPa \cdot s}$ for tap water [173–175]. The intermolecular forces between the molecules of the bulk solution are stronger at higher viscosity, and the evaporation rate can decrease as a result [24]. While the surface tension of tap water is approximately 73 mN/m, that of cooling tower water can drop to as low as 62 mN/m due to the addition of biodispersive agents employed to control biofilm growth [176, 177]. A lower surface tension is typically associated with a longer evaporation rate [171]. Non-volatile components, including biofilm, bacteria, viruses, disinfectants, salt, and organic matter, can also influence the evaporation dynamics from a thermodynamic point of view [24, 173]. Indeed, unless the relative humidity is very low, some water will remain in the droplet nucleus. This remaining water leads to an equilibrium diameter that increases with higher initial non-volatile solid concentrations [178]. However, the extent of the influence of surface tension, viscosity and non-volatile solids on evaporation dynamics remains not well-documented [20, 168].

2.5.4 Influence of environmental parameters

Multiple environmental parameters of the media surrounding the aerosol droplets affect evaporation [24, 153, 154]. These factors are especially important in the context of airborne transmission as they often cannot be controlled and can be rapidly changing. Temperature and relative humidity are the most dominant parameters influencing evaporation. Their effect on the evaporation of droplets is well documented.

As temperature increases, the kinetic energy of the molecules of the liquid droplet increases, allowing more molecules to escape the liquid phase and enter the gaseous phase. Higher temperatures also reduce the surface tension of the droplet, facilitating the release of water molecules into the air. Additionally, evaporation rates are faster in warmer environments

because the increased energy overcomes the molecular bonds holding the liquid together [153, 162, 179].

Relative humidity is the ratio of the partial pressure of water vapor in the air to the saturation vapor pressure of water at a given temperature [179]. Mechanistically, relative humidity affects the vapor pressure gradient between the droplet surface and the ambient air [24, 154]. At lower relative humidity levels, this gradient is steep, allowing for efficient water vapor diffusion away from the droplet. As relative humidity increases, the vapor pressure of the surrounding air approaches the vapor pressure at the surface of the droplet, diminishing the driving force for evaporation. It is therefore directly related to the capacity of the air to absorb additional water vapor. As relative humidity increases, the potential of the surrounding air to additional water vapor becomes limited, effectively slowing the evaporation process. At 100% relative humidity, evaporation halts because the air is saturated, and no additional moisture can be absorbed [161].

2.5.5 Droplet Evaporation Experiments

Comprehending the evaporation dynamics of pathogen-laden airborne particles is essential for accurately assessing contamination risks, yet this understanding remains incomplete. As previously discussed, particle size distribution plays a critical role in the contamination potential of specific pathogens. Therefore, gaining a deeper insight into the evaporation mechanisms of bacteria-laden droplets is crucial for predicting pathogen concentration, viability, and potential for contamination under various conditions [17]. Accurate data on aerosol droplet evaporation rates are also essential, as particles that are either too large to be inhaled or too small to carry pathogens do not contribute to contamination [180].

Most studies used direct measurement such as optical methods for droplet evaporation assessment. Researchers have observed particles with microscopic optical techniques [181] and different evaporation regimes have been evaluated with high-speed cameras [182]. However, monitoring aerosol evaporation with optical methods remains challenging because the size scale involved is very small and evolves rapidly. A refined technique for evaporation monitoring of free-falling aerosol droplets of 25-50 μm was proposed by Hardy et al. Droplets were injected in a column and illuminated during their free fall with a vertical laser strobed at the same frequency of the droplet generation, allowing the monitoring of the droplet evaporation with a high speed camera [183]. Some research groups have used acoustic levitation to study the behavior of a single droplet. However, it was shown that acoustically levitating droplets evaporate faster than free-falling droplets [170, 184]. Acoustically levitated droplets can oscillate and vibrate in the acoustic field, which can increase the surface area available

for evaporation. This dynamic movement allows for more efficient mass transfer of water vapor from the droplet to the surrounding air. Overall, there is a research need to define a robust method to characterize the evaporation of airborne contaminated aerosol droplets.

2.5.6 Aerosol generation

Multiple types of devices can accurately generate aerosol droplets using various aerosolization techniques. Most aerosol generators utilize spray atomization or ultrasonic nebulization principles, producing an aerosol with a consistent size distribution [185–187]. However, these aerosol generation mechanisms do not reliably produce monodispersed droplets. They also induce large strains on the bulk solution [188], making them unsuitable for airborne transmission contexts, as they could compromise the viability of pathogens contained in the aerosol droplets.

Monodispersed droplets can be generated through thermal jetting or piezoelectric droplet generation. In thermal jetting, heat forces ink from the print head to the substrate by powering microscopic resistors behind the nozzle. This intense heat vaporizes a small amount of ink, creating a rapidly expanding bubble that ejects a droplet from the orifice [185, 189]. In piezoelectric droplet generation, microscopic piezoelectric elements such as crystals or ceramics are positioned behind the nozzles. When an electrical charge is applied, these elements bend backward, forcing precise amounts of liquid through the nozzle. This method allows for excellent control over the ejection rate and results in perfectly spherical droplets of varying sizes. Because piezoelectric generation does not heat the bulk fluid, it is particularly well-suited for airborne transmission applications.

These monodispersed generation techniques are integral to inkjet printing, which is recognized as one of the most effective methods for accurate and reliable droplet generation. The underlying principle involves creating a pulse within the fluid; with each pulse, fluid is pushed outside the channel, and due to the surface tension of the bulk media, a droplet forms at the nozzle [190]. Inkjet technology offers a low-cost, reliable, and convenient method for generating droplets, making it increasingly relevant in a wide range of industrial applications. Although it has been around since the 1950s in specialty printing, its impact across various fields is becoming increasingly apparent, leading to a growing number of studies exploring inkjet printing as a droplet generation mechanism [191].

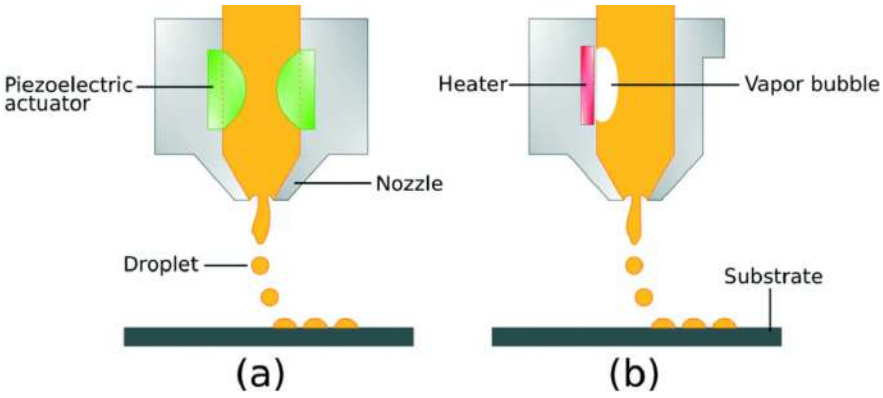

Figure 2.19 Schematic representation of thermal a) and piezoelectric b) inkjet printing. Reprinted with written permission from CCA [192].

CHAPTER 3 RESEARCH OBJECTIVES

3.1 Critical analysis of the literature

The risks posed by *Legionella* airborne transmission from cooling towers are substantial, with reported cases steadily increasing over the past 30 years. These risks are likely to be further exacerbated by the effects of climate change, which may create conditions more favorable for *Legionella* proliferation and transmission. The literature review identified several key research gaps that must be addressed to improve our understanding of the physical processes involved in the transmission of *Legionella* from cooling towers and to develop effective mitigation strategies. These gaps are summarized below.

3.1.1 Water-based aerosol droplet size distribution

The literature review highlights the importance of accurately characterizing the size distribution of water-based aerosol droplets and to characterize the viability and concentration of the pathogens they carry, in order to assess the associated contamination risks. However, no known instrument can achieve a high-resolution measurement of the size distribution while also allowing for microbial assessment of an aerosol flow. Therefore, data acquired from multiple instruments must be combined to fully characterize aerosol droplets. Few studies have investigated the correlation between different aerosol measurement instruments with different working mechanisms. This comparison is therefore necessary to link the results from different measurement instruments throughout the literature and improve our understanding of the mechanisms governing airborne transmission.

Furthermore, instruments used in the context of aerosol airborne transmission are typically designed for other purposes such as air pollution monitoring. Although they show promising results for water droplet characterization, their usage must be done with careful consideration when dealing with water-based particles subject to evaporation. These techniques often require thorough calibration processes and thoughtful assumptions about the optical and physical properties of the measured particles, which is even more challenging for droplets that evaporate over time and that contain biological material. There is also no consensus on the standard protocol to compare aerosol size distribution from different instruments, which can lead to different results for the same measurement, depending on the measurement technique employed. Hence, comparing size distribution measurement instruments is an essential foundation for accurate measurements of contaminated aerosol droplets and enables the combination of measurements from multiple instruments to assess the contamination

risks.

3.1.2 Cooling towers and drift eliminators

A broad overview of the challenges associated with *Legionella* contamination from the aerosol generated inside cooling towers was presented. Due to the complex fluid dynamics involved in aerosol generation and environmental transport, infections are often underdiagnosed, and accurately assessing the contamination risk is challenging. Indeed, there is a significant gap in the literature regarding the direct link between bacterial concentrations in cooling towers and the corresponding concentrations discharged into the environment. While some general relationships between ambient conditions and infection rates are known, the physical processes driving the generation of contaminated aerosol droplets are largely unexplored. Additionally, although several studies have investigated the efficiency of drift eliminators, many are outdated, rely on numerical models that do not accurately predict the behavior of operating cooling towers, or are based on wind tunnel experiments that fail to capture real-world conditions. These studies often focus more on the aerodynamics related to the energy efficiency of drift eliminators rather than their effectiveness in capturing bacteria-laden particles, and typically do not account for multiphase flows. To ultimately improve the understanding of aerosol generation processes inside cooling towers and its transport into the environment, it is primordial to conduct an *in situ* experimental sampling campaign. To the best of the author's knowledge, no comprehensive study has characterized aerosol generation and transport across a wide range of cooling towers.

3.1.3 Risk assessment

Numerous studies have assessed the risks associated with *Legionella pneumophila* and cooling tower systems. Some of these studies have employed risk assessment models such as Quantitative Microbial Risk Assessment (QMRA), a systematic approach based on statistical models that estimates the likelihood and severity of adverse health effects resulting from exposure. However, the QMRA model developed by Hamilton et al. for airborne transmission from cooling towers has notable limitations, particularly concerning aerosol generation, particle size distribution, and drift eliminator capture efficiency. Moreover, current regulatory action levels for *Legionella* in cooling towers are based not on quantitative risk assessments but rather on water bacteeria concentrations. Therefore, there is a need for an optimized and simplified risk assessment strategy to enhance regulatory frameworks and better mitigate the risks associated with *Legionella*.

It is well known that most cases of *Legionella* infection are sporadic. As a result, there is no established methodology to reliably link these sporadic cases to specific cooling towers,

particularly given the limited understanding of aerosol generation and transport. The presence of various types of cooling towers on large buildings further complicates the comparison of aerosol generation and transport across different systems. This lack of a robust foundation for investigations hampers the development of effective mitigation strategies. Moreover, as previously discussed, there are currently no regulations governing the release of airborne microbial loads into the environment. While general guidelines exist to advise cooling tower managers on water quality, there is no enforcement or oversight by authorities regarding what is actually emitted into the air. Consequently, there is a pressing need to deepen our understanding of the transmission process from cooling towers and to connect this knowledge to water quality. This will enable the amendment of regulations and the implementation of strategies to reduce the infection risks associated with *Legionella*.

3.1.4 Aerosol generation for droplet evaporation

Much of the existing literature on droplet evaporation addresses the simplified scenario of a single droplet in quiescent air, which fails to capture the complex fluid dynamics governing the evaporation of small-scale particles containing trapped solids. In reality, aerosol droplets generated and released by cooling towers exist within a turbulent aerosol plume, a condition that significantly alters the evaporation dynamics, but that is not well characterized. In such environments, the evaporation of aerosol droplets is likely influenced not only by the proximity of neighboring droplets but also by the thermo-physical properties of the plume itself. This reveals a critical gap in our understanding of the evaporation processes of airborne droplets within a plume. As highlighted in the literature review, inkjet printing technology has shown considerable promise for the simultaneous generation of closely spaced aerosol droplets of uniform size, offering a potential avenue for studying these complex evaporation dynamics.

3.1.5 Evaporation of contaminated aerosol droplets

The evaporation of water droplets containing *Legionella* is a critical factor in the airborne transmission from cooling towers. However, existing risk assessment models often neglect this process, leading to an underestimation of the associated risks. The evaporation dynamics of aerosol droplets can be influenced by various water properties, including the presence of non-volatile matter, viscosity, and surface tension. Despite this, the extent to which these factors affect evaporation remains inadequately documented. Furthermore, much of the existing research focuses on large droplets deposited on surfaces, which do not accurately represent the behavior of an aerosol. The fate of a water-based particle within a multiphase flow is intrinsically linked to its size and thus, its evaporation dynamics. Such information is

essential for assessing the contamination risks and there is a pressing need for experiments that precisely tracks the evaporation of airborne contaminated droplets. In essence, the complex fluid dynamics involved in the evaporation of small-scale particles that have trapped and transported solids remains largely an open subject, as few studies have targeted these phenomena.

Balachandar et al. developed a simplified framework for predicting aerosol generation, dispersion, and droplet evaporation in the context of anthropogenic airborne transmission. Despite their contributions, the authors identified a significant limitation in accurately determining the evaporation rate of droplets containing non-volatile substances. Their model assumes a uniform impact of non-volatile components on evaporation, which oversimplifies the issue. In contrast, Pruppacher and Klett presented a comprehensive evaporation model for water-based droplets related to the fields of cloud microphysics and aerosol science. This model accounts for the effects of non-volatile matter, viscosity, and surface tension on evaporation, as well as its impact on droplet nuclei size. However, it requires experimental validation for applications related to airborne transmission.

3.1.6 Cooling tower water filtration

Effective management of cooling tower systems requires thorough control of bacterial growth. While traditional chemical water treatment methods remain the most common strategy, they are costly, damaging to the system and yield limited results when used in isolation. Cross-flow microsand filtration systems present a promising alternative, with the added advantage of potentially enhancing evaporative cooling efficiency and saving energy. However, as the extent of the effect of the technology on the performance of cooling towers remains speculative, widespread adoption of this technology has been limited. As such, there is a need to quantify the effect of water filtration on the energetic performance of cooling towers to provide a basis for the adoption of this solution. Additionally, understanding the technology's efficiency in controlling the growth of *Legionella* and integrating this with its impact on cooling tower performance will contribute to the accurate assessment of the contamination risks and to the development of more comprehensive and safer management practices.

3.2 Research Objectives

Based on the aforementioned research needs, the following objectives are defined :

Objective 1 : Compare size distribution measurement instruments for water-based aerosol droplets, assessed in conditions where evaporation is ongoing.

Objective 2 : Characterize the aerosol generated by operating cooling towers fitted with different types of drift eliminators.

Objective 3 : Improve the risk assessment modelling of *Legionella* airborne transmission from cooling towers.

Objective 4 : Develop an experimental setup for the study of the evaporation of the droplets from an aerosol plume.

Objective 5 : Characterize the evaporation dynamics of contaminated droplets in the context of *Legionella* airborne transmission from cooling towers.

Objective 6 : Quantify the effect of water filtration on the cooling tower energetic performance.

3.3 Research Outcomes

The results of this research are discussed in the next five chapters of which four are presented as journal articles. The research outcomes are as follows :

ARTICLE 1 : Comparison of Aerosol Spectrometers: Accounting for Evaporation and Sampling Losses This article compares the performance of four different aerosol size distribution measurement instruments with a focus on water-based aerosols. It is the result of objective 2 and has been published in *Measurement Science and Technology* [193].

ARTICLE 2 : Identification and Mitigation of Operational Factors Increasing *Legionella* Risks in Cooling Towers A large-scale sampling campaign was conducted on 15 operating cooling towers fitted with different types of drift eliminators to characterize the aerosol generated. The data collected was used to improve the risk assessment model for *Legionella* airborne transmission from cooling towers. This article is the result of objectives 3 and 4 and has been submitted to *Water Research*.

ARTICLE 3 : Evaporation of aerosol droplets from contaminated cooling tower water This article characterizes the evaporation dynamics of airborne aerosol droplets, considering viscosity, surface tension and the presence of non-volatile matter, in the context of *Legionella* airborne transmission from cooling towers. It is the result of objective 5 and has been submitted to *Physics of Fluids*.

ARTICLE 4 : Evaporation of an Aerosol Plume from an Inkjet Printhead This extended abstract presents an experimental setup for the generation of aerosol droplets by inkjet printing technology to study of the effect of the proximity of droplets inside an aerosol plume. This work is the result of objective 6 and has been submitted to *Experiments in Fluids*.

ARTICLE 5 : Data-Driven Cooling Tower Optimization: A Comprehensive Analysis of Energy Savings Using Microsand Filtration This work quantifies the effect of a cross-flow microsand filtration system on the energetic performance of an operating cooling tower using a data-driven approach. A machine learning model also predicts the energy savings potential of the filtration system. This article is the result of objective 1 and was accepted for publication to *Applied Thermal Engineering* [194].

CHAPTER 4 ARTICLE 1: COMPARISON OF AEROSOL SPECTROMETERS : ACCOUNTING FOR EVAPORATION AND SAMPLING LOSSES

Published online in *Measurement Science and Technology* on January 12 2024 [193]

By

Xavier Lefebvre, Antonella Succar, Emilie Bedard, Michèle Prévost and Etienne Robert

4.1 Abstract

Measuring aerosol size distribution with precision is critical to understand the transmission of pathogens causing respiratory illnesses and to identify risk mitigation strategies. It is however a challenging task as the size of pathogen-carrying particles evolves over time due to evaporation. Although measurement techniques well established in the field of aerosol science are often used to characterize bioaerosols, their performance is seldom assessed with respect to evaporation and deposition in sampling lines. Four instruments providing aerosol size distribution were compared using oil and water-based particles. They each rely on different measurement principles: phase doppler anemometry, light scattering, electrical mobility and aerodynamic impaction. Size distributions of oil-based particles showed consistency across different measurement instruments, but significant discrepancies arose for water-based particles undergoing evaporation. These larger differences result from both evaporation and particle deposition in transit between the sampling point and the measurement inside the instrument. Phase doppler anemometry was best suited for precise size distribution measurement, as it eliminates the need for a sampling line, thereby preventing particle loss or evaporation during transit. With this instrument as a reference, empirical correction factors for evaporation and deposition were derived from dimensionless numbers and experimental data, enabling quantitative assessment of bioaerosol size distribution using different instruments. To obtain the size distribution at the source of the aerosol generation, complete drying of a salt solution was performed. Using the complete drying technique and accounting for losses, sampling instruments can reliably provide this critical information and allow for thorough risk assessment in the context of airborne transmission.

4.2 Introduction

The ability of aerosol particles to carry pathogens has been known for over a century [15] and their role as a means of infection has since been the subject of a sustained research

effort. The COVID-19 pandemic has highlighted the need to improve our understanding of pathogen dissemination to effectively prevent outbreaks [195]. Potentially infectious aerosol particles settle slowly or not at all depending on their size and on the air flow of indoor environments [17]. These droplets, dependent upon environmental conditions, will gradually lose part of their water content and shrink down to a small nucleus containing the solid matter initially comprised in the droplet, including potential pathogens [152]. Since most bioaerosol particles are water-based, they experience a decrease in size through evaporation immediately following their separation from the bulk solution, unless relative humidity is 100%, in which case particles grow [196]. Such sub-micron droplet nuclei can travel further from the source, remaining airborne until actively removed through ventilation systems [197], and can penetrate deep in the airways when inhaled. Measuring aerosol size distribution accurately is critical to predict the deposition site of particles within the respiratory tract, the size and dose of pathogens they contain, to improve the understanding of their dispersion in ambient air, as well as their settling and deposition dynamics, and to assess the performance of aerosol control procedures or tools. Recent investigations have demonstrated that even small differences in particle size can have a major effect on the behavior of pathogen-carrying particles in indoor air, in the airways and in aerosol treatment systems, especially in the sub-micron range [198–200].

Aerosol size distribution can be measured with a wide variety of instruments relying on different operating principles [138, 201]. The instrumentation currently used in experimental studies of bioaerosol particles consists mainly of impactors and filters [202]. These choices are motivated by the need to obtain cultivable samples and the typically low biological content in air, requiring large volumes to be sampled. However, filters and impactors provide only limited information on the size of the particles carrying pathogens in bioaerosol, and mostly do so when implemented in cascade arrangements that are cumbersome to use.

Risk assessment infection models require the estimations of the number of particles, their size distribution and their configuration-specific drying profile [108]. Research groups working with bioaerosol particles have explored the use of precise analytic tools to get this critical information, that can quickly and conveniently provide detailed particle size distributions [203,204] but are unable to capture culturable samples. As different physical phenomena are involved with each instrument, there is a need to provide guidelines for meaningful interpretation of experimental data combining size distribution information and the detection of pathogens.

In this study, a transversal comparison between four instruments using different measurement

techniques is performed. Two optical instruments are used: a Phase Doppler Anemometer (PDA) that detects single particles going through a measurement volume without sampling air [145], and a portable optical aerosol spectrometer (OAS) (GRIMM mini LAS 11-R) [142]. Detailed sub-micron size distributions are also obtained through the electrical mobility of particles using a Scanning Mobility Particle Sizer (SMPS) [144]. Finally, a Cascade Impactor is used to obtain the size distribution through the aerodynamic diameter of particles [139], a method adopted in most bioaerosol studies where the particle size is obtained [205]. As wet aerosol size changes dynamically due to evaporation, measurements are conducted on both drying and non-drying aerosol droplets.

The main objective of this study is to improve our understanding of the deposition in the transit and the drying behavior of water-based droplets in common aerosol spectrometers, using four different experimental approaches. First, a comparison is performed using oil-based and water-based particles suspended in air. Second, the effects of evaporation and deposition on the size distribution are studied using an OAS and a PDA with water-based droplets. Third, correction factors are defined to adjust the size distribution measurements of multiphase flows experiencing evaporation and deposition during transit, according to a reference instrument. Lastly, a technique is implemented based on the dried particle size distribution obtained from a saline solution, enabling the calculation of the initial diameter of the particles. These results allow for the use of cost-effective and portable spectrometers to achieve a more accurate estimation of the size distribution at a specific location. Therefore, the outcomes presented in this study serve as a valuable reference for characterizing droplets containing pathogens in a scientific context.

4.3 Methodology

4.3.1 Aerosol Generation

As droplet size for volatile liquids can change rapidly due to evaporation, measurements were conducted on both drying (water-based) and non-drying (Di-Ethyl-Hexyl-Sebacate (DEHS) oil-based) aerosol droplets. The four aerosol spectrometers considered were first compared using particles produced by a TOPAS GMBH model ATM 221 aerosol generator. This instrument can be operated with water, a saltwater solution or DEHS oil, generating a stable distribution of particles in the sub-micron range. The size distribution generated from this type of instrument fluctuates by a maximum of 2.5% over several hours of use [206]. Aerosol particles generated with DEHS, which has a density of 0.9 g/cm^3, are spherical and serve as a control for the aerosol emission size, as they dry very slowly over the course of a few hours. During operation, the aerosol generator was connected to a mass flow controller (Hastings

HFC 202), enabling regulation of the output flow rate of aerosol in the 0-25 standard liter per minute (SLPM) range.

The instruments were then compared using aerosol particles produced by a spray gun (1.0 mm Mini HPLV Air Spray Gun, Neiko) utilizing tap water. The spray gun, operated with 6 bars of pressurized air, yielded larger particles in comparison to the TOPAS aerosolizer and was more suitable for covering the entire size range of the measurement instruments employed in the study.

The last experiment was conducted with a solution of 10% m/m NaCl (density of 2.16 g/cm^3) dissolved in tap water, aerosolized with the spray gun. For saltwater-based measurements, aerosol particles were completely dried with a desiccator column filled with silica gel beads (Model DDU 570, TOPAS GMBH). The use of high salt concentration ensured the presence of a detectable nucleus after drying.

4.3.2 Aerosol characterization

Phase doppler anemometry (PDA)

The phase doppler anemometry (PDA/LDA system, Dantec Dynamics, Skovlunde, Denmark) technique is an extension of laser doppler anemometry. The measurement volume is defined by the intersection of two pairs of laser beams with wavelengths of 532 and 561 nm. As single particles flow through the measurement volume, light is scattered from the interference patterns created by the two laser beam pairs [145]. The particle velocity is obtained from the doppler shift of the interference fringes, while information on its size can be acquired from the phase shift. Since the measurement volume is very small, measurements are considered punctual, distinguishing the PDA from the other instruments, making it ideal for the measurement of spray particles [207]. The measurement size range was from 0,5 μm to 8000 μm for the instrument used in this study. Specific settings (Appendix), were selected to ensure that the maximum number of particles were detected by the PDA, without saturating the detectors. The PDA measurements, being made directly in the region of the flow where the aerosols are sampled for the other instruments, are used as reference.

Optical Aerosol Spectrometer (OAS)

An optical aerosol spectrometer (OAS) (MiniLAS model 11-R, GRIMM Aerosol Technik Ainring GmbH & Co, Ainring, Germany), is an optical instrument that measures the light scattering of single particles with a diode laser to obtain the size distribution of an aerosol [142]. It is usually employed for atmospheric measurements. However, when used to characterize the size distribution in a flowing aerosol, it is common to connect a sampling tube to the

inlet of the instrument [135, 136].

For this study, a 1.5 m sampling tube, of which the smallest section was 2 mm in diameter, was connected at the inlet of the instrument for particle measurements. It is recognized that employing a long sampling line may lead to sampling losses [208]. However, the functionality of the instrument was dependent on the use of a sampling line in the studied configuration and the objective was to evaluate and compare instruments under conditions that accurately reflect their typical use for bioaerosol [209] [210] [211]. The inlet sampling flow rate was set at 1.2 L/min. Particles with a size ranging from 0.25 to 32 μm were measured. The instrument requires knowledge of the particle density for mass distribution measurement. Repetitive measurements were taken every 6 seconds for 5 minutes and averaged in a single size distribution.

Scanning mobility particle sizer (SMPS)

The scanning mobility particle sizer (model 3938 L76, TSI Incorporated, Shoreview, MN, USA) used in the study, hereafter called SMPS, consists of a differential mobility analyzer (DMA model 3081A) and an ultrafine condensation particle counter (CPC model 3736), which is butanol-based [144]. In the DMA, the particles are drawn to an electrically charged rod at different rates as a function of their size, only letting one narrow particle size range go through to the CPC. The condensation particle counter finally counts the particles of each size and creates the size distribution.

Extensive literature, including studies by Wang and Flagan [212] and Watson et al. [213], underscores the reliability of SMPS measurements, with any discrepancies between water-based and calibration aerosols predominantly manifesting in the 10-30 nm range, deemed too small to be relevant in the context of airborne transmission. Therefore, deviations in the measurement efficiency of the SMPS were neglected for the size range considered here.

The DMA was fitted with a 71 μm impactor nozzle and a flow rate of 1.2 L/min was drawn with a sheath flow rate of 2.0 L/min. The scanning time was 60 seconds, the retrace time was 6 seconds and the purge time was 10 seconds, which yielded a total time of 76 s for each measurement. These settings resulted in a diameter measurement range of 22 nm to 671 nm. The samples were drawn through plastic tubes of 4 mm in diameter connected to a 2 m flexible silicone tube (TSI Conductive Silicone Tubing) at the inlet of the instrument. Results are presented with diffusion correction applied in the software. Repetitive measurements were performed every 2 minutes for a total of 3 scans, averaged in a single size distribution. The impactor nozzle was cleaned between every set of 3 scans.

Cascade Impactor

The aerosol flow was also measured with a Cascade Impactor (Dekati® Low Pressure Impactor DLPI+). Particles with sizes ranging from 0.16 to 10 μm were collected on 14 different stages based on their aerodynamic diameter, with a sampling flow rate of 10 L/min for 30 minutes. The size associated with each stage is a D50 value, implying that each particle with a given size or larger is collected with 50% efficiency. The larger particles have more inertia and are collected on the first stages while the smaller particles have less inertia and are found on the lower stages. The samples were drawn through a flexible plastic tube with a diameter of 12.7 mm and a length of 0.6 m. Each stage was cleaned with ethanol and water, and weighed before and after measurements. Number size distribution was then derived from the mass of particles collected on each stage, assuming sphericity and constant density.

The time delay between sampling and weighing was approximately 3 to 5 minutes. While the evaporation of Di-Ethyl-Hexyl-Sebacate (DEHS) droplets is negligible over this timeframe [214], for water-based droplets, substantial evaporation occurs, leaving only suspended and dissolved solids for mass measurement. To address this challenge, it was assumed that evaporation was complete and that the remaining solid particles were spherical, with their individual mass obtained from the characteristics of the stage considered. The assumption of complete evaporation was confirmed by visual inspection prior to weighting, although some water could remain in the particles at the moment of impaction.

4.3.3 Experimental facility

The experiment aimed at diluting aerosol particles with clean air to produce a well-mixed and low-speed flow into a sampling chamber common to all instruments (Figure 7.2). To enable the comparison of the size distribution measured with each instrument using the same aerosol, it was necessary to dilute with clean air to avoid saturation. The low flow speed into the sampling chamber and a sampling tube diameter adapted to each instrument flow rate resulted in equal velocities between the air around and inside the tube, which minimized the divergence of the flow lines at the sampler inlet [137]. This isokinetic condition prevents skewed size distribution measurements due to the inertial effects of particles entering the sampling tube. The sampling chamber had a volume of 53 L and was made of clear polymethyl methacrylate (PMMA, plexiglass) so that the optics of the PDA could measure particles through the side walls. Honeycomb material was fixed at the inlet and outlet of the mixing chamber to dampen large flow structures. During the measurements, the mean temperature in the laboratory was 25°C and the mean relative humidity was 42%.

For DEHS aerosol particles, the injection of aerosol particles was done perpendicularly to the

longitudinal direction of the tube and set by the flow controller at 4.2 L/min, for a dilution ratio of 1:5. The clean dilution air was injected from the other side of the tube, in the same manner as the aerosol. By injecting the particles and the air perpendicularly from the longitudinal direction of the tube, turbulence is created, and promotes the mixing of the two flows. To ensure that the flow was properly mixed and that a steady state concentration was reached, a tube of length 1.83 m with an inside diameter of 0.0762 m was used between the aerosol inlet and the sampling chamber (L/D = 24). Measurements were also started 3 minutes after flow initiation. Following every measurement, the chamber was drained by turning off the aerosol generator and injecting compressed air at 6.6 L/min for 10 minutes. For all experiments, the measurements were replicated three times to assess repeatability.

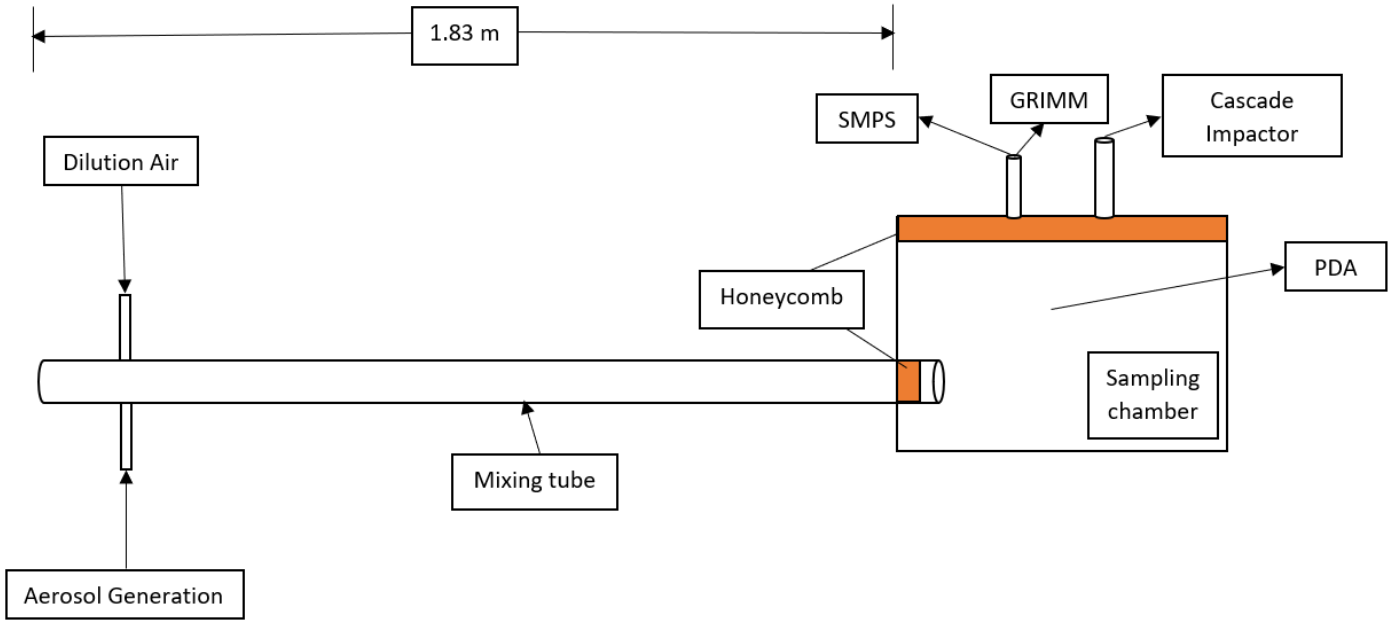

Figure 4.1 Schematic representation of the experimental facility

4.3.4 Aerosol Drying

Aerosol generation from DEHS was ideal for instrument comparison since the particles only dry over several hours in ambient conditions. Additionally, NaCl water-based aerosol particles were used to study evaporation. The use of a sampling line was investigated by comparing the size distribution measured by the OAS and the PDA, using the spray gun and salt water to generate larger aerosol particles compared to those obtained from DEHS in the TOPAS instrument. To remove the complexity associated with uneven evaporation for size distribution measurement, the droplets were also completely desiccated and measured from

the sampling chamber with the SMPS. The SMPS was used because dried particles are smaller and in the appropriate size range for measurement with this instrument. The size distribution was also measured without using the desiccator, for comparison.

Knowing the concentration of salt per volume of the water solution C_s (kg/m^3) as well as the measured mass of salt per volume of air M_f (kg/L$_{\text{air}}$), with the sampling flow rate $\dot{V}$ (L$_{\text{air}}$/s) and the measurement time t (s), the total volume of water for each size bin V (m^3) can be calculated.

$$V = \frac{M_f \dot{V} t}{C_s} \tag{4.1}$$

Then, knowing the number of particles for each size bin n, the diameter of the particles generated at the source D_s (m), was derived, assuming that the transfer rate of NaCl from the solution to the aerosol particles was constant and that the generated droplets were spherical. The source size distribution was then reconstructed from the diameter at the source for each size bin.

$$D_s = \sqrt[3]{\frac{6V}{n\pi}} \tag{4.2}$$

4.3.5 Number Concentration

To account for the fact that the number of size bins is not the same for every instrument, and that the bins are unequal in width, the y-axis on size distribution plots is normalized by dividing the number concentration of each bin by the logarithm of the bin width [134]. This results in a log-normal distribution. Some instruments such as the SMPS already provide a normalized size distribution, but for the OAS, the Cascade Impactor and the PDA, the concentration had to be normalized through data post-treatment. While the OAS and the SMPS produce the size distribution by volume of air sampled, the PDA only counts the number of particles passing through the measurement volume and the cascade impactor yields the cumulative mass of the particles collected on each stage. The particle concentration per liter of air N_C therefore needs to be calculated in the case of the PDA and the cascade impactor. For the latter, since the measurement was made over 30 min and the flow is pumped at a constant rate of 10 L/min, the mass concentration was obtained for each stage by dividing the accumulated mass M (kg/L$_{\text{air}}$) by the sampling flow rate $\dot{V}$ (L/s) and the time of measurement t (s). The number concentration was then calculated assuming sphericity and constant density ρ_p (kg/m^3), where V_p (m^3) is the volume of one particle of the measured

size.

$$N_C = \frac{M}{\rho_p V_p \dot{V} t} \tag{4.3}$$

For the PDA, the cross-section of the measurement volume perpendicular to the flow represents the measurement surface needed to calculate the volume of gas covered by the laser. The measurement volume provided by the supplier was verified by laser irradiance measurement [215], and confirmed at 2.6 mm by 153.1 μm. Assuming that the measurement volume is ellipsoidal, the measurement surface could be derived. The speed of the flow through the measurement volume is known, as the instrument also provides particle velocity, and the time of the measurement remains constant. The concentration of particles per liter of air N_P can therefore be obtained by dividing the counted particle number N by the mean flow velocity V_m (m/s), the time of measurement t (s) and the measurement surface S (m^2).

$$N_P = \frac{N}{S V_m t} \tag{4.4}$$

The SMPS and PDA distributions are composed of 100 size bins, while the OAS and the Cascade impactor only produced size distributions with 9 and 6 bins, respectively, for the DEHS measurements. The size resolution improved slightly for water-based droplets with respectively 11 and 7 bins used for the latter two instruments.

4.4 Results and Discussion

4.4.1 Instruments comparison

The size distributions of oil-based and water-based droplets were measured and compared with the OAS, the SMPS, the PDA and the Cascade Impactor (Figure 4.2). The peak concentration of DEHS particles in the air was found to be approximately 6×10^7 for all the instruments. However, the water-based measurements showed a wider range of peak concentrations, varying between 10^7 and 10^9 particles per liter of air. The modes of DEHS particles coincided for all instruments at approximately 0.3 μm with a variance a thousand times smaller than for the water-based measurements. Essentially, the size distribution statistically concurred for the measurement of DEHS droplets but not for water-based droplets and the discrepancies between both configurations are significant according to a T-test conducted on the modes of the distribution ($p<0.05$).

OAS and SMPS spectrometers as well as the cascade impactor require the use of a small inlet sampling tube, in which some particles may be lost by impaction on the walls or through evaporation. The use of a sampling line was investigated further by comparing the size distri-

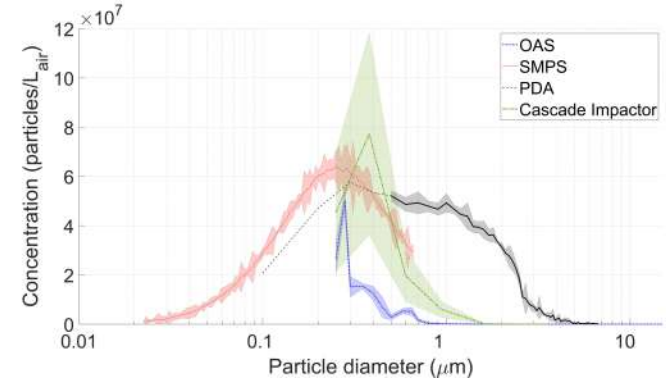

(a)

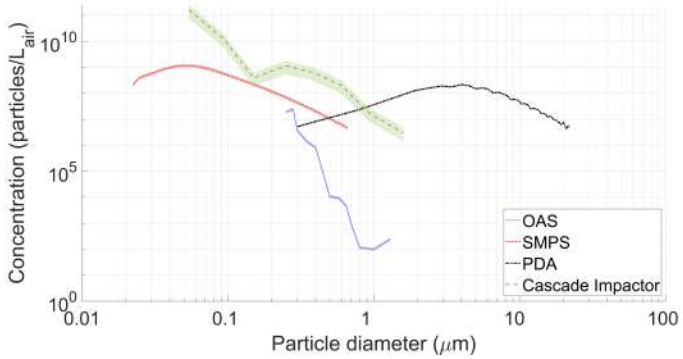

(b)

Figure 4.2 Comparison of the size distribution measurements from the four instruments a) with DEHS aerosol particles. b) with water-based aerosol particles. Results are averaged over three measurements. Shaded areas show the standard deviation within repeated runs.

bution obtained from the spray gun with the PDA and the OAS (Figure 4.3 a). In addition to the expected losses in measurement associated with particle deposition, it was observed that the size distribution of the OAS was shifted towards smaller particles. This shift indicated that the measurement process was also affected by evaporation, which occurred rapidly as the particles went through the sampling line (transit time of 1.16 seconds). Therefore, deposition and evaporation of particles are likely responsible for the significant discrepancies observed within the size distribution measurements conducted with instruments using different working mechanisms and their effects must be considered.

Evaporation does occur between the generation and sampling site and is of significant interest in the context of airborne transmission. However, the primary objective of this study aimed to offer a practical comparison of aerosol size distribution measurement instruments under consistent laboratory conditions. As such, the evaporation considered here pertains specifi-

cally to the interval from the sampling point to the measurement point inside the instrument. Thus, the measurement volume of the PDA could be considered as the source and coincident with the sampling point of the other instruments.

As the sampling flow rate through the different instruments is generally fixed (except for the SMPS for which a slight adjustment is possible), the sampling tube diameter is imposed to achieve isokinetic sampling. When comparing the concentration measured by the different instruments, the OAS measured up to 5 orders of magnitude fewer particles than the other instruments (Figure 4.2 a). For particles larger than 0.25 µm, differences in the measurement were at least 40%, and from 0.8 µm, reached close to 100%, revealing that larger particles are less likely to be detected by the OAS (Figure 4.3 b). Some particles are lost, others evaporate in transit and are detected at a lower size. This effect appears mostly significant with the OAS. However, as the mode and shape of the distribution were qualitatively in agreement, the results provided by this highly portable instrument remain valuable, especially when measuring either dry or slowly evaporating particles.

Due to the lower resolution inherent in its measurement principle, the cascade impactor showed the highest variability in the measurements (Figure 4.2). In effect, the use of cascade impactors to characterize the size distribution of droplet-laden flows poses significant challenges due to the inherent evaporation of droplets during sampling, following impaction and prior to mass measurement. This temporal gap introduces uncertainties, particularly for water-based droplets, as evaporation of the deposited droplets is significant. To mitigate this issue, assumptions were made to assume total evaporation and treat the remaining solid particles as spherical entities. While cascade impactors offer benefits in capturing particles based on their aerodynamic size, the limitations associated with evaporation and the subsequent conversion process make them suboptimal instruments for achieving precise size distribution characterization in the context of droplet-laden flows.

The PDA displayed among the most repeatable measurements and detected larger and more particles than the other instruments in all investigated configurations, since it does not require a sampling tube, minimizing evaporation and losses in the sampling line. Therefore, the PDA can be regarded as a reference over its size range. However, since the wavelengths of the lasers used in the PDA are approximately 0.5 μm, the measurements for smaller particles lacked precision, and are therefore illustrated as a dashed line. For particles smaller than 0.5 μm, the SMPS is considered the gold standard as very little losses are expected in transit for such small particles.

Decripancies arose within the size distribution measurements of both water-based and oil-

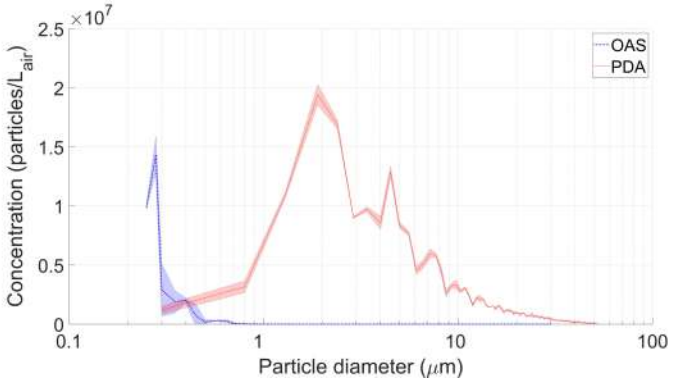

(a)

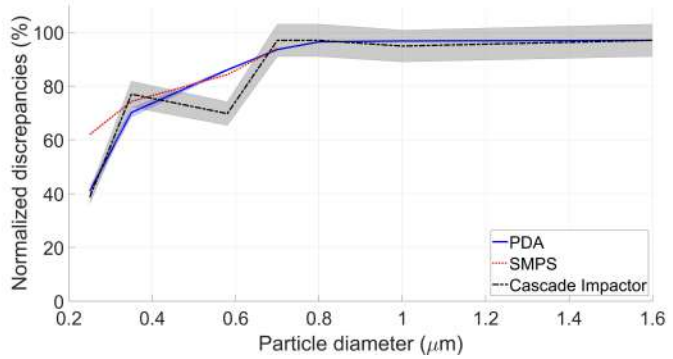

(b)

Figure 4.3 a) Comparison of the OAS and the PDA to show the effect of the sampling tube on the measurements. Results are averaged over three measurements. Shaded areas show the standard deviation within repeated runs. b) Sampling discrepancies observed with the OAS compared to the other three instruments.

based particles from different instruments. Although much slower than for water evaporation also occurs in oil-based particles, and the effect of particle deposition could be observed for the measurement of larger oil-based particles from the OAS and the cascade impactor. However, the effects of evaporation and particle deposition on the size distribution measurements were more significant for water-based particles because of their combined effect. The fact that evaporation was negligible for DEHS measurements [214] explains the much better agreement between the instrument than for water-based droplets, as only the effect of particle deposition caused the measurement discrepancies. As such, sections 3.2 to 3.4 will focus on the development of empirical correction factors, with the PDA as a reference, for configurations where evaporation and deposition in sampling lines are occurring.

4.4.2 Evaporation

The evaporation of the measured particles can be characterized by the dimensionless Sherwood number, which represents the ratio of the convective mass transfer h (m/s) to the mass diffusivity D (m^2/s). With knowledge of the particle diameter d_p (m), the Sherwood number can be calculated [154] :

$$Sh = \frac{h}{D/d_p} \tag{4.5}$$

While the Sherwood number itself may not explicitly include terms for temperature and relative humidity, the convective mass transfer coefficient (h) it includes is influenced by these ambient conditions [154]. The convective mass transfer coefficient h (m/s) is a function of the surface of the droplet A (m^2), the molar mass transfer $\dot{n}_A$ (mol/s) and the vapor concentration difference between the boundary surface and the ambient air Δc (mol/m^3):

$$h = \frac{\dot{n}_A}{A\Delta c} \tag{4.6}$$

Therefore, changes in temperature and relative humidity in the atmosphere can indirectly affect the Sherwood number and, consequently, the mass transfer characteristics of aerosol droplets during evaporation.

The mass diffusivity coefficient can be easily derived for DEHS and water with respect to ambient air, knowing the relative properties of the interacting fluids. As for the convective mass transfer coefficient h, it is a function of the mass transfer rate at the interface of the droplet, the area of the interface and a driving force coefficient, which is dependent upon the conditions, and complex to infer. However, using dimensional analysis for the evaporation of a spherical droplet, the Sherwood number can also be defined as the Froessling function, dependent upon the Reynolds and Schmidt numbers [216]. With knowledge of the density of the fluid ρ (kg/m^3), the dynamic viscosity of the fluid μ (kg/ms), and the velocity of the particles relative to the air u (m/s), it was calculated here using the following equation :

$$Sh = f(Re, Sc) = 2 + 0.552(Re)^{\frac{1}{2}}(Sc)^{\frac{1}{3}} \tag{4.7}$$

Where

$$Re = \frac{\rho u d_p}{\mu} \; ; \; Sc = \frac{\mu}{\rho D}$$

The rate of evaporation I (kg/s), characterized as the loss of water m (kg) over time t (s), is linearly proportional to the surface area of a liquid droplet of and thus to the square of the

droplet diameter d (m) [154].

$$I = \frac{-m}{t} \propto \pi d^2$$

Therefore, a correction factor for the evaporation of droplets before they are measured needs to consider the square root of the transit time (t). Also, although very slow due to the nature of the fluid, evaporation does occur for DEHS droplets. Because DEHS is used as a reference for evaporation, the correction factor must consider the Sherwood numbers of both oil-based (Sh_{DEHS}) and water-based droplets (Sh_{water}). Finally, the properties of the fluids and the aerosol generation mechanism influence the size of the generated droplets. As such, the correction factor must include the ratio of the modes of the water-based size distribution ($D_{p;m,water}$), over the DEHS size dsitribution ($D_{p;m,DEHS}$). In light of all these hypotheses, the following empirical correction factor can be used to adjust for the bias of the droplet diameters measured due to evaporation:

$$K_{evap} = \frac{D_{p;m,water}}{D_{p;m,DEHS}\sqrt{t}} \frac{Sh_{DEHS}}{Sh_{water}} \tag{4.8}$$

The transit time t was calculated by dividing the volume of the sampling line (m^3) by the sampling flow rate (m^3/s). The PDA was used as the reference instrument. As such, the correction factor was applied respectively to each of the particle sizes for all the instruments except for the PDA, and the correction factor incorporated the ratio of the modes from the size distribution of different fluid, measured with the PDA. As an example with the OAS, a transit time of 1.16 seconds, Sherwood numbers of 36.13 and 32.86 respectively for DEHS and water and the ratio of the modes of 13.33, yielded a correction factor K_{evap} of 13.60. For a particle size of 0.5 μm measured with the OAS, the corrected particle size was therefore 6.8 μm (Figure 4.5).

4.4.3 Sampling line deposition

The deposition of particles on the walls of the sampling line, resulting in measurement losses, can be characterized by the Stokes number and the length of the sampling line. The Stokes number quantifies the capacity of the particles to follow the streamlines of the flow. The length of the sampling line affects the particle essentially through the transit time available for deposition to occur. Sampling line deposition of particles mostly influences the measured concentration, which is not affected equally for all droplet sizes, as larger particles, with a larger Stokes number, exhibit a higher propensity for settling and colliding with the walls.

Both the length of the sampling tube and the Stokes number can be combined in a single parameter [217]. However, in this section, we will assess the effect of both phenomena on the measurement separately.

Particle transit

The likelihood of particle loss through settling in the sampling line during transit, before reaching the measurement point of the instrument, can be characterized by the dimensionless Stokes number, which is the ratio of the characteristic time of a particle t_0 to the characteristic time of the flow. Knowing the particle density ρ_p (kg/m^3), the diameter of the particles d_p (m), the dynamic viscosity of the air μ_g (kg/ms), and the flow speed u (m/s), the Stokes number is defined as :

$$Stk = \frac{t_0 u}{d_p} \tag{4.9}$$

where

$$t_0 = \frac{\rho_p d_p^2}{18\mu_g}$$

For large particles, the Stokes number is therefore large and impaction on the sampling line walls, which are bound to include bends, is more likely to occur because of the inertia of the particles. The flow rate was 1.2 L/min in the sampling line of the OAS, 2.0 L/min for the SMPS and 10 L/min for the cascade impactor. For a 0.5 μm particle, this resulted in Stokes number of 9.8×10^{-3}, 4.1×10^{-3} and 2.02×10^{-3}, respectively, inside the sampling lines of the OAS, the SMPS and the cascade impactor. The Stokes number for OAS measurements was more than twice that of the SMPS and was five times larger than that of the cascade impactor, explaining the losses in the sampling line for larger particles with the former. The differences here were exacerbated by the fact that these losses are strongly size dependent, as well as the ability of the OAS to detect much larger particles, up to 32 μm.

The Stokes number (Stk) depends on the droplet diameter and is therefore size specific. Thus, a correction factor for particle deposition inside the sampling line must affect the concentration differently depending on the particle size, the droplet fluid and the measurement instrument used. For a specific particle diameter, the Stokes number varies linearly with the properties of the fluid, so the correction factor is expected to be a linear function. Also, particle deposition occurs regardless of the fluid, but the properties of the fluid making up the droplets influence the behavior of the particles. Consequently, the correction factor should include the ratio of the density of DEHS and water as well as the viscosity of the ambient air.

The following empirical correlation can therefore be used to correct the bias of the droplet concentration measured due to particle deposition :

$$K_{dep} = \alpha Stk \tag{4.10}$$

Where

$$\alpha = \frac{0.87}{\mu_{air}} \frac{\rho_{DEHS}}{\rho_{water}} = 4285$$

In the correction factor, the factor of 0.87 is an empirical value that corrected for the differences in viscosity of the humid air surrounding the aerosol in relation to the ambient air [218]. The correction factor was multiplied by the concentration and was size-dependent. The reference for the calculation of the empirical correlation factor was the PDA, meaning that it was applied to the particle sizes of all the instruments except for the PDA. As an example, approximately 10^4 water-based particles of size 0.5 μm were measured with the OAS per liter of air. The Stokes number was 9.8×10^{-3}, which yielded a correction factor of approximately 42. The corrected particle concentration was therefore 4.2×10^5 particles per liter of air.

Effect of the sampling line length

The length of the sampling tube also affects the measured concentration through measurement losses. Here, the effect of the use of different sampling tube lengths was investigated experimentally, using DEHS particles to avoid the complications associated with evaporation. The size distribution obtained using the SMPS and sampling lines of 7 different lengths (0.5, 1.0, 1.5, 2.0, 3.0, 4.0 and 5.0 m) are shown in Figure 4.4 (a). If losses were only the results of inertial effects, the Stokes number reveals that particle deposition should be more significant for larger particles. In the SMPS however, selected based on its suitability for the sub-micron size range investigated, the measurement losses did not exhibit a significant change as a function of the particle size. It was therefore assumed that the correction factor for the sampling line length is not size-dependent.

By using the same measurement instrument, as well as DEHS aerosol droplets to characterize changes in the particle deposition from changes in the length of the sampling line, the resulting observations represent the added probability of particles interacting with the sampling line wall due to its extended length, without the combined effect of evaporation and Stokes number-dependent deposition.

The losses in the sampling line were approximately proportional to the cube of the sampling line length L (Figure 4.4 b). The correction factor for the measurement losses induced by the length of the tube is therefore in the form of a power law with empirical coefficients a,

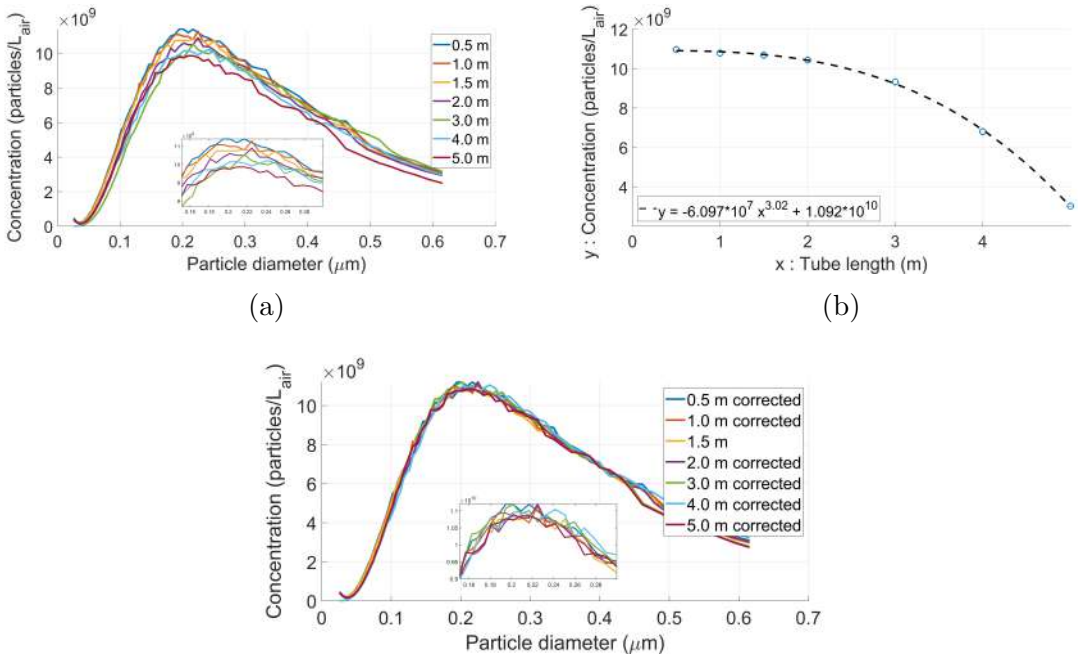

Figure 4.4 a) Average of SMPS measurement triplicates of the concentration as a function of droplet diameter for five sampling tube lengths (0.5, 1.0, 1.5, 2.0, 5.0 m). b) Curve fitting of the concentration (y) as a function of the tube length (x), for the mode of the size distribution. c) Corrected size distribution according to the sampling line length with reference to the 1.5-meter sampling line.

b and c. To correct for the length of the sampling line, the measured concentration can be multiplied by the ratio of the power law applied to the length of the sampling line of the corrected measurement instrument over the length of the sampling line of the instrument used as a reference. As an example, if the SMPS was used as the reference instrument and the size distribution of the OAS was to be corrected, the correction factor would be :

$$K_{lengthSMPS} = \frac{a(L_{OAS})^b + c}{a(L_{SMPS})^b + c} \tag{4.11}$$

Where Table 4.1 displays the empirical constants.

Applying a single fitting curve corresponding to the mode of the distribution (Figure 4.4 b) caused minimal disparities when the size distribution measured through the 7 sampling line lengths with the SMPS were corrected (Figure 4.4 c), especially when compared to the uncorrected measurements (Figure 4.4 a). This is convenient in this context due to the

Table 4.1 Empirical constants for the correction factor of the sampling line length with the SMPS

Empirical Constant	Value
a	-6.097×10^7
b	3.02
c	1.092×10^{10}

narrow size range measured using the SMPS.

A better reference to use when correcting for sampling losses is the PDA, which does not use a sampling line. In this case, a proportionality empirical correlation variable β can be used, calculated using the correlation applied to a sampling tube of length zero, multiplied by an empirical constant of 10, acquired through trial and error, which allowed for a better fit. The correction factor can be applied to all instruments covering a wide range of sizes, despite being derived from measurements in the sub-micron size range. The β variable is used to adjust the concentrations to the reference PDA, which is assumed not to be subjected to sampling and evaporation losses, as it performs direct measurements at the location where the other instruments are pulling aerosol. As such, this approach not only allows for a thorough comparison between different instruments, but also provides a means to improve the accuracy of results obtained from affordable tools such the OAS, which costs significantly less than the PDA but is subject to significant sampling and evaporative losses. Considering the PDA as the reference, the best fit for the mode of the concentration of the 7 investigated sampling lengths yielded the following correction factor :

$$K_{length} = \frac{\beta}{a(L)^b + c} = \frac{1.0915 \times 10^{11}}{-6.097 \times 10^7 (L)^{3.02} + 1.092 \times 10^{10}} \tag{4.12}$$

Where

$$\beta = 10(a(0)^b + c) = 1.0915 \times 10^{11}$$

4.4.4 Corrected comparison

The empirical correction factors presented in the previous sections were applied to the water-based size distribution produced with the spray grun (Figure 4.5). The evaporation correction factor K_{evap} was applied to the particle diameter and the correction factors for the sampling line losses K_{length} and K_{dep} were both applied to the particle concentration. A summary of the correction factors is presented in Table B.2.

The modes of the corrected size distribution (Figure 4.5) coincide very well, with a droplet

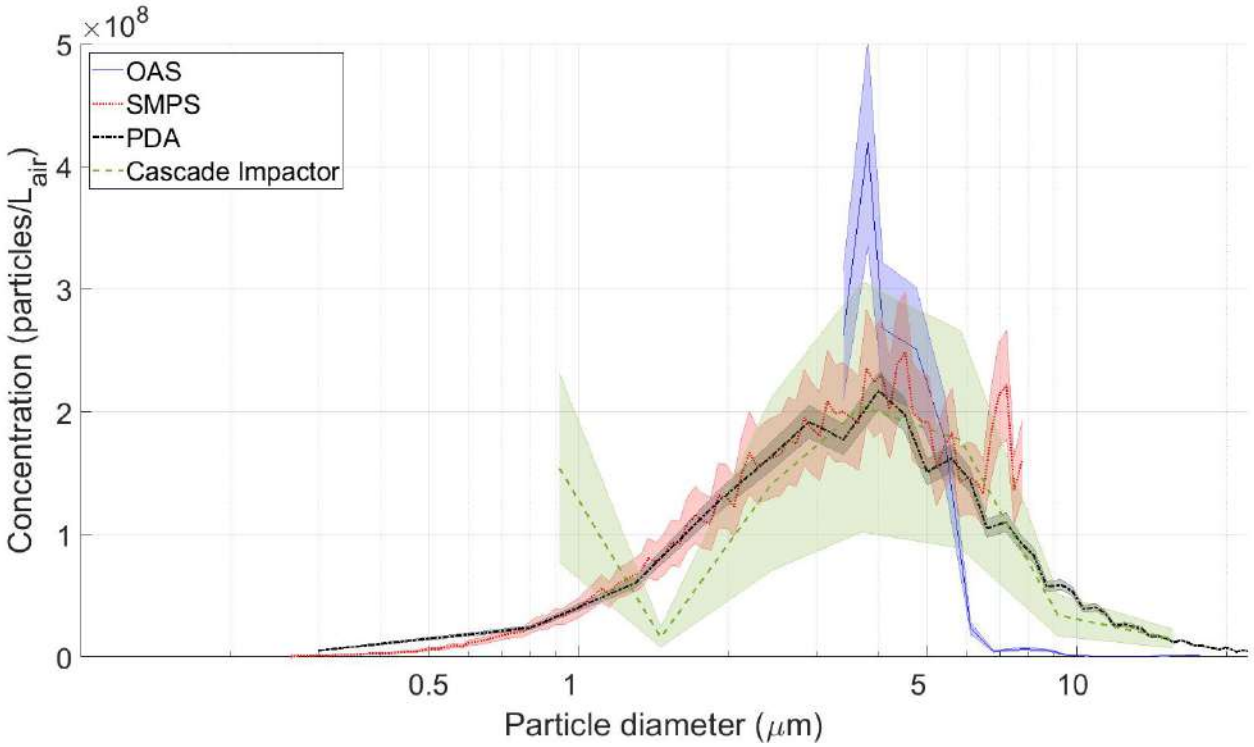

Figure 4.5 Comparison of the four instruments with water-based aerosol particles corrected empirically. Shaded areas show the standard deviation within repeated runs of the initial measurements.

diameter of approximately 4 μm, showing that the measured size distribution of water-based particles is not statistically different than that of DEHS particles when corrected with the approach described previously, according to a T-test on the modes ($p>0.05$). Therefore, the correction factors allow the comparison and combination of measurements obtained from different instruments relying on sampling lines and working with droplets undergoing evaporation.

As observed in Figure 2, where disparities in size distribution measurements were identified, the correction factor for evaporation needs to account for particle diameter. This approach was motivated by the significant impact of evaporation on size distribution, particularly for smaller droplets, as substantiated by previous studies [219] [220]. In contrast, the correction factor for sampling line length played a more pronounced role on aerosol concentration, with little effect observed on the particle size (Figure 4a), for the conditions investigated here. Although a particle size-dependence can be expected for the deposition in the sampling line, with bigger particles depositing more easily, we did not observe such a quantifiable effect for the size range considered here. The correction factors, detailed in Table B.2, target both

evaporation and deposition, acknowledging their preferential effects on size distribution and concentration.

The approach presented here based on correction factors can be adapted to other aerosol sizing measurements relying on sampling. Although the correction factors for evaporation and sampling line losses have been validated for the configuration described in Section 2, they can be calculated for different fluid systems or experimental facilities, as they essentially depend on flow conditions and particle characteristics, rather than instrumentation. Conversely, the correction factor for the length of the sampling line requires the availability of a reference instrument such as the SMPS or the PDA. In this study however, the empirical constants of the correction factor were derived from SMPS measurements of submicron DEHS droplets and were then successfully applied to larger water-based droplets measured with different instruments. The results from this investigation can be used to correct experimental data from sampling instrumentation such as optical aerosol spectrometers and impactors similar to those used here.

Finally, the specific measurement instruments used in this study also have their advantages and limitations which can influence the results depending on the application as further discussed in Appendix B. Applying these correlations to other measurement instruments besides those considered here may also introduce errors due to inherent differences in their measurement principles, as well as their sensitivity and measurement range.

Table 4.2 Summary of the correction factors for evaporation, as well as sampling line deposition during particle transit and the length of the sampling line.

Correcting for :	Correction factor	Applied to :
Evaporation	$K_{evap} = \frac{mo_{water}}{mo_{DEHS}\sqrt{t}} \frac{Sh_{DEHS}}{Sh_{water}}$	Particle diameter
Sampling line deposition during particle transit	$K_{dep} = \alpha Stk$ where $\alpha = \frac{0.87}{\mu_{air}} \frac{\rho_{DEHS}}{\rho_{water}}$	Aerosol concentration
Length of the sampling line	$K_{length} = \frac{\beta}{a(L)^b + c}$ $K_{length} = \frac{1.0915 \times 10^{11}}{-6.097 \times 10^7 (L)^{3.02} + 1.092 \times 10^{10}}$	Aerosol concentration

4.4.5 Circumventing Evaporation

The size distribution of NaCl droplets measured with the SMPS, with and without drying the aerosol in a desiccation column (representing the dried and wet distributions respectively), are presented along with the calculated initial size distribution (Figure 4.6). The particle size as they were generated (source distribution) was calculated following the procedure described in section 2, which avoids the complications associated with evaporation during measurement, or between the aerosol source and the measurement point. The concentration at the source was adjusted for the length of the sampling line. The maximum number of particles measured was approximately 2×10^9 particles per liter of air for the dried distribution, and was approximately three times more for the wet distribution, revealing significant particle losses in the drying process.

As expected, the measured particles were much smaller than at the source, due to evaporation. Particles at the source ranged from 0.65 μm up to 10 μm and covered a broader range of particles than the dried and wet measurements. 90 % of the generated particles were larger than 1 μm and once measured, all the particles were submicron. This further supports the signficance of the evaporation effect in the measurement process and the importance of considering the measurement biases induced by the use of a sampling line with an evaporating aerosol.

Mass conservation

Following the assumption that the solid concentration in each droplet is equivalent to the bulk solution concentration, it is possible to conduct a mass conservation analysis. Knowing the density of the bulk saline solution used to generate the measured droplets, the total volume of water aerosolized V_t (m^3) can be calculated by integrating the volume of a sphere with the diameter of a measured droplet across the size range of the size distribution at the source, multiplied by the number of measured droplets at that size N_s. The total mass of salt at the source M_s (kg) can then be inferred with the concentration of salt in the bulk saline solution C_s (kg/m^3). With knowledge of the measured mass of dried solids M_f (kg), mass conservation calculations can then provide the mass of solids lost during the measurement of the dried particles M_L (kg):

$$M_s = M_f + M_L \tag{4.13}$$

Where

$$M_s = C_s \times V_t$$

$$V_t = N_s \int_{d_{min}}^{d_{max}} \frac{\pi (d_p)^3}{6}$$

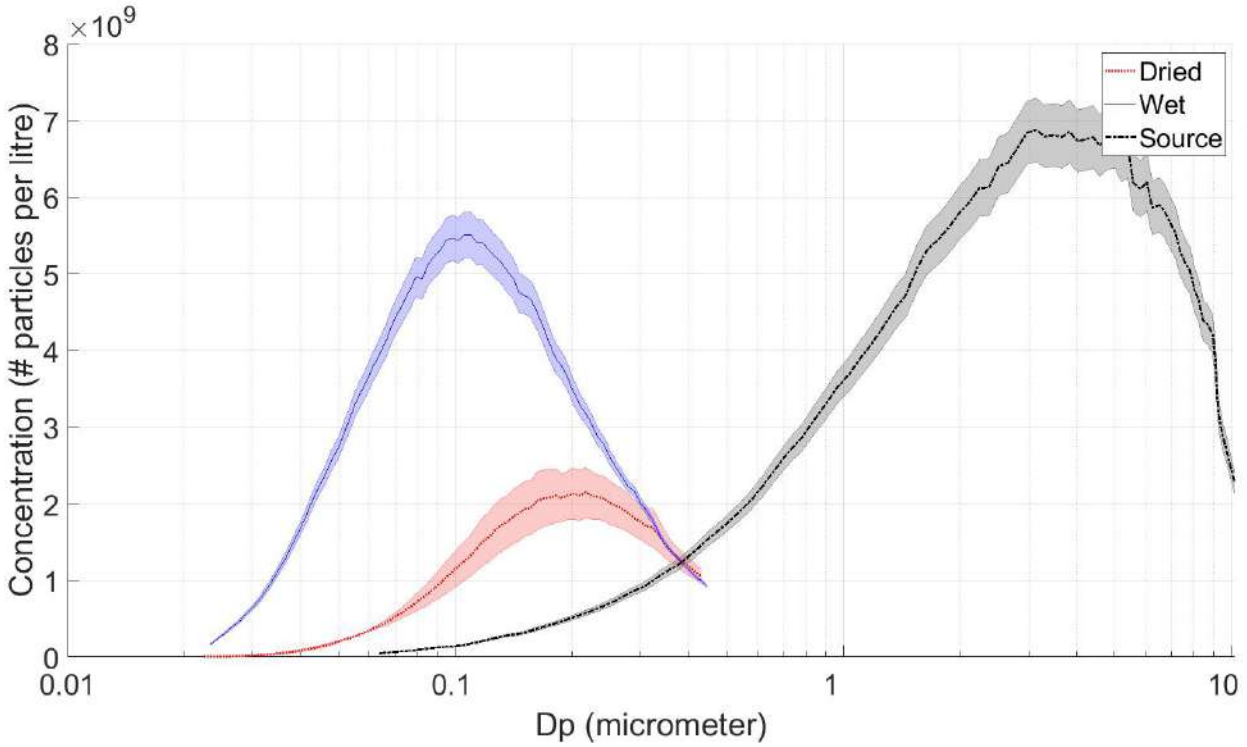

Figure 4.6 Size distribution from the SMPS with dried NaCl aerosol particles and the calculated size distribution at the source. Results are averaged over triplicate measurements. Shaded areas show the standard deviation within repeated runs.

The mass of the wet size distribution M_w (kg) can also be added to the calculations to isolate the losses in the sampling line and from evaporation M_L^* (kg):

$$M_s = M_w + M_L^* \tag{4.14}$$

Approximately 96% of the mass at the source was lost during measurement, attributed to water evaporation, as well as particle deposition in the sampling line and the desiccation column. Particle transit and Stokes number analysis indicated that these measurement losses were significantly exacerbated for larger particles. Wet and dried size distributions only showed a 4% mass difference, suggesting that most losses through evaporation occurred during particle transit, reinforcing the key advantage of the PDA as a reference instrument. Water content constituted 90% of the mass at the source, and over 15% of the total mass was lost through sampling line deposition. This entails that evaporation is the dominant factor in the differences between measurements, but that particle deposition also played a significant role. The losses in the desiccation column accounted for less than 5% of all losses, primarily affecting smaller particles due to Brownian motion-induced diffusion during evaporation.

This explains the shift towards larger particles in the dried size distribution, where the wet distribution measured with the SMPS had a maximum concentration at a diameter 2 times smaller than the dried distribution.

Significance of the complete evaporation approach

Research groups focusing on bioaerosols face limitations when using Phase Doppler Anemometry due to safety concerns and practical constraints. Nevertheless, the interest in understanding the size distribution of potentially contaminated droplets remains high. As an alternative, portable and user-friendly instruments like an OAS or impactors are commonly employed. However, these instruments suffer from losses during transit, primarily caused by particle deposition in the sampling line, and evaporation. The incomplete and unknown evaporation process makes the size distribution measurement largely arbitrary and dependent upon environmental conditions. To address this challenge, our approach involves complete evaporation of particles, allowing the calculation of the size distribution at the source by considering the solid content in the bulk solution and after complete drying. However, the significant losses during measurement must be considered. In this study, the PDA was used as a reference to account and correct for these losses. The process of completely drying water-based aerosol particles to then revert to their initial size also demonstrates the possibility of extending this methodology to dry aerosol particles, in that case disregarding the evaporation correction factor.

4.4.6 Applications

In the context of airborne transmission, the approach outlined also offers a valuable framework for advancing our understanding of respiratory particle dynamics. The choice of appropriate measurement techniques, including a combination of data from several instruments and empirical correction factors for evaporation and deposition, becomes particularly important when applied to the study of aerosols originating from the respiratory system [21]. However, a critical research gap lies in our understanding of aerosol size distribution within the airways themselves [221]. By adapting the methodology proposed here to focus on airway aerosols, a more accurate characterization of size distribution can be achieved, enabling researchers to extract meaningful results from a range of measurement instruments. As such, the use of a sampling line can be valuable to reach specific areas that are difficult to access. Incorporating the correction factors derived in this study can also address potential losses during sampling and transit. Moreover, the application of a complete drying technique allows for source characterization, providing insights into the initial composition and behavior of aerosols directly from the respiratory system. This comprehensive approach can contribute to a more robust

characterization of the risks associated with respiratory pathogen transmission, facilitating the development of targeted mitigation strategies.

4.5 Conclusions

A transversal comparison was presented between four aerosol size distribution measurement instruments with different working mechanisms, performed in a flow of water and DEHS aerosol particles suspended in the air. Instruments generally agreed when measuring particles that do not evaporate, but not when measuring water-based droplets. For DEHS (oil-based) particles, all instruments detected comparable size distributions and concentrations with minimal differences, except for the OAS, which generally measured at least 70% fewer particles for sizes larger than 0.25 μm, indicating that deposition was also significant for oil-based particles. For water-based aerosol particles, measurement discrepancies affected all the instruments, sometimes exceeding one order of magnitude.

These differences between the measurement of water-based and oil-based particles were explained by the evaporation of water-based droplets before the measurement was conducted, as well as measurement losses due to particle deposition in the sampling line. Empirical correction factors based on the Stokes and the Sherwood numbers, as well as the length of the sampling line were developed to account these measurement biases, using the PDA, which does not use a sampling line, as a reference. These results demonstrate that in the context of airborne transmission, employing size distribution measurement instruments that are not designed for bioaerosol measurements can provide actionable data for proper risk assessment if particle deposition and evaporation are accounted for.

Evaporation was then further investigated by conducting measurements on dried particles and subsequently reconstructing the size distribution at the source. Mass conservation allowed for a quantitative assessment of the measurement losses due to evaporation and deposition. Using this approach, affordable and portable OAS can be used to characterize size distribution at the source if the solid content is known, circumventing difficulties associated with the evaporation process. Therefore, the complete drying of the particles enables the evaluation of the initial size of the generated particles, a critical information in the context of airborne transmission.

Acknowledgements

This research was supported by a NSERC Alliance Grant (ALLRP545363/2019), Polytechnique Montréal. Xavier Lefebvre is supported by the Hydro-Québec excellence scholarship

as well as a NSERC scolarship (ES D) with a FRQNT supplement (B2X).

Ethical statement

Data Availability

Data that support the findings of this study are available from the corresponding author upon reasonable request.

Competing Interests

The authors declare no competing interests.

CHAPTER 5 ARTICLE 2: IDENTIFICATION AND MITIGATION OF OPERATIONAL FACTORS INCREASING *LEGIONELLA* RISKS IN COOLING TOWERS

Submitted to *Water Research* on October 29 2024

By

Xavier Lefebvre, Elliston Vallarino Reyes, Dominique Charron, Sebastien Faucher, Etienne Robert, Emilie Bedard and Michèle Prévost

5.1 Abstract

Cooling towers (CTs) have been identified as a main source of Legionnaires disease (LD) outbreaks but source attribution remains a challenge. A comprehensive study was completed to quantify spatial and temporal variability of CT emission of *Legionella pneumophila* (*L.p.*) aerosol droplets by conducting *in situ* sampling of 15 cooling towers. A wide range of inhalable aerosol emission rates spanning two orders of magnitude was measured and significant temporal variability (up to 10X) was observed. Site specific CT aerosol discharge rates of *L.p.* and *Legionella spp.* (*L.spp.*) not only reflected CT capacity but also operational rate and installation characteristics. At high cooling tower working capacity, the efficiency of drift eliminators for capturing potentially contaminated inhalable aerosol droplets dropped to less than 50%, a critical consideration for exposure assessment. Estimates of viable *L.p.* concentrations and transfer rates from water to aerosol droplets were generated from qPCR and Intact Cell Counts (ICC) at each CT. Site-specific data were then used to assess the impact of emission rates on viable *L.p.* concentrations, on daily risks using Quantitative Microbial Risk Assessment (QMRA). Water-based airborne viable *Legionella* concentrations, operating rates and the efficiency of drift eliminators in capturing potentially contaminated inhalable particles were combined in an improved emission model. Viable *Legionella* emission rates varied in a 5,000-fold range spanning over 5 logarithmic units, driven mostly by the *Legionella* concentration in water and the aerosol emission rate. QMRA derived risk estimates spanned over 3 orders of magnitude across the monitored CTs, underscoring the potential for extreme values associated with the large spatial and temporal variability to substantially influence the risks associated with cooling towers. QMRA based risks suggest that, in the absence of site-specific data, risk assessment should be conducted with the system operating at maximum capacity, particularly when water concentrations are at their peak. From these results, a generalized QMRA emission framework which considers the transfer rates,

drift eliminator capture efficiencies and the aerosol emission rates acquired throughout the sampling campaign was formulated to provide CT managers and public health authorities with an improved risk estimate, facilitating informed mitigation strategies and source investigation. More frequent *L.p.* monitoring and drift eliminator optimization appear as key elements to mitigate the risks associated with the airborne transmission of *Legionella* from cooling towers.

5.2 Introduction

Legionnaires' disease (LD) is responsible for an estimated health care cost of 402 M$ per year in the United States [11, 71, 72] and 1.2 B$ in Europe [222, 223]. *Legionella* can cause Legionnaire's disease (LD), a serious pneumonia with a 10% mortality rate, as well as Pontiac fever, a self-limited illness [224–226]. *Legionella pneumophila* (*L.p.*), specifically serogroup 1 (*L.p. SG1*) and *Legionella* species (*L.spp.*) have been targeted by public health regulations due to their persistence [227], prompting strict guidelines for water system management and monitoring [104]. Infections occur via the inhalation or respiration of contaminated aerosol droplets, making this transmission route critical epidemiologically [66, 115].

Community acquired sporadic cases account for most LD cases and the exposure source is typically unknown [8, 9, 79]. Sporadic cases displaying clear seasonal patterns have increased 9-fold between 2000 and 2020, leading to 1.9 and 2.4 yearly cases per 100 000 people in North America and Europe respectively [8, 105, 106]. Cooling towers (CTs) have been identified as the primary source of LD outbreaks associated with *L.p.* [80, 228–231] and a probable source of sporadic disease when spatial association can be made [232].

CTs are specialized heat exchangers that generate an aerosol plume of potentially contaminated droplets capable of traveling over long distances up to 12 kilometers as a by product of their working mechanism [79, 233, 234]. Their complex network of heat exchangers, chillers and piping offers large surface areas at conditions favorable for biofilm and *Legionella* growth [74, 234, 235] operated at optimal temperatures and in many cases intermittently [101, 236], making it challenging to efficiently implement control measures across the CT system [235, 237]. The barrier against the dissemination of contaminated droplets is the drift eliminator. However, drift eliminators are designed to limit water losses through the aerosol plume, not to capture aerosol droplets of a size relevant to lowering the risk of *Legionella* transmission [53, 59, 238].

Quantitative microbial risk assessment (QMRA) statistical models are commonly used to quantify the infection risks of airborne disease, and hav been applied to CTs [81, 101, 239].

However, when applying these models to assess *L.p.* exposure risks from CTs, several challenges remain, particularly regarding key parameters such as droplet emission rate and size distribution within the 1-10 μm exposure range, as well as the pathogen concentration and viability within the aerosol plume [101, 108, 239, 240].

To improve the impact of QMRA scenario analysis, it would be beneficial to select scenarios on their applicability to best inform policy [241]. That is we aim to identify critical periods of exposure by monitoring the spatial and temporal variability of the bioburden of *Legionella* that considers both aerosol emission rate and pathogen viability, as outlined by [115].

The main objective of this study was to determine the spatial and temporal variability of the bioburden of contaminated aerosol droplets released by cooling towers in order to improve risks assessment of *Legionella*. The secondary objectives include: (1) documenting the spatial and temporal variations in aerosol emission rates and size distribution of total and intact bacterial cells, including *L.p.* and *L.spp.*, from 15 CTs, (2) assessing the efficacy of drift eliminators under varying operating conditions, (3) improving the estimates of pathogen transfer from water to aerosol droplets, (4) conducting site-specific QMRA estimates using real data to identify key parameters that could reduce risks and (5) proposing a conservative generic framework to estimate the bioburden of contaminated *Legionella* aerosol droplets in the absence of site-specific data.

5.3 Materials and methods

5.3.1 Selection of study sites

A total of 25 sites (labeled S1, S2, S3, etc.) were visited, with 15 CTs selected for further investigation (Table C1 - Appendix). The CTs, located on municipal and institutional rooftops or at ground level, varied in operation, some seasonal (March to September) and others year-round. Full details of the CTs and their respective drift eliminators are in Appendix C. Key characteristics include the operating rate, calculated as the ratio of current to maximal operation for fan speed and water pump [127], and the CT capacity, the amount of heat that the tower can remove from the circulating process water, measured in tons of heat removed. The study included crossflow, counterflow, and forced draft CTs, with capacities from 50 to 5,000 tons.

5.3.2 Experimental approach

The sampling campaign was divided into two parts: a one-time sampling blitz and a longitudinal monitoring effort. The sampling blitz involved the measurement of 15 different CT

systems in the span of two weeks. The longitudinal monitoring sampling included 8 visits between May and August 2022 at three CTs, which were also included in the blitz. Measurements were conducted under varying atmospheric conditions, but never during heavy rains or thunderstorms. Temperature and relative humidity were recorded throughout. More information on the sampling sites, dates and psychrometric parameters is provided in Appendix C.

Location of aerosol measurements

Aerosol droplets were characterized at different locations in and around the CTs to calculate the drift eliminator capture efficiencies (Figure 5.1). The first sampling point established the background aerosol in the ambient air, and was collected 5 to 10 meters upwind from the CT. The second measurement point was located inside the CT and represented the concentration of generated particles per liter of air inside the CT. The third sampling point was at the exhaust air outlet of the CT and was a measure of the particles released to the environment. One liter of water from the CT basin was sampled in sterile low-density polyethylene bottles for physico-chemical assessment and microbial detection.

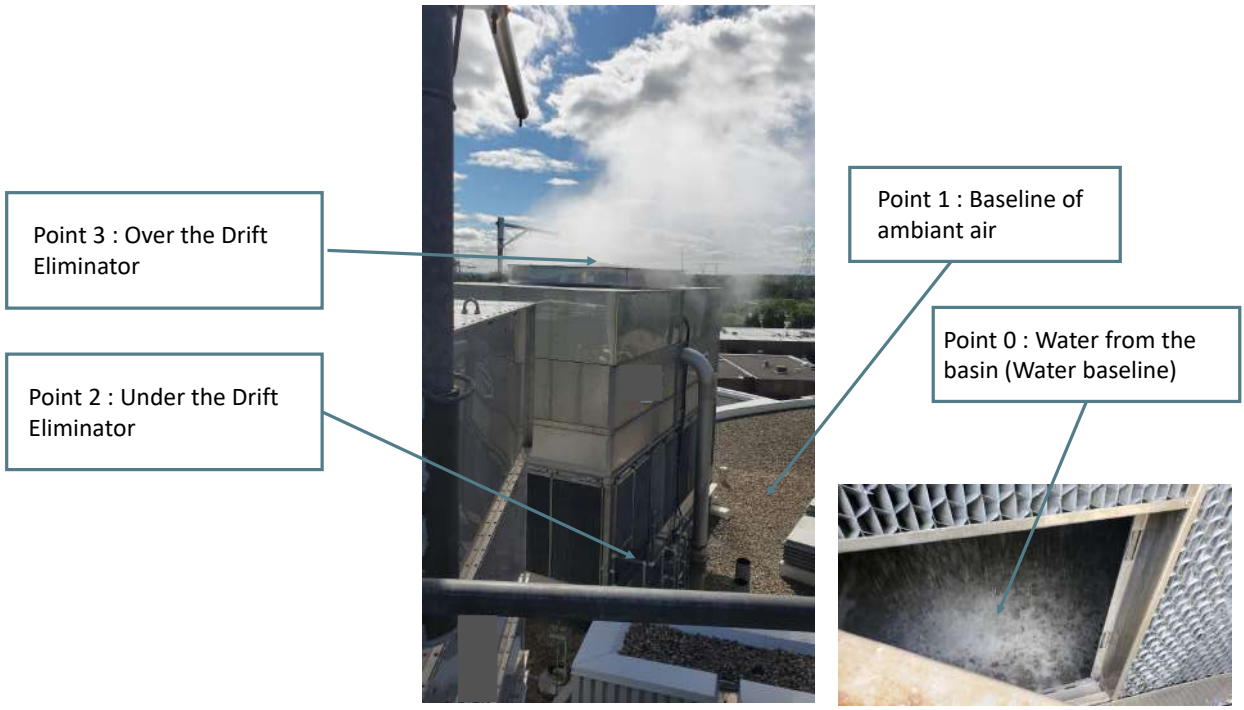

Figure 5.1 Sampling points on the CTs, showed for S1.

Optical aerosol spectrometer

Aerosol size distributions were obtained using an optical aerosol spectrometer (MiniLAS model 11-R, GRIMM Aerosol Technik Ainring GmbH & Co, Ainring, Germany), hereafter called the OAS. This instrument measures the size of individual particles from light scattering [142]. Particles with a size ranging from 0.25 to 32 μm were measured. A 1.5 m sampling line was connected at the inlet for particle measurements. The inlet flow into the instrument was 1.2 L/min. Repetitive measurements were taken every 6 seconds for 3 minutes at each sampling point and repeated 3 times, then averaged in a single size distribution per measurement point. Particles were completely dried before being measured to avoid saturation of the sampling instrument with the high humidity present within and around the CT, using a desiccator column filled with silica gel beads (Model DDU 570, TOPAS-GMBH). The actual wet size distribution at the measurement point was then back calculated from the dried size distribution according to the methodology of Lefebvre et. al [193].

Cascade Impactor

The aerosol flow was sampled with a Cascade Impactor (Dekati® Low Pressure Impactor DLPI+). Each stage was cleaned with ethanol and water before measurements. Particles with sizes ranging from 0.16 to 10 μm were collected on 0.05 μm Millipore filters disposed on 10 different stages based on their aerodynamic diameter, with a sampling flow rate of 10 L/min for 30 minutes [193]. The samples were drawn through a flexible plastic tube with a diameter of 12.7 mm and a length of 0.6 m. The filters were pooled together into a standard liquid saline solution (0.9% w/v NaCl in MiliQ water) after the measurement.

SASS 3100

The SASS® 3100 dry air sampler (Research International, Inc., Seattle, USA) was used at an inlet flow rate of 300 L/min, allowing for larger sample volumes to be collected. It was fitted with a custom-made sampling tube of 0.025 m in diameter and 0.30 m in length to safely reach deeper into the CTs. The microbial load was collected on standard bioaerosol electret filters. Sampling was conducted at the outlet of the CT for 80 minutes. Elution of the electret filters was conducted for microbial assessment using the SASS® 3010 Particle Extractor (Research International, Inc., Seattle, USA), yielding 7 mL of solution [242]. This volume was vacuum filtered on sterile 0.2 μm (Ø47 mm) Supor® PES membranes (PALL Corp., Mississauga, ON, Canada). Membranes were then gently folded and processed within 2 hours.

Flow velocity

The flow velocity at the CT outlets was measured using a telescopic hot wire anemometer (VelociCalc Air Velocity Meter 9515, TSI, MN, USA) calibrated for instantaneous velocity [243]. The anemometer, fixed to a tripod, took five equally spaced measurements along the outlet fan radius. The volumetric flow rate was calculated by multiplying the average flow velocity by the outlet's surface area, assuming constant velocity. This rate was used to normalize aerosol particle concentrations for comparison across systems. For non-circular outlets, measurements were taken over a 1.5 m^2 area instead of the total outlet area.

Physico-chemical parameters

Conductivity (0.01-200 mS/cm) and dissolved oxygen (0-20 mg/L) were assessed with the HQ40d™ portable meter (HACH, London, ON, Canada). The probes were inserted in a beaker containing approximately 150-200 mL of a well-mixed water aliquot taken from the sample. Total dissolved solids (TDS), which refers to the combined content of all inorganic and organic substances, were estimated from the conductivity using the correlation proposed by Brown et. al [244, 245]. Two successive aliquots of 10 mL were withdrawn from the well-mixed water sample for assessment of free and total chlorine equivalent concentrations (0 to 2.00 mg/L), based respectively on the HACH DPD Powder Pillows methods 8021 and 8167, with the portable DR 2800™ spectrophotometer (HACH, London, ON, Canada). Whenever free chlorine equivalent concentrations exceeded 0.05 mg/L, one mL of sodium thiosulfate (10% v:v) was added.

Flow cytometry

Flow cytometry was conducted using a BD Accuri™ C6 Plus flow cytometer along with the BD CSampler™ autosampler (BD-Biosciences, Mississauga, ON, Canada) to enumerate total (TCC) and intact cell counts (ICC) based on the integrity of cell membranes as the viability criteria. Quantification of cells was performed in duplicate with aliquots of 300 μL per sample to discriminate between dead and live cells. TCC were stained with 3 μL of SYBR Green fluorochrome and 3 μL of a mix of SYBR Green and propidium iodide fluorochromes stained damaged (dead) cells (ICC). 3 μL of EDTA was also added to each aliquot. Before the addition of dyes, aliquoted samples were incubated at 37 °C for three minutes. Samples with dyes were incubated once again at 37 °C for 10 min in the dark. Cells were enumerated using the FL3 (670 nm) and FL1 (530–533 nm) density plots, and bacteria gating was assessed according to the EAWAG water quality template previously developed to discriminate TCC and ICC [246, 247].

qPCR

For water samples, 1 L was vacuum filtered on 0.45 μm pore size MF-Millipore™ membranes (47 mm in diameter, gridded) (Sigma-Aldrich, Oakville, ON, Canada). For aerosol droplets sampled with the SASS 3100, 7 mL of the eluted solution was filtered. The quantification of *L.p.*, *L.spp* and *L.p. SG1* DNA was conducted in triplicates by real-time qPCR according to the instructions of the microproof® *Legionella* Quantification LyoKit - LP *L.p.* Real-Time PCR kit (Hygiena/Biotechon). Fluorescence curves were recovered on the Bio-Rad CFX Opus 96 Real-Time PCR Instrument and results were expressed in genomic units (GU) per liter. For samples where inhibition was detected in only one of the triplicates, the inhibited triplicate was therefore not included in the analysis. The limits of detection and quantification were of 3 and 10 GU per reaction respectively.

5.3.3 Data analysis

Size distribution and capture efficiency

The theoretical size-dependant drift eliminator capture efficiency η_t (%) was calculated assuming spherical particles. It depends on the density of the particle ρ_p (kg/m^3), the particle diameter D_p (m), the airflow velocity U_e (m/s), the viscosity of the bulk liquid μ (kg/ms), the width of the channels of the drift eliminator w (m) and the angle of the direction change of the drift eliminator θ (°), and is given by the following equation [248]:

$$\eta_t = \frac{\rho_p (D_p)^2 U_e}{18 \mu w} \theta \tag{5.1}$$

The theoretical capture efficiencies were compared to the results from the *in situ* measurements. Equation 5.2 was used to determine the drift eliminator capture efficiency η (%), where C_o and C_u are the size-dependant concentration of particles, respectively over and under the drift eliminator, and b is the baseline concentration (particles/L_{air}):

$$\eta = 1 - \frac{C_o - b}{C_u - b} \tag{5.2}$$

The baseline size distribution was subtracted from the concentrations measured around the CTs to only consider the particles generated inside the CT.

Relationship between water and air

To ensure a consistent comparison, *Legionella* concentrations were evaluated in the bulk water of the CT or in the cumulative water sampled from aerosol droplets generated and

released from the CT. To maintain clarity throughout the article, we refer to these compared concentrations as water and airborne.

The relationship between bacteria in water and aerosolized bacteria concentrations was calculated by combining airborne size distribution assessments with qPCR detection. It was assumed that the solid mass concentration in water remained constant during aerosolization until evaporation. Using the sampled air volume, V_{air} (L_{air}), mass-based particle size distribution, D_{air} (kg/L_{air}), and total dissolved solids (TDS, kg/L_w) for each water sample, the total aerosol water volume, V_w (L_w), was calculated. This was based on particle diameter x (µm) within the OAS detection range, assuming droplet sphericity. The airborne water volume was obtained by summing the volumes from each particle concentration and diameter combination in the studied size range :

$$\begin{aligned} V_w &= \sum_{n=1}^{+\infty} D_{air} * \frac{\pi x^3}{6} * \frac{V_{air}}{TDS} \\ V_w &= \frac{V_{air}}{TDS} \int_{0.25}^{32} D_{air} * \frac{\pi x^3}{6}\, dx \end{aligned} \tag{5.3}$$

After calculating the airborne water volume, the ratio of sampled air volume to airborne water volume, R_h, was compared to the ratio of solution volume (used for microbial burden estimation by PCR) to sampled air volume, R_s, to characterize the relationship between bacteria in water and aerosolized bacteria concentrations. The airborne particle concentration per liter of water, C_w (particles/L_w), was then derived from the solution concentration assessed by qPCR, C_{sol}, using the volumetric relationship between the two media :

$$C_w = C_{sol} * R_s * R_h \tag{5.4}$$

where

$$R_s = \frac{V_{sol}}{V_{air}}; R_h = \frac{V_{air}}{V_w}$$

5.3.4 Quantitative Microbial Risk Assessment (QMRA)

The QMRA methodology was adapted from Hamilton et. al. [81, 108]. It assumes that *L.p.* exposure risks are based on the emission of potentially contaminated aerosol droplets from a CT, the atmospheric dispersion of the generated particles, the inhalation and deposition of the particles in the alveoli depending on their size, and finally the pathogenic dose-response specific to *L.p.*. In this study, the emission rate of *L.p.* Q_{em} (particles/s) was calculated considering the pathogen concentration per volume of water C_w (particles/L_w) as well as

the volumetric air flow rate of the CT $\dot{V}_{air}$ (L_{air}/s), the drift eliminator capture efficiency (η [-]), the ratio of bacteria in water transferred to the airborne aerosol droplets, the volume of water aerosolized V_w (L_w), the volume of air sampled by the OAS V_{air} (L_{air}) and the ratio of accuracy for the detection method R_m [-]:

$$Q_{em} = \frac{C_w \dot{V}_{air} V_w R_{wa} \eta}{V_{air} R_m} \tag{5.5}$$

The QMRA model considers the emission rate of inhalable droplets in the 1-10 μm size range, which was used for the aerosolized water volume. Parameters for the dose-response model, the inactivation during dispersion model, and the inhalation model were taken from Hamilton et. al [81]. Exposure was assumed to last 1 hour, and daily risks were calculated as per Signor and Ashbolt [249] to account for CT variability (Table C7 - Appendix). Daily DALY was calculated by dividing the annual DALY by 365 [249]. A common health based target for infection rates in drinking water is 10^{-4} infections per person per year [81,101,250]. The daily DALY target of 2.7×10^{-7} was calulated as 10^{-4} divided by 365 days per year, as recommended by [249].

5.4 Results and discussion

5.4.1 Space-time variability of aerosol emission rate

The size distributions of aerosol discharged from the 15 CTs sampled during the blitz, sorted by total emission rate in the inhalable size range, are displayed in Figure 5.2 a. A large variability was observed in the size-dependent aerosol concentration from each CT. S2, S11, S21, S22_1, and S22_2, exhibited similar average emission rates of approximately 10^{12} particles/s, while disparities of over three orders of magnitude were evident between S16 and S6B, the CTs with the highest and lowest emission rates, respectively. The distribution across droplet sizes remained relatively constant, suggesting that when a CT produces more droplets, it does so for all sizes. This phenomenon is typical of the main generation mechanisms associated with CTs (bubble bursting, droplet impaction and atomization) [3, 26], and consistent size distributions were also observed in *Legionella*-laden aerosol droplets generated through nebulization [66].

The large variability observed in the emission rates was expected, as each CT system's capacity is set to meet its building's energy needs. However, multiple factors can influence CT emission rates, such as capacity, operating rate, and the drift eliminator's efficiency in capturing aerosol droplets. For instance, combined capacity and operating rate influence the airflow that carries droplets out of the CT and into the environment. Discharge flow rates varied between 5- to 10-fold across the 15 systems (Figure 5.2 b). The emission rate of S16 was exacerbated by its high airflow, whereas S22_2 displayed an average emission rate across the monitored CTs due to its low airflow, despite generating the third-highest volumetric droplet rate at almost 10^6 particles/$L_a$ir (Figure 5.2 c).

Particle emission rates varied considerably over time for the three CTs monitored longitudinally (Figure 5.3 a). Despite similar mean emission rates and total particles emitted, fluctuations of more than an order of magnitude occurred across measurements. For instance, S1 discharged over 10^8 particles/s during the June 2nd sampling, compared to approximately 10^6 on August 16th. However, the size distribution remained relatively constant week to week, regardless of operating rate differences (Figure 5.3 b).

As the CT operating rate only partially explains the large spatio-temporal variability in the emission rate, other factors, such as drift eliminator capture efficiency and bacteria transfer rates from CT water to discharged aerosol, are investigated in the following sections.

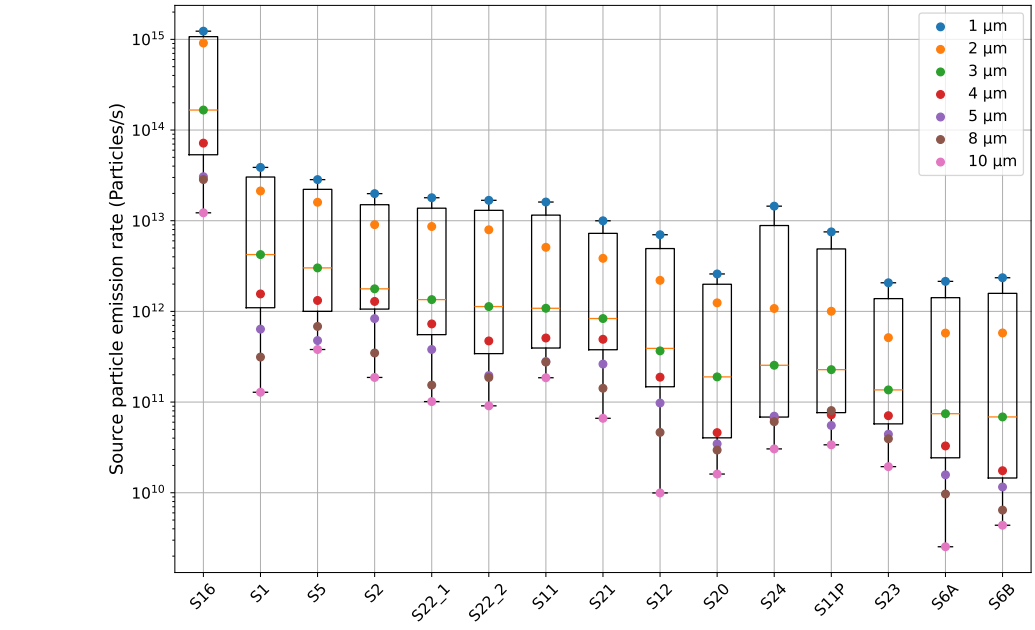

(a)

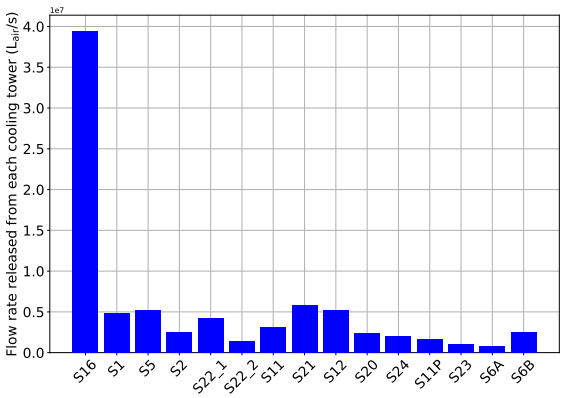

(b)

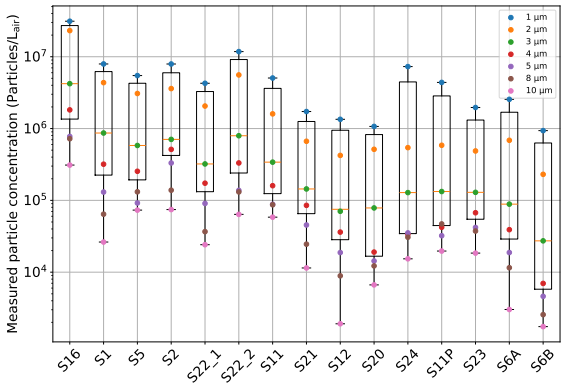

(c)

Figure 5.2 a) Comparison of the average emission rate for the sampled CTs (n=3). The box's central mark shows the median, while the bottom and top edges represent the 25th and 75th percentiles. Whiskers extend to the 5th and 95th percentiles, with points beyond considered outliers. b) Air flow rate at the outlet of the CTs during the blitz. c) Measured particle concentration for the inhalable size range for the CTs sampled during the blitz.

5.4.2 Drift eliminator capture efficiency

Site-specific drift eliminator capture efficiency varied over time for the three CTs monitored longitudinally (Figure 5.3 b). During weeks 4 and 5 of the longitudinal monitoring (July 12th to August 4th) notably poor capture efficiencies were noted for S1 and S11, corresponding periods of high operating rates ($> 90\%$). A potential association between efficiency variations and wet-bulb temperature, typically used as a design criterion for CTs [251], was explored. Weeks 4 and 5 were associated with wet-bulb temperatures above 18 °C, corresponding to high thermal loads and thus conditions in which evaporative cooling is less efficient [28] (Figure 5.4 a). The drift eliminator capture efficiency of S1 was observed to be linearly proportional to the CT operating rate for inhalable aerosol droplets (Figure 5.4 b). Thus, when CTs operate at high capacity, the ability of drift eliminators to capture inhalable aerosol particles decreases.

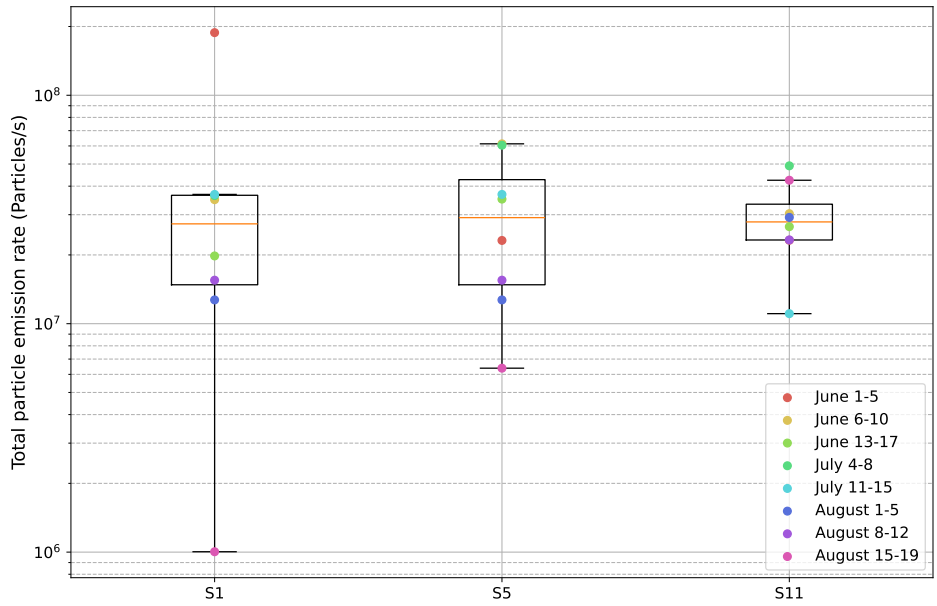

(a)

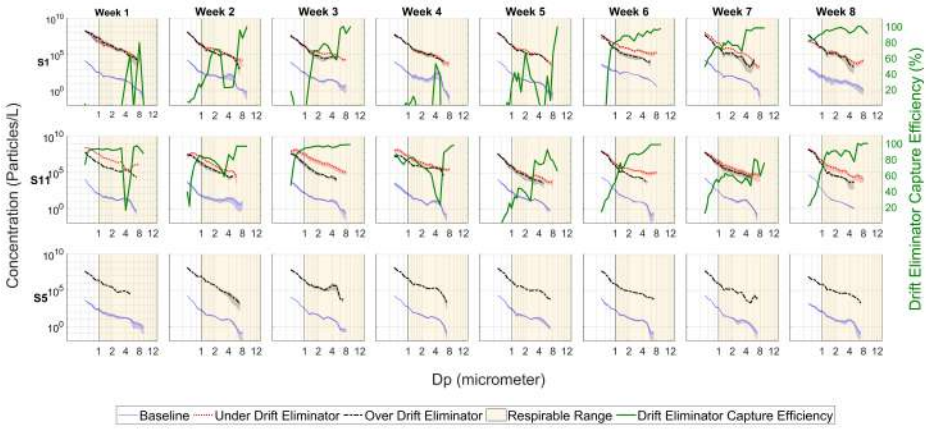

(b)

Figure 5.3 a) Comparison of the average emission rate for the three monitored CTs through the 8 sampling weeks (n=3). b) Comparison of the size distribution and drift eliminator capture efficiency from the longitudinal monitoring. Results are averaged over three measurements (n=3). Shaded areas show the standard deviation within the repeated runs.

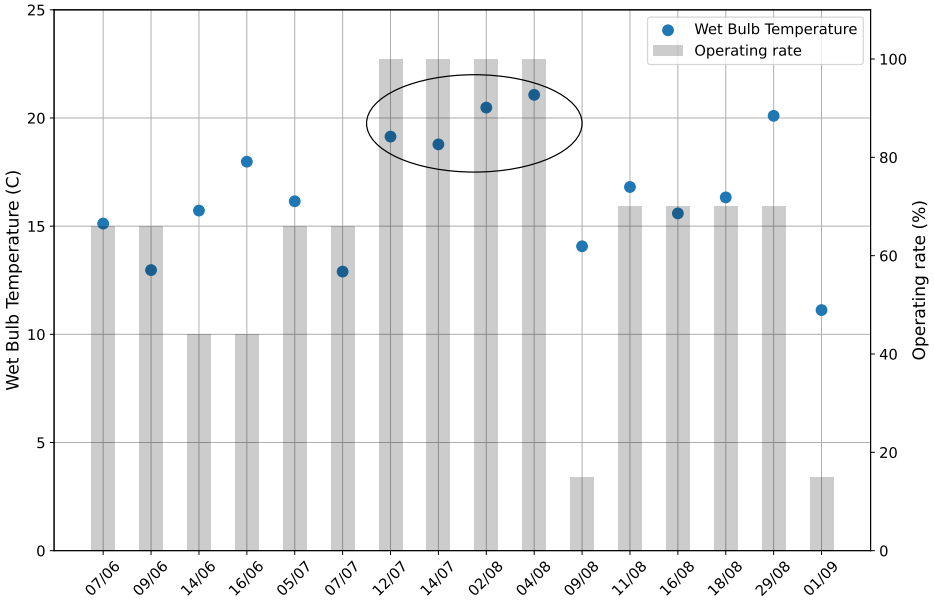

(a)

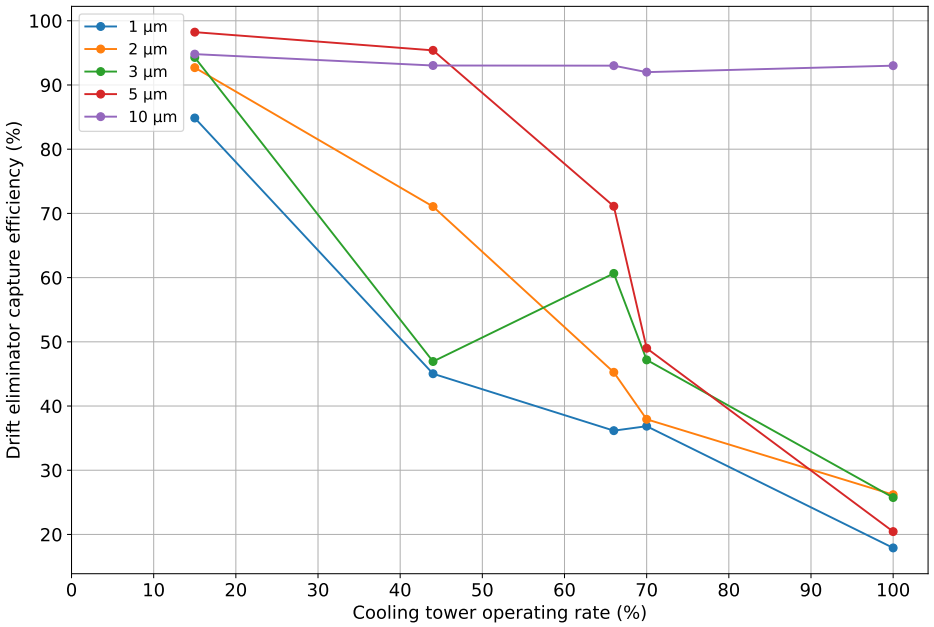

(b)

Figure 5.4 a) Wet-bulb temperatures and the operating rates of S1 monitored during the sampling campaign. The circled datapoints represent periods of high temperature and relative humidity. b) Drift eliminator capture efficiency for different droplet sizes as a function of CT operating rate for S1.

The average drift eliminator capture efficiency of the CTs monitored longitudinally, as a function of droplet diameter, was compared with the theoretical collection efficiency calculated using equation 5.1 for the average mass distribution collected in towers S1 and S11 (Figure 5.5). S1 was fitted with a cellular-type drift eliminator, while S11 used a blade-type drift eliminator, with $U_e = 3$ m/s, $\mu = 0.3$ kg/ms, $w = 2.2$ cm, $\theta = 53°$ for the cellular type, and $w = 2.54$ cm, $\theta = 35°$ for the blade type. These parameters were representative of the drift eliminators installed on S1 and S11.

Experimental results confirm the theoretical expectation that cellular-type drift eliminators would be more efficient at capturing particles than blade-type drift eliminators, mainly due to increased surface area [53, 59, 238]. The blade type drift eliminator from S11 exhibited approximately 20-30% better capture efficiency than S1 for particles sized between 1 and 10 μm (Figure 5.5). However, the large variability in capture efficiency (Figure 5.3 b) underscores the importance of CT operating conditions on capture efficiency. Additionally, as depicted in Figure 5.2 a, a considerable quantity of droplets was discharged into the environment despite the presence of drift eliminators. Thus, due to their inherent design limitations in capturing inhalable droplets and reduced efficiency at high operating rates, drift eliminators appear insufficient to effectively mitigate exposure risks.

Regardless of operational conditions, theoretical capture efficiencies for both types of drift eliminators remained below 80% for droplets in the 5-10 μm size range and below 40% for particles smaller than 5 μm. While both types generally followed theoretical trends, they demonstrated capture efficiencies up to 40% higher than predicted in the 1-10 μm size range. Drift eliminators are designed to balance power consumption and water losses, with manufacturers claiming they can capture over 99% of the mass of water discharged from CTs [252]. Drift eliminators achieve this goal by capturing larger droplets to conserve water. Despite droplets in the 1-10 μm size range constituting the majority of the total number discharged droplets (Figure 5.2 b) and being associated with *Legionella* risks, they represented only approximately 25% of the mass fraction of aerosolized water in the size range of the OAS. Interestingly, for S1, droplets sized 1-4 μm accounted for only 5% of the total mass sampled whereas droplets sized 5-10 μm accounted for 20%.

To limit *Legionella* risks associated with CTs, the target performance and resulting design of drift eliminators need to be reevaluated to enhance their capture of smaller droplets in the inhalable size range. Improvements of drift eliminators should consider the trade-off between all aspects of CT operation including energy usage, including water conservation, head losses due to inertial disturbances in the flow. The incorporation of *Legionella* into very small

aerosol droplets (1-2 μm) remains to be investigated, considering the size of *Legionella*. As the droplets sized 1-4 μm accounted for a small fraction of the sampled mass of water, improving the capture of the droplet sizes ranging between 5-10 μm could be prioritized focus to reduce exposure risks. Nonetheless, since the theoretical capture model was conservative for the inhalable range, it can serve as a default value when considering the impact of operational range on potential removal of inhalable droplets.

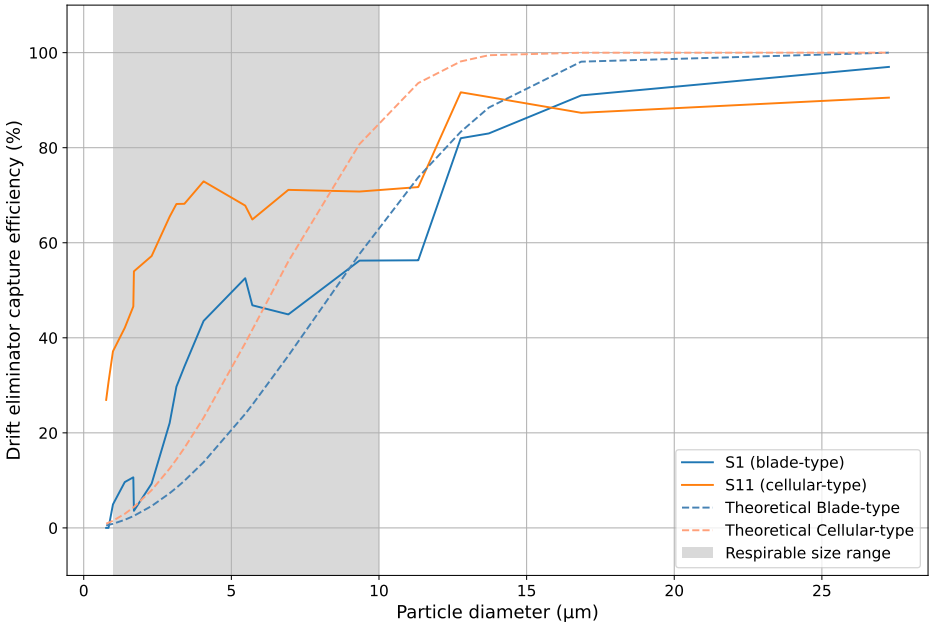

Figure 5.5 Comparison of the average drift eliminator capture efficiency from the sampled CTs with theoretical calculations. The grey section of each plots represents the size range between 1 and 10 μm.

5.4.3 *Legionella* transfer from water to aerosol droplets

Water *L.spp.* concentrations measured by qPCR for the 15 investigated CTs ranged from 10^2 to 10^5 GU/L during the monitoring of S1, S11, and S5 (Table C3 - Appendix).

Figure 5.6 a and b show flow cytometry and qPCR results for CT water and discharged aerosol droplets across the 15 sampled CTs. Airborne and water concentrations refer to bacterial concentration in water or in the water volume in a given volume of air (bacteria/L_{water}). On average, airborne bacteria concentrations were within one order of magnitude of water concentrations for both flow cytometry and *Legionella spp.* qPCR results. *L.p.* and *L.p. SG1* were undetected in aerosol samples, likely due to low water concentrations. Longitudinal monitoring also revealed bacteria concentrations in water consistently within one order of magnitude of airborne concentrations (Figure 5.6 c). Notably, data points clustered along the diagonal ($R^2 = 0.89$), indicating a strong correlation between airborne concentrations and in the water, with no systematic enrichment observed. These findings align with previous studies reporting similar bacterial concentrations during aerosolization [253–255].

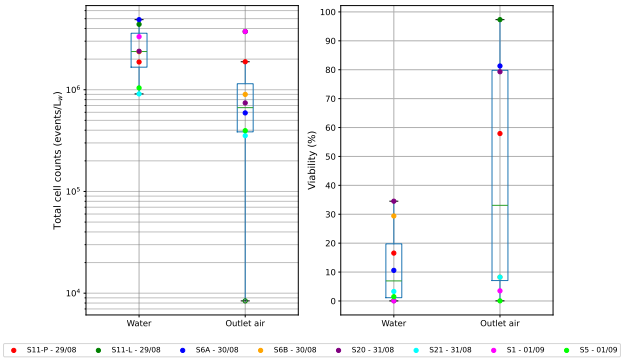

(a)

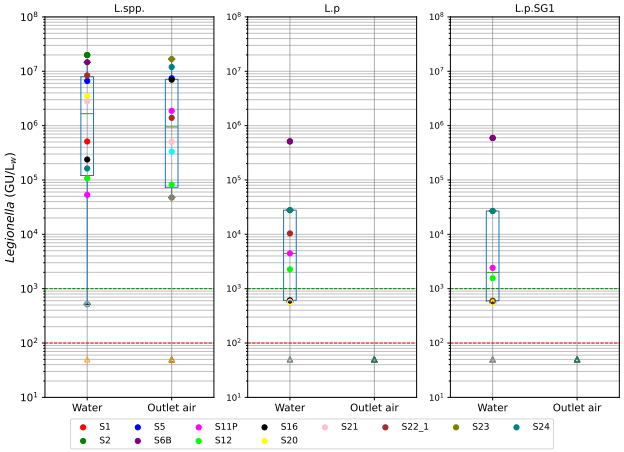

(b)

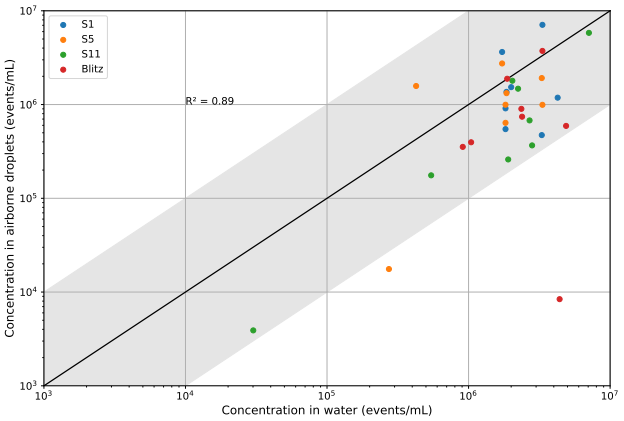

(c)

Figure 5.6 a) Flow cytometry results of total cell counts and viability ratio for the blitz sampling campaign. b) qPCR results of the detected *Legionella spp.*, *L.p.* and *L.p. SG1* for the blitz sampling campaign. Green and red dashed lines represent the quantification and detection limits, with points below these limits shown as open-faced or triangular markers. c) Bacterial concentration in airborne droplets versus CT water. The shaded area indicates a difference of less than one order of magnitude. The coefficient of determination (R^2) was calculated using logarithmic values.

Assessment of airborne viability revealed significant spatial variability (Figure 5.7 a). Notably, S11 exhibited nearly no viability in water and close to 100% airborne viability, while S6A showed approximately 10% viability in water and 80% airborne viability. Overall, airborne viability was generally higher than viability in water. Residual chlorine equivalent concentrations (0.2 to 2 mg/L) were measured in most CTs, potentially explaining lower viability in water samples (Figure 5.7 b). Although extensive work links chlorine residual to viability in water, its effect on airborne viability within aerosol droplets is unclear [256]. Chlorine is likely to be stripped during aerosolization and early transport due to the large surface area of aerosol droplets. This could be contributing to the higher airborne viability. Viable bacteria also tend to agglomerate at the water-air interface due to surface tension effects and increased oxygen content, which could also be a contributing factor [3].

Multiple studies suggest that ICC determined through flow cytometry is applicable to qPCR assessments [115, 257–259]. Therefore, airborne *Legionella* viability can be assumed to be reflected by the viability ratio measured by flow cytometry. However, the absence of a correlation between airborne viability and chlorine residual, combined with high temporal variability and a limited sample size, prevented the fitting of a statistical distribution to airborne viability data. To provide a conservative risk assessment, a viability associated with the maximum observed value (approximately 100%) could be used as a point in time estimation. Such a conservative approach would reflect critical conditions such as inadequate treatment often cited as the cause of LD outbreaks.

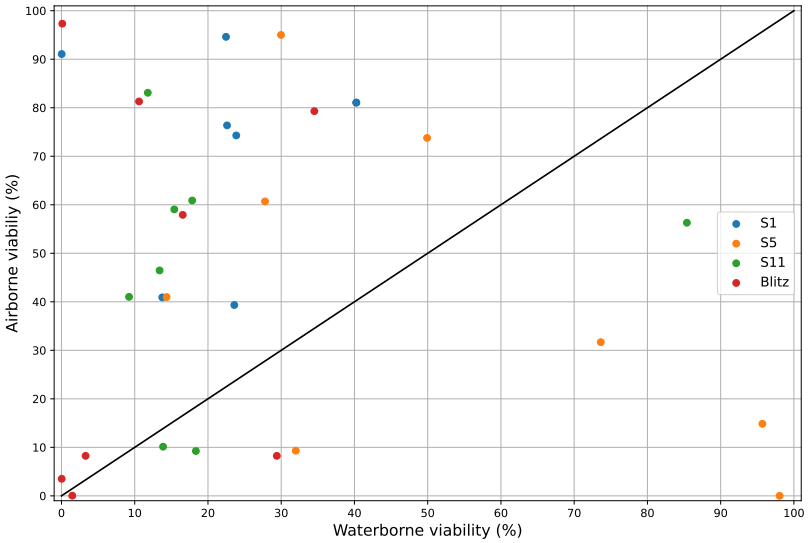

(a)

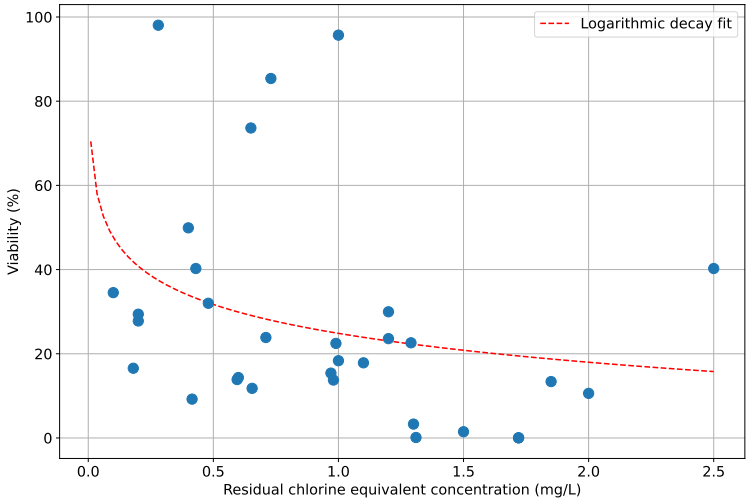

(b)

Figure 5.7 a) Airborne viability as a function of the viability in the water. The shaded area represents a difference of less than one order of magnitude. b) Residual chlorine equivalent concentration in the CT water monitored during the sampling blitz.

5.4.4 Bioburden : Viable *Legionella* emission rate

The bioburden described by Nocker et. al [115] is defined as the rate of *Legionella* discharged from CTs, thus combining both the aerosol emission rate and the viable *Legionella* concentration inside the aerosol droplets. The bioburden for *L.p.* is equivalent to the emission model in the QMRA. Theoretically, modelling it would simply involve a function of the airborne viable bacterial concentration discharged from the CT C_{air} (particles/L_{air}) and the volumetric flow rate $\dot{V}$ (L_{air}/s):

$$Q_{em} = C_{air}\dot{V} \tag{5.6}$$

However, the challenge of detecting airborne *Legionella* through qPCR (Figure 5.6 b) makes this strategy unreliable for risk assessment. Consequently, the methodology outlined in equation 5 was used to calculate the emission rate from the *Legionella* concentration in water (Figure 5.8 a). On average, between 5×10^4 and 2.5×10^8 viable *Legionella* were released in the environment per hour for S1. This emission rate was on average 10X higher than depicted in a similar study [115]. Given that even a small concentration of *L.p.* can lead to severe health outcomes near large emitters, the release of such a large number of potentially contaminated aerosol droplets raises concerns for public health, especially considering the large distance contaminated droplets can travel [78, 83].

During the periods of August 8-12 and 15-19 (Weeks 7 and 8 of the longitudinal monitoring), S1 exhibited emission rates two to three orders of magnitude lower than in preceding weeks (Figure 5.8 a). This difference can be attributed to the viable *Legionella* concentration in water and the concentration of discharged inhalable droplets. Indeed, the viability of the airborne *Legionella* was lower during these two weeks (Figure 5.6 a). Also, while the *L.spp.* concentrations in water remained similar between August 8-12, *L.p.* and *L.p. SG1* levels were below detection limits (Figure 5.8 b), explaining the lower emission rate for *L.p.* and *L.p. SG1* during this period. Conversely the lowest aerosol emission occurred between August 15-19, coinciding with lower wet-bulb temperature and accounting for the low emission rates observed across all species that week (Figure 5.2 a). Furthermore, a linear regression revealed that both factors explain most of the variability in the emission rate, yielding a combined R^2 of 0.92 (Figure 5.9 a). Individually, the concentration in water and droplet concentration had similar correlations, with R^2 values of 0.49 and 0.47, respectively (Figure 5.9 b). Thus, weekly variability of the viable *Legionella* emission rate was driven by both the concentration of *Legionella* in water and the concentration of inhalable droplets discharged.

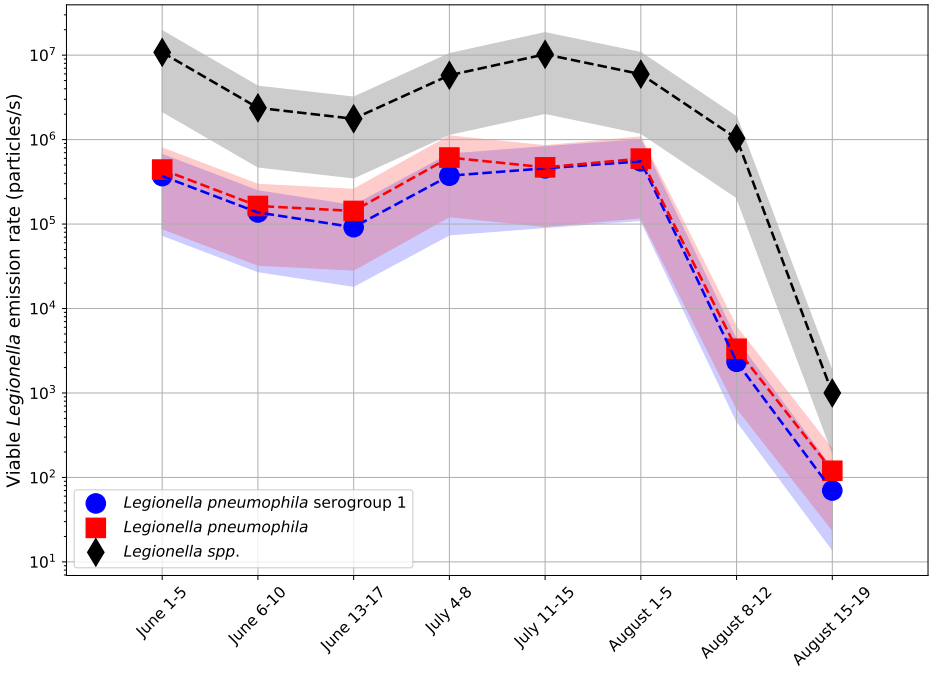

(a)

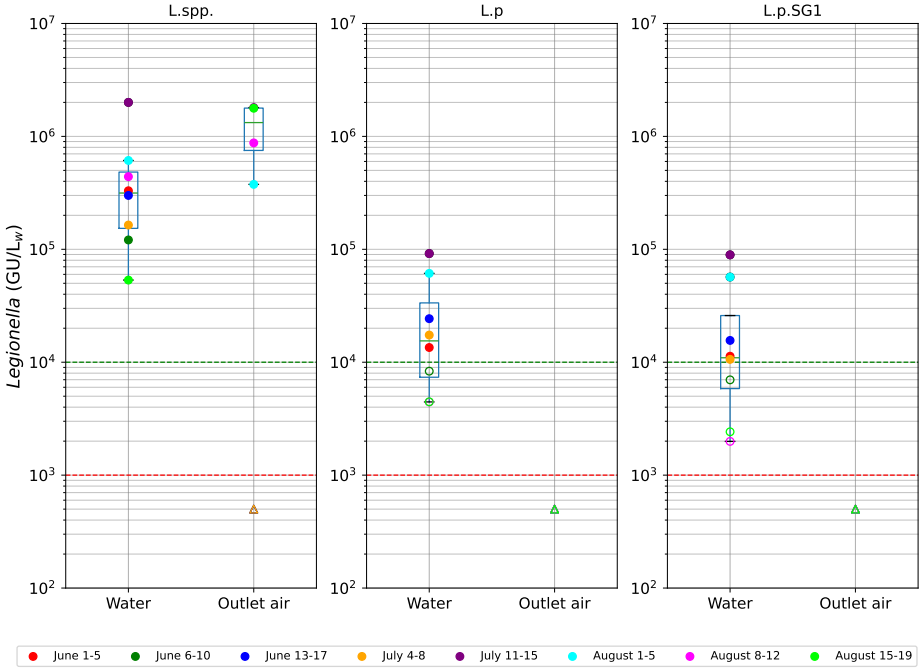

(b)

Figure 5.8 a) Viable *Legionella* emission rate from S1 during the monitoring sampling campaign. b) qPCR results of the detected *Legionella spp.*, *L.p.* and *L.p. SG1* for the monitoring sampling campaign of S1, S5 and S11. The green and red dashed line represents the quantification and detection limits respectively. Measurements below the quantification limit are displayed as open-faced scatter points. Measurements below the detection limit are shown as half the detection limit in the open-faced triangular scatter points.

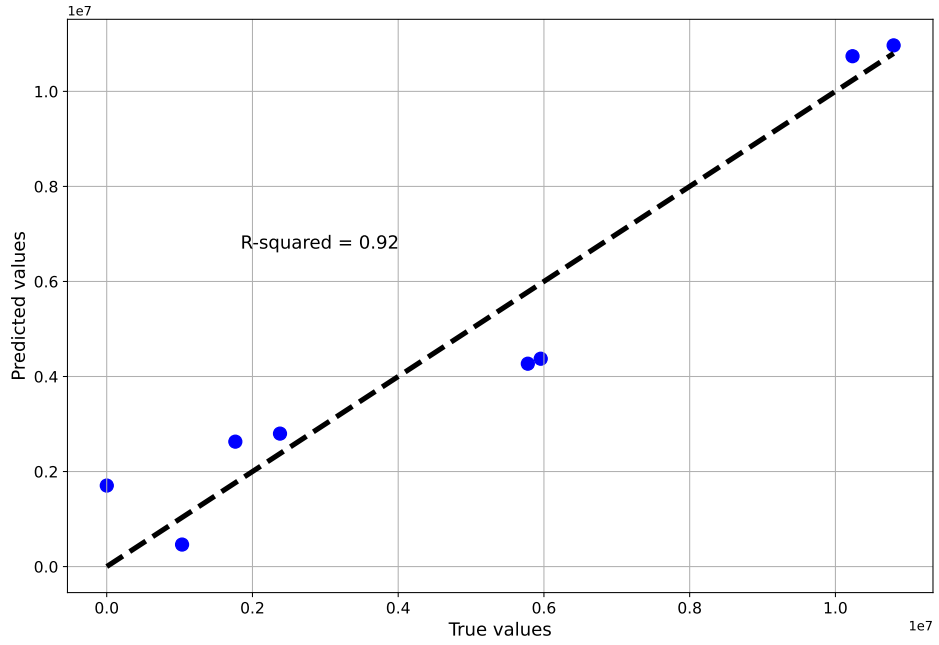

(a)

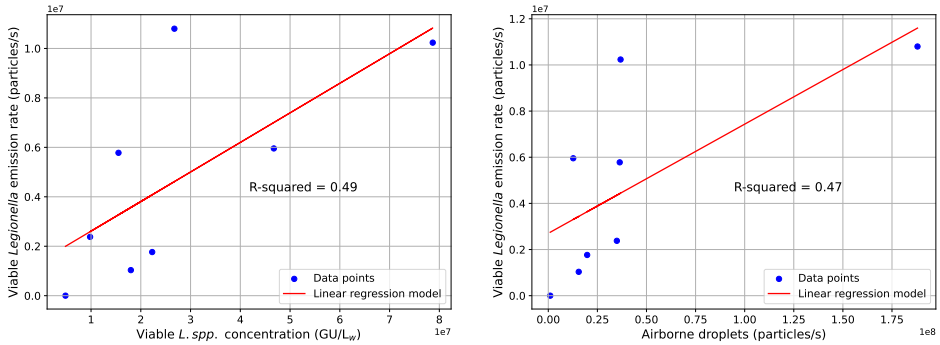

(b)

Figure 5.9 a) Linear regression of the viable *Legionella* emission rate from S1 during the monitoring sampling campaign with three features: Airborne viability, concentration of *L.spp.* in the water and Airborne droplet concentration. b) Linear regression of the viable *Legionella* emission rate from S1 with each feature individually.

5.4.5 Effect of emission rates on contamination risks

The daily Disability-Adjusted Life Year (DALY) values from the QMRA model were compared across the 15 CTs sampled during the blitz (Figure 5.10), utilizing the proposed viable *Legionella* emission rate from the previous section. Minor differences in the size distribution measured across the 15 CTs (Figure 5.2 a) did not affect infection risks, resulting in identical DALY values when using a size distribution averaged across the sampled CTs, as shown on Figure 5.10 by the overlapping of the results obtained by the proposed method using site specific size distribution (orange bars) and average size distribution (hatched bars). An average size distribution can therefore be used as a reference rather than a site specific one and still provide sufficient resolution for risk assessment.

Resulting daily DALYs can be compared to the World Health Organization (WHO) risk threshold of 10^{-6} yearly outcomes, adjusted for daily risks [260]. S6B exceeded the daily target, while DALYs for S22_1 and S16 were within the same order of magnitude as the target (Figure 5.10). In contrast, the DALYs for S1, S6A, and S11P were three orders of magnitude lower, suggesting low associated risks. However, these risk estimates are derived from the results obtained in a one-time sampling event, not reflective of the range of risk that can be encountered throughout the year.

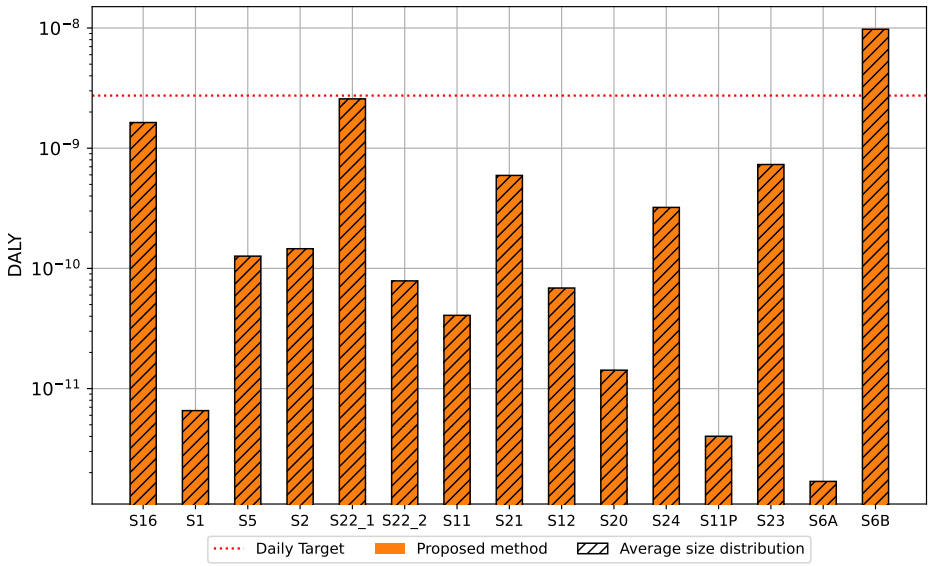

Figure 5.10 Daily QMRA results (DALY) The proposed method's DALY, using individual droplet size distributions, is compared to results using the average distribution. The red dashed line in the figure indicates the WHO target of 10^{-6} yearly outcomes [260], adjusted for daily risks.

The combination of aerosol emission rates and viable *Legionella* concentrations directly im-

pact risks. For example, although S6B and S16 displayed a difference of almost 3 orders of magnitude in their emission rates (Figure 5.2 a), their DALY values were within the same order of magnitude. Further investigation into their QMRA results highlighted that the viable *L.p.* concentration was nearly three orders of magnitude higher in S6B than in S16. In contrast, S16 discharged over 10^{16} inhalable droplets per second, compared to 10^{13} for S6B. Moreover, S6A had a much lower *L.p.* concentration and exhibited DALY values three orders of magnitude lower than S6B. This example underscores the significant impact of effective water management [32, 101, 236, 237] and highlights the importance of both viable *L.p.* concentration and aerosol emission rates regarding exposure risks.

The original QMRA model by Hamilton et al. effectively identifies the impact of *L.p.* concentration in water on risks [81] (Figure C1 - Appendix) but uses a fixed transfer coefficient. As a result, when comparing with DALY values obtained with the proposed method, results for S6B were within the same order of magnitude, while S16 showed a two-order-of-magnitude difference. This indicates that using a fixed transfer coefficient for aerosolized inhalable droplets, as hypothesized in the original model due to a lack of empirical data, does not capture the wide range of contaminated aerosol emissions. By directly measuring the size distribution and concentration of droplets from various CTs, the novel methodology presented in this study can reflect more accurately the varying aerosol emission conditions encountered in the field.

The effect of the aerosol emission rate on the risks could explain why CTs with viable *Legionella* concentrations below action thresholds were still identified as the source of outbreaks in multiple locations (Norway, Netherlands, and China) [8, 9, 79]. In these cases, exposure was higher than suggested by the *Legionella* concentration in water due to large quantities of inhalable aerosol droplets discharged into the air. These findings have important implications for CT management as they emphasize the role of drift eliminators as a crucial last barrier before aerosol discharge into the environment, especially in periods of elevated *Legionella* concentrations.

When using QMRA to assess the risks associated with a single system, it is important to consider the wide variations of *Legionella* concentrations and of emission rates that can typically occur over time. Single point assessments may not be representative of the risks associated with a specific cooling tower.

Weekly variations of up to two orders of magnitude were observed (Figure 5.11), which was previously reported for individual CT systems [79–81, 115, 235]. These variations indicate that *Legionella* levels may exceed action thresholds while remaining undetected between

regulatory sampling events if the time interval between samplings is large [239].

The variability of the daily probability of infection and DALY were estimated ffrom longitudinal monitoring of three CTs (Figure 5.11). Results show strong spacial en temporal variability. The mean daily probability of infection was 3×10^{-5} for S1 and 6×10^{-6} for S5, both exceeding the daily target by at least an order of magnitude. S11 also had exceedances, but its mean daily probability was only slightly below the threshold. This indicates a potential populational burden on the probability of infection, but more importantly high DALY impact. Indeed, DALYs are typically considered more stringent risk assessment as they consider the severity of the health outcomes of infections [101]. S1's mean DALY was above the daily target (Figure 5.11), while the blitz sampling reflected the lowest value recorded during monitoring (Figure 5.10). This underscores the importance of longitudinal assessments for comprehensive risk evaluation. S5's mean DALY was approximately at the daily target, with exceedances for S11 as well. Consequently, QMRA indicates significant mean exposure risks for the three CTs monitored longitudinally, despite undetectable viable *L.p.* in the air.

DALY values at least an order of magnitude larger than all other values, and categorized as statistical outliers in the boxplot were observed during the longitudinal monitoring of the three CTs (Figure 5.11). These DALY values can statistically be categorized as extreme values according to the definition of Haan and Ferreira, as they exceed the 95th percentile of the distribution [261]. Each of the three systems experienced at least one extreme value, but during different weeks of the longitudinal monitoring. For instance, while S11 displayed an average DALY more than one order of magnitude lower than the threshold, an event still exceeded it in the week of June 13-17. This extreme value can be explained in retrospective by a higher measured aerosol emission rate during this week. By definition, extreme values are rare events, but they are also hard to predict statistically [261] and their importance in the context of airborne transmission lies in their potential to drive sporadic cases of *Legionella* infections [262–264]. Consequently, the potential for extreme values to increase the risks associated with CTs suggests that QMRA should be conducted under conditions where the system operates at maximum capacity and pathogen concentrations are at their peak.

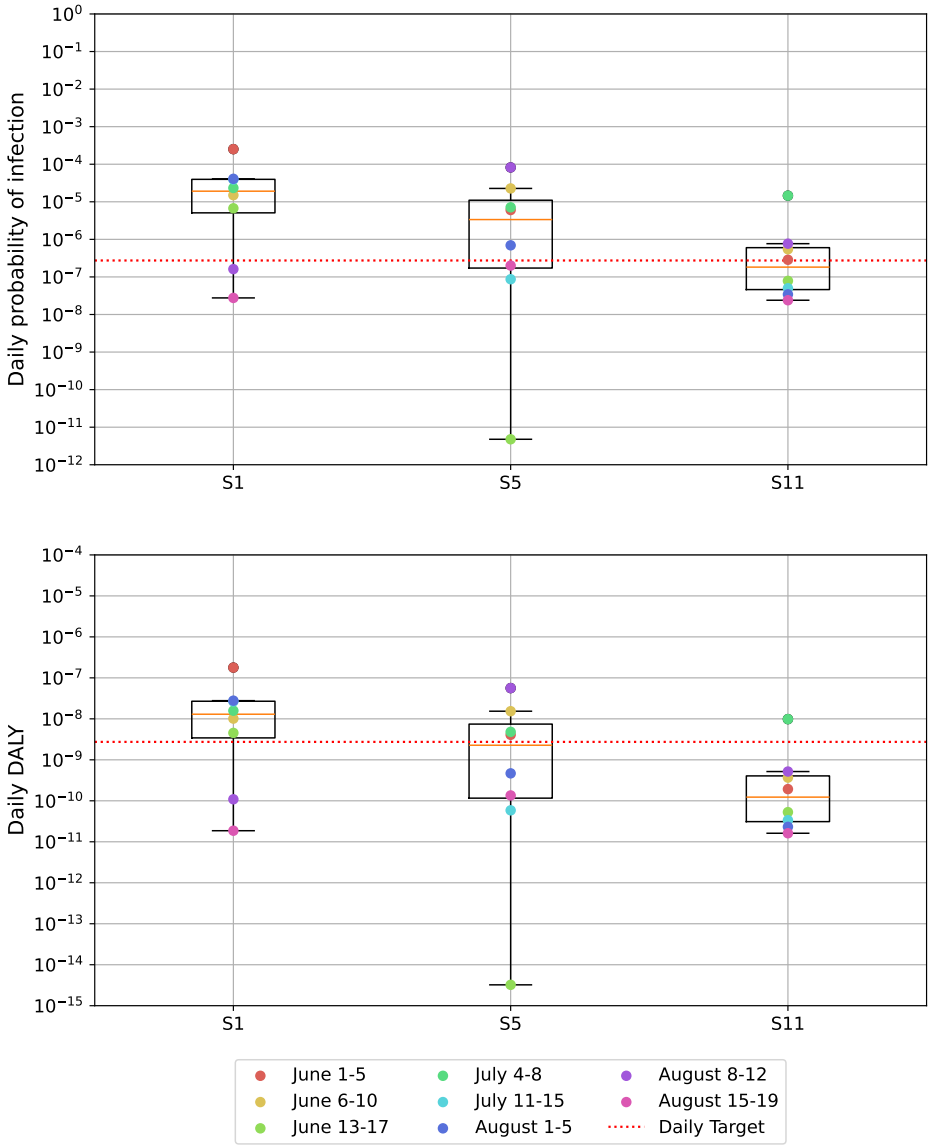

Figure 5.11 QMRA results for CTs S1, S5, and S11, showing daily risks against targets for annual infection probability and DALY.

5.4.6 Generalized QMRA emission model

The improved emission model proposed in this study requires detailed aerosol measurements, which may limit its wide application. Building on the recent QMRA models [101, 108, 240], a generalized emission model with an improved and more conservative emission rate, default aerosol sieze distribution and drift eliminator efficacy is proposed. This streamlined approach can help operators assess more effectively exposure risks for individual CTs and adopt appropriate risk mitigation strategies.

Typically, operators have access to information regarding the operating rate, the concentration of *L.p.* in the water, and the capacity of their system. The generalized emission model Q_{em} (particles/s) can be tailored using these accessible parameters. Following the trend of Figure 5.4 b, a negative sigmoid function can accurately describe the drift eliminator capture efficiency η (-) according to the average operating rate O_p (-) which ranges between 0 and 1 (Equation 5.7).

$$\eta = \frac{1}{1 + e^{((2e)O_p - e)}} \tag{5.7}$$

The discharge rate D_r (L_w/s) represents the quantity of aerosolized water in the form of droplets in the 1-10 μm size range. The extensive dataset generated during the blitz sampling campaign can be used to define multiple options for the discharged rate according to the size of the CT and its operating rate (Table 5.1). The average of the operating rate of the CT O_p (-) can also be considered. The ratio of accuracy of 0.7 for the detection method R_m (-), introduced by Hamilton et. al in their QMRA model, must also be considered so as to not underestimate the risks [81]. The viability rate R_v (-) of the airborne *L.p.* can be simply represented by the Gaussian distribution presented in section 3 and randomly selected from the probability density function of the Gaussian viability distribution (Figure 5.7 c). The generalized emission model Q_{em} (particles/s) is therefore given by:

$$Q_{em} = \frac{C_w D_r O_p R_v (1 - \eta)}{R_m} \tag{5.8}$$

The proposed generalized emission model was compared with the methodology of Hamilton et al. (Figure 5.12). The proposed generalized model predicted a higher emission rate for 12 of the 15 sampled CTs. The emission rates obtained with the proposed generalized model were up to four orders of magnitude higher than the original model. The only three instances where the original model predicted a higher emission rate than the proposed model were for

Table 5.1 Emission rate as a function of the CT capacity

Capacity (Tons)	Emission rate D_r (L_w/s)
50 (Small-size)	0.01
500 (Medium-size)	0.3
5000 (Large-size)	0.9

S11P and S6A during the sampling blitz, as well as one instance during the longitudinal monitoring of S1. These values were associated with the lowest DALY values and were observed during colder days of the sampling campaign (Figure 5.10 and Figure 5.11). The proposed generalized emission model is thus conservative in terms of risks and can be used as the emission model in the QMRA methodology of Hamilton et. al [81] to obtain an estimate of the exposure risks for CT operators and surrounding population.

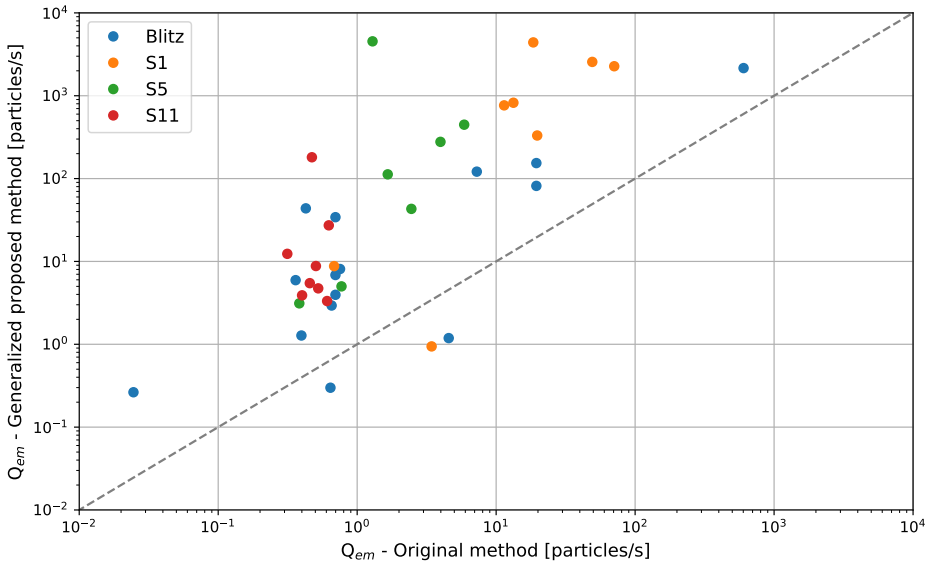

Figure 5.12 Proposed generalized emission model compared with the methodology of [81]. The diagonal line represents a perfect fit between the two models.

5.4.7 Risk mitigation strategies

The combined effect of the aerosol emission rate and the concentration of viable *Legionella* on the exposure risks suggests that a multifaceted approach is essential to mitigate the risks associated with the airborne transmission of *Legionella* from CTs. Current guidelines only consider the *Legionella* concentration in water and typically require periodical, usually monthly sampling [104]. Our results show that weekly variations of *Legionella* concentrations and aerosol emission rates can lead to rapid and frequent changes in LD risks.

Extreme events should be considered in the risk assessment by considering systems operating at maximum capacity and elevated pathogen concentrations documented on site. Collectively, these risk mitigation strategies can serve as proactive measures to curtail the airborne transmission of *Legionella* from CTs and safeguarding public health.

The proposed generalized QMRA model can easily be used by a CT operator in the absence of site specific aerosol measurements. This simplified approach combines a conservative default emissions rates based on capacity and site specific historical peak concentration of viable *Legionella*. The model output could guide water treatments and CT improvements to meet the health-based thresholds recommended to lower the probability of infection and the DALY.

The following risk mitigation strategies are thus proposed based on the results of this study:

First, implementing a robust and stringent control regime maintaining low *Legionella* concentrations in water is is a critical element of risk control. Furthermore, control should be conducted at a point representative of water entering the cooling tower (not the basin) to provide early detection of deviations and prompt intervention.

Second, drift eliminators should be redesigned to increase their capture efficiency for droplets in the inhalable size range, specifically in the 5-10 μm size range. This can be achieved by increasing the surface area of the drift eliminators and enhancing the flow deflections, while considering the trade-off between energy usage and head losses due to inertial disturbances. Each drift eliminator should be aerodynamically customized for a specific CT and the design point should be set to the maximum operating rate of the system.

Third, CTs should rarely operate above 50% of the operating rate to minimize particle emission in the inhalable range. To maximize the current capture efficiency of drift eliminators for inhalable droplets, another CT can be activated when the operating CT exceeds 50% of the operating rate. Even if maintained and monitored regularly to ensure optimal performance, drift eliminators should not be assumed to provide a large reduction in the exposure risks as peak cooling tower working capacity.

5.5 Conclusions

- The large scale *in situ* sampling campaign conducted on 15 CTs provided evidence to improve risks assessment and define risk mitigation strategies.
- Longitudinal monitoring of three CTs highlighted major weekly variations in *Legionella* concentrations (up to two orders of magnitude) and aerosol emission rates (up to three

orders of magnitude) can lead to rapid changed in LD risks.

- When CTs were working at high capacity, drift eliminators lost their ability to capture aerosol particles, specifically small particles in the inhalable size range.
- For QMRA analysis, airborne *Legionella* concentration within the same range as the concentrations found in water can be considered. The maximum observed value (100%) can be used as a conservative estimation of the airborne viability for conservative risk assessment.
- Risk assessment must consider both the concentration of viable *Legionella pneumophila* and the aerosol emission rate.
- The potential for extreme values to significantly influence the risks associated with CTs suggests that QMRA should be conducted under conditions where the system operates at maximum capacity and concentrations in water are at their peak.
- A generalized QMRA emission model can be used by managers to estimate the magnitude of the exposure risks and identify risk mitigation strategies.

Funding

This research was supported by a NSERC Alliance Grant (ALLRP545363/2019), Polytechnique Montréal. Xavier Lefebvre is supported by the Hydro-Québec excellence scholarship as well as a NSERC scolarship (ES D) with a FRQNT supplement (B2X).

Data Availability

Data that support the findings of this study are available from the corresponding author upon reasonable request. The authors declare no competing interests.

Acknowledgements

We want to acknowledge the contribution of Yves Fontaine, Tetiana Elyart, Julie Philibert, Mélanie Rivard and Jacinthe Mailly. This project would not have been possible without their help in the laboratory, field support and training. Special Thanks to the study sites managers for access to their building.

CHAPTER 6 ARTICLE 3: EVAPORATION OF AEROSOL DROPLETS FROM CONTAMINATED COOLING TOWER WATER

Submitted to *Physics of Fluids* on October 30 2024

By
Xavier Lefebvre, Mathieu Chartray-Pronovost, Caroline Duchaine, Emilie Bedard, Michèle Prévost and Etienne Robert

6.1 Abstract

. The evaporation dynamics of water-based aerosol droplets carrying pathogens such as *Legionella* from cooling towers is critical for assessing the risks of airborne transmission. Yet the evaporation of contaminated aerosol droplets remains poorly understood, and is often overlooked by current risk assessment models. Changes in water properties such as viscosity and surface tension, induced by the presence of non-volatile solids or contaminants, affect the evaporation time, the droplet nuclei size, and the time resolved size evolution. The effect of these parameters was experimentally and analytically studied. Surfactants lowering surface tension introduced non-linearity in droplet size evolution, extending evaporation time by up to 14% and halting it at high concentrations. Increased viscosity delayed evaporation onset without affecting nuclei size, which remained around 8-9 μm compared to 0.5 μm for reference water droplets. High concentration of solids, covering over 60% of the droplet surface, nearly doubled the evaporation time and increased nuclei size to 20 μm. Existing evaporation models do not fully account for temporal size changes and the variability in nuclei size due to solids concentration. Improving evaporation models and incorporating them into microbial contamination risk assessments is critical to develop effective mitigation strategies, such as using efficient drift eliminators for cooling towers.

6.2 Introduction

The global challenge of airborne disease transmission has emphasized the need to improve our understanding of diseases spreading through aerosol pathways. This includes transmission originating from human activities (anthropogenic) or engineered water systems harboring pathogens [265]. Waterborne diseases such as legionellosis pose significant challenges, particularly in light of the complex multiphase flow dynamics which govern aerosol-mediated infections [81]. This disease, associated with a 10% mortality rate, is transmitted through the airborne dispersion of aerosol droplets transporting the bacteria *Legionella*. The prevalence

of this disease has increased worldwide by 9-fold since 2000, leading to infection rates of 1.9 and 2.4 yearly cases per 100 000 people in North America and Europe respectively [266, 267]. The primary contamination source is cooling towers, efficient heat exchangers installed on large buildings [11]. They provide the right conditions for *Legionella* to thrive, and generate large quantities of potentially contaminated aerosol droplets [79]. Drift eliminators are installed at the outlet of cooling towers and serve as the last barrier before contaminated droplets are released into the environment. However, their capture efficiency is low for the inhalable size range, defined between 1 and 10 μm in diameter [53, 59, 238].

Upon generation, water from an aerosol droplet evaporates partially, leaving a stable nucleus with a smaller size [161]. Water droplets initially a few hundred microns in diameter typically reach the inhalable size range over no more than a few seconds, when accounting for mass and energy balance at the droplet surface at approximately 20°C and 30-50% relative humidity [161]. However, the precise evaporation dynamics of contaminated aerosol droplets from relevant water sources are not well understood. Yet, accurate information is critical to quantify infection risks. A longer evaporation time can increase the at-risk area associated with a source of pathogens as the aerosol droplets take longer to reach an inhalable size. Thus, the size evolution of a contaminated droplet, its capacity to reach an inhalable size upon evaporation, and the ability of the airborne pathogens to remain infectious under the conditions of the dried-up nuclei collectively determine if it can serve as a vector for transmission via the aerosol route [3]. Consequently, an accurate understanding of the underlying phenomena governing the evaporation dynamics of contaminated aerosol droplets is critical for a thorough assessment of the risks associated with airborne transmission [268].

In cooling towers, water properties such as viscosity and surface tension differ markedly from other water systems, potentially influencing evaporation. Viscosity can increase with the presence of biofilm, reaching up to 1.25 mPa $\cdot$ s compared to 1 mPa $\cdot$ s for tap water [173–175]. The intermolecular forces between the molecules of the bulk solution are stronger at higher viscosity, and the evaporation rate can decrease as a result [24]. While the surface tension of tap water is approximately 73 mN/m, that of cooling tower water can decrease to as low as 62 mN/m due to the addition of biodispersive agents employed to control biofilm growth [176, 177]. A lower surface tension is typically associated with a longer evaporation rate [171]. Non-volatile solid contaminants, both soluble and non-soluble, including biofilm, bacteria, viruses, disinfectants, salt, and organic matter, can also influence the evaporation dynamics from a thermodynamic point of view [24, 173]. Indeed, unless the relative humidity is very low, some water will remain in the droplet nucleus. This remaining water leads to an equilibrium diameter that increases with higher initial solid concentrations [178]. However,

the extent of the influence of surface tension, viscosity and solids on evaporation dynamics remains not well-documented [20, 168].

Current risk assessment models for waterborne diseases often overlook evaporation, thus failing to account for scenarios where large quantities of suspended solids may become aerosolized into large droplets that eventually reach inhalable sizes upon evaporation [108]. Balachandar et. al developed a simplified framework to predict aerosol generation, dispersion and droplet evaporation in the context of anthropogenic airborne transmission [20]. Despite their efforts, the authors identified a crucial gap in accurately determining the evaporation rate of droplets containing solids [20]. It simplistically treats all non-volatile components as having a uniform impact on evaporation. Conversely, Pruppacher and Klett developed an extensive evaporation model for water-based droplets in the context of cloud microphysics and aerosol science [159]. This model considers the effect of solids, viscosity and surface tension on evaporation, as well as the effect of solids on the droplet nuclei size, but requires experimental validation for airborne transmission applications [269]. Consequently, there is a strong research need to validate these models in the context of airborne transmission scenarios involving complex liquid compositions such as those encountered in cooling towers.

The objective of this experimental and analytical study was to characterize the effect of surface tension, viscosity, as well as the concentration of dissolved and suspended solids on the evaporation of aerosol droplets. This will provide important information to refine evaporation models by defining the size range of droplets to be considered based on the fluid properties.

6.3 Methodology

The time-resolved characterization of the evaporation of water-based aerosol droplets with different compositions was obtained by measuring the size distribution and velocity of monodispersed droplets at different positions along their free-falling path.

6.3.1 Bulk aerosolized solutions

A reference solution consisted of a standard phosphate-buffered saline (PBS) solution composed of 0.8% m/m of sodium chloride ($NaCl$), 0.02% m/m of potassium chloride (KCl), 0.144% m/m of sodium phosphate dibasic (Na_2HPO_4) and 0.0245% m/m of potassium phosphate monobasic (KH_2PO_4) [270]. Non-volatile components were added to the reference solution (PBS) to conduct a parametric study. Between 5 and 8 solutions were made for each of the investigated parameters (Table Table 6.1). The parametric study was conducted independently for each parameter.The concentrations were chosen to cover the typical and marginal

ranges observed in cooling tower water. Aerosol droplets were then generated from different solutions to isolate the effect of surface tension, viscosity, as well as the concentration of dissolved and suspended solids on the evaporation dynamics. As a control experiment, one liter of water from the cooling tower basin was sampled in sterile polyethylene bottles to compare with the evaporation of pure water (MiliQ).

The presence of surfactants affecting the surface tension of droplets was assessed by adding between 0.025 and 1% m/m of Polysorbate 20 (Tween 20, Thermo Fisher Scientific, MA, USA). The presence of polymers affecting the viscosity of the solution was assessed by adding between 2.5 and 10% m/m of Polyethylene glycol (PEG 1000, Thermo Fisher Scientific, MA, USA). PEG is composed of long polymer chains with hydrophilic and lipophilic properties mimicking the presence of biofilm in terms of viscoelasticity and surface properties. PEG is highly soluble due to its ability to form hydrogen bonds, which increases the viscosity of the media [271]. Thus, in all the tested solutions, PEG was fully dissolved in the solution. The presence of dissolved solids was assessed by modulating the concentration of salt between 5 and 100 g/L, while maintaining a consistent PBS concentration ratio. Finally, the presence of suspended solids was assessed by adding between 10^2 and 10^{13} polystyrene microbeads of 2 μm in diameter with a carboxylate coating (Thermo Fisher Scientific, MA, USA) per liter of PBS, chosen to be representative of suspended bacteria. Each solution was at a temperature of 21°C and was tested individually.

6.3.2 Droplet generation

A commercial Vibrating Orifice Aerosol Generator (VOAG, Model 3450, TSI Corporation, MN, USA) was employed to generate a stream of single-file liquid droplets (Figure 7.2). Droplets are generated by forcing a liquid through an orifice subjected to mechanical perturbations, which breaks it up into individual droplets [272]. It was oriented with the orifice pointing downwards so that the droplets were free-falling after generation. In this configuration, droplets take approximately 0.16 seconds to break up from the orifice [273]. An orifice of 35 μm in diameter allowed the generation of 60 μm droplets, with a standard deviation

Table 6.1 Composition of the tested solutions. Each parameter was tested over 5 to 8 solutions, without changing any of the other parameters.

Additive	Solution 1	Solution 2	Solution 3	Solution 4	Solution 5	Solution 6	Solution 7	Solution 8
Tween (% m/m)	0	0.025	0.050	0.075	0.100	1.00	-	-
PEG (% m/m)	0	2.5	5.0	7.5	10.0	-	-	-
Salt (g/L)	0	5.0	10.0	15.0	20.0	100.0	-	-
Microbeads (beads/L)	0	10^2	10^4	10^6	10^8	10^{10}	10^{12}	10^{13}

of ± 0.2 μm at the generation site [274]. Droplets were produced at a frequency of 15 kHz, corresponding to the modulation of the orifice disk by a piezoelectric ceramic transducer. In this configuration, the droplets were spaced out by approximately 200 μm. The bulk solution to be aerosolized was injected from a 60 mL Luer taper polypropylene syringe at a constant speed of 4.2×10^{-4} cm/s controlled by a syringe pump (KDS 100, KD Scientific, MA, USA). The pressure of the solution at the orifice plate was approximately 70 kPa.

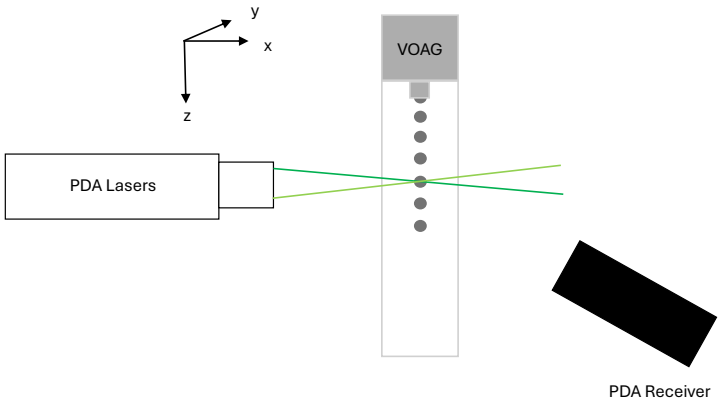

(a)

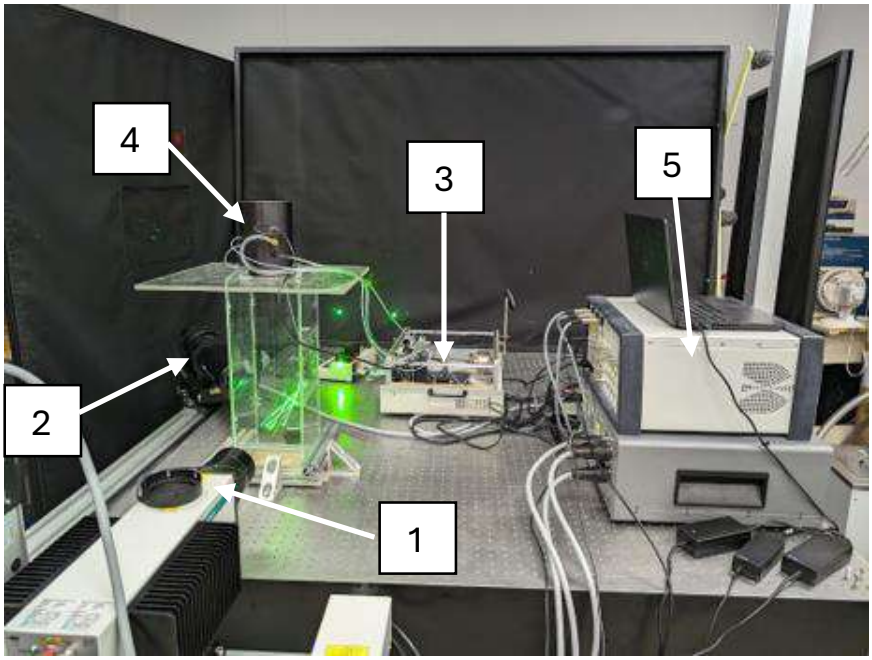

(b)

Figure 6.1 (a) Schematic representation of the droplet generation (VOAG) and the particle characterization (PDA). The reference coordinates are also displayed. The origin point was located 1 mm under the VOAG nozzle. (b) Overview of the experimental setup: 1) PDA laser and 2) receiver, 3) VOAG control box, 4) VOAG and measurement chamber, 5) controls of the PDA and the traverse.

6.3.3 Dispersion air

The multiphase flow, consisting of the aerosol droplets dispersed in air, was generated within a rectangular sampling chamber measuring 0.15 m × 0.15 m × 0.6 m, with an opening at the bottom to ensure a laminar flow. Air was supplied from the VOAG at a constant flow rate of 30 SLPM. The temperature and relative humidity of the flow were measured by a digital sensor module (DHT22) placed at the entrance of the sampling chamber and controlled by a microcontroller (Arduino Uno).

An aerosol generator (TOPAS GMBH model ATM 221) was used to seed the pressurized air with water and thus control the relative humidity. During operation, the aerosol generator was connected to a mass flow controller (Hastings HFC 202), enabling regulation of the flow rate of water droplets in the 0-25 SLPM range and allowing for the relative humidity to be adjusted between 30 and 90%. The temperature of the air was constant at 21°C.

6.3.4 Droplet characterization

The Phase Doppler Anemometry (PDA, Dantec Dynamics, Skovlunde, Denmark) technique was used to characterize the aerosol droplets. The measurement volume is defined by the intersection of two pairs of laser beams with wavelengths of 532 and 561 nm. As single droplets flow through, light is scattered from the interference pattern created by the two laser beam pairs, allowing for size distribution and velocity characterization [275]. The droplet velocity is obtained from the Doppler shift of the interference fringes, while information on its size can be acquired from the phase shift. Since the measurement volume is very small (approximately .15 x 0.15 x 2.6 mm), measurements are considered punctual, making it ideal for the characterization of individual droplets generated from the VOAG [276]. The PDA can detect particles between 0.5 and 8000 μm, covering the range of the generated droplets from their inception down to their size stabilization as evaporated nuclei.

The PDA was mounted on a traverse to map the evolution of the droplets. For each solution, a scan was conducted starting 1 mm under the nozzle and moving progessively 250 mm downwards, with steps of 10 mm in the z-direction (Figure 7.2 a). Slight adjustments in the x and y directions at each measurement point allowed for maximal droplet detection. Each point was sampled for 120 seconds, thus measuring between 2000 and 80 000 droplets. PDA settings were selected to achieve adequate detection (See Appendix A).

6.3.5 Evaporation metrics

Three evaporation metrics were used to compare the effect of the different parameters on the evaporation dynamics: The droplet nuclei size, the evaporation time and the time-resolved

size evolution of the droplet diameter. The droplet nuclei size, defined as the diameter of the droplet after complete evaporation, was measured as the average size of the droplet once it stabilizes at the end of the experiment. This stabilization criteria also defines the evaporation time. The size evolution refers to the mean droplet size as a function of the residence time of the droplet. It is therefore a measure of the evaporation rate of the droplet at each instant of the evaporation.

6.3.6 Data analysis

The size evolution of the droplets was acquired according to their position in the z direction (Figure 7.2 a). The position of the droplets was converted to the cumulative residence time, according to the distance between two measurement points L (0.01 m) and the velocity from the previous measurement point v (m/s).

$$t_n = \sum_{i=2}^{n} \frac{L}{v_{i-1}} \tag{6.1}$$

6.3.7 Evaporation models

Two evaporation models were used to compare the experimental results. The Balachandar et. al model was developed for the evaporation of droplets in the context of anthropogenic airborne transmission [20]. Assuming that the droplet is spherical, the rate at which a small sphere loses mass through evaporation is influenced by the diffusion of the vapor layer away from the surface of the droplet. The rate of evaporation is given by the following equation [156, 157]:

$$-\frac{dm}{dt} = \pi d D \rho_p Nu \ln(1 + B_m) \tag{6.2}$$

Here, m (kg) is the mass of a droplet with diameter d (m), D (m^2/s) is the diffusion coefficient of the vapor in the surrounding air, and ρ_p (kg/m^3) is the density of the surrounding air. The dimensionless Spalding mass number B_m (-) is given by $B_m = \frac{Y_d - Y_p}{1 - Y_s}$, where Y_d (-) is the mass fraction of water vapor at the droplet surface, and Y_p (-) is the mass fraction of water vapor in the surrounding air. Nu (-) is the dimensionless Nusselt number and is calculated from the Reynolds number, Re, and the Prandtl number, Pr, knowing the velocity and viscosity of the surrounding air v (m/s) and μ ($N \cdot s/m^2$) respectively, according to the following equations:

$$Nu = 2 + 0.4 Re^{1/2} Pr^{1/3} \tag{6.3}$$

$$Re = \frac{d\rho_p v}{\mu} \tag{6.4}$$

$$Pr = \frac{\mu}{\rho_p D} \tag{6.5}$$

Assuming that Nu and B_m remain nearly constant for small droplets, equation 2 can be integrated to derive the following relationship for the evolution of the droplet, defined as the squared law of evaporation [158]:

$$d(t) = \sqrt{d_e^2 - k't} \tag{6.6}$$

Where

$$k' = 4DNu\ln(1 + B_m) \tag{6.7}$$

In these equations, d_e (m) is the initial diameter of the droplet, and k' represents an effective evaporative diffusivity with units of m^2/s.

The Pruppacher-Klett model is more complex, considering the effect of Stefan flow and the temperature dependence of diffusion coefficients [159,160]. The evaporation rate $\frac{dm}{dt}$(kg/s) is given by:

$$-\frac{dm}{dt} = \frac{2\pi d M_w D C_T p \mathrm{Sh}}{RT_\infty} \ln\left(\frac{p_s - p}{p_{sat} - p}\right)$$

Where

$$C_T = \frac{T_\infty - T_p}{T_\infty - 1.6}\left(\frac{2-k}{T_\infty^{2-k} - T_p^{2-k}}\right) \tag{6.8}$$

In the previous equations, M_w (kg/mol) is the molecular weight of water and p ($kg/m \cdot s^2$) is the atmospheric pressure of air. C_T (-) is a correction factor accounting for the temperature dependence of the diffusion coefficient, with k (-) being a constant between 1.6 and 2. The partial pressure of vapor on the droplet surface is given by p_s and p_{sat} ($kg/m \cdot s^2$) is the saturation vapor pressure. T_∞ (K) is the temperature far from the droplets, Sh is the dimensionless Sherwood number, calculated from the Reynolds number, Re, and the Schmidt number, Sc, which are given by the following equations:

$$Sh = 2 + 0.6\mathrm{Re}^{1/2}\mathrm{Sc}^{1/3} \tag{6.9}$$

$$Sc = \frac{\mu}{\rho_p D} \tag{6.10}$$

p_s can be calculated from the following equation:

$$\ln \frac{p_s}{p_{sat}} = \frac{4 M_w \sigma_{LV} q_w}{R T_1 \rho_w d_e} \tag{6.11}$$

Where σ_{LV} (kg/s^2) is the surface tension of the droplet, q_w (-) is the mass fraction of water in the droplet and R (J/(mol $\cdot$ K)) is the universal gas constant.

The final size of the droplet nuclei d_{dr} (m) is given by the following equation and is equivalent for both models. It is a function of ψ (-), the volume fraction of solids suspended initially in the droplet [20, 159]:

$$d_{dr} = d_e \psi^{1/3} \tag{6.12}$$

6.4 Results and Discussion

6.4.1 Relative humidity

The effect of relative humidity on the evaporation time and the size evolution of the pure water droplets was assessed experimentally (Figure 6.2). The resulting evaporation curve displays the droplet mean diameter as a function of the residence time with the dispersion air being injected at a relative humidity between 30 and 90%. As expected, higher humidity resulted in slower evaporation rates, delaying size reduction and increasing evaporation time. This effect was also observed in the two evaporation models (Figure 6.2). The Pruppacher-Klett model predicted a slower evaporation rate than the Balachandar et. al model for approximately two thirds of the evaporation time, before surpassing it in the latter stages. Both models predicted the absence of droplet nuclei, as pure water was used to generate the droplets. Experimental results closely matched the models, with the largest discrepancies at the start where the evaporation rate was slower than predicted (Figure 6.2). This observation was expected, given the documented impact of relative humidity on evaporation, a factor both models incorporate [20, 159, 161]. Consequently, these findings not only validate the experimental approach but also corroborate that the models can capture the dynamics of droplet evaporation under varying humidity conditions.

The effect of relative humidity on the evaporation rate is important because it can influence

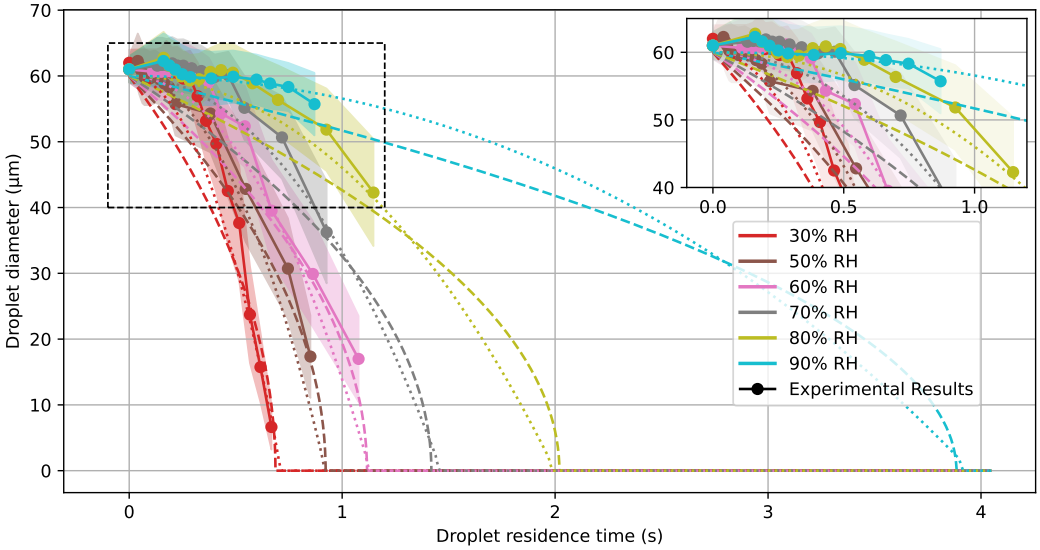

Figure 6.2 Experimental results of the mean diameter as a function of the residence time for different levels of relative humidity on pure droplets. The standard deviation of measurements is shown as shaded error bars. Results from the Balachandar et. al model and the Pruppacher-Klett model are also displayed.

the size evolution of the droplet, as well as the evaporation time. Indeed, as relative humidity increased, the evaporation rate slowed down. Droplets at 30% relative humidity were almost completely evaporated after 0.5 seconds, while they only lost approximately 10% of their diameter after 1 second at 90% relative humidity. Cooling towers typically release contaminated droplets in a plume that ranges between 90 and 100% relative humidity [173]. Therefore, droplet evaporation is considered to occur in mostly in very humid conditions [265], fostering large evaporation time and thus the possibility for contaminated droplets to diffuse further into the environment and potentially increase the exposure risks [3]. Thus, the experiments should ideally be conducted at high humidity rates. However, the final size could not be assessed at high relative humidity with the available experimental setup because the droplets were not completely evaporated at the end of the experiment (Figure 6.2 a). Nonetheless, as the experimental results and both models agreed on the evaporation with different relative humidity values, it can be assumed that the results obtained at 30% relative humidity could easily be scaled for different relative humidities. Consequently, the subsequent experiments were conducted at 30% relative humidity to ensure that the droplets were completely evaporated at the end of the experiment.

6.4.2 Cooling tower water

To understand the discrepancies in evaporation dynamics depending on the properties of the bulk solution, the mean diameter of droplets initially at 60 μm was compared to their residence time for pure water and cooling tower water droplets (Figure 6.3). Notably, cooling tower water droplets did not fully evaporate, reaching a diameter of 27 μm after 1.5 seconds for an initial diameter of 60 μm, whereas pure water droplets completely evaporated in approximately 0.6 seconds. The standard deviation of the measurements was also significantly higher for droplets of cooling tower water. These results highlight the effect of non-volatile constituents and particulate content (colloids, bacteria, particles) on the evaporation dynamics, as well as the need to understand the underlying mechanisms.

The rapid evaporation timescale of between 0.5 and 1.5 seconds is crucial for the development of strategies to mitigate the exposure risks associated with *Legionella* from cooling towers. Drift eliminators are essential for capturing droplets generated inside cooling towers before they are released into the environment. Promoting impaction through rapid flow deflections, drift eliminators are generally ineffective at capturing droplets in the inhalable size range. Improving their capture efficiency requires a thorough understanding of the evaporation dynamics, as droplets travel through the eliminators within the first 2 seconds upon generation [238]. Furthermore, the time-resolved size evolution of the contaminated droplets scales with relative humidity, where higher relative humidity is associated with longer evaporation time (See Appendix A). The results are thus applicable to a broad range of airborne transmission scenarios.

The composition of cooling tower water influenced the evaporation dynamics, which can in turn impact the exposure risks. Indeed, a longer evaporation time could increase the risk of exposure by allowing contaminated droplets to travel further and remain airborne longer [81]. Droplet nuclei size is also closely related to the exposure risks, as larger droplets can carry more contaminants, while droplets that are too large cannot be inhaled [277]. These factors, as well as the evaporation rate of the droplets, can also influence the viability of the contaminants transported in aerosol droplets. Therefore, a model that accurately predicts the size evolution of contaminated droplets could lead to better risk assessment with high time and spatial resolution. As such, the effect of surface tension, viscosity, as well as the concentration of dissolved and suspended solids on the evaporation dynamics was assessed. The results were compared to two evaporation models, the Balachandar et. al model and the Pruppacher-Klett model.

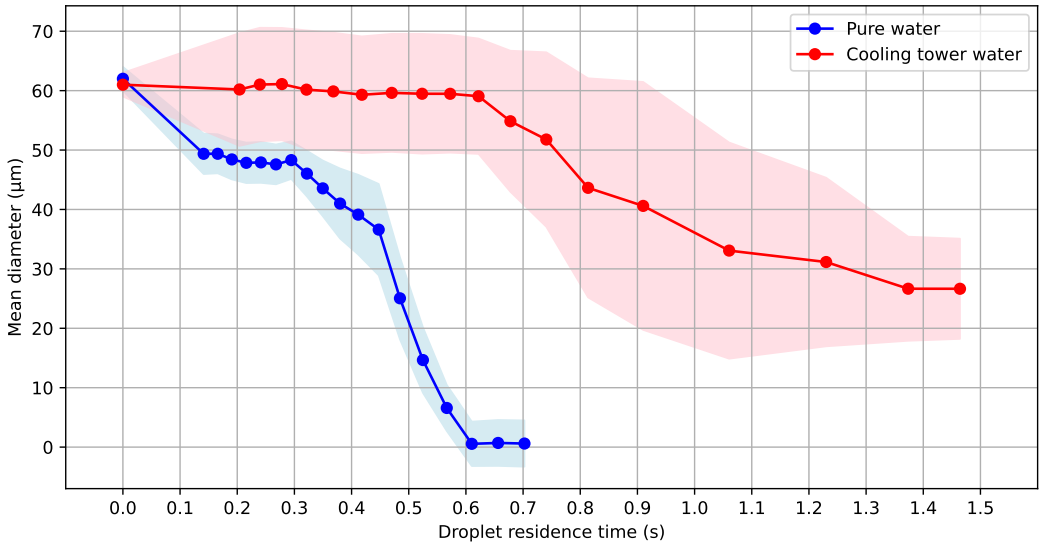

Figure 6.3 Mean diameter as a function of residence time for pure water and cooling tower water. The standard deviation of measurements is shown as shaded error bars.

6.4.3 Baseline water-based aerosolized solution

The concentration of solids, including bacteria, biofilm, and minerals, varies significantly across different water systems such as cooling towers, and over time [278]. Therefore, using cooling tower water as a basis for droplet generation may not accurately represent every cooling tower and could hinder the reproducibility of our experiments. Instead, phosphate-buffered saline (PBS), a standard in microbiology with well-characterized properties and minimal impact on bulk physical properties [270], was used as the baseline solution for the aerosol droplets.

Pure water droplets were experimentally compared to droplets generated from PBS in terms of evaporation time, nuclei size and time-resolved size evolution (Figure 6.4). For both substances, evaporation was slow for the initial 0.3 seconds, with minimal reduction in mean diameter. Subsequently, the evaporation rate increased, but PBS droplets evaporated slower than their pure water counterparts. Their evaporation time was 0.67 seconds compared to 0.56 seconds for pure water droplets. PBS droplets did not completely evaporate, leaving droplet nuclei of approximately 8-9 μm compared to 0.5 μm for pure water droplets. The observed droplet nuclei for pure water droplets did not reach zero due to the detection limit of the PDA, at 0.5 μm. Therefore, PBS droplets exhibited similar evaporation patterns to pure water but with a slower rate and larger nuclei size. Furthermore, fewer droplets were

detected by the PDA when pure water was used in the experiment setup. PBS measurements were conducted in duplicate and the resulting evaporation curves were almost identical. The repeatability of the PBS droplet measurements further validated the experimental approach and the choice of PBS as a baseline solution.

The results were compared to the two evaporation models (Figure 6.4). The time-resolved size evolution of the droplets was different between the experimental results and both models. Indeed, the slow onset of the evaporation was well captured by the Pruppacher-Klett model, but not by the Balachandar et. al model. Both models predicted a faster evaporation rate than the experimental results for most of the evaporation but agreed with the experimental data for the last 0.1 second. The experimental droplet nuclei size was approximately 9 μm, which was in line with the predictions of the two models at 9.5 μm. The experimental evaporation time of 0.67 seconds was close to the 0.65 seconds predicted by the Balachandar et al. model and the 0.7 seconds by the Pruppacher-Klett model. The models therefore agreed with the experiments on the evaporation time and the nuclei size, but not on the time-resolved size evolution.

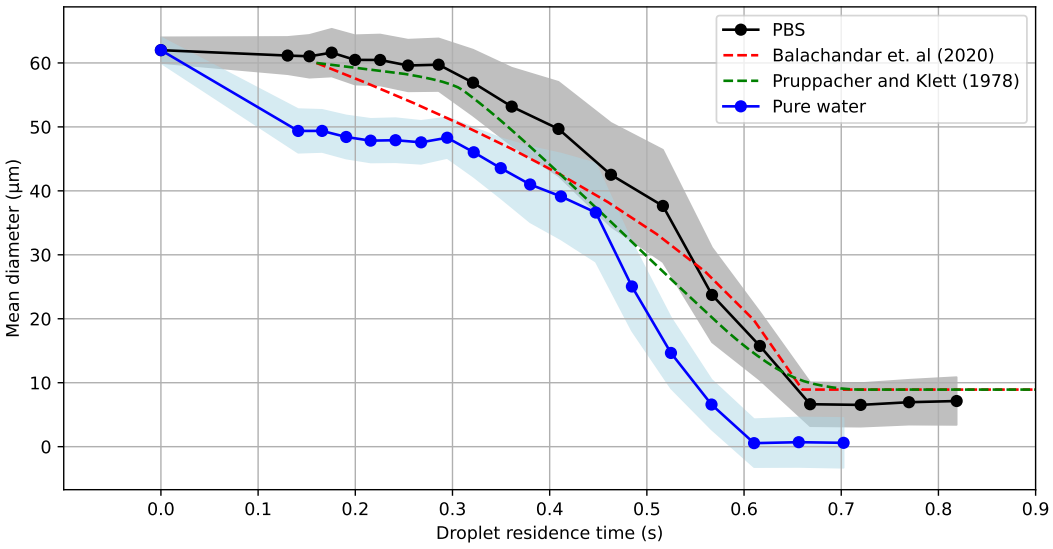

Figure 6.4 Mean diameter as a function of residence time for pure water and PBS droplets. The standard deviation of particle size measurements is shown as shaded error bars. Comparison of the experimental results with the Balachandar et. al and Pruppacher-Klett models.

6.4.4 Surface tension

The effect of surface tension on droplet evaporation was assessed by adding between 0.025 and 1% m/m of Tween 20 to the PBS solution. The mean droplet size was measured as a function of the residence time for each surfactant concentration (Figure 6.5 a). The evaporation time increased by almost 14% with a concentration of 0.1% m/m compared to PBS droplets. The nuclei size remained at approximately 9 μm for concentrations up to 0.1% m/m, similar to PBS droplets. However, it was approximately 45 μm at 1% m/m, as the evaporation was halted after 0.5 seconds. These discrepancies in the evaporation time and droplet nuclei size are likely due to the high concentration of surfactant at the droplet surface. Indeed, surfactants, such as biodispersive agents in cooling towers, decrease surface tension, which in turn increases evaporation time for airborne droplets [177, 279]. This occurs due to the dual interfacial properties of surfactants. Polysorbate in Tween 20, like most surfactants, has a hydrophilic head and a hydrophobic tail [172]. Consequently, once the droplet is generated, a surfactant lipid layer gradually forms on its surface, reducing surface tension [171] and decreasing the availability of water molecules at the surface, thus impeding mass transfer into the surrounding air and lowering the evaporation rate [156].

The minimum concentration at which surfactants aggregate, called the critical micelle concentration, was approximately 0.02% m/m in the experimental conditions [280]. All experimental concentrations exceeded this threshold. Due to the propensity of surfactant molecules to be at the free surface, a lipid layer was formed at the droplet surface, thus confirming the impact of the surfactant on the evaporation dynamics. As droplets evaporate, surfactant concentration increases, eventually halting evaporation if the droplet surface is completely covered in surfactant [281]. Given that Tween 20 has a surface density of approximately 10^{12} molecules/m^2 and that a gram of Tween 20 contains on average 4.91 $\times 10^5$ molecules of Polysorbate, complete surface coverage occurs for concentrations of 0.5% m/m.

The two investigated models considered the effect of surfactant on droplet evaporation (Figure 6.5 b). In the Balachandar et al. model, surfactant presence at the droplet surface reduced the Spalding number (B_m) by decreasing the water molecule concentration at the surface (Y_d), assuming other parameters involved in the Spalding number remained constant [282]. The reduction in Y_d is directly proportional to the surface density of the surfactant, allowing the quantification of this reduction in surface tension [176] (See Appendix B). The Pruppacher-Klett model also accounts for surfactants through a surface tension term [159]. The surface tension of the droplet decreased from 73 (mN/m) for PBS to 68 (mN/m) for droplets with 0.05% m/m of Tween 20 [283, 284]. This reduction in surface tension lowers the partial pressure of vapor on the droplet surface, p_s, and the evaporation rate of the droplet. Exper-

imental results matched the models in terms of evaporation time and nuclei size (Figure 6.5 b).

The experiments and models however showed significant discrepancies in the time-resolved size evolution of droplets (Figure 6.5b). Both models predicted a steady increase in evaporation rate, underestimating the droplet size for most of the residence time compared to the experiments. Experimental results revealed a three-stage non-linear size evolution (Figure 6.6 a). Initially, the evaporation rate was similar to PBS due to the uniform dispersion of surfactant within the droplet, (first stage). As evaporation progressed, the surfactant concentration increased while it migrated to the droplet surface, forming a lipid layer that slowed the evaporation rate (second stage). Finally, depending on surfactant concentration, either the lipid layer became too thick to allow evaporation or the lipid layer did not cover the whole surface area of the droplet, allowing the water molecule diffusion to reach the droplet nuclei equilibrium (third stage).

The transition between stages 2 and 3, where evaporation was halted and then resumed, could be attributed to Marangoni instabilities induced by the non-uniform distribution of surfactants and other solids from the PBS. These surface tension gradients drive internal fluid flows that disrupt the lipid layer, causing localized thinning or rupture, which in turn enables water vapor diffusion to resume in some regions of the droplet [24]. These instabilities are not commonly observed for airborne aerosol droplets, but have been reported for sessile droplets [285–287]. The models did not account for these instabilities, leading to discrepancies in the time-resolved size evolution of the droplets. For surfactant concentrations under 1%, the lipid layer coverage was insufficient, allowing the droplet to continue evaporating, whereas at 1% concentration, the lipid layer fully covered the droplet surface, explaining the evaporation being stopped after 0.5 seconds (Figure 6.6 b).

The surfactant concentrations inside cooling towers typically range between 0.025 and 0.1% m/m, but they can reach up to 1% upon injection of biodispersive agents [288]. These agents work by dispersing biofilm from the piping system into the cooling tower water to make them more susceptible to disinfectants. However, it can also introduce more pathogens into the generated aerosol. These results show that the evaporation dynamics of potentially contaminated droplets released from cooling towers could vary significantly with the presence of surfactants, thus impacting the exposure risks.

6.4.5 Viscosity

The effect of viscosity on evaporation was assessed experimentally by adding between 2.5 and 10% m/m of polyethylene glycol (PEG 1000) to the PBS solution. The mean droplet size was measured as a function of the residence time for each PEG concentration (Figure 6.7 a). The droplet diameter decreased slowly over the first 0.4 seconds, 0.1 seconds longer than for PBS droplets. After this initial delay in evaporation, the size evolution was essentially similar to that of PBS, yet yielded a longer evaporation time, increasing from 0.67 seconds for PBS droplets to 0.79 seconds for droplets with 10% m/m of PEG. This longer evaporation time was observed to be small, but significant in the range of viscosity studied, which is typical for cooling tower water.

The Balachandar et al. model did not capture the effect of viscosity on the evaporation rate and thus predicted the same droplet size evolution, regardless of the viscosity of the bulk (Figure 6.7 b). Conversely, the Pruppacher-Klett model predicted a slower evaporation rate for droplets with higher viscosity, leading to a longer evaporation time. Indeed, the Balachandar et al. model does not account for viscosity, while the Pruppacher-Klett model does consider it through a correction factor in the evaporation rate which accounts for the effect of this parameter on the diffusion of water molecules towards the droplet surface. None of the models predicted the delay of the onset of evaporation observed in the experiments. This caused a constant discrepancy of approximately 0.1 seconds for the evaporation time between the experiments with the Prupacher-Klett model (Figure 6.7 b). The Balachandar et al. model first overestimated the evaporation time and then underestimated it at higher viscosity.

The effect of viscosity on the evaporation rate and thus the droplet size evolution stems from the intermolecular forces holding the droplet together, which tend to increase with viscosity [289, 290]. The higher the intermolecular forces, the harder it is for water molecules to detach from the surface of the droplet and diffuse into the environment [291]. The viscosity of a liquid η ($\mathrm{N \cdot s/m^2}$) is related to the Gibbs free energy of activation through the Eyring equation [292, 293]:

$$\eta \propto \frac{k_B T}{h} \exp\left(\frac{\Delta G}{RT}\right) \tag{6.13}$$

In the previous equation, k_B is the Boltzmann constant (J/K), T (K) is the temperature of the liquid, h ($\mathrm{kg \cdot m^2/s}$) is the Planck constant and ΔG (J/mol) is the Gibbs free energy of activation and R ($\mathrm{J/mol \cdot K}$) is the universal gas constant. For water molecules to escape the droplet surface, they must overcome the Gibbs free energy of activation.

In liquids with higher viscosity, the intermolecular forces such as hydrogen bonding in water, are stronger. These forces increase the Gibbs free energy of activation, making it more difficult for water molecules to escape into the vapor phase. The rate of a process that involves overcoming an energy barrier can often be described by the Arrhenius equation [294]. The evaporation rate J, with A as a constant, is thus given by:

$$J = A \exp\left(-\frac{\Delta G}{RT}\right) \propto -\eta \tag{6.14}$$

According to equations 13 and 14, as viscosity increases, the evaporation rate decreases linearly. This would explain the delay in the onset of evaporation (Figure 6.7), which increased with an increase in viscosity. However, after onset, the evaporation rate followed the same trend as for PBS droplets. Therefore, the effect of viscosity was more prominent at the early stages of the evaporation. The early onset of evaporation in quiescent air is typically dominated by the diffusion of water molecules at the droplet-air interface, while the later stages are governed by thermal effects that sustain the evaporation [24]. Even though the droplets ejected from cooling towers cannot be considered to be in quiescent air, the effect of viscosity on the evaporation rate is likely to be more significant in the early stages of the evaporation.

The small discrepancies observed in typical viscosity ranges for cooling tower water yielded significant differences in the evaporation time and could affect the associated exposure risks. However, this phenomenon is particularly relevant in the context of anthropogenic airborne transmission, involving droplets made from mucus and saliva, which are typically 30-50% more viscous than cooling tower water [295]. These results demonstrate that current evaporation models do not accurately capture the effect of viscosity.

6.4.6 Effect of solids

Evaporation models do not typically differentiate non-volatiles between dissolved and suspended solids. In this section, they were analyzed separately to highlight their distinct influence. Their impact on droplet nuclei size was also investigated statistically.

Suspended solds

The effect of suspended solids on the evaporation time and the size evolution of the droplets was assessed experimentally by adding between 10^2 and 10^{13} microbeads/L to the PBS solution. It is acknowledged by the authors that microbeads are not exactly representative of all the suspended solids contained in cooling tower water, but it is believed that they are a good proxy for the effect of bacteria such as *Legionella* on evaporation. To best imitate

the behavior of bacteria in the bulk solution, polystyrene was chosen to provide hydrophobic properties and the microbeads were coated with a carboxylate coating to provide hydrophilic properties. Using microbeads as a proxy for bacteria in aqueous media was also done in studies focused on microfluidic water treatment [296, 297]. The size of 2 μm was selected to be representative of *Legionella* bacteria (typically in cylindrical shape, approximately 0.3-0.9 by 1.5-5 µm [298]) in terms of volume occupied and surface properties. According to equation 12, the driving factor determining droplet nuclei size is the total volume occupied by the suspended solids, rather than the individual size of each particle [20, 299]. However, the effect on the size evolution and the evaporation time might slightly differ because of the surface area that the microbeads can occupy compared to *Legionella* bacteria. Nonetheless, the effect of the microbeads on the evaporation dynamics can be considered similar to that of *Legionella* bacteria.

The mean droplet size was measured as a function of the residence time for each microbead concentration (Figure 6.8 a). This was also observed in the literature where the presence of particles changes the surface energy of liquid droplets [300, 301] . The evaporation time was not influenced by the smaller concentrations of microbeads, up to 10^8 microbeads/L. Indeed, at this concentration, on average only 1% of the droplets contained one microbead. However, for higher concentrations, the evaporation time was significantly larger. A concentration of 10^{13} microbeads/L (with each droplet containing on average approximately 1000 microbeads), yielded an evaporation time of 1.1 seconds, compared to 0.67 seconds for PBS droplets (Figure 6.8 b) . The nuclei size was approximately 9 μm for concentrations up to 10^8 microbeads/L, but was 20 μm for 10^{13} microbeads/L. When comparing the average volume that would be occupied by the microbeads to the volume of the droplet nuclei for this concentration, the droplet nuclei contained almost only microbeads for 10^{13} microbeads/L (less than 1% of water per volume), whereas it was closer to 90% at a concentration of 10^8 microbeads/L. As the concentration of suspended solids typically ranges from 10^7 to 10^{15} particles/L in cooling tower water [173, 302], this change can influence the viability of the bacteria by changing the amount of water remaining in the droplet nucleus and thus the infection risks.

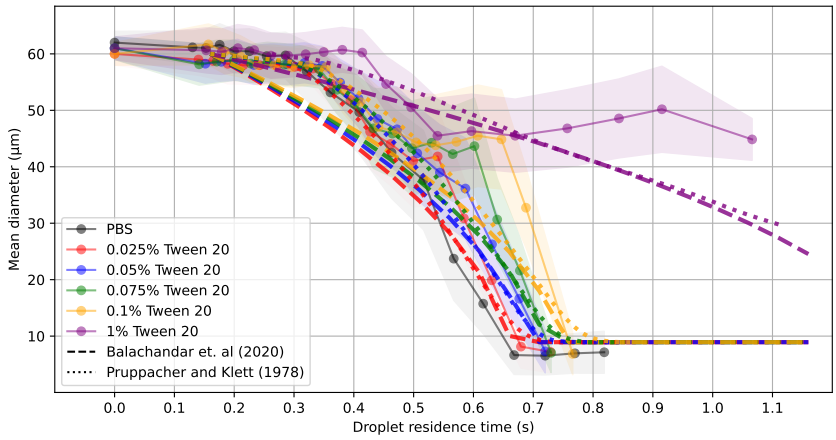

(a)

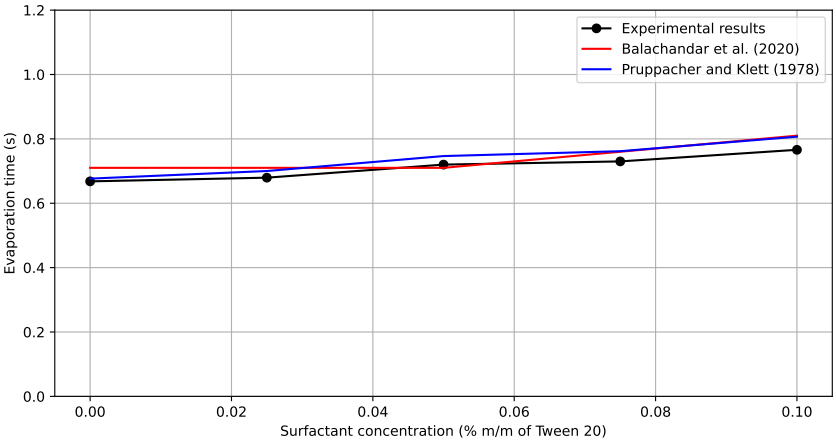

(b)

Figure 6.5 (a) Left: Mean diameter as a function of residence time for different concentrations of surfactant compared to the Balachandar et. al and Pruppacher-Klett models for different concentrations of surfactant. The standard deviation of measurements is shown as shaded error bars. (b) Evaporation time as a function of surfactant concentration for the experimental results and the two models.

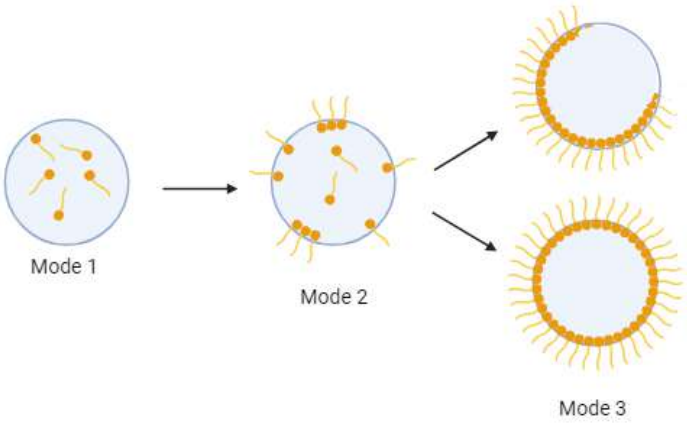

(a)

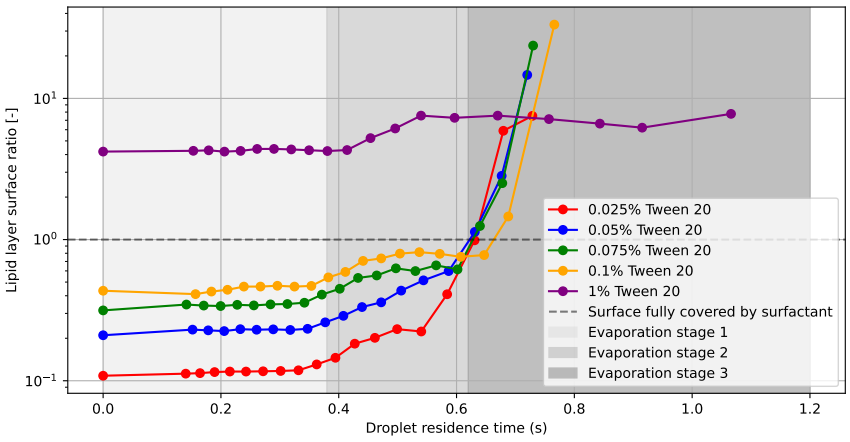

(b)

Figure 6.6 (a) Schematic representation of the surfactant distribution inside droplets, showing 3 evaporation stages. (b) Ratio of the droplet surface covered by a lipid layer of surfactant as a function of the droplet residence time for different concentrations. The ratio shown is the maximum possible value, where all the surfactant is assumed to be at the droplet surface.

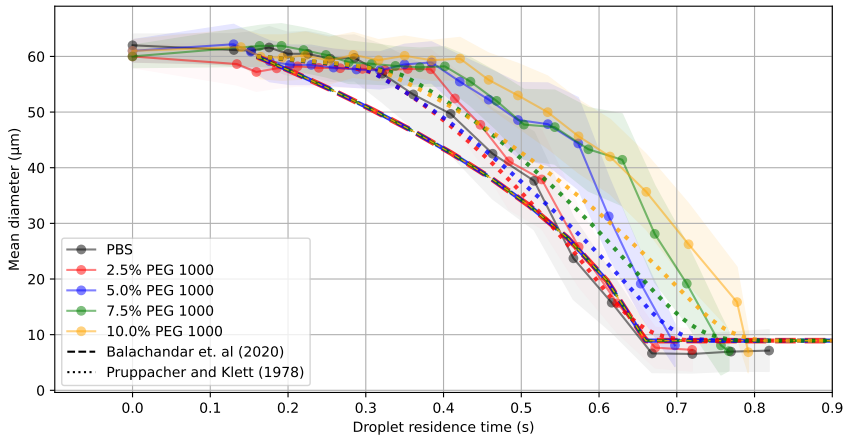

(a)

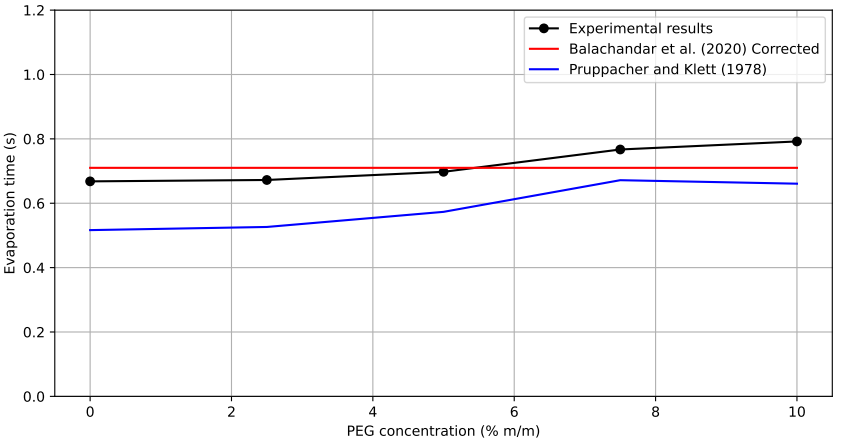

(b)

Figure 6.7 (a) Left: Evolution of the mean diameter with residence time for different concentrations of Polyethylene glycol (PEG) compared to the Balachandar et. al and Pruppacher-Klett models for different concentrations of PEG. The standard deviation of measurements is shown as shaded error bars. (b) Evaporation time as a function of PEG concentration for the experimental results and the two models.

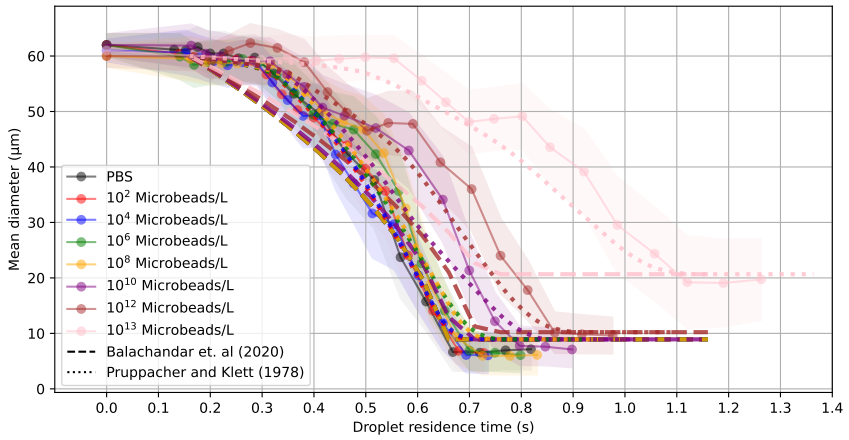

(a)

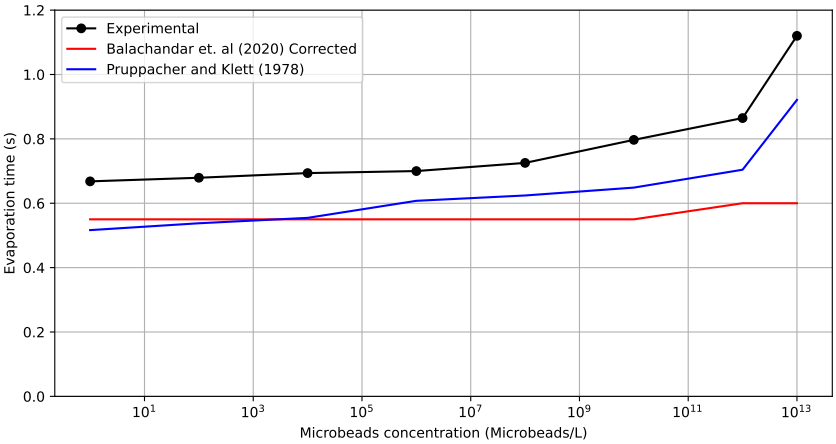

(b)

Figure 6.8 (a) Left: Mean diameter as a function of residence time for different concentrations of microbeads compared to the Balachandar et. al and Pruppacher-Klett models for different concentrations of microbeads. The standard deviation of measurements is shown as shaded error bars. (b) Evaporation time as a function of the microbeads concentration for the experimental results and the two models.

The microbeads behaved similarly than bacteria in the bulk solution in that they were dispersed randomly in the bulk solution [239]. Contrary to surfactants where most of the concentration was located at the droplet-air interface during the evaporation, the number of microbeads located at the air-droplet interface at any point, thus impeding the evaporation, was stochastic. By comparing the size and concentration of the microbeads to the surface area of the droplet, the average ratio of the surface occupied by the microbeads was inferred (See Appendix C). Statistically, for concentrations up to 10^8 microbeads/L, less than 9% of the surface was initially occupied by microbeads. However, between 60 and 98% of the surface of the droplet was occupied by microbeads for concentrations between 10^{10} and 10^{13} microbeads/L. This caused significant discrepancies in the evaporation dynamics. Indeed, a non-linearity in the size evolution, where the evaporation is slowed down after the initial onset of size reduction, was observed for the two largest concentrations of microbeads assessed, between 0.5 and 0.6 seconds for 10^{12} microbeads/L and between 0.7 and 0.82 seconds for 10^{13} microbeads/L (Figure 6.8 a).

As evaporation occurs, a fraction of the surface is occupied by suspended solids, which makes evaporation longer as fewer water molecules can diffuse from the surface. Both the Balachandar et al. model and the Pruppacher-Klett model account for the effect of suspended solids on the evaporation rate. However, they assume this effect remains constant over time, which leads to an overestimation of the evaporation rate [20]. Indeed, both models underestimated the evaporation time, especially for larger concentrations of microbeads. For both models however, the droplet nuclei size was predicted accurately, even for a concentration of 10^{13} microbeads/L, which yielded a droplet nuclei size of 20 μm (Figure 6.8 b). There was also a significant discrepancy between the models and the experiments for the time-resolved size evolution, as the models did not predict the non-linearity observed in the experiments at higher concentrations of suspended solids.

Large variations in bacteria concentration are typically observed over time in cooling tower water and the generated droplets, both within a single cooling tower and across different systems [115]. The results demonstrate that associated risks can be influenced by the concentration of suspended solids in the water, as microbeads had a tangible effect on the evaporation time, the size evolution and the nuclei size. However, thermodynamic factors such as temperature and relative humidity have a much more significant influence on evaporation dynamics than the concentration of suspended solids [154]. Nonetheless, it remains that the exposure risks are dominated by the concentration of bacteria in the water and evaporation can significantly affect these risks.

Dissolved solids

The effect of dissolved solids on the evaporation time and the size evolution of the droplets was assessed experimentally by adding different concentrations of salt to the bulk solution. The mean droplet size was measured over the residence time for each concentration of salt (Figure 6.9 a). The concentration of dissolved solids did not influence the evaporation dynamics. However, for a high concentration of dissolved solids, the final size and the size evolution were influenced similarly to the case of high concentrations of suspended solids. Indeed, at a salt concentration of 100 g/L, the onset of the evaporation was delayed by approximately 0.1 second, but the final evaporation time was still approximately 0.5 seconds, or almost 30% faster than at the lower concentrations. Finally, the droplet nuclei size was approximately 40 μm, compared to 9 μm for PBS droplets.

As the droplet experiences evaporation, it loses water which increases the dissolved solid concentration. If the concentration is at any point higher than the saturation concentration (solubility) of the bulk solution, then the solid will precipitate. The saturation concentration of PBS in water is approximately 320 g/L [303]. The initial concentrations of salt were all under this threshold, but as the droplet evaporated, the concentration increased. For a concentration of 100 g/L, the salt precipitated, which led to the early formation of the droplet nuclei (Figure 6.9 b). Conversely, the smaller salt concentrations only surpassed the solubility threshold after 0.6 seconds, when they had almost already reached the droplet nuclei size. The same phenomenon was observed for the addition of PEG 1000 (Figure 6.7 a). The solubility of PEG 1000 in water is very high due to its ability to form hydrogen bonds. Thus, even with the decrease in the droplet size due to evaporation, the droplets did not surpass the solubility ratio of PEG 1000 in water. This is why the droplet nuclei size was not affected by the concentration of PEG 1000.

Cooling tower water typically contains a small concentration of between 5 and 25 g/L of dissolved solids [235]. However, after adding disinfectants (typically chlorine compounds) in the cooling tower water, the solid contents can remain at concentrations closer to 100 g/L for multiple hours in the bulk water [174]. If the concentration is too large in droplets, it can affect their evaporation and thus the associated exposure risks. Even though high chlorine residuals are typically associated with low concentrations of viable *Legionella* bacteria in the cooling water, the effect of disinfection is not immediate [237]. The exposure risks can thus remain high over a significant period, as evaporation is hindered by the high solid solids concentration.

Droplet nuclei size

The average droplet nuclei size was previously assessed for the two models and the experimental results for each parameter influencing evaporation. The presence of solids had a significant effect on the nuclei size. To further understand the extent of their influence, the size distribution of the nuclei size was compared for the different concentrations of suspended solids (Figure 6.10 a). At lower concentrations, for which the nuclei size was largely unaffected (Figure 6.8 a), the size distribution was relatively narrow, ranging between 4 and 10 μm. Conversely, at the two highest concentrations, not only was the mean nuclei size larger, but the variability was also larger, with nuclei diameters ranging between 6 and 14 μm for a concentration of 10^{12} microbeads/L and between 10 and 30 μm for a concentration of 10^{13} microbeads/L.

Generally, the two models predicted the droplet nuclei size to be within the range measured by the experiments (Figure 6.10 b). However, the observed variability was not predicted by the models and can make a significant difference in terms of the risk assessment. The 10^{13} microbeads/L concentration yielded a nuclei size of 20 μm on average, too large to be inhaled, which would therefore decrease the exposure risks. However, the size distribution ranged between 5 and 30 μm. This entails that a significant quantity of potentially contaminated particles were small enough to be inhaled. In that case, the model would have underestimated the risks.

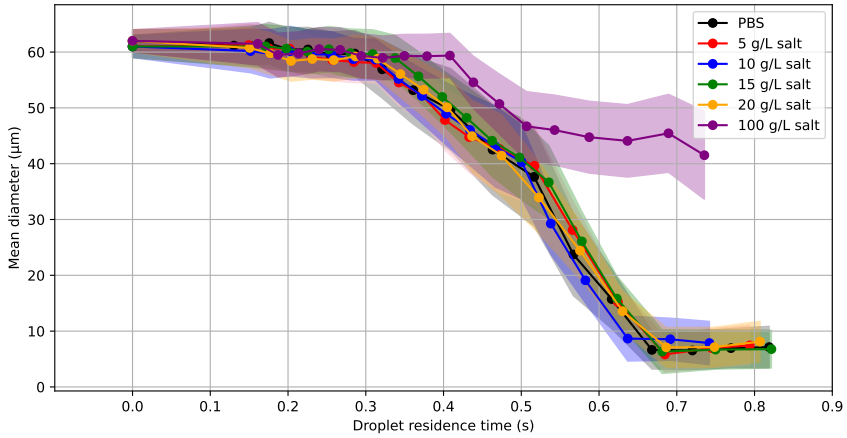

(a)

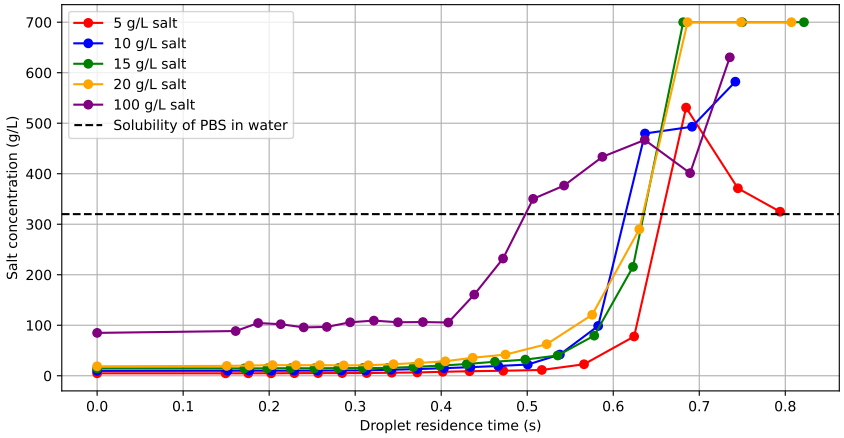

(b)

Figure 6.9 (a) Mean diameter as a function of residence time for different concentrations of dissolved solids. The standard deviation of measurements is shown as shaded error bars. (b) Evolution of the salt concentration with the droplet airborne residence time.

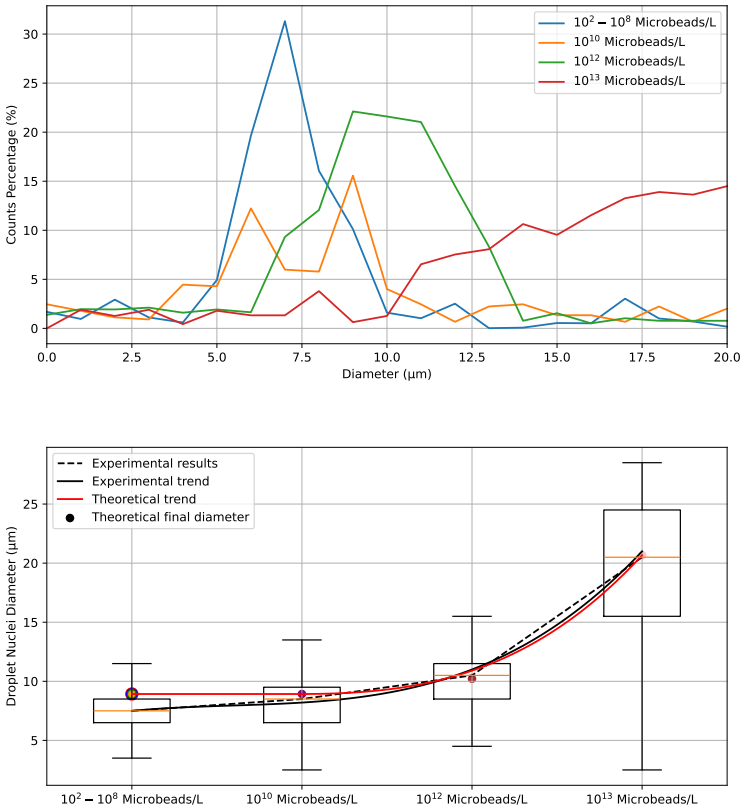

(a)

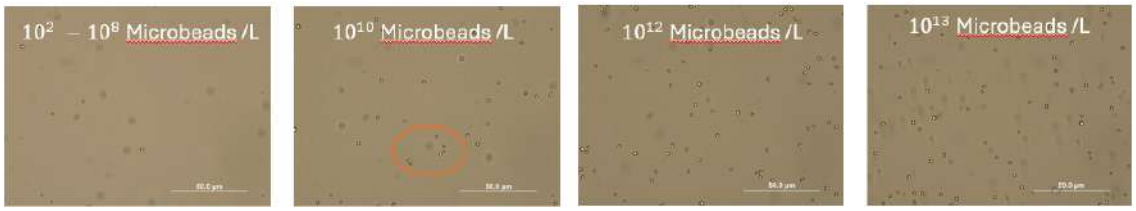

(b)

Figure 6.10 (a) Left: Final size distribution for different microbeads concentrations. Counts percent are displayed as a function of diameter. Right: Box plot of the nuclei size for the different microbeads concentrations. On each box, the central mark indicates the median and the bottom and top edges of the box indicate the 25th and 75th percentiles respectively. The whiskers extend to the 5th and 95th percentiles. The trends of the average nuclei size is compared between the two models and the experiments. (b) Microscope images of solutions with different microbeads concentrations. The circled microbeads highlight the random distribution of the microbeads in the bulk and the possibility that clusters can form.

Most interestingly, the size distribution was bimodal for a concentration of 10^{10} microbeads/L, with a final size peak at 6 μm and another at 9 μm (Figure 6.10 a). This phenomenon can be explained by the fact that this concentration in the bulk solution yielded droplets containing on average 1.2 microbeads. Therefore, according to the assumption that microbeads behave like bacteria such that they are distributed randomly in the bulk solution, some droplets contained more than 1 microbead whereas some droplets contained one or none [239]. This can be observed in the microscope, where random distribution of microbeads leads to clusters and empty areas (Figure 6.10 b). The droplets with one microbead or none had a droplet nuclei diameter of 6 μm, while the droplets with more than 1 microbeads reached a droplet nuclei closer to 9 μm.

The bimodal final size distribution highlights the variability in the concentration of contaminants. Indeed, some droplets will contain more viable bacteria than others, which can increase the risks of infection. In the context of the airborne transmission of *Legionella* bacteria from cooling towers, where low doses are often required to cause infections in vulnerable individuals [304], and where most cases are sporadic, this result entails that outliers in droplet concentrations and nuclei size can drive the exposure risks. As such, when considering evaporation in a risk model, the variability of both the solids concentration and the droplet nuclei size must also be considered.

6.5 Conclusion

An experimental and analytical study was conducted to characterize the effect of surface tension, viscosity, as well as the concentration of dissolved and suspended non-volatile solids on the evaporation time, the size of the droplet nuclei and the time-resolved size evolution of aerosol droplets. Surfactants introduced non-linearity to the size evolution of evaporating droplets due to the surface properties of surfactant molecules, significantly impeding the evaporation time by as much as 14% and halting the evaporation at high concentrations. Higher viscosity increased the evaporation time because of a delay in the early onset of evaporation due to higher intermolecular forces. It did not affect the droplet nuclei, always at approximately 8-9 μm. The results also demonstrated that high concentrations of at least 10^{10} particles/L of suspended solids almost doubled the evaporation time, led to droplet nuclei size up to 20 μm and significantly impacted the size evolution. As for dissolved solids, when its concentration surpassed the solubility threshold of the bulk solution, precipitation affected evaporation in the same way as suspended solids. The effects of the studied parameters on the evaporation dynamics are not fully encompassed in the current models, which can lead to an underestimation of the exposure risks. The models however accurately predicted the ultimate

droplet nuclei size in cases representative of cooling tower water conditions. Furthermore, taking into account the variability of solids concentration in the aerosol and in the droplet nuclei size is essential for accurate risk modeling, as some large droplets can still become small enough to be inhaled post-evaporation, and potentially cause infection. The results of this study can thus be used to improve the accuracy of the risk assessment models by including the evaporation of contaminated droplets through evaporation models.

Acknowledgements

This research was supported by a NSERC Alliance Grant (ALLRP545363/2019), Polytechnique Montréal. Xavier Lefebvre is supported by the Hydro-Québec excellence scholarship as well as a NSERC scholarship (ES D) with a FRQNT supplement (B2X).

Conflict of interest

The authors declare no competing interests.

Supporting Information

The data that support the findings of this study are available upon reasonable request from the authors.

CHAPTER 7 ARTICLE 4: EVAPORATION OF AN AEROSOL PLUME FROM AN INKJET PRINTHEAD

Submitted to *Experiments in Fluids* on October 30 2024

By
Xavier Lefebvre and Etienne Robert

7.1 Abstract

The size of aerosol droplets is a critical factor in evaluating the risks associated with airborne pathogen transmission, yet it is highly variable due to evaporation. Additionally, the close proximity of water droplets within an aerosol plume can slow their evaporation, thereby further complicating risk assessments. To investigate these complexities, a versatile experimental setup was developed using the XAAR XJ128 inkjet printhead to generate droplets of 50 μm in diameter for detailed evaporation characterization within a plume. The droplet evaporation process was monitored via Phase Doppler Anemometry (PDA), which provided size distribution and velocity measurements at various positions along the vertical axis of the falling droplets. These experimental results were compared to a theoretical model for isolated droplet evaporation in quiescent air. Droplet number density significantly influenced evaporation, with measured evaporation rates in the plume, originally at a relative humidity of 30%, comparable to the theoretical model under 60-80% relative humidity when nearly all printhead nozzles were active. The effect of number density on evaporation was also analytically evaluated. Notably, the complete evaporation of droplets in this configuration could theoretically increase relative humidity up to 89% locally when all nozzles were used, while using about one-third of the nozzles resulted in a local relative humidity up to 33%. These insights underscore the importance of further investigating the evaporation dynamics of airborne aerosol droplets in the context of pathogen transmission. The use of an inkjet printhead demonstrates its significant potential for generating a controlled aerosol plume, offering a promising avenue for future research in this critical area.

7.2 Introduction

Aerosol droplet evaporation is a critical process in the transmission of airborne diseases. It has been extensively studied in the context of illnesses such as tuberculosis, influenza, and COVID-19 [165, 305]. However, much of this research has focused on the simplified scenario of a single droplet evaporating in quiescent air [24]. In contrast, work by Bourouiba

et al. has demonstrated that contaminated droplets are typically expelled from humans within a turbulent aerosol plume, through coughing, sneezing, talking or singing [3, 23]. This phenomenon similarly applies to engineered sources such as showers, faucets, toilets, or cooling towers, where potentially contaminated water-based droplets are released in a plume capable of transporting pathogens over greater distances [306]. In these scenarios, the evaporation dynamics of the aerosol are likely influenced by the proximity (number density) of the droplets with each other and the thermo-physical properties of the plume [20]. This phenomenon was thoroughly investigated for sessile droplets [307], but not for airborne contaminated droplets. As evaporation dynamics were shown to differ significantly between airborne and sessile droplets in the context of airborne transmission [3], this highlights a significant research gap in the understanding of droplet evaporation in the context of airborne transmission.

Laboratory experiments have employed various aerosol generation mechanisms for droplet production, including spray atomization, ultrasonic nebulization, and single droplet-on-demand techniques [185–187]. Each of these methods offers distinct advantages and disadvantages. However, none can consistently and simultaneously control droplet direction, frequency, quantity, and size distribution, nor provide a homogeneous spatial concentration. As a result, these techniques are inadequate for the precise study of evaporating droplets within a plume. Conversely, piezoelectric inkjet printing is recognized as one of the most effective ways to achieve accurate and reliable droplet generation [189]. The underlying principle behind the technology involves the creation of a pressure pulse inside the fluid with a piezoelectric element. At every pulse, a precise amount of fluid is pushed outside of the channel through a thin nozzle and because of the surface tension of the bulk media, a droplet is generated. Although commonly used in standard paper printers, this method can also be applied to various fluids beyond ink. The pulse frequency of the piezoelectric elements controls the droplet production rate, enabling their generation in close proximity to one another. Additionally, inkjet printheads typically feature multiple nozzles, which can be controlled independently, facilitating the precise arrangement of droplets in the transverse direction. This technique allows for continuous droplet generation with high precision, accommodating a wide range of fluid types and the possibility to vary the number density of the droplets [308].

A versatile experimental setup that generates droplets suitable for the evaporation characterization of droplets within a plume was developed using the inkjet printhead technology. The objective of this study was to investigate the effect of the number density of water-based droplets on their evaporation dynamics.

7.3 Methodology

The commercial XAAR XJ128 printhead was selected for its versatility in accommodating fluids with various properties. It was operated according to the guidelines provided in the XAAR operation manual [309], utilizing custom control electronics. An Arduino Uno module was employed to control the jetting frequency and the number of generated droplets from the printhead. The full Arduino code to operate the printhead is provided in the Supplementary information section. To supply the necessary 35 V power to the printhead, two 36 V power supplies were used, with relay modules managing the electronic power delivery to the printhead. The XAAR XJ128 inkjet printhead, equipped with 30 pins, was connected and controlled via Serial Peripheral Interface (SPI) protocol [310]. The detailed connections are illustrated in Figure 7.1.

Water droplets of approximately 50 μm (80 pL) in diameter were reliably generated through its 128 nozzles with a maximum frequency of 4.25 kHz. Droplets were generated inside a sampling chamber designed to isolate the generated droplets from ambient air currents, measuring 0.15 m $\times$ 0.15 m $\times$ 0.6 m, with an opening at the bottom to induce laminar circulation. A 30 SLPM laminar flow of pressurized air at 30% relative humidity was injected into the sampling chamber in the same direction as the droplets to facilitate the measurement (Figure 7.2).

The Phase Doppler Anemometry (PDA system, Dantec Dynamics, Skovlunde, Denmark) technique was used to characterize the aerosol droplets. The measurement volume is defined by the intersection of two pairs of laser beams with wavelengths of 532 and 561 nm. As single droplets flow through, light is scattered from the interference pattern created by the two laser beam pairs, allowing for size distribution and velocity characterization [275]. The droplet velocity is obtained from the Doppler shift of the interference fringes, while information on its size can be acquired from the phase shift. Since the measurement volume is very small, measurements are considered punctual, making it ideal for the characterization of individual droplets generated from the inkjet nozzles [276]. The PDA can detect particles between 0.5 and 8000 μm, covering the range of the generated droplets from their inception down to their size stabilization as evaporated nuclei.

The evaporation of the generated droplets was assessed with the PDA by measuring their size distribution and velocity at several positions along the vertical axis in line with the falling droplets. The PDA was mounted on a traverse to map the evolution of the droplets. For each solution, a scan was conducted starting 1 mm under the nozzle and moving progressively 200 mm downwards, with steps of 10 mm (Figure 7.2 a). Each point was sampled for 10 seconds

and the printhead stopped between the measurement points to allow for slight adjustments and refilling with water. Two configurations of the printhead were tested: 120 working nozzles were used to generate droplets in high number density horizontally, or 40 nozzles (one operating out of every three) to generate a less dense aerosol. For both configurations, the jetting frequency was set at 1 kHz.

Data analysis

The size evolution of the droplets was acquired as a function of to their position downwards from the generation site (Figure 7.2 b). The position of the droplets was converted to the cumulative residence time, using the known distance between two measurement points L (0.01 m) and the velocity from the previous measurement point v (m/s).

$$t_n = \sum_{i=2}^{n} \frac{L}{v_{i-1}} \tag{7.1}$$

The evaporation of the droplets was compared to the theoretical evaporation of a single droplet of pure water in quiescent air at different relative humidities. From the squared law of evaporation [24, 153, 154], the radius of the droplet r (m) as a function of time t (s) can be expressed as follows, knowing the initial radius r_0 (m), the diffusion coefficient D (m^2/s), the density of the air ρ (kg/m^3), the saturation concentration of water in air c_s (kg/m^3) and the concentration of water in air c_∞ (kg/m^3) :

$$r(t) = \sqrt{r_0^2 - 2\frac{D(c_s - c_\infty)}{\rho}t} \tag{7.2}$$

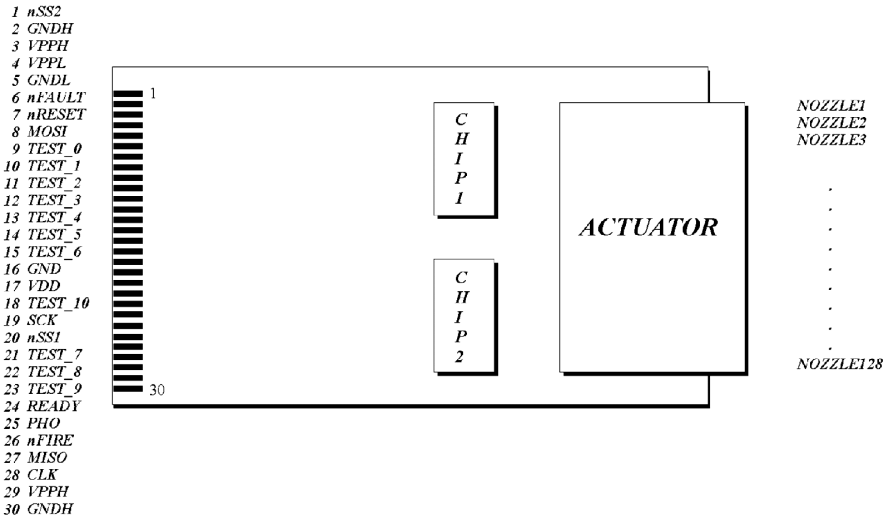

(a)

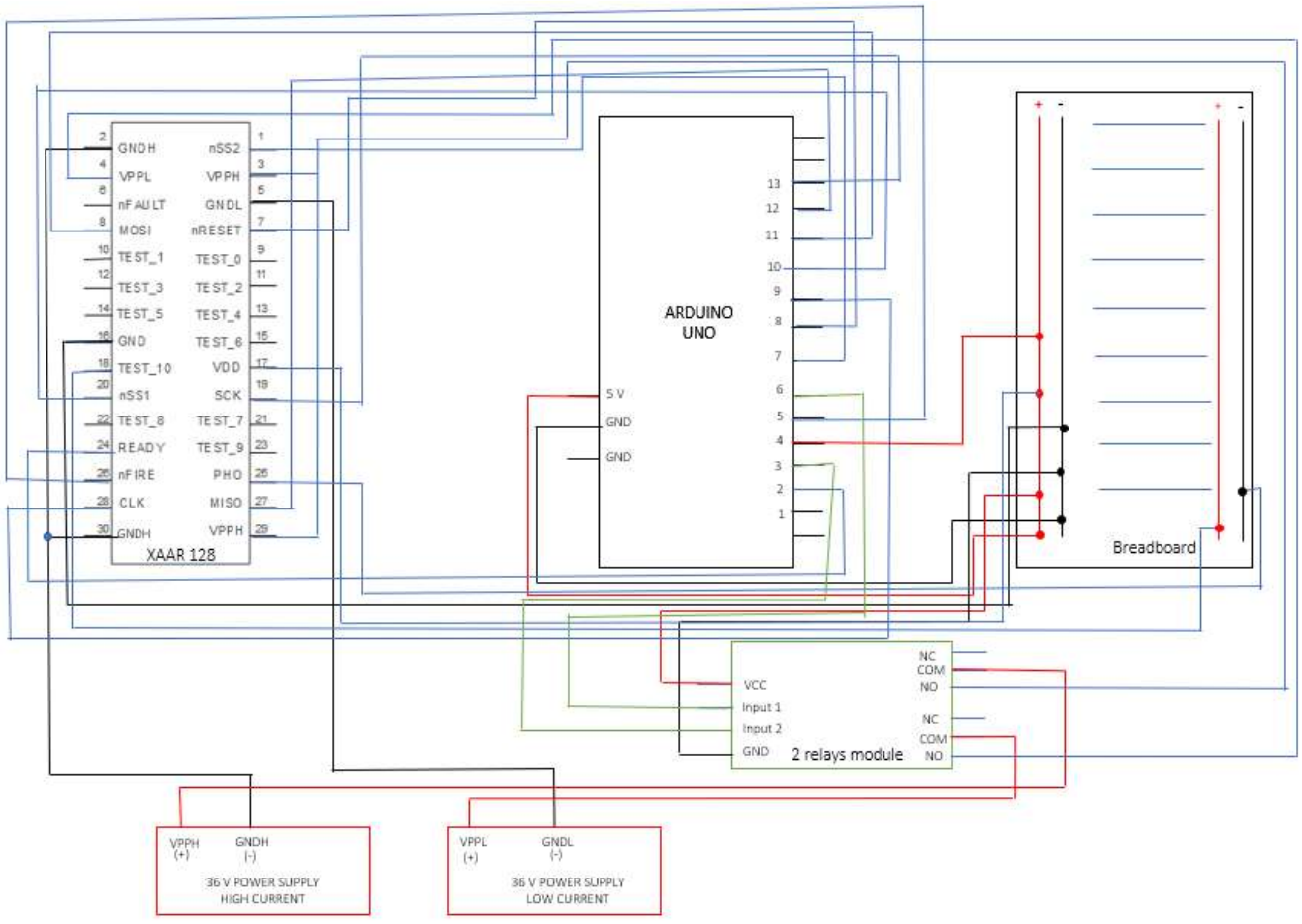

(b)

Figure 7.1 (a) Pins of the XAAR printhead with their respective SPI signal identification. (b) Connections of the XAAR printhead to the hardware.

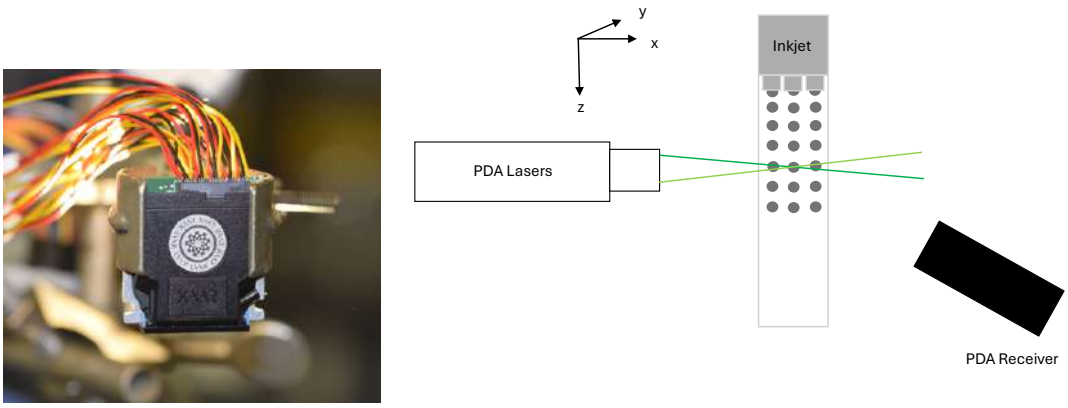

(a)

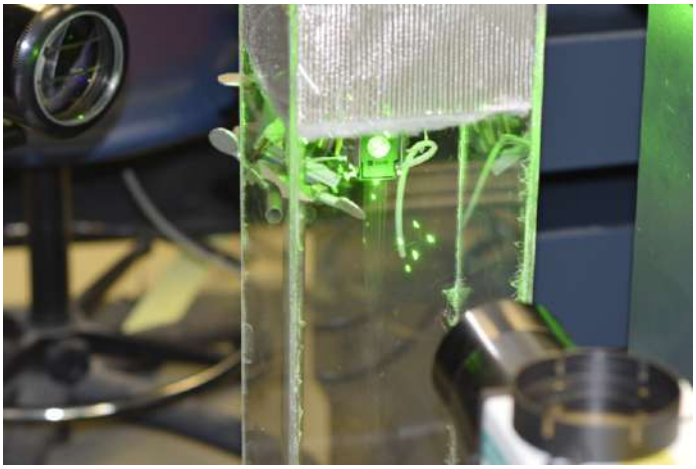

(b)

Figure 7.2 (a) Left: XAAR XJ128 inkjet printhead. Right: Schematic of the sampling chamber and the PDA measurement. (b) XAAR aerosol generation and measurement with the PDA.

7.4 Results and Discussion

7.4.1 Multiphase flow characterization

Measurements of droplet velocity and mean diameter as a function of the position of the PDA with 40 operating nozzles on the printhead are displayed in Figure 7.3 a) and b). Upon generation, droplets travelled at approximately 1.65 m/s and their velocity decreased to 0.75 m/s at the bottom of the test section. This velocity decrease is expected as the co-flow of air injected at 30 LPM travels at 0.025 m/s. The droplets are subject to drag, which slows them down. Droplets fully evaporated before the terminal velocity was reached (Figure 7.3 b). From the size distribution and velocity measurements, the mean diameter of the droplets was calculated as a function of the residence time, as described in equation 1 (Figure 7.3 c).

The variability of the velocity measurement increased with distance from the droplet generation site (Figure 7.3 a). 175 mm away from the generation site, the standard deviation was more than 5 times larger than at the generation site. This was likely due to the high exiting velocity of the generated droplets compared to the co flow velocity, which can create local disturbances in the co-flow due to the drag [311]. This variability in the velocity of the droplets did not affect the evaporation curve, which displayed small measurement errors (Figure 7.3 b). Also, these small disturbances in the flow did not affect the trajectory of the droplets either. Indeed, the Reynolds number (Re) of the co-flow was approximately 250, indicating laminar flow with linear streamlines moving downward. At the droplet generation site, the Stokes number (St) was 0.3, meaning the droplets closely followed the streamlines. As the droplets evaporate, the Stokes number decreased further, reinforcing the assumption that the droplets generally traveled in a straight downward path. Furthermore, the distribution of the velocity measurements was Gaussian (Figure 7.4), justifying the use of the average velocity over the 10 000 droplets measured at each point for the evaporation curve.

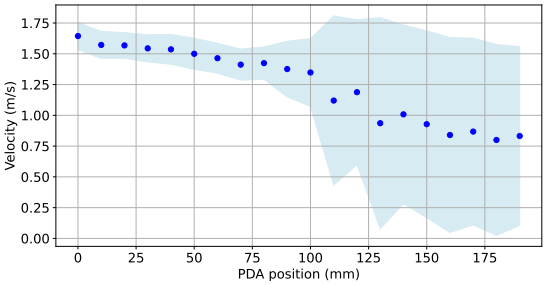

(a)

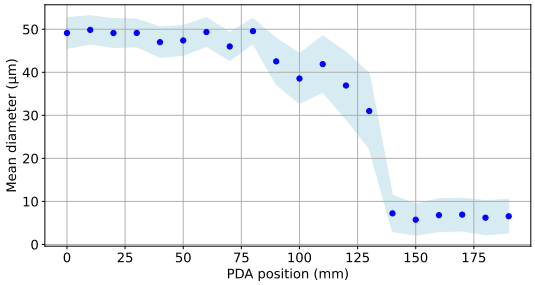

(b)

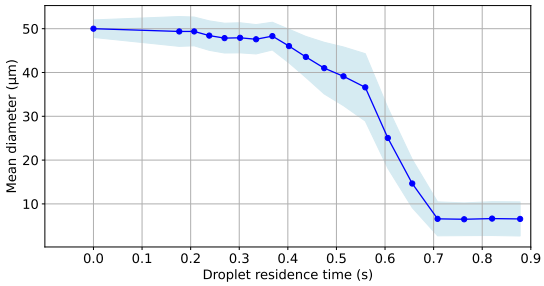

(c)

Figure 7.3 (a) Droplet velocity as a function of the position of the PDA. (b) Mean diameter of the droplets as a function of the position of the PDA. (c) Mean diameter according to residence time. The standard deviation of measurements is shown as shaded error bars.

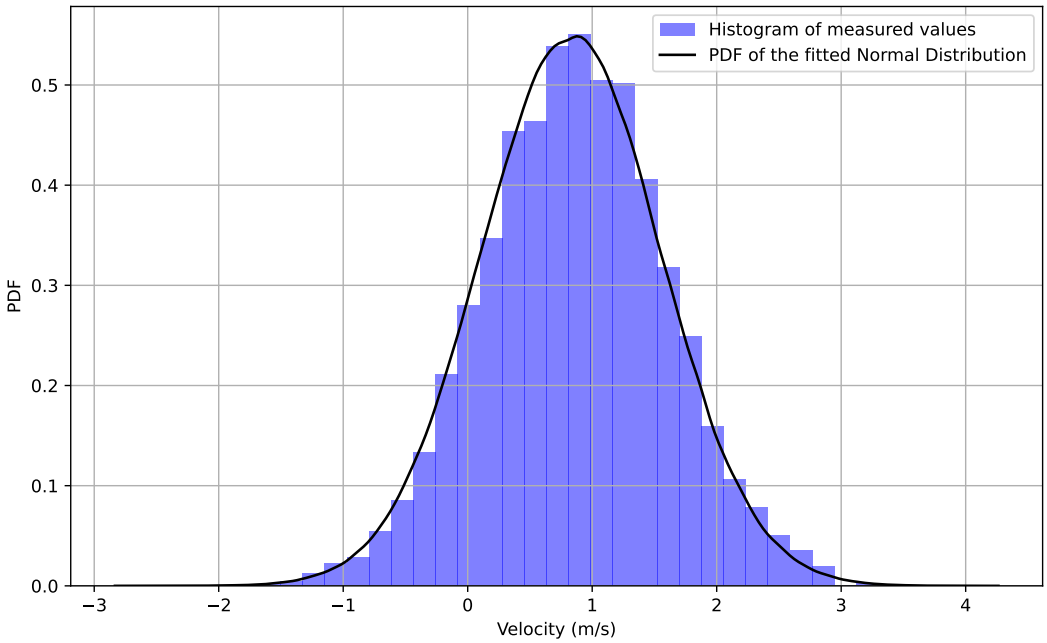

Figure 7.4 Probability distribution function (PDF) of the droplet velocity at 175 mm downwards from the generation site.

7.4.2 Effect of number density on pure water droplet evaporation

The evaporation results were compared to the theoretical evaporation of a single droplet of pure water in quiescent air at different relative humidities (Figure 7.5). When using approximately a third of the nozzles from the printhead, the droplets evaporated at a similar rate than predicted by the model for 30-40% relative humidity. However, when employing almost all the nozzles of the printhead, the droplet evaporation followed the theoretical curves for 60-80% relative humidity. The pressurized air injected into the experimental setup was always at approximately 30% relative humidity. Thus, the number density of the droplets influenced the evaporation process by increasing the local moisture concentration.

The droplet evaporation time was approximately 0.7 seconds using a third of the nozzles and 1.3 seconds with all the nozzles, corresponding to a 85% increase due to number density of the droplets. A similar phenomenon was also observed by Hatte et. al who observed a 65% increase in evaporation time for a sessile droplet with similar droplet density [307]. The different magnitude of this effect on evaporation time could be due to the airborne configuration as opposed to the sessile droplet experiment from the Hatte et. al.

7.4.3 Local effect of droplet number density on relative humidity

To assess the effect of the number density of the droplets on the relative humidity, it was necessary to determine the spacing between the droplets, which can be defined as the distance between the edges of two adjacent droplets. The vertical spacing between two generated droplets Δz can be calculated with the following equation, knowing the droplet generation frequency f and the droplet initial velocity V_d :

$$\Delta z = \frac{1}{f} \times V_d \tag{7.3}$$

With a generation frequency of 1 kHz and an initial velocity of approximately 1.5 m/s measured with the PDA, the 50 μm droplets were vertically spaced by 375 μm. Horizontally, the droplets were 137 μm apart when 120 nozzles were fired and 511 μm when 40 nozzles were fired, according to the spacing between two adjacent nozzles. The disposition of the droplets upon generation is shown in Figure 7.6.

The effect of the number density of the droplets on the relative humidity can be assessed analytically. Considering an arbitrary volume composed of inkjet printed aerosol droplets in air, as shown in Figure 7.6, it initially contains a specific mass of water vapor. This mass of water vapor in the air can be calculated using the ideal gas law, knowing the relative

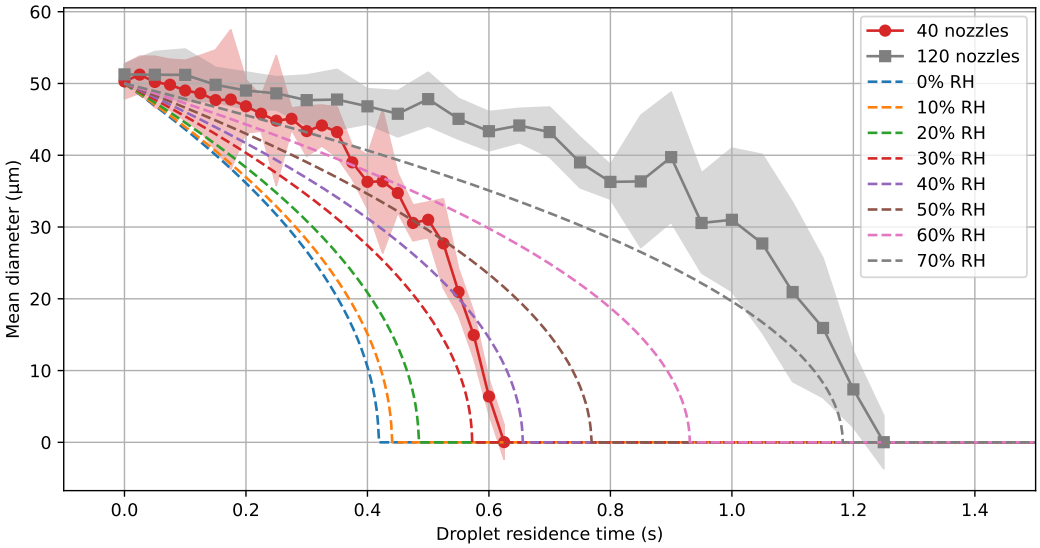

Figure 7.5 Mean diameter as a function of residence time for pure water droplets using a 40 nozzles and 120 nozzles from the printhead. The standard deviation of measurements is shown as shaded error bars. The experimental results are compared to the evaporation equation for the evaporation of pure water droplets in quiescent air at different relative humidity rates.

humidity of the air flowing in the sampling chamber, which was approximately 30%.

$$PV = \frac{m_w}{M} RT \tag{7.4}$$

Where P (kPa) is the vapor pressure at the specific relative humidity, V (m^3) is the volume, m_w (kg) is the mass of water vapor, M (kg/mol) is the molar mass of water, R ($J/mol \cdot K$) is the ideal gas constant and T (K) is the temperature.

As droplets are generated from the printhead, a specific number of droplets, and thus water molecules, occupy the considered volume of air (Figure 7.6). The mass of water vapor of the volume of air will gradually increase locally depending on the number density of the droplets. The added mass of water vapor in the volume of air at the end of the evaporation process can be calculated using the mass of the droplets, assuming complete evaporation of the pure water droplets.

$$m_d = n_d \rho_w \frac{\pi d^3}{6} \tag{7.5}$$

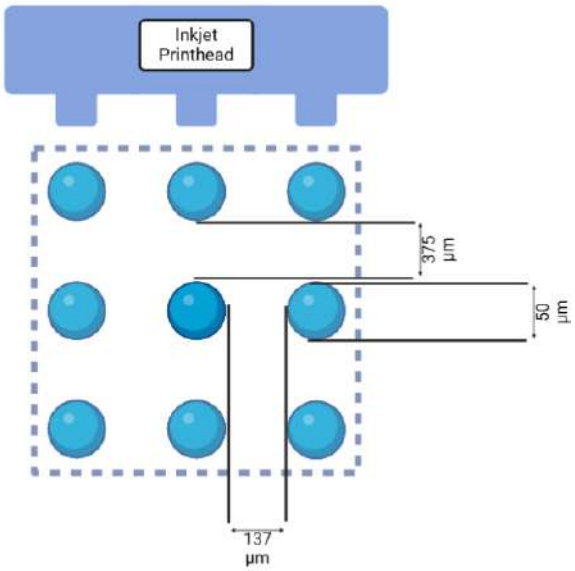

Figure 7.6 Schematics representation of the disposition of the aerosol droplets generated by the XAAR XJ128 inkjet printhead upon generation. The number density of the droplets when 120 nozzles are employed is displayed. The volume of air considered for the calculation of the effect of the droplets on the relative humidity is shown as the dotted square and encompasses 9 droplets from edge to edge. The figure is not to scale.

Where m_d (kg) is the mass of the droplet, n_d is the number of droplets, ρ_w (kg/m^3) is the density of water and d (m) is the diameter of the droplet.

Finally, the effect of the number density of the droplets on the local relative humidity ΔRH (%) can be calculated by comparing the mass of water vapor in the air at the end of the evaporation process with the mass of water vapor in the air at 30% relative humidity using the following equation where m_{sat} (kg) is the mass of water vapor in the air at 100% relative humidity:

$$\Delta RH = \frac{m_d + m_w}{m_{sat}} - RH_{initial} \tag{7.6}$$

A volume of air encompassing 9 droplets generated from center jets was considered for calculations. At standard laboratory conditions of 25°C, 1 atm and 30% relative humidity, the complete evaporation of the droplets could increase the local relative humidity up to approximately 89% when employing all the nozzles of the printhead. Conversely, when using only 40 of the nozzles, it would increase locally up to approximately 33%. The difference between

the two configurations is expected. As the 120 nozzle configuration generates 3 times more water droplets than the 40 nozzle configuration, the local relative humidity increase is also 3 times higher.

This increase in relative humidity explains the slower evaporation of the droplets when they are generated in high number density. The evaporation curve of droplets generated in the 40 nozzle configuration matched the theoretical curve for 30-40% relative humidity and match with the calculated local relative humidity of 33%. The 120 nozzle configuration matched the theoretical curve for 60-80% relative humidity, slightly lower than the 89% local relative humidity calculated. This difference can be due to the large differences between the global and local relative humidity. Indeed, due to this increasing relative humidity gradient, the diffusion rate of water vapor from the area of higher partial pressure to the lower one will be greater. Thus, the local relative humidity can be lower than theoretically calculated.

As such, it can be assumed that the droplet generation influences the evaporation process and that our experimental setup was suitable for evaporation characterization of an aerosol plume. Understanding these evaporation dynamics is essential not only for experimental precision but also for broader implications, particularly in the context of airborne transmission. The rapid size changes due to evaporation directly impact the transport, deposition, and inhalation of aerosol droplets, and even the extent to which a pathogen remains virulent. Thus, characterizing evaporation timing is critical for accurate risk assessments in pathogen transmission models.

7.5 The experimental potential of the inkjet printhead

The experimental setup using an inkjet printhead and the PDA offers notable advantages, including high-resolution size and velocity measurements, as well as suitability for detailed evaporation characterization of aerosol droplets within a plume. These features make it a valuable tool for precise and nuanced studies. However, the setup is not without its limitations. Issues with clogged nozzles on the printhead have posed challenges, making droplet generation cumbersome and occasionally inconsistent. Additionally, the XAAR XJ128 printhead is fragile and requires careful handling to avoid damage. Despite these drawbacks, the experimental setup provides significant potential benefits for advanced aerosol research, highlighting the need for ongoing improvements to address its limitations.

Inkjet printing, originally developed in the 1950s, has predominantly been used for paper printing. However, the technology holds significant potential beyond its conventional applications [308]. The capabilities of the technology extend to environmental and occupational health studies, offering possibilities for aerosol characterization, air quality monitoring, pollution analysis, and the study of airborne contaminant dispersion. In drug delivery systems, piezoelectric inkjet printing can enable precise respiratory drug delivery [312]. In biological and medical research, it has the potential to facilitate advancements in cell culture and tissue engineering [313]. Additionally, it could play a crucial role in material deposition within material science and in the fabrication of printed electronics [314, 315]. Furthermore, it could be used in combustion studies through the aerosolization of fuels [316]. This potential for diverse applications highlight the untapped versatility of piezoelectric inkjet printing technology, suggesting a promising future in various scientific and industrial fields.

7.6 Conclusion

In this study, a versatile experimental setup was developed using the XAAR XJ128 inkjet printhead to generate droplets for examining evaporation dynamics within a plume. The droplet size distribution and velocity was measured at various vertical positions using PDA to assess the evaporation process. The observed evaporation behavior was then compared with theoretical models of a single droplet of pure water in quiescent air at 30% relative humidity. Results indicated that the number density of droplets within the plume significantly impacted the evaporation rate. When nearly all printhead nozzles were active and the generated droplets were in high number density, the evaporation rate aligned with the theoretical model under 60-80% relative humidity. According to analytical calculations, full evaporation of droplets increased local moisture concentration up to 89% when all nozzles were used, whereas employing only a third of the nozzles resulted in a 33% local relative humidity. This

characterization of evaporation dynamics is crucial for improving our understanding of airborne transmission risks. Additionally, the versatility of the experimental setup suggests its potential for further applications in aerosol research and environmental studies.

Supplementary information

The full Arduino code to control the XAAR XJ128 printhead is available on github at the following link: `https://github.com/xalef/xaar128/tree/main`

Acknowledgements

This research was supported by a NSERC Alliance Grant (ALLRP545363/2019), Polytechnique Montréal. Xavier Lefebvre is supported by the Hydro-Québec excellence scholarship as well as a NSERC scholarship (ES D) with a FRQNT supplement (B2X).

Declarations

The authors have no conflicts of interest to declare that are relevant to the content of this article.

CHAPTER 8 ARTICLE 5: DATA-DRIVEN COOLING TOWER OPTIMIZATION: A COMPREHENSIVE ANALYSIS OF ENERGY SAVINGS USING MICROSAND FILTRATION

Accepted for publication in *Applied Thermal Engineering* on October 25 2024 [194]

By

Xavier Lefebvre, Vaishali Ashok, Dominique Claveau-Mallett, Etienne Robert and Emilie Bedard

8.1 Abstract

Effective management of cooling tower systems requires thorough water quality control. While traditional chemical water treatment methods are currently the most prominent strategy, they are costly and may yield limited results when relied upon as the sole approach. Cross-flow microsand filtration systems offer an interesting alternative with the added benefit of potentially increasing evaporative cooling efficiency, thus saving energy. The focus of the study was to evaluate the effect of these filtration systems on cooling tower operation. A comprehensive data-driven analysis over two cooling seasons evaluated the energetic performance of a system equipped with and without an operating filter using continuous monitoring and statistical modeling. For similar environmental conditions, the coefficient of performance was on average 18% higher and was higher 63% of the time when the filter was operating, indicating superior heat transfer efficiency and significant energy savings. It was also 41% higher during periods of high cooling demand. Consequently, the filter and the system work more efficiently at high wet-bulb temperature and thermal load. Machine learning modeling suggested that operating the filter year-round could save between 5% and 13% of the energy bill, primarily during the cooling season. Continuous filter operation is essential as it mitigates biofouling, underscoring its long-term significance, even during periods of lower thermal loads. The results of this study are significant for sustainability, public health and hold broader implications for cooling tower management. Integrating filtration systems into cooling tower management therefore fosters sustainable practices by decreasing energy consumption and biofouling. This study presents a novel approach by demonstrating, for the first time, the significant impact of continuous cross-flow microsand filtration on cooling tower efficiency, both in terms of energy savings and biofouling mitigation.

Nomenclature

Nomenclature

E	Energy (kWh)
$\dot{Q}$	Heat absorbed from the building (W)
$\dot{m}$	Mass flow rate of the process water (kg/s)
T	Temperature (K)
c_p	Heat capacity of the water (J/kg K)
ΔT	Temperature difference (K)
P	Power consumption (kW)
V	Working voltage (V)
I	Operating electric current (A)
N	Operating speed (RPM)

Greek Symbols

η	Coefficient of performance

Subscripts

in	Entering the system
out	Exiting the system
w	Water
air	Air
co	Electric energy consumed by the system
ex	Thermal energy exchanged inside the system
$Vortisand$	Electric energy consumed by the Vortisand filter
fan	Fan
$pump$	Pump
$HeatExchanger$	Heat exchanger
$load$	Thermal load
$Chiller$	Chiller
ON	Filter operating
OFF	Filter not operating
0	Nominal value

Abbreviations

COP	Coefficient of performance
MLJ	Machine Learning Julia

8.2 Introduction

Operating on the principle of evaporative heat transfer, cooling towers expose warm process water to ambient air, efficiently lowering its temperature [35]. The evaporative cooling efficiency, or performance, can be defined as the ratio of the energy to be evacuated by the tower (thermal load) to the energy required to operate the system [120]. This metric is called the coefficient of performance (COP) and is a measure of the effectiveness of transferring heat between two fluids [121]. Understanding the complex interplay of factors influencing cooling tower performance is essential for optimizing energy efficiency and reducing operational costs. Factors such as the wet-bulb temperature, the lowest atmospheric temperature achievable by evaporating water into a volume of air at constant pressure, as well as water quality and control strategies, all contribute to the overall efficiency of cooling tower operation [118]. Additionally, thermal inertia, a measure of heat gradually stored and released in a building, also plays a significant role in determining operational efficiency [119]. However, despite technical advancements in cooling tower design, most systems still operate below their optimal efficiency levels [129]. This inefficiency results in increased energy consumption, higher operating costs, and potentially negative environmental impacts [130–132]. Collectively, these studies highlight the multifaceted challenges in cooling tower operation, indicating that while individual factors like wet-bulb temperature and thermal inertia have been explored extensively, there remains a gap in integrated approaches that simultaneously address these variables for holistic system optimization. As such, there is a strong need to address these inefficiencies through the integration of innovative technologies.

Inefficiencies in cooling tower systems can stem from bad original design, but it is typically because of a deteriorating system accompanied by an accumulation of biofilm. Cooling tower systems are not only comprised of the tower itself but also include pumps, heat exchangers and chillers. These elements are typically connected via a piping network, offering a large surface area for biofilms to develop and thrive [76]. Biofilm is a structured community of microorganisms attached to the surfaces, and its accumulation can act as an insulating layer, decreasing the heat transfer rate by up to three orders of magnitude [122]. Biofilms can also reduce the effective diameter of pipes, impeding the flow of water and reducing the heat transfer efficiency as less water is exposed to the surrounding air [123]. Thorough removal of biofilm is particularly difficult due to its complex structure and the presence of protective extracellular polymeric substances, which shield embedded microorganisms from antimicrobial agents, thus necessitating comprehensive strategies for effective control [317]. Furthermore, the large surface present in cooling tower systems makes it even more challenging to efficiently disinfect contaminated cooling towers [32]. This underscores the pervasive challenge

of biofilm formation in cooling systems, highlighting the critical need for integrated control strategies that address both the mechanical and biological aspects of biofilm management.

Typical cooling tower water disinfection and conditioning strategies can cost from 50 000 to 300 000 USD annually [93]. These strategies are often damaging to the cooling tower system over time, inducing significant corrosion and scale formation, which can reduce the heat transfer efficiency by up to two orders of magnitude, and compromise cooling tower performance, potentially causing operational issues [40, 94]. Thus, sustainable methods such as mechanical filtration of the process water have become more relevant in recent years. Cross-flow microsand filtration effectively removes particulate matter and microorganisms larger than 1 μm from water [96, 97]. These systems are usually combined with a lower dosage of the chemical treatment. This approach not only enhances microbial control but also contributes to a reduction of corrosion and scale formation [98, 99], thereby improving the overall physical state of cooling tower systems. This reflects a growing consensus on the importance of integrating mechanical filtration with chemical treatment as a more sustainable alternative to traditional methods, addressing both efficiency and longevity of cooling tower systems. Given the potential of this technology in terms of water treatment, an important question therefore needs to be investigated and quantified: Can the process of filtering the cooling tower water with a microsand filter increase the coefficient of performance of the system?

Cooling tower operation and management typically display significant variability over timescales ranging from minutes to months [32]. This highlights the importance of continuously monitoring operating cooling towers using a data-driven approach, which can provide information on the validity of the treatment strategy, as well as the effect of external factors such as thermal load on the operation of the system [41, 318]. However, because of the technical challenges involved in the longitudinal monitoring of cooling towers, such studies are scarce in the literature. A data-driven approach can provide high resolution information on the operation of a cooling tower system and is thus the ideal approach to improve their efficiency. Furthermore, limited research has been conducted to explore the impact of filtration on the operational efficiency of cooling towers. The majority of studies have been either analytical [118, 319] or conducted experimentally at reduced size and time scales, rather than being performed *in situ* [320]. This research gap underscores the necessity for comprehensive, in situ investigations that can more accurately capture the operational dynamics and long-term effects of filtration technologies. To address this research need, a data-driven comprehensive analysis was conducted on the performance of a cooling tower system equipped with a cross-flow microsand filtering system over 18 months to quantify the effect of this approach

on the energy performance. The analysis was carried out on the basis of a system operating alternatively with and without a filter.

Previous work conducted on this topic have attempted to address some of the highlighted research gaps. However, each of them falls short of addressing the totality of the research gaps tackled by this study. For instance, Song et al. [321] explored a data-driven approach using deep learning models to predict the energy efficiency of natural draft cooling towers, but they did not consider forced draft cooling towers nor the impact of cross-flow microsand filtration, which are central to this investigation. Similarly, Silverwood et al. [322] evaluated cross-flow microsand filtration using computational fluid dynamics, but their study was limited to particulate removal and did not assess the impact on cooling tower efficiency, a gap that this work explicitly addresses through in situ analysis. Furthermore, foundational work by Melo and Bott [124–126], as well as Wang et al. [323] delve into biofouling and its effects on heat transfer, yet they do not provide quantitative assessments or solutions applicable to real-world cooling tower operations this study does. Recent studies have also investigated on the energy efficiency of cooling towers, but with marked differences : None of them involved the microsand filtration technology and none of them were data-driven in situ investigations [324–328]. This study addresses these gaps by providing a novel, *in situ*, long-term data-driven analysis of a cooling tower system equipped with a cross-flow microsand filtering system, providing new insights into its effectiveness under real operating conditions.

The next section details the methodology, including sampling procedures and data-driven analysis techniques. Following that, the data-driven methodology is first validated and the results of the effect of the filtration on the performance of the system is then presented discussed. Predictions of the potential energy savings from a machine learning model are then discussed. Finally, the effect of intermittent operation of the filter is assessed and the implications of the results are discussed.

8.3 Methodology

A large-scale data acquisition campaign was conducted over two cooling seasons (2022-2023) on an operating cooling tower system. Data from May to September 2022 and from March to September 2023 was considered, as these months are representative of the typical cooling season, associated with high thermal loads [129]. In Quebec, Canada, the cooling season is typically defined as starting between March and May and running through September due to higher atmospheric temperatures and increased humidity during this period. The exact duration can vary based on the specific climate of the region [329].

8.3.1 Site description

The cooling tower system investigated is implemented in a large building in Montreal, Canada. It can be considered as a large-size system in terms of power consumption [330]. It is composed of three standard 400-ton (1400 kW) counterflow cooling towers (500-TOE-01, 500-TOE-02 and 500-TOE-03), as well as subsystems including two plate heat exchangers (500-EEE-001 and 500-EEE-003) and one water-cooled chiller (500-REF-01) (Figure 8.1). Three vertical centrifugal pumps (500-PET-01, 500-PET-02 and 500-PET-03) feed the water from a basin to each of the subsystems. The water is sprayed inside the cooling towers while ambient air is drawn in with a pair of 10 HP (7.457 kW) axial fans for each cooling tower (not shown in the figure). During the heat transfer, the process water percolates inside the cooling towers and is drained back into a common water basin. Each of the three cooling towers operates independently, based on the total thermal load of the building.

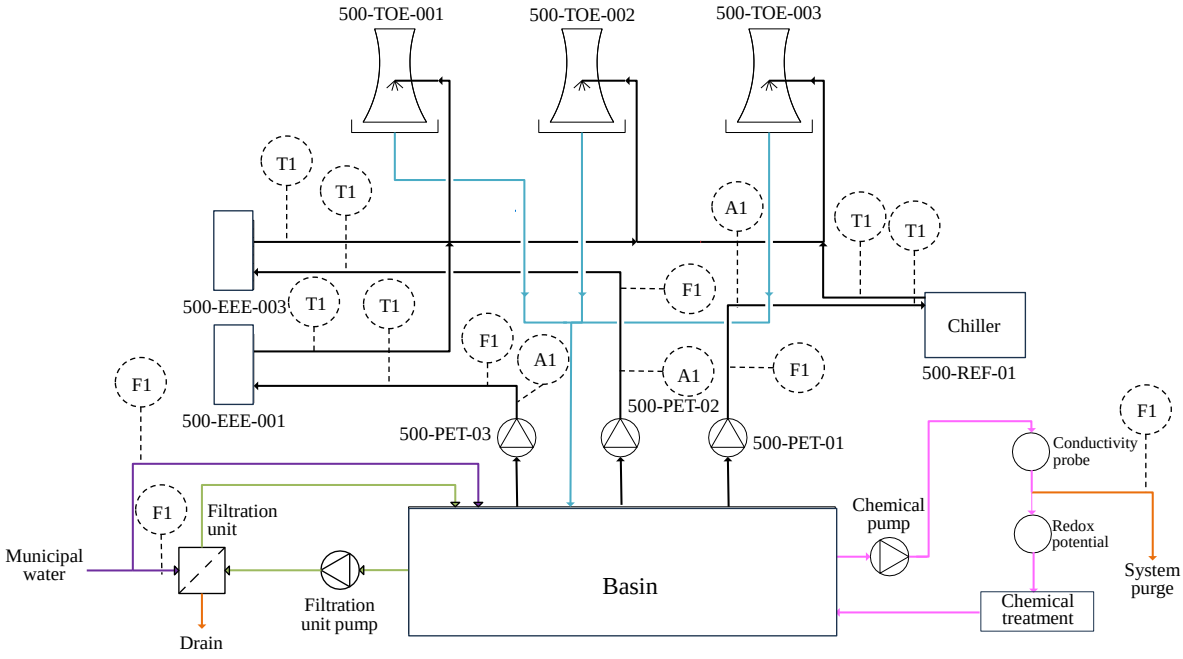

Figure 8.1 Schematics of the cooling tower system and the position of the sensors. Tl are the temperature sensors, Fl the flowmeters and Al the current measurement.

Approximately 20% of the process water flow rate is also circulated through a cross-flow granular microsand industrial filtration system (VORTISAND® Crossflow Microsand Filter) from Xylem+Evoqua. This process is ongoing whenever the filter is active. Standard chemical

treatment is configured and was operated throughout the investigation, with part of the water continuously pumped from the basin to the chemical station and recirculated. This implies that 100% of the water is eventually both filtered and chemically treated when the filter is operational. When the filter is not in use, the water is treated chemically only.

The filter generates a cross-flow water pattern that holds the particles in suspension so as not to obstruct the filtering media. This allows the use of a filtering media composed of fine 0.15 mm microsand, resulting in very efficient capture of suspended particles. The filter was initially installed in 2014 and has been running since, except for the intentional breaks in operation for this study. The original installation was done in 2009. The installation date of 2014 refers to the new patented crossflow injectors and media configuration that was installed for the first time *in situ* for final proofing. The microsand filtration system has been well maintained through the years, with a comprehensive maintenance program including bi-annual verification of the filtration level layer and chemical cleaning of the media. The Vortisand filter was operational for the period between May 2022 to March 6th, 2023, and was first shutdown on March 6th, 2023. It was reactivated from June 26th to July 11th, 2023, then shutdown between July 11th and August 10th, 2023 (Figure 8.2). Between May and September 2022, when the filter was always operating, only heat exchanger 1 (500-EEE-01) was operated. Between March and September 2023 however, heat exchanger 2 (500-EEE-03) was also operated.

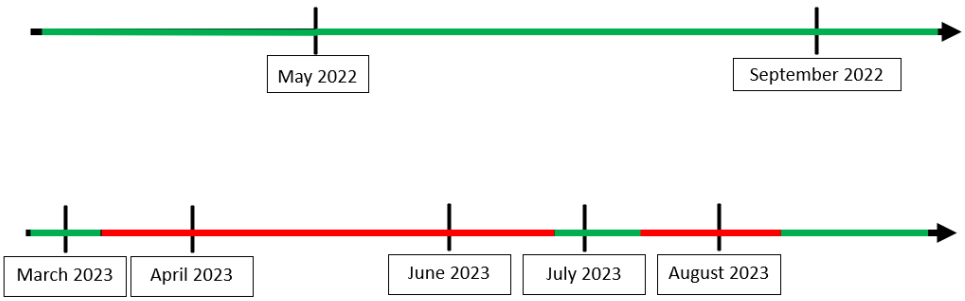

Figure 8.2 Timeline of the Vortisand filtration system operation with regards to the data acquisition campaign. The green line represents the configuration where the filter was operating and the red line configurations where the filter was not operating.

8.3.2 Data Collection

The dataset was acquired through strategically positioned sensors in the cooling tower system (Figure 8.1). To capture the mass flow rate, three flow meters were positioned downstream of each pump (Fl). The temperature profiles within the subsystems were recorded using six sensors (Tl) positioned both downstream and upstream from each heat exchanger and three

more temperature sensors monitored the cooled water temperature inside each cooling tower after the heat transfer (not shown in figure). The ambient wet-bulb temperature and pressure were also collected from the meteorological data of Environment Canada [331]. Additionally, the electric current consumption for each pump (Al) as well as the operational speed and nominal power consumption of the cooling tower fans were recorded. Finally, the duty cycles of each component of the system were deduced from the power consumption data. Datapoints for the temperature were acquired at regular 5-minute intervals throughout the two years of the data acquisition campaign. Datapoints for the mass flow rate were acquired at regular 30-minute intervals and assumed to be constant for 5-minute subintervals.

8.3.3 Thermodynamic energy balance

To assess the effect of filtration on the performance of the system, a thermodynamic energy balance on the whole cooling tower system was conducted (Figure 8.3 a). Because the cooling towers are interconnected and part of the same system, they can thermodynamically be considered as a singular entity rather than individual units. For each of the 5-minute intervals of data recorded, the system was assumed to be in steady state, the heat transfer process was considered isobaric and possible changes in kinetic and potential energy were neglected, the specific heat of water was considered constant. Finally, the heat released into the environment by the cooling tower was considered equivalent to the heat exchanged in the subsystems.

The principle of evaporative cooling involves heat transfer between the cooling tower water and the colder ambient air circulating through the system. From the first law of thermodynamics, the energy balance,can be expressed as a function of the energy carried by the water E_w and by the air E_{air} as well as the work required to draw the air and the water into the system W_{tot} (Equation 8.2):

$$E_{in} = E_{out} \tag{8.1}$$

$$E_{w_{in}} + E_{air_{in}} + W_{tot} = E_{w_{out}} + E_{air_{out}} \tag{8.2}$$

From this energy balance, two important parameters were defined: $E_{co} = W_{tot}$, the electric energy consumed to operate the system and E_{ex}, the thermal energy exchanged inside the system, which is the energy associated with the thermal load (Equation 8.3).

$$E_{ex} = E_{w_{in}} - E_{w_{out}} \tag{8.3}$$

These two parameters were used to assess the coefficient of performance of the system and thus, the efficiency of the system at conducting heat exchange with and without the filter

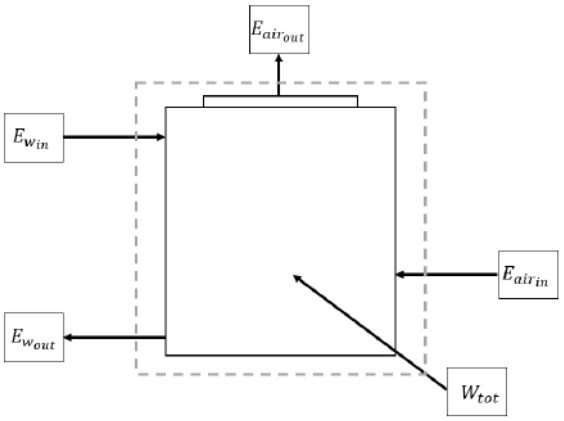

(a)

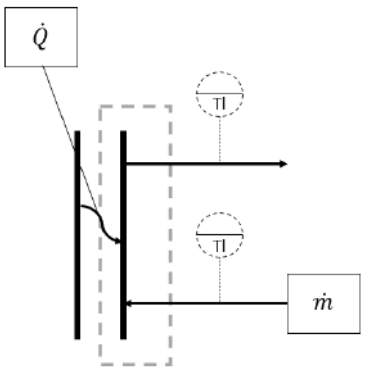

(b)

Figure 8.3 a) Thermodynamic energy balance on the cooling tower, showing the system boundary (dotted square), energy flows (E_w and E_{air}), and work input (W_{tot}). b) Schematic of heat exchanger 1 (500-EEE-01) with temperature sensor positions, illustrating the thermal load ($\dot{Q}$), mass flow rate ($\dot{m}$), and temperature changes (Tl) in the cooling tower system.

operating.

Energy performance parameter

A modified coefficient of performance (COP), was applied to the whole cooling tower system instead of the typical definition for subsystems (Equation 8.4):

$$COP = \frac{E_{ex}}{E_{co}} \tag{8.4}$$

Electric energy consumed by the system

E_{co} was calculated from the electric energy consumed by each pump and fan, as well as by the pump of the filter.

The electric energy consumed by the pumps was calculated from their power consumption P_{pump} (W), knowing the constant working voltage V (V) of 575 V and the measured operating electric current I (A).

$$P_{pump} = VI \tag{8.5}$$

The electric energy consumed by the pairs of cooling tower fans was calculated from their power consumption P_{fan} (kW) using the fan affinity law for power [332], with knowledge of the fan operating speed N_{fan} (RPM) and the nominal power consumption P_0 (kW), which was of 8.3375 kW when the fan is operating at a nominal speed N_0 of 60 RPM.

$$P_{fan} = P_0 \left(\frac{N_{fan}}{N_0} \right)^3 \tag{8.6}$$

From the power consumption of the pumps and the pairs of fan, the respective energy consumed (kWh) was calculated by multiplying the power consumption P (kW) of each of the elements with the time of use t (h). The electric energy consumed by the Vortisand filter $E_{Vortisand}$ was constant at 0.31 kW. This energy need remains constant as the filter is backwashed once a day, thus reducing the increase in resistance. The energy needed for the backwash is included in the 0.31 kW. Finally, the total electric energy consumed by the system E_{co} over time t was given by the sum of the energy consumed by each of the elements.

$$E_{co} = \sum Pt \tag{8.7}$$

$$E_{co} = E_{Pump1} + E_{Pump2} + E_{Pump3} + E_{Fan1} + E_{Fan2} + E_{Fan3} + E_{Vortisand} \tag{8.8}$$

Thermal energy exchanged inside the cooling towers

Likewise, the thermal energy exchanged by the cooling towers between the building and the environment E_{ex} (kWh) was given by the sum of the energy exchanged by each subsystem (both heat exchangers and the chiller).

$$E_{ex} = E_{HeatExchanger1} + E_{HeatExchanger2} + E_{Chiller} \tag{8.9}$$

E_{ex} was calculated from the heat absorbed from the building, equivalent to the thermal load on the system $\dot{Q}_{load}$, multiplied by the time of use t (h)

$$E_{ex} = \sum \dot{Q}_{load} t \tag{8.10}$$

$$\dot{Q}_{load} = \dot{Q}_{HeatExchanger1} + \dot{Q}_{HeatExchanger2} + \dot{Q}_{Chiller} \tag{8.11}$$

The heat absorbed from each subsystem $\dot{Q}$ (J/s) was calculated, knowing the mass flowrate of the process water $\dot{m}$ (kg/s), the heat capacity of the water c_p (J/kg K) and its temperature difference from before and after the heat transfer ΔT (K), measured on either side of the subsystem inside the cooling tower system (Figure 8.3):

$$\dot{Q} = \dot{m} c_{\mathrm{p}} \Delta T \tag{8.12}$$

8.3.4 Data analysis

To assess the effect of the filter on the coefficient of performance, two configurations of the cooling tower system were compared: with and without the filter operating (filter ON and OFF). Time series were defined to compare the configurations during intervals where the cooling tower system experienced similar environmental conditions. A large dataset with more than 890 000 entries was considered. The data analysis was conducted using the Julia programming language [333].

Time series

The wet-bulb temperature was initially identified as a comparison metric to evaluate the coefficients of performance of the system. Three parameters were considered to define the time series: First, *margin*, the root mean square difference between the wet-bulb temperature of both datasets (°C), second *range*, the duration of the period considered for the time series (hours) and third, *inertia* the thermal inertia on the building. The assessment of thermal inertia was considered by making sure that the slope of the wet-bulb temperature was of the same sign for a defined period (hours), before the start of the time series. An in-house algorithm scanned through the data to locate temporal correspondences between two input vectors, the wet-bulb temperatures for each configuration of the system, based on the *margin* and *inertia*. The algorithm employed a sliding window approach, a standard algorithm used in time series analysis, to compare all the possible time series combinations for the two configurations (Vortisand ON and OFF). It involves moving a fixed-size window across the data, one step at a time, and comparing the subsets within each window (See Appendix E).

The algorithm started with with a subset of the input vector for the configuration with the filter operating, starting with the first value and tried to find a match in the other input vector, iteratively analyzing subsequences of length *range* of the input vectors. Then, the algorithm evaluated the next subset, starting at the second value of the input vector, and repeated the process until all values of the dataset were assessed. When two time series were matching, they were appended in another variable. To enhance computational efficiency, parallel processing was leveraged to concurrently explore potential matches.

A convergence analysis was conducted to select the three parameters defining the time series (See Appendix E). Values for each of the parameters were individually progressively increased until the number of time series reached a plateau, indicating optimal parameter configuration to maximize the size of the dataset. The objective was to strategically select parameter values that would maximize the number of time series generated, while still offering a good resolution on the obtained results. Following this optimization process, a carefully chosen set of parameters for *margin* (0.5 °C), *range* (6 hours), and *inertia* (6 hours) yielded a total of 28 265 time series after outliers were filtered out.

Machine learning

A machine learning model was defined to predict how much energy would be saved in a given timeframe if the filter was operating throughout (ON), compared to if it was not operating (OFF). The random forest regressor model from the MLJ.jl package in Julia was adopted due to its overfitting mitigation and improved accuracy by using multiple decision trees [334] (See Appendix E). These hierarchical structures recursively partition the data based on the parameters of interest to make sequential decisions. MLJ (Machine Learning Julia) provides a composable framework for building, evaluating, and deploying machine learning models. The Random Forest Regressor model in MLJ was imported from the TensorFlow package of the Python language [335]. It uses features (parameters of interest selected from the dataset) to predict the value of a target variable after having been trained on part of the data to build the relationship between the features and the target variable [334, 336].

Using cross-validation principles, the dataset was separated into the two aforementioned configurations for the predictions, when the filter was operating (ON) and when it was not (OFF). A random set of 80% of the data was used to train the model and the remaining 20% was used to test it. The target variable adopted was the electric energy consumed by the system E_{co}. The features used were the thermal load, the water temperature inside each cooling tower, the wet-bulb temperature, the thermal energy exchanged inside the system E_{ex}, the coefficient of performance, and the configuration of the filter (ON or OFF). All

features were scaled from 0 to 1 using a sigmoid function before building the model, and training it [337]. The model was then validated on the testing data using the R-squared metric calculated between the observed and predicted values. To optimize performance, key parameters such as the number of trees (n_estimators =100), maximum tree depth (set to "None"), and maximum number of features (set to "auto") were fine-tuned [335]. Once fitted accordingly, the model was then applied to the respective data for the years 2022 and 2023. The machine learning model did not predict the COP directly. Instead, it estimated the energy savings for 2022 and 2023 assuming continuous filter operation. Therefore, the reported improvement in COP is a result of the experimental observations rather than a direct prediction of the machine learning model.

8.4 Results and Discussion

8.4.1 Time series validation

As year-on-year comparisons were not possible because key parameters (wet-bulb temperature, thermal load) could change drastically, time series based on the wet-bulb temperature were adopted. However, given the significant variability associated with the dataset, the definition of the time series can substantially impact the obtained results. Consequently, it was necessary to first validate the chosen parameters before delving into assessment of the energetic performance of the system with or without an operational filter. This validation involves a convergence analysis and a subsequent examination of the coefficient of variation across the selected time series, a ratio of the variability to the mean. The objectives were to maximize data resolution and mitigate the bias associated with the dataset, as well as the impact of variability on the outcomes

A convergence analysis was first undertaken to select the three parameters defining the time series (Figure S1 - Appendix E). The intent was to maximize the number of time series, while reducing the variability of the dataset, thus facilitating the development of correlations between the performance of the system and the environmental conditions. Increasing the *margin* parameter from 0.4 to approximately 1°C resulted in a linear increase of the number of time series up to more than 94 000. Further increase did not change the number of time series significantly. However, a *margin* parameter larger than 0.5 introduced significant variance in the time series (Figure S2 - Appendix E). A value of 0.5°C was therefore selected for this parameter to minimize the noise in the time series, and yielded more than 40 000 time series. Conversely, decreasing the values beyond 6 hours for the *range* and *inertia* parameters reduced the number of series. This value was therefore selected for both parameters. From this convergence analysis, and after filtering out the outliers, maintaining a maximal

root mean square difference of 0.5°C in wet-bulb temperature between configurations and considering the thermal load over the preceding 6 hours, 28 265 six-hour time series were generated. The extensive dataset therefore provided sufficient information to define a large number of time series to thoroughly investigate the intricate dynamics of the cooling tower system. Measurement errors were minimal, with maximum variability of 0.1°C in water temperature and 3% for the flow rate. As the measurements were conducted on the same system throughout the investigation, the same systematic errors are present in both datasets being compared. Additionally, the relative errors are small and do not compromise the conclusions drawn from comparing the two datasets.

Wet-bulb temperatures ranging from nearly 0 to 25°C were recorded throughout the investigation, with an average coefficient of variation of between 14.6 and 15.4 % depending on the filter configuration (Table 8.1). These values highlight the significant variability of the environmental conditions throughout the investigation and thus the potential impact on the system through the thermal load. The coefficient of variation was used to compare the extent of variability between the individual time series, as well as across all the time series. Figure 8.4 (a) displays the wet-bulb temperature for a single time series with the selected parameters. As an example, in that specific period of 6 hours, the wet-bulb temperature oscillated between 18 and 20°C when the filter was operating, and when it was not. As can be observed, the difference in wet-bulb temperature between both filter configurations is minimal. Furthermore, the difference between the wet-bulb temperature of each configuration represents a coefficient of variation of less than 2%. This indicates that for each time series, the variability in the wet-bulb temperature was small, but that between all the selected time series, a broad range of wet-bulb temperatures was covered.

Table 8.1 Coefficient of variation (%) for individual time series and across all time series for the wet-bulb temperature, for configurations where the filter was and was not operating.

	Configuration of the filter	Average coefficient of variation of individual time series (%)	Average coefficient of variation across all time series (%)
Wet-bulb Temperature	ON	1.52	14.58
	OFF	1.78	15.39

These results highlight the representativeness of the time series for a broad range of environmental conditions during a typical cooling season, reflecting low-bias data selection and further validating the choice of parameters for the time series.

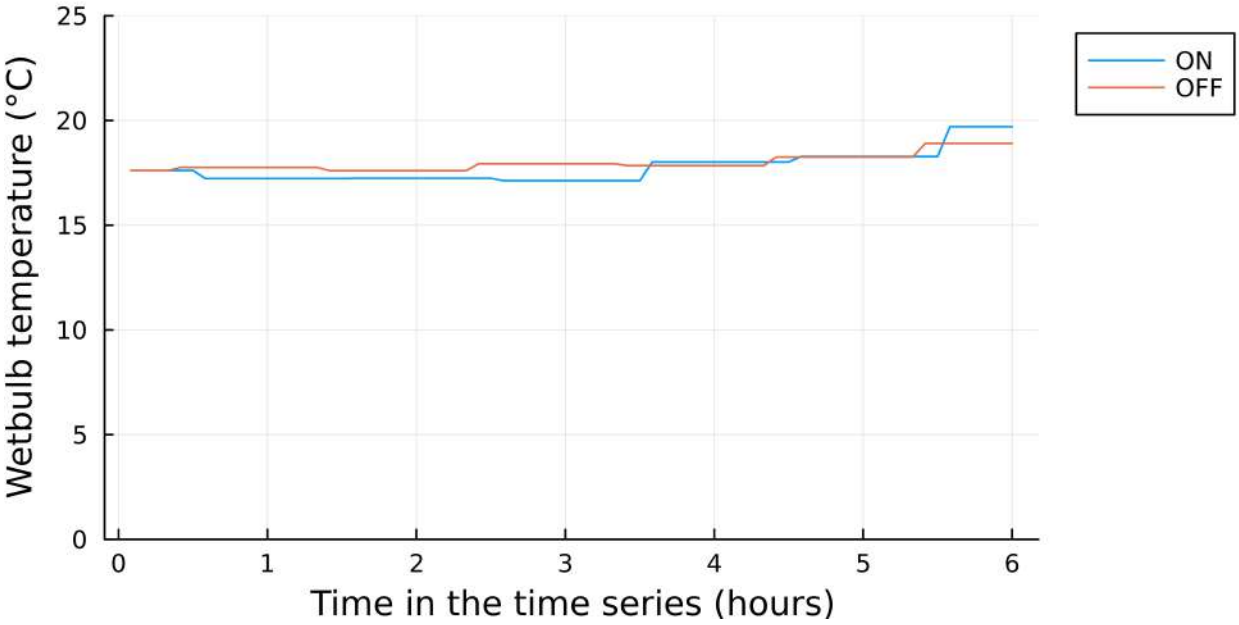

Figure 8.4 Results of the wet-bulb temperature for a single period of 6 hours. Configurations where the filter was operating (ON) and not operating (OFF) are displayed.

8.4.2 Effect of the filtration system on performance

The coefficient of performance was calculated across all the 28 265 time series, and ranged from 2.2 to 6 when the filter was not operating and from 3.2 to 4.1 when the filter was operating, showing more stability for the latter configuration (Figure 8.5). These values for the coefficient of performance are high and underscore the efficiency of cooling tower systems in terms of heat transfer for large buildings. The coefficient of performance, usually calculated for each subsystem, typically ranges between 1 and 5 [338, 339], meaning that the thermal energy transferred inside the system is higher than the mechanical energy provided to the system [117, 340]. The modified metric used in this study, calculating a global COP for the cooling tower system, was slightly higher because of the compounding effect of the multiple subsystems (heat exchangers and chillers). Across all time series, the coefficient of performance was on average 18% higher and was higher 63% of the time when the filter was operating, revealing that over time, the cooling tower system was more efficient at conducting heat transfer when the filter was operating. This 18% increase in performance is significant and highlights the important effect of the filter on the cooling tower system. The fact that the coefficient of performance was higher 63% of the time with the filter operating also shows that this effect is compounded with time.

However, these results also indicate that under specific conditions, the system was more effi-

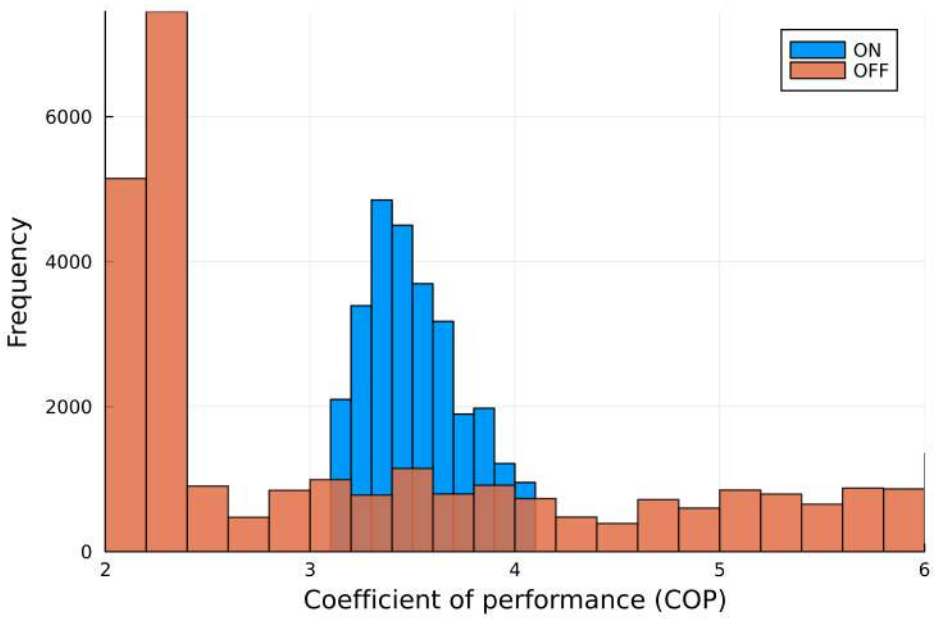

Figure 8.5 Coefficient of performance of the system across all time series.

ciently conducting heat exchange when the filter was not operating. These performance peaks were associated with periods of low wet-bulb temperature and thermal loads not characteristic of the cooling season. Further investigation was performed to understand conditions affecting the coefficient of performance.

The wet-bulb temperature was found to be a critical factor influencing the coefficient of performance (Figure 8.6 a). As can be observed, the coefficient of performance decreased linearly with increasing wet-bulb temperature, likely caused by the combination of the increased load on the system and potential biofilm accumulation (See Appendix E) [341]. The slope was steeper (approximately -6% compared to -2%) in the configuration where the filter was not operating, indicating that the filter enables the system to work more efficiently at high wet-bulb temperature, associated with the most energy-consuming periods. These results underscore the important effect of environmental factors on the operation of cooling towers through the thermal load. This phenomenon is of significance for energy conservation because it highlights the potential benefits of implementing strategies to mitigate the impact of higher wet-bulb temperatures on cooling tower behavior and performance.

The thermal load was also significantly correlated to the energy exchanged inside the system. The difference in the coefficient of performance between the configuration with the filter ON and with the filter OFF was found to vary according to the thermal load (Figure 8.6 b). A positive difference in the coefficient of performance indicates a higher coefficient of

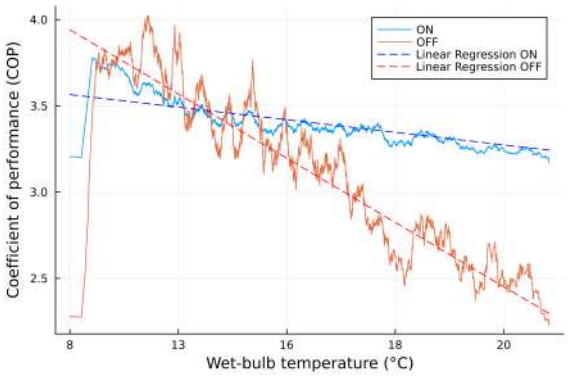

(a)

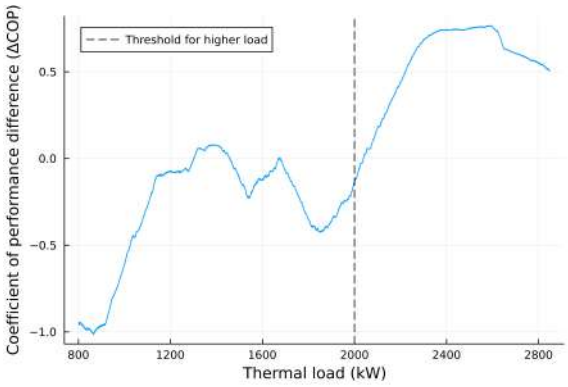

(b)

Figure 8.6 a) Coefficient of performance of the system across all time series as a function of the wet-bulb temperature. Wet-bulb temperatures larger than 10 °C were considered for the regression. b) Difference of the coefficient of performance when the filter is ON and when the filter is OFF for wet-bulb temperatures larger than 10 °C. Configurations where the filter was operating (ON) and not operating (OFF) are displayed.

performance when the filter was operating than when it was not. Although not linearly, the difference in the coefficient of performance increased with the thermal load. Instances where the coefficient of performance was larger when the filter was not operating occurred only for thermal loads smaller than approximately 2000 kW, which can be associated with periods of low to medium cooling demand for a large cooling tower such as the investigated system [330, 341, 342]. This indicates that the effect of the filter on the coefficient of performance was more prominent for higher thermal loads.

When considering only periods of high cooling demand, associated with thermal loads higher than approximately 2000 kW and wet-bulb temperatures higher than 10 °C, the coefficient of performance was always higher with the operating filter (Figure 8.7). More than half

of the time series respected these thresholds, which yielded a coefficient of performance 41 % higher when the filter was operating, as well as a standard deviation of approximately 0.1, indicating high consistency when the cooling demand is high. Thus, the system was found to be more efficient for 81% of the total transferred energy during the investigation, most markedly during periods of high cooling demand. This increase in the coefficient of performance associated with peak conditions show important potential for the improvement of cooling tower systems operation.

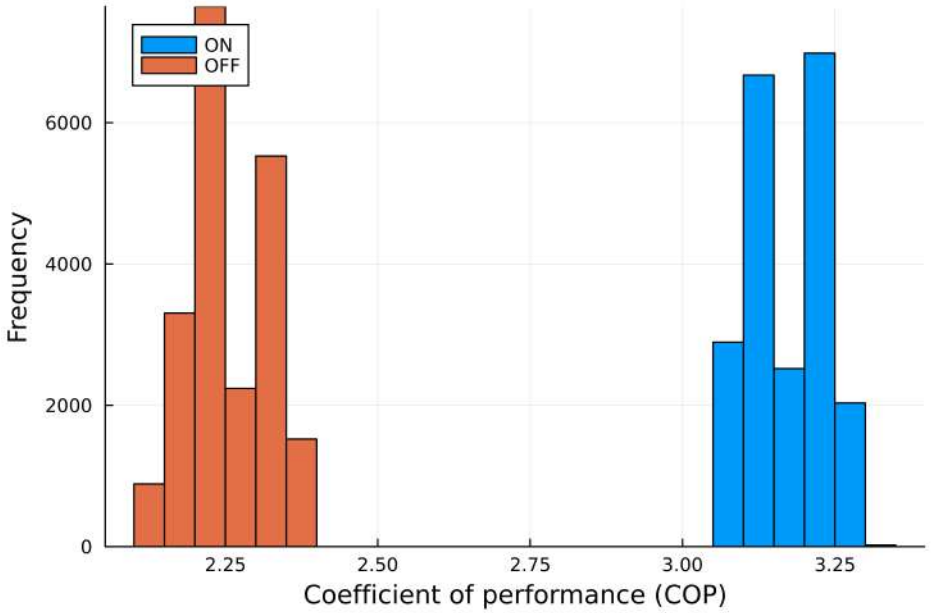

Figure 8.7 Coefficient of performance of the system for wet-bulb temperatures larger than 10°C and thermal load larger than 2000 kW. Configurations where the filter was operating (ON) and not operating (OFF) are displayed.

8.4.3 Energy Savings Prediction

This investigation revealed a consistent trend wherein the cooling tower system demonstrated superior heat transfer efficiency over time when employing filtration, irrespective of prevailing conditions. The microsand filtering system only recirculates 20% of the flow rate of the cooling water at any given time during operation, while the remaining 80% continues to flow throughout the rest of the system. As such, in a well-designed system, less than 80% of the flow rate of the cooling water should be needed for heat transfer purposes at any given instant. Therefore, the increase in energy needed to operate the cooling tower system with the filter is limited to the energy needed to operate the filter and its pump, which was minimal at 0.31 kW in total. Moreover, higher cooling demands corresponded to an increase in the system efficiency at conducting heat transfer, which was particularly evident when the filter was

operational. During periods of high thermal load, the electricity demand for cooling tower operation increases significantly. Consequently, any reduction in electricity consumption, particularly during these peak periods, is not only beneficial in terms of immediate energy savings but also contributes to the overall durability of the system. By mitigating energy demand during peak times, filtration systems offer a sustainable solution for managing cooling tower operations efficiently while reducing strain on the power grid and minimizing the environmental footprint of industrial processes. Consequently, the integration of filtration technologies is promising for long-term energy conservation. However, the precise extent of energy savings attributable to filter usage could not be established for a full year due to the intermittent activation and deactivation of the filter during the investigation.

To quantify the potential energy savings associated with specific operational scenarios, a predictive model was developed to estimate the energy consumed throughout the year based on observed external conditions affecting the cooling tower system. Figure 8.8 displays the strength of the correlation between different environmental parameters within the cooling tower system. This heat map was used to determine which external conditions should be considered to define the model. The highest correlation observed for the electric energy consumed was with the wet-bulb temperature at 0.51, but the other displayed parameters were also significantly correlated to the consumed energy. A correlation of 1 would mean that the parameter is directly related to the target variable, so having multiple parameters correlated to the target at approximately 0.5 indicates a potential for high accuracy predictions. These parameters were thus selected to develop the machine learning model.

The machine learning model was trained to account for both investigated configurations of the filter (Figure 8.9). The model exhibited an R-squared value of 0.99 between the predicted and observed values across both the training and testing datasets. This coefficient of determination implies that 99% of the variance in the predictions was accurately captured by the model, showcasing significant predictive ability. Such high accuracy was also observed for models associated with the energy efficiency of cooling towers in the literature [321]. This trained model was then compared to the available data. Because the filter was operated throughout the 2022 cooling season, the electric energy consumed, as well as information on all the necessary features, was available. As can be observed in Figure 8.10 (a), the prediction of the model for the electric energy consumed by the system almost perfectly matched the observed values, further indicating the reliability of the model. Indeed, the line for the 2022 data with the filter operating and the line for the predicted data with the filter ON are superposed (Figure 8.10 a).

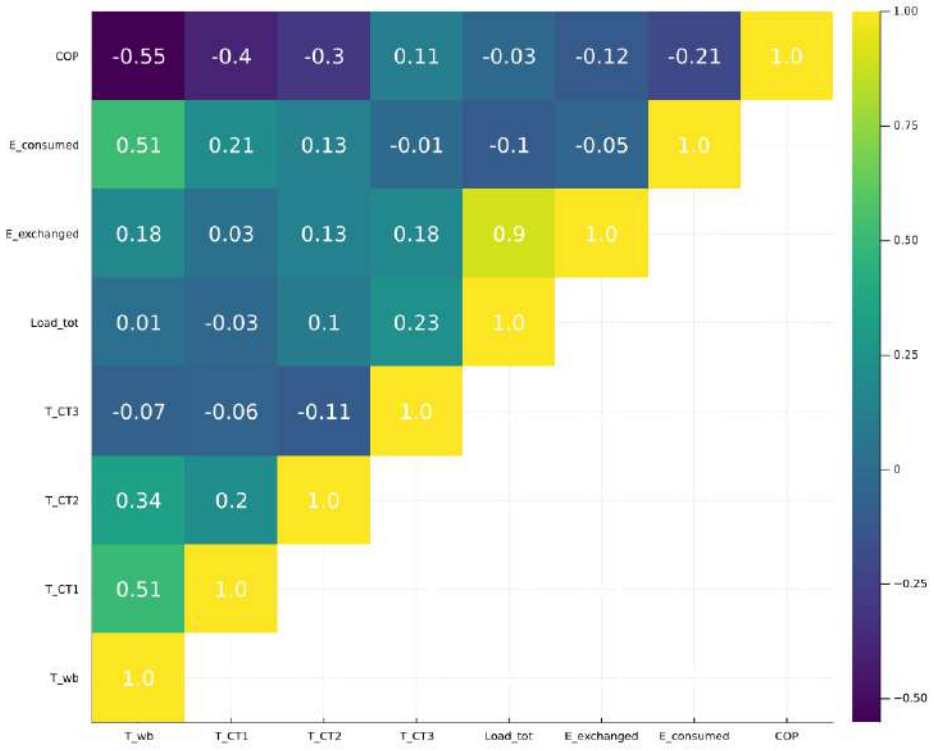

Figure 8.8 Heatmap of the correlations between the different features (the wet-bulb temperature T_{wb}, the temperature of the water inside each cooling tower T_{CT1}, T_{CT2} and T_{CT3}, the thermal load $Load_{tot}$, the thermal energy exchanged $E_{exchanged}$ and the coefficient of performance COP) and the target (The electric energy consumed by the system $E_{consumed}$). A positive correlation indicates that when one of the variables increases, the other increases as well. A negative correlation indicates that when one of the variables increases, the other decreases. The higher the value of the correlation the more important the increase or decrease.

The predicted electric energy consumed by the system during 2022 showed little variability between May and August for both configurations, but the configuration with the filter operating displayed a standard deviation an order of magnitude higher during the month of August (Figure 8.10 a). Nonetheless, if the filter had been OFF in 2022, the system would have consumed 218 000 more kWh, equivalent to 5% of the total consumed energy. This is a significant quantity of energy that can be saved, highlighting the potential of microsand filtration systems. As the year 2023 featured record high temperatures, causing higher thermal loads during the cooling season [343], the average predicted consumed electric energy was 26% higher (Figure 8.10 a). The model predicted that the system would have saved 714 000 kWh between March and September 2023, equivalent to 13% of the consumed energy, with the filter operating. Cumulatively, the energy saved increased linearly between May and September 2022 and during the cooling season in 2023, from May to September (Figure 8.10

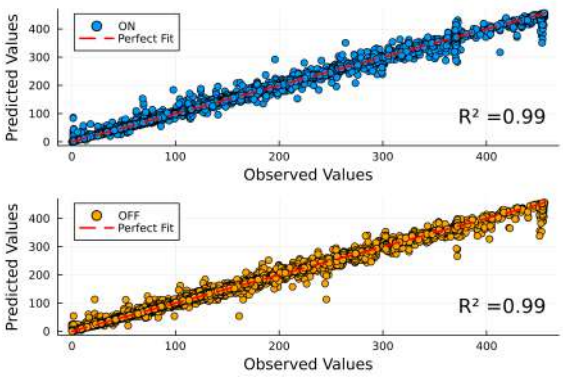

(a)

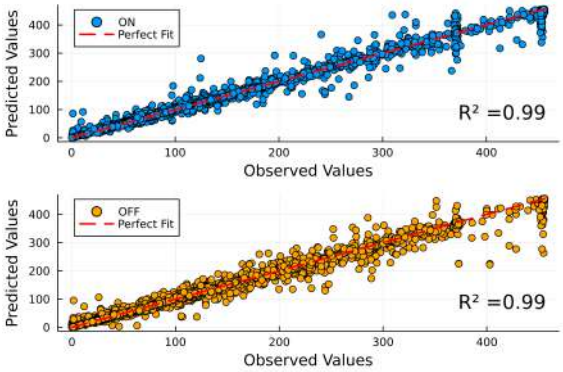

(b)

Figure 8.9 a) Evaluation of the machine learning model on the training data. b) Evaluation of the model on the testing data. the diagonal dashed line represent where datapoints should fall if there was a perfect match between experimental data and model.

b). Assuming the typical industrial energy cost of 0.07 USD/kWh in North America for large-power consumers [330], 15 265 USD would have been saved after 2022 and a cumulative total of 62 530 USD would have been saved after 2023. These important energy savings underscore the extent at which energy can be saved over time in a cooling tower system using microsand filtration.

As can be observed in Figure 8.10, the energy saved was most significant during the main cooling season (between May and September). The difference between the consumed energy for each configuration was not as significant between March and mid-April, as the cumulative saved energy only increased by 5% during that period. It can thus be concluded that during the colder months, between September and March, energy savings would be marginal. As was also observed in Figure 8.6, the operation of the filter during periods of lower thermal loads and wet-bulb temperatures sometimes led to slightly less efficient heat transfer when

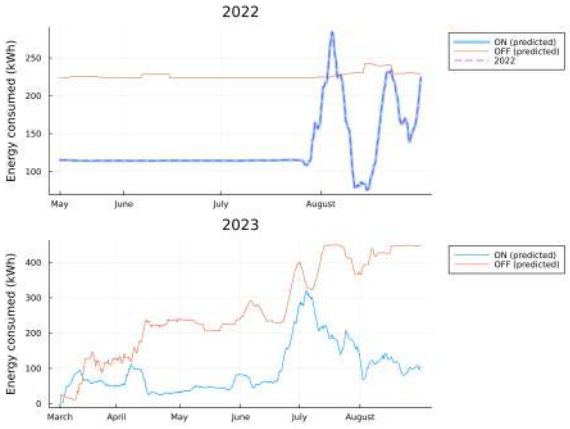

(a)

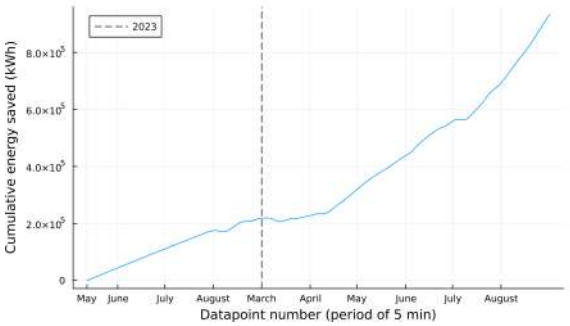

(b)

Figure 8.10 a) Predicted energy saved in 2022 and 2023 with the filter always operating for periods of 5 minutes. b) Predicted cumulative energy saved between 2022 and 2023 with the filter always operating. The vertical dashed line represents the rupture in the dataset between September 2022 and March 2023.

the filter was operating. Therefore, it might be more costly to operate the system with the filter ON during that period. Given that the primary objective was to compare the effect of having a filter versus no filter on the energetic efficiency of the cooling tower system, the lifespan of the filter did not directly impact our analysis as the same filter was used throughout the investigation. Additionally, incorporating an older filtration system into the study potentially mitigated a statistical bias where a newer filter might show an exaggerated effect on the performance of the system. Maintaining continuous filter operation throughout the year significantly mitigates biofouling on the surfaces of the cooling tower system, thereby improving evaporative cooling efficiency, suggesting potential long-term reductions in maintenance costs [344]. Thus, while the benefits mostly manifest during the cooling season (high thermal loads), they are contingent upon year-round filter operation. Moreover, the benefits would be extended in geographical regions where the cooling season is longer.

8.4.4 Effect of intermittent operation

The intermittent operating pattern of the filter on the coefficient of performance of each of the heat exchangers was investigated (Figure 8.11). At the beginning of the cooling season in May 2022, the coefficient of performance of heat exchanger 1 was 4.5, its highest during that year. Similar results were also observed at the beginning of March 2023, as well as with the coefficient of performance of heat exchanger 2, albeit slightly lower at approximately 3. Thus, the highest coefficient of performance observed was at the beginning of the cooling season during both years of the investigation. In 2022, the performance of heat exchanger 1 decreased slightly during the cooling season to approximately 3, equivalent to a 50% decrease in performance, even though the filter was always operating. This phenomenon of steady decrease in performance throughout the cooling season was also observed for both heat exchangers during the 2023 cooling season with a decrease of 50% in performance for heat exchanger 1 and 25% for heat exchanger 2 between March and September. It is typical for the performance of heat exchangers to decrease up to 50% during the cooling season because of the biofilm accumulation, as well as because of the increased load on the system, which can be unevenly distributed between the subsystems [341]. As such, the coefficient of performance of the subsystems tends to decrease even with the filter operating.

When the operation of the filter was first stopped at the end of March, the coefficient of performance started to decrease linearly almost immediately for both heat exchangers (Figure 8.11 b). A decrease of 28% and 20% was observed within 8 weeks for heat exchangers 1 and 2 respectively. When the operation of the filter was resumed in June, the coefficient of performance of both heat exchangers increased to levels almost as high as at the beginning of the year. Recovery time was approximately 4 weeks, just before the second filter shutdown. A decrease of 25% and 16% in the coefficient of performance for heat exchangers 1 and 2 respectively was observed again when the filter stopped operating a second time in July (Figure 8.11 b). The decrease of the coefficient of performance was almost three times faster (steeper slope) during the second shutdown, likely because the wet-bulb temperature was higher and biofilm could develop faster. Furthermore, while the filter was operated between September 2022 and March 2023, the coefficient of performance of heat exchanger 1 increased from approximately 3 to 4.5, indicating that when the filter is operated during periods of lower thermal load, the coefficient of performance of the subsystems tends to increase. This suggests that operating the filter slows down the decrease in the coefficient of performance of individual subsystems during the cooling season.

These results indicate that the filter has a tangible effect on reducing the biofouling inside the heat exchangers as well as throughout the cooling tower system. They agree with other

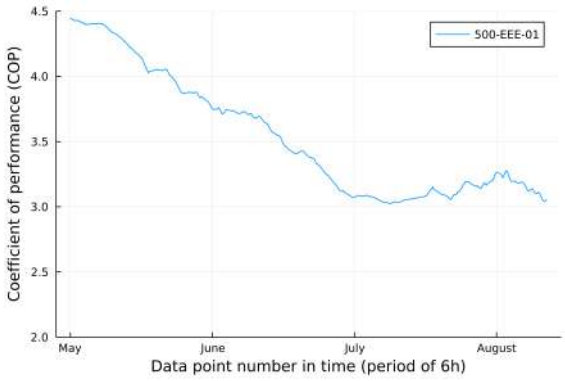

(a)

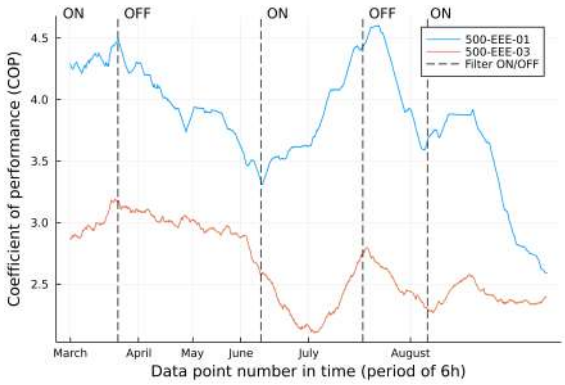

(b)

Figure 8.11 a) Behavior of heat exchanger 1 in 2022. b) Behavior of heat exchanger 1 and 2 in 2023.

studies that characterized the effect of biofilm on heat exchanger using models and small scale experiments [325]. The effect of biofouling on the performance of a cooling tower system can impede the heat transfer capacity by up to 50% [76, 123]. As the performance of the heat exchangers decreased by up to 28% when the filter was not operating, the biofilm formation likely increased significantly after the filter was stopped [344]. After resuming the operation of the filter, the observed linear increase in the coefficient of performance was likely due to the cleaning effect of the filter on the cooling tower water in the system. These results further emphasize the importance of operating the filter all year. Filtering cooling tower water in conjunction with standard chemical water treatment appears to offer a notable advantage by substantially mitigating the buildup of biofilm, increasing the evaporative cooling efficiency of the cooling tower system while concurrently minimizing the risks of bacterial contamination.

The insights gained from the study on the use of cross-flow microsand filtration systems offer significant contributions to energy efficiency and sustainability across various industrial

cooling processes. These findings are particularly relevant to industries focused on reducing environmental impact and achieving energy savings. Additionally, the methodologies and results hold broader implications for engineers and researchers in the field of heating, ventilation, and air conditioning (HVAC) systems. By enhancing the understanding of thermal management in cooling systems, this work may guide the design and optimization of HVAC systems in both commercial and industrial settings. Moreover, the findings highlight the importance of reducing biofouling and improving overall system hygiene for increased energetic performance, which may in turn also help prevent health risks associated to pathogens such as *Legionella*.

8.5 Conclusion

A data-driven comprehensive analysis was conducted over two cooling seasons (2022 and 2023) on the energetic performance of a cooling tower system using a cross-flow microsand filtering system. The results underscore the intricate relationship between wet-bulb temperature, thermal load and cooling tower performance. As wet-bulb temperature and thermal load rise, the efficiency of cooling tower systems tends to decrease. This study is the first to provide a long-term, in situ evaluation of cross-flow microsand filtration's impact on cooling tower efficiency, offering novel insights into its effectiveness under real-world conditions. A time series analysis demonstrated that the coefficient of performance was on average 18% higher, was higher 63% of the time when the filter was operating and for 81% of the total transferred energy, most markedly at higher thermal loads. These results reveal that over time, the cooling tower system was more efficient at conducting heat transfer when using filtration. Furthermore, during periods of high cooling demand characterized by increased wet-bulb temperatures and thermal loads, the performance gap widened significantly, with the system operating 41% more efficiently with the filter in operation. Predictions for the energy saved over time with the filter operating were conducted using a machine learning model and indicated that 5 and 13% of the energy bill could have been saved during the 2022 and 2023 cooling seasons respectively by operating the filter all year long, including the periods where the operation of the filter is more energetically costly. Notably, most energy savings occur during the cooling season, thus enhancing overall system durability and minimizing environmental impact. In addition, the biofouling mitigation provided by continuous filter operation [344] enabled higher performance of the system, underscoring the importance of continuous filter operation. Integrating cross-flow microsand filtration systems into cooling tower management not only optimizes performance but also aligns with sustainable practices, mitigating microbial risks and conserving energy resources.

The efficiency of microsand filtration systems at reducing the concentration of suspended matter in cooling water has been well documented. However, the energy savings potential on cooling tower systems related to this technology remained unexplored. While there is plenty of literature on the loss of energy efficiency in heat exchangers due to fouling, the effect of filtration, and especially of crossflow microsand filtration on an in-situ large scale cooling tower system had not been studied before this work. The in situ aspect of the study is also novel, as a longitudinal sampling campaign was conducted on an operating cooling tower system, yielding a rich dataset over 18 months. The results are therefore more representative of real-world conditions than those of previous studies conducted in laboratory settings or numerically, but also added the challenge of dealing with the variability of the system. Finally, the use of machine learning to predict the saved energy is also novel. The model was able to predict the energy savings with a high degree of accuracy and could easily be implemented to other cooling tower systems with similar data.

The findings of this study are particularly significant for industries that rely on cooling tower systems, such as Heat, ventilation and air conditioning (HVAC), energy, and manufacturing sectors, where optimizing energy efficiency and reducing operational costs are critical. By demonstrating the effectiveness of cross-flow microsand filtration, this work provides a practical solution that can be readily adopted in these industries to improve system performance and sustainability. Moreover, this study lays the groundwork for future research in several key areas, including the long-term effects of filtration on system durability, the role of filtration in reducing microbial risks, and the broader environmental impact of implementing such systems on a larger scale. Future studies could explore these aspects in more depth, as well as investigate the applicability of similar filtration systems in other thermal management applications.

Acknowledgements

This research was supported by the MITACS Accelerate program with Evoqua+Xylem industrial partner (project Mitacs IT27607). Xavier Lefebvre is supported by the Hydro-Québec excellence scholarship as well as a NSERC scolarship (ES D) with a FRQNT supplement (B2X).

We want to acknowledge the contribution of Alain Silverwood, Technical Director R&D at Xylem / Evoqua Water Technologies, this project would not have been possible without his vision, his continuous support for experiment design, data collection, field support and training.

Special Thanks to the study site managers for access to their building and data.

Thank you also to Nils Frejinger Robert for his contribution to the time series algorithm that was implemented into the code.

Conflict of interest

The authors declare no competing interests.

Supporting Information

The data that support the findings of this study are available upon reasonable request from the authors.

CHAPTER 9 GENERAL DISCUSSION

Most of the literature on the transmission of *Legionella* from cooling towers focuses on the presence of bacteria within the system. While the presence of *Legionella* is necessary for contamination to occur, the associated risks are not solely dependent on its concentration in the water. Indeed, airborne transport of contaminated aerosol droplets plays an essential role in the contamination process and pathogenicity, which is influenced by the drying process of the aerosol and the *Legionella* strain present. A holistic approach including the characterization of the multiphase flow dynamics governing the transport of *Legionella* via the airborne route, for which significant research gaps exist, was thus needed for a thorough assessment of the contamination risks and the development of mitigation strategies. These two aspects were thus investigated from a contaminated aerosol perspective, as the articles of this thesis were based on the assumption that cooling towers are inherently contaminated by *Legionella*.

9.1 Assessment of the exposure risks

9.1.1 Aerosol droplet size distribution

The challenge of accurately tackling the characterization of size distributions of potentially contaminated aerosol droplets was addressed experimentally in the first article. Four measurement instrument with different working mechanisms, which are typically used to measure the size distribution of small particulate matter without biological considerations, were compared on a flow of evaporating aerosol droplets. The results offered an original contribution, enabling the possibility to select and apply such measurement instruments to the field of airborne transmission.

The size distribution of droplets from a potentially contaminated aerosol plume is closely related to the contamination risks. With the size of the contaminated droplets changing due to evaporation, and their size-dependant deposition inside the sampling line of some instruments, the accurate measurement of the size distribution at the source is challenging. Currently widespread size distribution measurement instruments are not adapted to accurately measure water-based aerosol droplets. As such, instruments based on different operating principles provide different size measurements which makes the associated risk assessment highly variable. The main question is therefore the following: which instrument, if any, measures the most accurate droplet size as a function of operating and sampling conditions?

Out of the four instruments compared in this study, the PDA is most adapted to measure the size distribution of aerosol droplets. Indeed, this laser based technique can accurately measure the size distribution without sampling the flow and therefore does not need to consider the evaporation and deposition of the droplets. This work, as well as multiple other studies in the literature, showed that the technology of the PDA can be considered as the gold standard for aerosol measurement in the context of airborne transmission. However, such an expensive instrument is not widely available and not easily transportable. Article 1 thus provided correction factors for the three other studied instruments so that adequate size distribution characterization can be achieved with widespread measurement instruments. Finally, to be able to compare different sources in terms of the airborne transport of contaminated droplets, the initial size of the droplets must be known. The novel approach involving the complete drying of the droplets proposed in this study enables the evaluation of the initial size of the droplets. This approach not only provides a more accurate estimation of droplet size at the source by circumventing evaporation during measurement but also offers a practical solution for in-field applications, allowing for more reliable comparisons between different systems and environmental conditions. This technique was used on operating cooling tower systems in article 2 and the PDA served as the experimental foundation for articles 3 and 4. The improvement of the characterization of aerosol droplets resulting from this article therefore laid a solid foundation for the risk assessment of the airborne transmission of *Legionella* from cooling towers.

9.1.2 Size evolution of aerosol droplets

The size evolution of contaminated aerosol droplets through evaporation, a critical aspect of airborne transmission, and one of the least understood, was assessed in articles 3 and 4. The effect of various liquid feedstock properties on the evaporation of water-based aerosol droplets was experimentally investigated in article 3. Decreased surface tension extended evaporation time by up to 14% and halted the process at high concentrations. Increased viscosity delayed the evaporation onset but did not affect the droplet nuclei size. High concentrations of non-volatile matter nearly doubled the evaporation time and predictably resulted in a larger droplet nuclei size. Furthermore, the results showed that the larger variability of the droplet nuclei size associated with higher non-volatile concentration, and the variability of the concentration of non-volatile matter between droplets can drastically influence the contamination risks. Article 4 focused on the development of a versatile experimental setup leveraging the inkjet printhead technology to generate aerosol droplets. The effect of the number density of aerosol droplets on their evaporation was also investigated. The evaporation of pure water droplets was significantly affected by the presence of other droplets in the

vicinity, as the local moisture concentration increased.

The characterization of the effect of surface tension, viscosity and non-volatile matter on the evaporation of aerosol droplets can be considered as original contributions to the fields of aerosol science and disease transmission. Furthermore, the experimental setup developed in article 4 provides a novel application for inkjet printhead technology, and can be used to further investigate the evaporation of aerosol droplets. The results of articles 3 and 4 provide insights into the evaporation of contaminated droplets and are crucial for the accurate assessment of the risks associated with the airborne transmission of *Legionella* from cooling towers.

9.1.3 *In situ* aerosol characterization

In the context of airborne transmission, a complete characterization of aerosol droplets requires the measurement of their size distribution, as well as the assessment of pathogen content and the evaluation of pathogen viability within the droplets. However, no single instrument currently exists that can reliably and accurately measure these parameters simultaneously for water-based aerosol droplets. As a result, a combination of instruments and techniques is necessary to achieve a full characterization, taking into account the evolution of droplet size over time. In article 1, a methodology was developed to integrate multiple instruments for this purpose, which was subsequently applied *in situ* in article 2.

With the 15 cooling towers sampled over two weeks and the 3 cooling towers monitored over 8 weeks, the *in situ* sampling campaign of article 2 provided a unique and large-scale dataset. This extensive dataset enabled an analysis of how environmental factors, such as temperature and humidity, as well as the operating rate of the cooling towers, influence the release of inhalable aerosol droplets, shedding light on the variability of droplet formation and dissemination under real-world conditions. Different types and sizes of cooling towers were investigated and compared, which allowed for a newfound understanding of these complex systems as it pertains to the airborne transmission of *Legionella*. The combined microbiology and aerosol science methodologies used to compare the concentration and viability of *Legionella* in the cooling tower water and in the aerosol droplets, provided novel results in the field of airborne transmission and critical information for the assessment of the contamination risks.

9.1.4 Risk assessment modelling

A thorough risk assessment of the airborne transmission of *Legionella* from cooling towers was conducted in the second article using QMRA. The acquired data allowed to improve the

risk assessment model in terms of the emission of contaminated droplets. Results showed that thorough risk assessment must consider both the concentration of viable *Legionella* and the aerosol emission rate. The results of the study highlight the significant risks of infection from *Legionella* originating in cooling towers, emphasizing that current mitigation strategies are not sufficient in protecting public health and underscoring the urgent need to refine and improve risk mitigation approaches. Accurate risk assessments are crucial for developing comprehensive mitigation strategies that not only limit the growth of *Legionella* in the water but also minimize the release and exposure of contaminated droplets.

Existing risk assessment models typically overlook evaporation, thus underestimating the associated risks. Indeed, without accounting for evaporation, these models fail to consider the risks posed by aerosol droplets that, while initially too large to be inhaled, shrink through evaporation to a size that can be respirable and potentially harmful to exposed individuals. They also fail to account for other extreme statistical events, outlined as important risks factors in article 2, where the right combinations of environmental conditions meet for contamination to occur, and where the properties of the aerosol droplets can be a determining factor. Furthermore, there are currently no evaporation modelling framework that are applicable to the airborne transmission of *Legionella* from cooling towers, as most evaporation studies are focused on anthropogenic airborne transmission, for which the aerosol droplets have different thermo-physical properties. The results of articles 3 and 4 can help to fill this gap in terms of the effects of the water properties and the number density of droplets. By integrating a precise evaporation model with a dispersion model, the risks of *Legionella* infection from cooling towers can be assessed with greater precision, leading to more targeted and effective risk mitigation strategies.

9.2 Development of mitigation strategies

9.2.1 Cooling tower efficiency with microsand filtration

The last article of this thesis focused on the effect of microsand filtration on the efficiency of the cooling tower system as a basis for the adoption of this solution. This case study presented a data-driven comprehensive analysis conducted on the performance of a cooling tower equipped with a cross-flow microsand filtering system. It was shown in the literature that this technology can reduce the fouling of the heat exchangers and increase the working efficiency of the cooling tower system. For similar environmental conditions, the coefficient of performance of the studied cooling tower system was on average 18% higher and was higher 63% of the time when the filter was operating, indicating superior heat transfer efficiency and significant energy savings. It was also 41% higher during periods of high cooling demand.

Consequently, the filter and the system work more efficiently at high wet-bulb temperature and thermal load. Machine learning modeling suggested that operating the filter year-round could save between 5% and 13% of the energy bill, primarily during the cooling season. From these results, it was concluded that the use of microsand filtration systems in cooling towers can lead to significant energy savings.

Following the holistic approach outlined at the beginning of this section, an underlying objective from the study and this thesis was to investigate the adoption of different strategies to mitigate the risks associated with the airborne transmission of *Legionella*. Efficient chemical disinfection poses a significant challenge for cooling tower managers, as *Legionella* displays an impressive ability to survive. Microsand filtration systems are not widely adopted in the industry even though they have been proven to be effective at limiting the growth of *Legionella* in the cooling tower water. As less suspended solids are present in the cooling tower water due to the filtering efficiency of the microsand filtration system and less dissolved solids are present due to the reduced use of chemical products, the generated aerosol droplets are likely to evaporate faster, thus reducing the exposure range associated with the cooling tower. The results also show that the energy savings potential is significant, especially during the cooling season, associated with the largest concentrations of *Legionella* and the peak in legionellosis cases. Furthermore, the adoption of different strategies to limit the growth of *Legionella* can drastically influence the contamination risks. This study can thus be used to guide the adoption of microsand filtration systems in cooling towers, with the intent of reducing the contamination risks.

9.2.2 Recommendations to mitigate the risks

Current guidelines only consider the water *Legionella* concentration. The use of chemical water treatment combined with microsand filtration can minimize *Legionella* concentrations in water. Nonetheless, the combined effect of the aerosol emission rate and the concentration of viable *Legionella* on the exposure risks observed in article 2 suggests that a multifaceted approach is essential to mitigate the risks associated with the airborne transmission of *Legionella* from cooling towers. The following risk mitigation strategies are thus proposed.

Ideally, continuous monitoring should be implemented to ensure that the water treatment is adjusted to minimize the concentration of viable *Legionella* in the cooling tower water. However, continuous monitoring is not always feasible due to the high cost and the lack of available technology. In such cases, a monitoring schedule which can provide early detection of deviations and prompt intervention should be implemented, especially during the cooling season when the concentration of *Legionella* is at its peak. Monitoring should be conducted

at a point representative of water entering the cooling tower to provide early detection of deviations and prompt intervention.

An original contribution of article 2 was the quantification of drift eliminator capture efficiency from experimental data on operating cooling towers. The results revealed the limitations associated with drift eliminators. Despite being a critical line of defense before potentially contaminated droplet are discharged into the environment, they are often inefficient in capturing inhalable aerosol droplets and thus currently not reliable as a risk mitigation strategy by themselves.

This finding calls for the redesign of drift eliminators to enhance their efficiency in reducing exposure risks, ultimately bolstering public health protection. This can be achieved by increasing the surface area of the drift eliminators and increasing the flow deflections, while considering the tradeoff between energy usage and head losses due to inertial disturbances. Risk assessment models typically consider a size range between 1 and 10 μm, for which aerosol droplets can carry pathogens and be inhaled. However, the incorporation of *Legionella* in aerosol droplets sized 1-2 μm remains to be investigated. Therefore, droplets are more likely to be contaminated with *Legionella* in the upper inhalable droplet size range (5-10 μm). As such, the redesign of drift eliminators should focus on capturing droplets in this size range. By focusing on the upper inhalable droplet size range, the exposure risks can be minimized while maintaining the energy efficiency of the cooling tower system. Furthermore, each drift eliminator should be aerodynamically customized for a specific CT and the design point should be set to the maximum operating rate of the system.

With the current design ignoring the capture of inhalable and potentially contaminated aerosol droplets, drift eliminators cannot be assumed to provide a large reduction in the exposure risks. Nonetheless, drift eliminators are the last line of defense before droplets contaminated with *Legionella* are discharged into the environment. As such, they should be maintained and monitored regularly to ensure optimal performance. To maximize the current capture efficiency of drift eliminators for inhalable droplets, CTs should rarely operate above 50% of the operating rate to minimize particle emission in the inhalable range. If possible, another CT can be activated when the operating CT exceed 50% of the operating rate. Considering the potential energy savings from the use of microsand filtration systems, the higher operating costs associated with the operation of multiple CTs can be at least partly offset.

A generalized contaminated droplet emission framework was introduced to provide cooling tower managers with an estimate of infection risks, facilitating informed mitigation strategies.

This generalized framework can be used as the emission model in the QMRA model adapted to *Legionella* from cooling towers. Thus, this generalized QMRA, encompassing the effect of aerosol emission rate and the concentration of viable *Legionella* on the exposure risks, should be performed and the water treatments should be adjusted upon exceedances of the health-based thresholds. An evaporation model adapted to the water properties of the cooling tower should be integrated into the QMRA model to provide a more accurate assessment of the risks.

Extreme statistical events are relevant in the context of disease transmission because they represent rare but high-impact occurrences. For *Legionella* and cooling towers, these events most likely correspond to sudden peaks of the concentration of viable *Legionella* in the water combined with higher aerosol emission rate due to an increase load demand on the building. Such circumstances can lead to disproportionate exposure and be responsible for sporadic cases, while remaining undetected due to the sudden onset of the conditions. Understanding these events is crucial for accurately modeling transmission dynamics and implementing effective mitigation strategies, especially in scenarios where extreme events can drive significant public health outcomes. The assessment of the risks should thus be conducted on systems operating at maximum capacity with peak water concentrations to account for these extreme events.

9.3 General impact

The concept of pandemics and infectious diseases is far from new, with historic events such as the Spanish flu and the Black Death leaving a lasting impact on humanity. Yet, the airborne transmission of diseases remains a relatively misunderstood and poorly documented subject, even though the air mediated transmission route had been recognized as early as the 19th century. While significant progress has been made in various aspects of airborne transmission, advancements specifically in the fluid dynamics underlying this process remain limited and continue to be an area of active research. As such, we remain reactive in our approach to managing airborne diseases, with the same basic principles of quarantine and social distancing being applied to the COVID-19 pandemic as they were to the Spanish flu 100 years prior. We continue to struggle with controlling nosocomial infections and still have limited knowledge of the physics that drive *Legionella*-laden aerosol droplets from cooling towers to human hosts.

The emerging field of airborne disease transmission has been rapidly evolving in recent years, bridging the gaps between microbiology, aerosol science, and multiphase fluid dynamics. *Legionella* transmission from cooling towers however, a topic historically primarily studied

in microbiology, had seen little exploration of the fluid dynamics involved in its airborne transport before this work. The applications of fluid dynamics in health and infectious diseases have led to the discovery of new processes and the development of innovative tools with broader applications beyond their original fields. In this thesis, significant advancements were made in measurement techniques for characterizing wet aerosol droplet size distributions, as well as in the use of inkjet technology to generate monodispersed aerosol droplets. The findings of this thesis, such as the characterization of water-based contaminated aerosol droplets and their evaporation dynamics offer improved methods for assessing contamination risks. This was achieved through a large-scale *in situ* investigation on operating cooling towers leading to improved QMRA, ultimately aiming to inform the development of more effective mitigation strategies.

Modern medicine treats diseases as isolated entities, with their own set of symptoms, treatments, and prevention strategies. However, the fluid dynamics of diseases transmitted via the airborne route underscore a universal process evolved throughout a wide range of pathogens. While each pathogen may have unique biological characteristics, the physical processes governing their transport, such as droplet formation, evaporation, and deposition, follow the same fluid dynamics principles. Some of the findings of this thesis, such as the characterization of the size distribution and evaporation dynamics of airborne aerosol droplets are not only relevant in the context of *Legionella* and cooling towers, but also contribute to a deeper understanding of the fundamental fluid dynamics pertaining to disease transmission. These results can thus potentially at least partly be applied to most diseases transmitted via the airborne route, such as tuberculosis, which is again becoming a major public health concern worldwide, or viruses responsible for COVID-19, the common flu and future pandemics. In this regard, this work highlights the importance of understanding airborne disease transmission generalized to a wide range of pathogens.

We might forever have to deal with challenges associated with disease transmission and the way we handle pathogens has long lasting effects. Indeed, the growing issue of antibiotic resistance, involving *Legionella* among other pathogens, further underscores how our approaches to managing the associated contamination risks can have widespread, unintended consequences. Indeed, evolutionary pressures naturally selects for robust, selfish mechanisms favoring gene survival in pathogens. Nevertheless, unraveling the fluid dynamics processes associated with the airborne transmission of pathogens offers a largely untapped opportunity for developing innovative control and mitigation strategies. This thesis is a step towards a future where the fluid dynamics of disease transmission are understood and harnessed to protect public health.

CHAPTER 10 CONCLUSION

10.1 Summary

In-depth risk assessment requires the precise characterization of aerosol droplets generated and released from cooling towers, which is challenging as they undergo evaporation during transport. The performance of various measurement techniques, well established for particulate matter for characterization in aerosol science, was evaluated for water-based droplets. Discrepancies observed in the size distributions of water droplets, due to evaporation and particle deposition, highlighted the need for empirical correction factors. By applying these corrections and utilizing a proposed drying technique, the reliability of results generated by different sampling instruments was improved, enabling accurate measurement of aerosol size distribution. This drying technique was crucial for comprehensive risk assessment in the context of airborne transmission.

Building upon the accurate measurement of aerosol droplets, we improved the QMRA model using data acquired through large-scale *in situ* sampling campaign. Results showed that risk assessment must consider both the concentration of viable *Legionella* and the aerosol emission rate. The potential for extreme values to significantly influence the risks suggests that QMRA should be conducted under conditions where the system operates at maximum capacity and water concentrations are at their peak. A generalized QMRA emission model can be used to obtain an estimation of the exposure risks for managers and operators. Risk mitigation strategies include more frequent monitoring of the water concentration of *Legionella*, redesigning drift eliminators to increase their capture efficiency for droplets in the inhalable size range, and performing generalized QMRA to assess the risks associated with cooling towers.

The evaporation of water-based droplets containing *Legionella* is a critical yet often overlooked factor in risk assessments. Our investigation into the impact of various water properties on droplet evaporation revealed that parameters such as surface tension, viscosity, and non-volatile matter concentration significantly influence evaporation dynamics. These fluid properties can vary in cooling tower water compared to drinking water with the accumulation of biofilm, as well as the addition of biodispersive agents (surfactants) and chemical disinfection products. Decreased surface tension extended evaporation time, while high concentrations of non-volatile matter nearly doubled it, resulting in larger droplet nuclei and increased variability in contamination risks. These findings highlight the need for more accu-

rate evaporation models adapted to various water characteristics to improve risk assessment and inform the development of efficient mitigation strategies.

To further understand the dynamics of droplet evaporation, a versatile and novel experimental setup was developed using the XAAR XJ128 inkjet printhead, which allowed for the controlled generation of droplets. Monitoring these droplets with PDA across different stages of evaporation provided insights into how number density and relative humidity influence evaporation rates. The results showed that the number density of airborne droplets could significantly alter their evaporation rate. This nuanced understanding of droplet evaporation within plumes is crucial for accurate risk assessments and the design of targeted mitigation strategies.

One of the major challenges in cooling tower management is the effective decontamination of water to reduce *Legionella* contamination. Traditional chemical disinfection methods are widely used but have their limitations. As an alternative or a complement, microsand filtration technology has shown promise not only in reducing contamination risks but also in enhancing the energetic efficiency of cooling tower systems, as shown in this thesis. Through a data-driven approach, it was determined that operating this filtration system could increase the coefficient of performance, especially during the cooling season. The integration of such filtration systems into cooling tower management could therefore promote more sustainable practices by reducing both energy consumption and biofouling.

In conclusion, the research presented in this thesis not only improves the understanding of contamination risks in cooling tower systems but also proposes practical solutions that can be implemented to enhance safety and efficiency. By combining innovative decontamination technologies, precise aerosol measurement techniques, and refined risk assessment models, this work contributes to the development of more sustainable and effective approaches to managing airborne transmission risks in industrial settings.

10.2 Future Research

A limitation of the work from this thesis lies in the assumption that contaminated droplets are inherently generated from cooling towers. Indeed, the assessment of the risks associated with *Legionella* was conducted assuming a consistent combination of different aerosolization mechanisms. While it is true that aerosol droplets are indeed generated inside cooling towers and released into the environment as a by-product of their operation, the propensity of these droplets to be contaminated depends on how they are generated. Multiple aerosolization mechanisms can be responsible for the generation of the aerosol inside each unique system.

These different mechanisms can drastically influence the concentration of the aerosol droplets, as well as the concentration of viable pathogens they carry. As such, future works are required to fundamentally characterize the aerosolization mechanisms within the cooling towers responsible for the generation of contaminated droplets.

The work presented in this thesis focused on the assessment of the risks associated with *Legionella* in cooling towers. The application to other pathogens was briefly discussed, but not the consideration of other sources of *Legionella*. Indeed, although the most prominent, cooling towers are not the only source of *Legionella* in the environment. Other sources, such as showers, hot tubs, and decorative fountains, have been identified as potential outbreak vectors and the aerosol generation inside these sources potentially differs significantly. The work presented in this thesis could be extended to assess the risks associated with *Legionella* from these sources. Specifically, the number of legionellosis cases in Switzerland has increased dramatically over the past few years. The main source of these infections is not well understood, as very few water cooling towers are operated in Switzerland. As such, it is likely that sources of *Legionella* that are unaccounted for could be responsible for the rise in cases. An emerging hypothesis is that soil is a potential source of *Legionella*. Indeed, *Legionella* has been found in soil samples, and the bacteria has been shown to be able to survive in soil. Unrelated work involving the characterization of petrichor, the distinct smell of rain, has demonstrated that soil can be aerosolized and transported over long distances. As such, it is possible that soil could be a source of *Legionella* outbreaks. Future works could focus on the assessment of the risks associated with *Legionella* from soil sources.

REFERENCES

[1] U. Nations, "United nations comprehensive response to covid-19," 2020.

[2] Members and C. of Congress, "Global economic effects of covid-19," 2021.

[3] L. Bourouiba, "The fluid dynamics of disease transmission," *Annual Review of Fluid Mechanics*, vol. 53, pp. 473–508, 2021.

[4] T. M. Daniel, "The history of tuberculosis," *Respiratory medicine*, vol. 100, no. 11, pp. 1862–1870, 2006.

[5] D. Huremović, *Brief History of Pandemics (Pandemics Throughout History)*. Cham: Springer International Publishing, 2019, pp. 7–35. [Online]. Available: https://doi.org/10.1007/978-3-030-15346-5_2

[6] E. Barclay, "Predicting the next pandemic," *The Lancet*, vol. 372, no. 9643, pp. 1025–1026, 2008.

[7] G. Churchyard, P. Kim, N. S. Shah, R. Rustomjee, N. Gandhi, B. Mathema, D. Dowdy, A. Kasmar, and V. Cardenas, "What we know about tuberculosis transmission: an overview," *The Journal of infectious diseases*, vol. 216, no. suppl_6, pp. S629–S635, 2017.

[8] C. K. McMullen, B. Dougherty, D. T. Medeiros, G. Yasvinski, D. Sharma, and M. K. Thomas, "Estimating the burden of illness caused by domestic waterborne legionnaires' disease in canada: 2015–2019," *Epidemiology & Infection*, vol. 152, p. e18, 2024.

[9] N. A. of Sciences Engineering and Medicine, *Management of Legionella in Water Systems*. Washington, DC: The National Academies Press, 2020. [Online]. Available: https://www.nap.edu/catalog/25474/management-of-legionella-in-water-systems

[10] A. J. Prussin II, D. O. Schwake, and L. C. Marr, "Ten questions concerning the aerosolization and transmission of legionella in the built environment," *Building and environment*, vol. 123, pp. 684–695, 2017.

[11] S. A. Collier, L. Deng, E. A. Adam, K. M. Benedict, E. M. Beshearse, A. J. Blackstock, B. B. Bruce, G. Derado, C. Edens, K. E. Fullerton *et al.*, "Estimate of burden and

direct healthcare cost of infectious waterborne disease in the united states," *Emerging infectious diseases*, vol. 27, no. 1, p. 140, 2021.

[12] B. f. G. BAG, "Legionellosis (legionärskrankheit) report," 2023. [Online]. Available: https://www.bag.admin.ch/bag/de/home/krankheiten/krankheiten-im-ueberblick/legionellose.html

[13] J. Walker, "The influence of climate change on waterborne disease and legionella: a review," *Perspectives in public health*, vol. 138, no. 5, pp. 282–286, 2018.

[14] World Health Organization, *WHO global air quality guidelines: particulate matter (PM2.5 and PM10), ozone, nitrogen dioxide, sulfur dioxide and carbon monoxide*, 2021, no. June. [Online]. Available: https://www.who.int/publications/i/item/9789240034228?ua=1

[15] M. W. H. Horrocks, "Experiments made to determine the conditions under which specific bacteria derived from sewage may be present in the air ventilating pipes, drains, inspection chambers, ans sewers," *Public Health*, pp. 495–506, 1906.

[16] World Health Organization, *Infection prevention and control of epidemic- and pandemic-prone acute respiratory diseases in health care*, 2007, no. June. [Online]. Available: http://apps.who.int/iris/handle/10665/69707

[17] T. Dbouk and D. Drikakis, "On coughing and airborne droplet transmission to humans on coughing and airborne droplet transmission to humans," *Physics of Fluids*, 2020.

[18] J. S. Kutter, M. I. Spronken, P. L. Fraaij, R. A. M. Fouchier, and S. Herfst, "Transmission routes of respiratory viruses among humans," *Current Opinion in Virology*, pp. 142–151, 2018.

[19] Y. Y. Zuo, W. E. Uspal, and T. Wei, "Airborne transmission of covid-19: Aerosol dispersion, lung deposition, and virus-receptor interactions," *ACS Nano*, vol. 14, no. 12, pp. 16 502–16 524, 2020, pMID: 33236896. [Online]. Available: https://doi.org/10.1021/acsnano.0c08484

[20] S. Balachandar, S. Zaleski, A. Soldati, G. Ahmadi, and L. Bourouiba, "Host-to-host airborne transmission as a multiphase flow problem for science-based social distance guidelines," *International Journal of Multiphase Flow*, vol. 132, p. 103439, 2020.

[21] L. Bourouiba, "Turbulent gas clouds and respiratory pathogen emissions: Potential implications for reducing transmission of covid-19," *Jama*, vol. 323, no. 18, pp. 1837–

1838, 2020.

[22] S.-A. Tabatabaeizadeh, "Airborne transmission of covid-19 and the role of face mask to prevent it: a systematic review and meta-analysis," *European Journal of Medical Research*, vol. 26, 01 2021.

[23] L. Bourouiba, E. Dehandschoewercker, and J. W. Bush, "Violent expiratory events: on coughing and sneezing," *Journal of Fluid Mechanics*, vol. 745, pp. 537–563, 2014.

[24] C. E. Brennen and C. E. Brennen, "Fundamentals of multiphase flow," 2005.

[25] H. Kanamori, D. Weber, and W. Rutala, "Healthcare-associated outbreaks associated with a water reservoir and infection prevention strategies," *Clinical Infectious Diseases*, vol. 62, p. ciw122, 03 2016.

[26] Y. S. Joung and C. R. Buie, "Aerosol generation by raindrop impact on soil," *Nature Communications*, vol. 6, no. 1, 2015.

[27] M. Otero Fernandez, R. Thomas, N. Garton, A. Hudson, A. Haddrell, and J. Reid, "Assessing the airborne survival of bacteria in populations of aerosol droplets with a novel technology," *Journal of The Royal Society Interface*, vol. 16, p. 20180779, 01 2019.

[28] G. Ferron and S. Soderholm, "Estimation of the times for evaporation of pure water droplets and for stabilization of salt solution particles," *Journal of Aerosol Science*, pp. 415–429, 1990.

[29] J. H. Schreck, M. J. Lashaki, J. Hashemi, M. Dhanak, and S. Verma, "Aerosol generation in public restrooms," *Physics of Fluids*, vol. 33, no. 3, p. 033320, 2021.

[30] S. Hall, "2 - heat exchangers," in *Branan's Rules of Thumb for Chemical Engineers (Fifth Edition)*, fifth edition ed., S. Hall, Ed. Oxford: Butterworth-Heinemann, 2012, pp. 27–57. [Online]. Available: https://www.sciencedirect.com/science/article/pii/B9780123877857000025

[31] "Most compact cooling towers," https://www.baltimoreaircoil.com/products/cooling-towers/pt2-cooling-tower, accessed: 2022-04-29.

[32] E. Bédard, C. Laferrière, E. Déziel, and M. Prévost, "Impact of stagnation and sampling volume on water microbial quality monitoring in large buildings,"

PLOS ONE, vol. 13, no. 6, pp. 1–14, 06 2018. [Online]. Available: https://doi.org/10.1371/journal.pone.0199429

[33] K. M. Carlson, L. A. Boczek, S. Chae, and H. Ryu, "Legionellosis and recent advances in technologies for legionella control in premise plumbing systems: A review," *Water*, vol. 12, no. 3, 2020. [Online]. Available: https://www.mdpi.com/2073-4441/12/3/676

[34] [Online]. Available: https://m.systemsra.com/index.php?ws=services&cid=1764&sid=7017&lang=en

[35] G. Hill, E. Pring, and P. Osborn, *Cooling Towers: Principles and Practice*. Butterworth-Heinemann, 1990. [Online]. Available: https://books.google.ca/books?id=oeFSAAAAMAAJ

[36] J. M. Donohue, "Water conditioning, industrial," in *Encyclopedia of Physical Science and Technology (Third Edition)*, third edition ed., R. A. Meyers, Ed. New York: Academic Press, 2003, pp. 671–697. [Online]. Available: https://www.sciencedirect.com/science/article/pii/B012227410500819X

[37] B. K. Naik and P. Muthukumar, "A novel approach for performance assessment of mechanical draft wet cooling towers," *Applied Thermal Engineering*, vol. 121, pp. 14–26, 2017.

[38] "How cooling towers work," https://www.coolingtowerproducts.com/blog/how-cooling-towers-work-diagram-pictures-2015.htm, accessed: 2022-05-10.

[39] F. Afshari and H. Dehghanpour, "A review study on cooling towers; types, performance and application," 09 2018.

[40] G. F. Cortinovis, J. L. Paiva, T. W. Song, and J. M. Pinto, "A systemic approach for optimal cooling tower operation," *Energy Conversion and Management*, vol. 50, no. 9, pp. 2200–2209, 2009. [Online]. Available: https://www.sciencedirect.com/science/article/pii/S0196890409001721

[41] Y. Anchan, S. Khan, S. Lad, D. Patel, D. Patel, and J. Variava, "Performance analysis of cooling tower in process industry," *International Journal Of Advance Research And Innovative Ideas In Education*, vol. Vol-3, p. 9, 12 2017.

[42] "Sw guidelines for legionella control in cooling water systems," https://www.health.nsw.gov.au/environment/legionellacontrol/Pages/guidelines-legionella-control.aspx, published: Sydney, Australia. 2018.

[43] C. G. Cutillas, J. Ruiz Ramírez, and M. Lucas, "Optimum design and operation of an hvac cooling tower for energy and water conservation," *Energies*, vol. 10, p. 299, 03 2017.

[44] D. J. Viljoen, "Evaluation and performance prediction of cooling tower spray zones," Ph.D. dissertation, Stellenbosch: University of Stellenbosch, 2006.

[45] M. Dupuy, S. Mazoua, F. Berne, C. Bodet, N. Garrec, P. Herbelin, F. Ménard-Szczebara, S. Oberti, M.-H. Rodier, S. Soreau, F. Wallet, and Y. Héchard, "Efficiency of water disinfectants against legionella pneumophila and acanthamoeba," *Water Research*, vol. 45, no. 3, pp. 1087–1094, 2011. [Online]. Available: https://www.sciencedirect.com/science/article/pii/S0043135410007207

[46] P. Dennis and J. Lee, "Differences in aerosol survival between pathogenic and non-pathogenic strains of legionella pneumophila serogroup 1," *Journal of Applied Bacteriology*, vol. 65, no. 2, pp. 135–141, 1988.

[47] X. Zhou, S. P. D'Aniello, and H.-Z. Yu, "Spray characterization measurements of a pendent fire sprinkler," *Fire Safety Journal*, vol. 54, pp. 36–48, 2012.

[48] P. K. Quinn, D. B. Collins, V. H. Grassian, K. A. Prather, and T. S. Bates, "Chemistry and related properties of freshly emitted sea spray aerosol," *Chemical reviews*, vol. 115, no. 10, pp. 4383–4399, 2015.

[49] H. Lhuissier and E. Villermaux, "Bursting bubble aerosols," *Journal of Fluid Mechanics*, vol. 696, pp. 5–44, 2012.

[50] F. Resch and G. Afeti, "Film drop distributions from bubbles bursting in seawater," *Journal of Geophysical Research: Oceans*, vol. 96, no. C6, pp. 10 681–10 688, 1991.

[51] E. Villermaux, "Fragmentation," *Annu. Rev. Fluid Mech.*, vol. 39, pp. 419–446, 2007.

[52] J. Stodůlka and R. Vitkovicova, "Estimation of the drift eliminator efficiency using numerical and experimental methods," *EPJ Web of Conferences*, vol. 114, p. 02111, 01 2016.

[53] J. K. Chan and M. W. Golay, "Comparative evaluation of cooling tower drift eliminator performance," 1977.

[54] P. Foster, M. Williams, and R. Winter, "Droplet behaviour and collection by counterflow cooling tower eliminators," *Atmospheric Environment (1967)*, vol. 8,

no. 4, pp. 349–360, 1974. [Online]. Available: https://www.sciencedirect.com/science/article/pii/0004698174901279

[55] S. C. Yao and V. E. Schrock, "Aerodynamic design of cooling tower drift eliminators," *NASA STI/Recon Technical Report N*, vol. 75, p. 24149, 1974.

[56] J. López, A. Káiser, B. Zamora, A. Viedma, J. Vera, M. Jiménez, J. Ruiz, and M. Lucas, "Analysis of the impact of droplets onto water films in drift eliminators," *International Journal of Computational Methods and Experimental Measurements*, vol. 4, no. 1, pp. 24–32, 2016.

[57] A. Burkholz, *Droplet separation*. VCH Publishers, 1989.

[58] D. Marmer, "Water conservation equals energy conservation," *Energy Engineering*, vol. 115, no. 5, pp. 48–63, 2018.

[59] B. Zamora and A. Kaiser, "Comparative efficiency evaluations of four types of cooling tower drift eliminator, by numerical investigation," *Chemical Engineering Science*, vol. 66, no. 6, pp. 1232–1245, 2011. [Online]. Available: https://www.sciencedirect.com/science/article/pii/S0009250910007360

[60] T. Sriveerakul, I. McLaine-cross, and M. Behnia, "Performance prediction for cooling tower eliminators," in *En The 17th Annual Conference of Mechanical Engineering Network, Prajinburi, Tailandia*, 2003.

[61] A. Mohiuddin, R. Saidur, M. Sattar, and A. Rahman, "Comparison of drift eliminators characteristics in evaporative condenser and spray-filled tower," *International Energy Journal*, vol. 8, pp. 155–162, 09 2007.

[62] B. Becker and L. Burdick, "Effect of drift eliminator design on cooling tower performance," 1992.

[63] Z. Yu, C. Sun, J. Fang, L. Zhang, Y. Hu, B. Bao, S. Bu, W. Xu, and Y. Ji, "Water recovery efficiency improvement using the enhanced structure of the mist eliminator," *Process Safety and Environmental Protection*, vol. 154, pp. 433–446, 2021.

[64] M. Lucas, J. Ruiz Ramírez, P. Martínez, A. Kaiser, A. Viedma, and B. Zamora, "Experimental study on the performance of a mechanical cooling tower fitted with different types of water distribution systems and drift eliminators," *Applied Thermal Engineering*, vol. 50, p. 282–292, 01 2013.

[65] Z. Yang, R. Tao, H. Ni, K. Zhong, and Z. Lian, "Performance study of the internally-cooled ultrasonic atomization liquid desiccant dehumidification system," *Energy*, vol. 175, pp. 745–757, 2019.

[66] S. Allegra, L. Leclerc, P. A. Massard, F. Girardot, S. Riffard, and J. Pourchez, "Characterization of aerosols containing legionella generated upon nebulization," *Scientific Reports*, vol. 6, no. 1, 2016.

[67] B. Rahimi and A. Vesal, "Antimicrobial resistance properties of legionella pneumophila isolated from the cases of lower respiratory tract infections," *Biomedical and Pharmacology Journal*, vol. 10, no. 1, pp. 59–65, 2017.

[68] N. A. of Sciences Engineering and Medicine, *Management of Legionella in Water Systems*. Washington, DC: The National Academies Press, 2020. [Online]. Available: https://nap.nationalacademies.org/catalog/25474/management-of-legionella-in-water-systems

[69] P. Ulleryd, A. Hugosson, G. Allestam, S. Bernander, B. E. Claesson, I. Eilertz, A.-C. Hagaeus, M. Hjorth, A. Johansson, B. de Jong *et al.*, "Legionnaires' disease from a cooling tower in a community outbreak in lidköping, sweden-epidemiological, environmental and microbiological investigation supported by meteorological modelling," *BMC infectious diseases*, vol. 12, no. 1, pp. 1–9, 2012.

[70] S. Mubareka, N. Groulx, E. Savory, T. Cutts, S. Theriault, J. A. Scott, C. J. Roy, N. Turgeon, E. Bryce, G. Astrakianakis *et al.*, "Bioaerosols and transmission, a diverse and growing community of practice," *Frontiers in public health*, vol. 7, p. 23, 2019.

[71] M. Baker-Goering, K. Roy, C. Edens, and S. Collier, "Economic burden of legionnaires' disease, united states, 2014," *Emerging Infectious Diseases*, vol. 27, no. 1, p. 255, 2021.

[72] M. E. Gerdes, S. Miko, J. M. Kunz, E. J. Hannapel, M. C. Hlavsa, M. J. Hughes, M. J. Stuckey, L. K. F. Watkins, J. R. Cope, J. S. Yoder *et al.*, "Estimating waterborne infectious disease burden by exposure route, united states, 2014," *Emerging Infectious Diseases*, vol. 29, no. 7, p. 1357, 2023.

[73] J. Beaute, P. Zucs, and B. de Jong, "Legionnaires disease in europe, 2009-2010," *Euro surveillance : bulletin européen sur les maladies transmissibles = European communicable disease bulletin*, vol. 18, 03 2013.

[74] E. Bédard, S. Fey, D. Charron, C. Lalancette, P. Cantin, P. Dolcé, C. Laferrière,

E. Déziel, and M. Prévost, "Temperature diagnostic to identify high risk areas and optimize legionella pneumophila surveillance in hot water distribution systems," *Water research*, vol. 71, pp. 244–256, 2015.

[75] C. Caicedo, K.-H. Rosenwinkel, M. Exner, W. Verstraete, R. Suchenwirth, P. Hartemann, and R. Nogueira, "Legionella occurrence in municipal and industrial wastewater treatment plants and risks of reclaimed wastewater reuse," *Water research*, vol. 149, pp. 21–34, 2019.

[76] A. T. Paniagua, K. Paranjape, M. Hu, E. Bedard, and S. P. Faucher, "Impact of temperature on legionella pneumophila, its protozoan host cells, and the microbial diversity of the biofilm community of a pilot cooling tower," *Science of The Total Environment*, vol. 712, p. 136131, 2020.

[77] D. L. Johnson, K. R. Mead, R. A. Lynch, and D. V. Hirst, "Lifting the lid on toilet plume aerosol: a literature review with suggestions for future research," *American journal of infection control*, vol. 41, no. 3, pp. 254–258, 2013.

[78] T. M. Nhu Nguyen, D. Ilef, S. Jarraud, L. Rouil, C. Campese, D. Che, S. Haeghebaert, F. Ganiayre, F. Marcel, J. Etienne, and J.-C. Desenclos, "A Community-Wide Outbreak of Legionnaires Disease Linked to Industrial Cooling Towers—How Far Can Contaminated Aerosols Spread?" *The Journal of Infectious Diseases*, vol. 193, no. 1, pp. 102–111, 01 2006. [Online]. Available: https://doi.org/10.1086/498575

[79] S. M. Walser, D. G. Gerstner, B. Brenner, C. Höller, B. Liebl, and C. E. Herr, "Assessing the environmental health relevance of cooling towers–a systematic review of legionellosis outbreaks," *International journal of hygiene and environmental health*, vol. 217, no. 2-3, pp. 145–154, 2014.

[80] P. Lapierre, E. Nazarian, Y. Zhu, D. Wroblewski, A. Saylors, T. Passaretti, S. Hughes, A. Tran, Y. Lin, J. Kornblum *et al.*, "Legionnaires' disease outbreak caused by endemic strain of legionella pneumophila, new york, new york, usa, 2015," *Emerging infectious diseases*, vol. 23, no. 11, p. 1784, 2017.

[81] K. A. Hamilton, M. T. Hamilton, W. Johnson, P. Jjemba, Z. Bukhari, M. LeChevallier, and C. N. Haas, "Health risks from exposure to legionella in reclaimed water aerosols: Toilet flushing, spray irrigation, and cooling towers," *Water research*, vol. 134, pp. 261–279, 2018.

[82] H. Grythe, J. Ström, R. Krejci, P. Quinn, and A. Stohl, "A review of sea-spray

aerosol source functions using a large global set of sea salt aerosol concentration measurements," *Atmospheric Chemistry and Physics*, vol. 14, no. 3, pp. 1277–1297, 2014. [Online]. Available: https://acp.copernicus.org/articles/14/1277/2014/

[83] S. Ishimatsu, H. Miyamoto, H. Hori, I. Tanaka, and S.-i. Yoshida, "Sampling and detection of legionella pneumophila aerosols generated from an industrial cooling tower," *The Annals of occupational hygiene*, vol. 45, no. 6, pp. 421–427, 2001.

[84] L. Duchemin, S. Popinet, C. Josserand, and S. Zaleski, "Jet formation in bubbles bursting at a free surface," *Physics of fluids*, vol. 14, no. 9, pp. 3000–3008, 2002.

[85] L. Hung and S. Yao, "Experimental investigation of the impaction of water droplets on cylindrical objects," *International journal of multiphase flow*, vol. 25, no. 8, pp. 1545–1559, 1999.

[86] C. Tan, M. Papadakis, D. Miller, T. Bencic, P. Tate, and M. Laun, "Experimental study of large droplet splashing and breakup," in *45th AIAA Aerospace Sciences Meeting and Exhibit*, 2007, p. 904.

[87] R. F. Berendt, "Survival of legionella pneumophila in aerosols: effect of relative humidity," ARMY MEDICAL RESEARCH INST OF INFECTIOUS DISEASES FORT DETRICK MD, Tech. Rep., 1980.

[88] J. Oliver, "The viable but nonculturable state in bacteria," *Journal of microbiology (Seoul, Korea)*, vol. 43 Spec No, pp. 93–100, 03 2005.

[89] J. M. Blatny, B. A. P. Reif, G. Skogan, O. Andreassen, E. A. Høiby, E. Ask, V. Waagen, D. Aanonsen, I. S. Aaberge, and D. A. Caugant, "Tracking airborne legionella and legionella pneumophila at a biological treatment plant," *Environmental science & technology*, vol. 42, no. 19, pp. 7360–7367, 2008.

[90] P. Hambleton, M. Broster, P. Dennis, R. Henstridge, R. Fitzgeorge, and J. Conlan, "Survival of virulent legionella pneumophila in aerosols," *Epidemiology & Infection*, vol. 90, no. 3, pp. 451–460, 1983.

[91] K. M. Carlson, L. A. Boczek, S. Chae, and H. Ryu, "Legionellosis and recent advances in technologies for legionella control in premise plumbing systems: a review," *Water*, vol. 12, no. 3, p. 676, 2020.

[92] J. P. Springston and L. Yocavitch, "Existence and control of legionella bacteria in building water systems: A review," *Journal of occupational and environmental hygiene*,

vol. 14, no. 2, pp. 124–134, 2017.

[93] D. S. Cutler, J. D. Dean, J. A. Daw, and D. Howett, "Alternative water treatment technologies for cooling tower applications," National Renewable Energy Lab.(NREL), Golden, CO (United States), Tech. Rep., 2019.

[94] J. W. Shea, A. F. I. O. T. W.-P. A. O. S. O. SYSTEMS, and LOGISTICS, "A comparative analysis of three water treatment programs for cooling tower systems," Ph.D. dissertation, Air Force Institute of Technology, 1991.

[95] V. A. Mouchtouri, G. Goutziana, J. Kremastinou, and C. Hadjichristodoulou, "Legionella species colonization in cooling towers: risk factors and assessment of control measures," *American journal of infection control*, vol. 38, no. 1, pp. 50–55, 2010.

[96] E. Udwin, "Side stream filtration for cooling towers," *Proc. Cooling Tower Inst. Ann. Mtg*, 1974.

[97] S. Daalach, "Étude de la performance des filtres vortisand en présence d'un balayage de surface," Ph.D. dissertation, École de technologie supérieure, 2017.

[98] S. Chien, M. Hsieh, H. Li, J. Monnell, D. Dzombak, and R. Vidic, "Pilot-scale cooling tower to evaluate corrosion, scaling, and biofouling control strategies for cooling system makeup water," *Review of Scientific Instruments*, vol. 83, no. 2, 2012.

[99] X. Duan, J. Williamson, and K. McMordie, "Side stream filtration for cooling towers," *Federal Energy Management Program US Department of Energy*, 2012.

[100] L. Trudel, M. Veillette, L. Bonifait, and C. Duchaine, "Management of the 2012 legionella crisis in quebec city: need for a better communication between resources and knowledge transfer," *Frontiers in Microbiology*, vol. 5, p. 182, 2014.

[101] E. National Academies of Sciences and Medicine, *Management of Legionella in Water Systems*. Washington, DC: The National Academies Press, 2020. [Online]. Available: https://nap.nationalacademies.org/catalog/25474/management-of-legionella-in-water-systems

[102] G. Cadieux, J. Brodeur, F. Lamothe, C. Lalancette, P. A. Pilon, D. Kaiser, and É. Litvak, "Éclosion communautaire et nosocomiale de legionella pneumophila à montréal, québec, 2019," *Relevé des maladies transmissibles au Canada*, vol. 46, no. 78, pp. 246–254, 2020.

[103] ASHRAE, *Legionellosis: risk management for building water systems.* ASHRAE, 2018.

[104] E. Van Kenhove, K. Dinne, A. Janssens, and J. Laverge, "Overview and comparison of legionella regulations worldwide," *American journal of infection control*, vol. 47, no. 8, pp. 968–978, 2019.

[105] M. A. Moffa, C. Rock, P. Galiatsatos, S. D. Gamage, K. J. Schwab, and N. G. Exum, "Legionellosis on the rise: A scoping review of sporadic, community-acquired incidence in the united states," *Epidemiology & Infection*, pp. 1–15, 2023.

[106] J. Beauté, D. Plachouras, S. Sandin, J. Giesecke, and P. Sparén, "Healthcare-associated legionnaires' disease, europe, 2008- 2017," *Emerging Infectious Diseases*, vol. 26, no. 10, p. 2309, 2020.

[107] Public Works and Government Services Canada, *control of Legionella in mechanical systems : standard for building owners, design professionals, and maintenance personnel /Mechanical and Electrical Engineering*, 2013, no. 15161. [Online]. Available: https://publications.gc.ca/site/eng/9.800838/publication.html

[108] K. Hamilton and C. Haas, "Critical review of mathematical approaches for quantitative microbial risk assessment (qmra) of legionella in engineered water systems: research gaps and a new framework," *Environmental Science: Water Research & Technology*, vol. 2, no. 4, pp. 599–613, 2016.

[109] Á. Leelőssy, F. Molnár, F. Izsák, Á. Havasi, I. Lagzi, and R. Mészáros, "Dispersion modeling of air pollutants in the atmosphere: a review," *Open Geosciences*, vol. 6, no. 3, pp. 257–278, 2014.

[110] J. Seinfeld and S. Pandis, *Atmospheric Chemistry and Physics: From Air Pollution to Climate Change*. Wiley, 2016. [Online]. Available: https://books.google.ad/books?id=n_RmCgAAQBAJ

[111] T. W. Armstrong and C. N. Haas, "A quantitative microbial risk assessment model for legionnaires' disease: Animal model selection and dose-response modeling," *Risk Analysis: An International Journal*, vol. 27, no. 6, pp. 1581–1596, 2007.

[112] R. Fitzgeorge, A. Baskerville, M. Broster, P. Hambleton, and P. Dennis, "Aerosol infection of animals with strains of legionella pneumophila of different virulence: compari-

son with intraperitoneal and intranasal routes of infection," *Epidemiology & Infection*, vol. 90, no. 1, pp. 81–89, 1983.

[113] T. W. Armstrong and C. N. Haas, "Legionnaires' disease: evaluation of a quantitative microbial risk assessment model," *Journal of Water and Health*, vol. 6, no. 2, pp. 149–166, 2008.

[114] A. van Lier, S. A. McDonald, M. Bouwknegt, E. group, M. E. Kretzschmar, A. H. Havelaar, M.-J. J. Mangen, J. Wallinga, and H. E. de Melker, "Disease burden of 32 infectious diseases in the netherlands, 2007-2011," *PloS one*, vol. 11, no. 4, p. e0153106, 2016.

[115] A. Nocker, L. Schulte-Illingheim, J. Frösler, L. Welp, O. Sperber, and A. Hugo, "Microbiological examination of water and aerosols from four industrial evaporative cooling systems in regard to risk of legionella emissions and methodological suggestions for surveillance," *International Journal of Hygiene and Environmental Health*, vol. 229, p. 113591, 2020. [Online]. Available: https://www.sciencedirect.com/science/article/pii/S143846392030537X

[116] J. Ruiz, A. Kaiser, M. Ballesta, A. Gil, and M. Lucas, "Experimental measurement of cooling tower emissions using image processing of sensitive papers," *Atmospheric environment*, vol. 69, pp. 170–181, 2013.

[117] M. G. Davies, *Building heat transfer*. John Wiley & Sons, 2004.

[118] D. Baker and D. Baker, *Cooling tower performance*. Chemical Publishing, 1984.

[119] S. Verbeke and A. Audenaert, "Thermal inertia in buildings: A review of impacts across climate and building use," *Renewable and sustainable energy reviews*, vol. 82, pp. 2300–2318, 2018.

[120] O. Levenspiel, *Engineering flow and heat exchange*. Springer Science & Business Media, 2013.

[121] B. Linnhoff, D. R. Mason, and I. Wardle, "Understanding heat exchanger networks," *Computers & Chemical Engineering*, vol. 3, no. 1-4, pp. 295–302, 1979.

[122] L. Habbart *et al.*, *Treatment of cooling water*. Springer Science & Business Media, 2009.

[123] E. L. Sciuto, P. Laganà, S. Filice, S. Scalese, S. Libertino, D. Corso, G. Faro, and

M. A. Coniglio, "Environmental management of legionella in domestic water systems: Consolidated and innovative approaches for disinfection methods and risk assessment," *Microorganisms*, vol. 9, no. 3, 2021.

[124] L. Melo and T. Bott, "Biofouling in water systems," *Experimental thermal and fluid science*, vol. 14, no. 4, pp. 375–381, 1997.

[125] T. R. Bott, *Industrial biofouling*. Elsevier, 2011.

[126] T. Bott, "Techniques for reducing the amount of biocide necessary to counteract the effects of biofilm growth in cooling water systems," *Applied thermal engineering*, vol. 18, no. 11, pp. 1059–1066, 1998.

[127] N. Milosavljevic and P. Heikkilä, "A comprehensive approach to cooling tower design," *Applied thermal engineering*, vol. 21, no. 9, pp. 899–915, 2001.

[128] T. Nishizaki, K. Miyamoto, and K. Yoshida, "Coefficients of performance of hydride heat pumps," *Journal of the Less Common Metals*, vol. 89, no. 2, pp. 559–566, 1983.

[129] T. Jagadeesh and K. S. Reddy, "Performance analysis of the natural draft cooling tower in different seasons," *IOSR JOURNAL OF MECHANICAL AND CIVIL ENGINEERING (IOSR-JMCE)*, vol. 7, no. 5, pp. 19–23, 2013.

[130] C. Schulze, S. Thiede, and C. Herrmann, "Life cycle assessment of industrial cooling towers," *Progress in Life Cycle Assessment*, pp. 135–146, 2019.

[131] C. Schulze, B. Raabe, C. Herrmann, and S. Thiede, "Environmental impacts of cooling tower operations–the influence of regional conditions on energy and water demands," *Procedia CIRP*, vol. 69, pp. 277–282, 2018.

[132] R. Saidur, E. Abdelaziz, M. Hasanuzzaman, and M. Mamun, "A study of energy efficiency, economic and environmental benefits of a cooling tower," *International Journal of Mechanical and Materials Engineering*, vol. 5, no. 1, pp. 87–94, 2010.

[133] K. Xhaxhiu and V. Adam, "Particle size distribution analyses," 08 2015.

[134] S. Sousan, K. Koehler, L. Hallett, and T. M. Peters, "Evaluation of the alphasense optical particle counter (opc-n2) and the grimm portable aerosol spectrometer (pas-1.108)," *Aerosol Science and Technology*, pp. 1352–1365, 2016.

[135] K. Ardon-Dryer, M. C. Kelley, X. Xueting, and Y. Dryer, "The aerosol research

observation station (aeros)," *Atmospheric Measurement Techniques*, vol. 15, no. 8, pp. 2345–2360, 2022. [Online]. Available: https://amt.copernicus.org/articles/15/2345/2022/

[136] S. Horender, G. Tancev, K. Auderset, and K. Vasilatou, "Traceable pm2.5 and pm10 calibration of low-cost sensors with ambient-like aerosols generated in the laboratory," *Applied Sciences*, vol. 11, no. 19, 2021. [Online]. Available: https://www.mdpi.com/2076-3417/11/19/9014

[137] J. D. Wilcox, "Isokinetic flow and sampling," *Journal of the Air Pollution Control Association*, vol. 5, no. 4, pp. 226–245, 1956. [Online]. Available: https://doi.org/10.1080/00966665.1956.10467715

[138] G. Hidy, "Atmospheric aerosols: Some highlights and highlighters, 1950 to 2018," *Aerosol Science and Engineering*, vol. 3, 02 2019.

[139] C. Garcia-Jares, R. Barro, and M. Llompart, "Indoor air sampling," *Comprehensive Sampling and Sample Preparation*, p. 125–161, 2012.

[140] L. Heining, L. Welp, A. Hugo, M. Elsner, and M. Seidel, "Bioaerosol sampling and bioanalysis: Applicability of the next generation impactor for quantifying legionella pneumophila in droplet aerosols by flow cytometry," *Journal of Aerosol Science*, p. 106460, 2024.

[141] M.-È. Benoit, M. Prévost, A. Succar, D. Charron, E. Déziel, E. Robert, and E. Bédard, "Faucet aerator design influences aerosol size distribution and microbial contamination level," *Science of The Total Environment*, vol. 775, p. 145690, 2021.

[142] H. Grimm and D. J. Eatough, "Aerosol measurement: The use of optical light scattering for the determination of particulate size distribution, and particulate mass, including the semi-volatile fraction," *Journal of the Air & Waste Management Association*, vol. 59, no. 1, p. 101–107, 2009.

[143] E. Knutson and K. Whitby, "Aerosol classification by electric mobility: apparatus, theory, and applications," *Journal of Aerosol Science*, vol. 6, no. 6, pp. 443–451, 1975. [Online]. Available: https://www.sciencedirect.com/science/article/pii/0021850275900609

[144] K. T. Whitby and W. E. Clark, "Electric aerosol particle counting and size distribution measuring system for the 0.015 to 1 μ size range," *Tellus*, vol. 18, no. 2-3, p. 573–586,

1966.

[145] H.-E. Albrecht, *Laser Doppler and phase Doppler measurement techniques*. Springer, 2011.

[146] R. B. Jørgensen, "Comparison of four nanoparticle monitoring instruments relevant for occupational hygiene applications," *Journal of Occupational Medicine and Toxicology*, pp. 1–14, 2019.

[147] M. Joshi, B. K. Sapra, A. Khan, S. N. Tripathi, P. M. Shamjad, T. Gupta, and Y. S. Mayya, "Harmonisation of nanoparticle concentration measurements using grimm and tsi scanning mobility particle sizers," *Journal of Nanoparticle Research*, 2012.

[148] R. H. Moore, E. B. Wiggins, A. T. Ahern, S. Zimmerman, L. Montgomery, P. Campuzano Jost, C. E. Robinson, L. D. Ziemba, E. L. Winstead, B. E. Anderson, C. A. Brock, and M. D. Brown, "Sizing response of the ultra-high sensitivity aerosol spectrometer (uhsas) and laser aerosol spectrometer (las) to changes in submicron aerosol composition and refractive index," *Atmospheric Measurement Techniques*, pp. 4517–4542, 2021.

[149] R. Sijs, S. Kooij, H. J. Holterman, J. Van De Zande, and D. Bonn, "Drop size measurement techniques for sprays: Comparison of image analysis, phase doppler particle analysis, and laser diffraction," *AIP Advances*, 2021.

[150] L. G. Dodge, "Comparison of performance of drop-sizing instruments," *Applied Optics*, p. 1328, 1987.

[151] E. Vo, M. Horvatin, and Z. Zhuang, "Performance comparison of field portable instruments to the scanning mobility particle sizer using monodispersed and polydispersed sodium chloride aerosols," *Annals of Work Exposures and Health*, pp. 711–720, 2018.

[152] W. Wells, "On air-borne infection study ii. droplets and droplets nuceli," *Am. J. Epidemiol*, pp. 611–618, 1934.

[153] W. A. Sirignano, *Fluid dynamics and transport of droplets and sprays*. Cambridge university press, 2010.

[154] N. A. Fuchs, *Evaporation and droplet growth in gaseous media*. Elsevier, 2013.

[155] J. C. Maxwell, *The Scientific Papers of James Clerk Maxwell...* University Press, 1890, vol. 2.

[156] I. Langmuir, "The evaporation of small spheres," *Physical review*, vol. 12, no. 5, p. 368, 1918.

[157] M. Pirhadi, B. Sajadi, G. Ahmadi, and D. Malekian, "Phase change and deposition of inhaled droplets in the human nasal cavity under cyclic inspiratory airflow," *Journal of aerosol science*, vol. 118, pp. 64–81, 2018.

[158] A. De Rivas and E. Villermaux, "Dense spray evaporation as a mixing process," *Physical Review Fluids*, vol. 1, no. 1, p. 014201, 2016.

[159] H. R. Pruppacher, J. D. Klett, and P. K. Wang, "Microphysics of clouds and precipitation," 1998.

[160] J. Kukkonen, T. Vesala, and M. Kulmala, "The interdependence of evaporation and settling for airborne freely falling droplets," *Journal of aerosol science*, vol. 20, no. 7, pp. 749–763, 1989.

[161] W. F. Wells, "On air-borne infection: study ii. droplets and droplet nuclei." *American journal of Epidemiology*, vol. 20, no. 3, pp. 611–618, 1934.

[162] V. Vlasov, "On a theory of mass transfer during the evaporation of a spherical droplet," *International Journal of Heat and Mass Transfer*, vol. 178, p. 121597, 2021.

[163] R. Hołyst, M. Litniewski, D. Jakubczyk, K. Kolwas, M. Kolwas, K. Kowalski, S. Migacz, S. Palesa, and M. Zientara, "Evaporation of freely suspended single droplets: experimental, theoretical and computational simulations," *Reports on progress in physics*, vol. 76, no. 3, p. 034601, 2013.

[164] H. Chen, L. Zhan, L. Gu, Q. Feng, N. Zhao, Y. Feng, H. Wu, and L. Yang, "Chloride release characteristics of desulfurization wastewater droplet during evaporation process using the single droplet drying method," *Fuel*, vol. 305, p. 121551, 2021.

[165] M. Rezaei and R. R. Netz, "Airborne virus transmission via respiratory droplets: Effects of droplet evaporation and sedimentation," *Current Opinion in Colloid & Interface Science*, vol. 55, p. 101471, 2021.

[166] X. Shao, Y. Hou, and X. Zhong, "Modulation of evaporation-affected crystal motion in a drying droplet by saline and surfactant concentrations," *Colloids and Surfaces A: Physicochemical and Engineering Aspects*, vol. 623, p. 126701, 2021.

[167] S. Basu, P. Kabi, S. Chaudhuri, and A. Saha, "Insights on drying and precipitation

dynamics of respiratory droplets from the perspective of covid-19," *Physics of Fluids*, vol. 32, no. 12, p. 123317, 2020.

[168] M. Alsved, L. Bourouiba, C. Duchaine, J. Löndahl, L. C. Marr, S. T. Parker, A. J. Prussin, and R. J. Thomas, "Natural sources and experimental generation of bioaerosols: challenges and perspectives," *Aerosol Science and Technology*, vol. 54, no. 5, pp. 547–571, 2020.

[169] E. Hernandez, C. Chen, J. Johnson, and R. Carter, "Viscosity changes in orange juice after ultrafiltration and evaporation," *Journal of Food Engineering*, vol. 25, no. 3, pp. 387–396, 1995.

[170] C. Lieber, S. Melekidis, R. Koch, and H.-J. Bauer, "Insights into the evaporation characteristics of saliva droplets and aerosols: levitation experiments and numerical modeling," *Journal of aerosol science*, vol. 154, p. 105760, 2021.

[171] M. Rabe, A. Kerth, A. Blume, and P. Garidel, "Albumin displacement at the air–water interface by tween (polysorbate) surfactants," *European Biophysics Journal*, vol. 49, no. 7, pp. 533–547, 2020.

[172] Z. Zhang, S. Orski, A. M. Woys, G. Yuan, I. E. Zarraga, N. J. Wagner, and Y. Liu, "Adsorption of polysorbate 20 and proteins on hydrophobic polystyrene surfaces studied by neutron reflectometry," *Colloids and Surfaces B: Biointerfaces*, vol. 168, pp. 94–102, 2018.

[173] J. C. Hensley, *Cooling tower fundamentals*. Marley Cooling Tower Company Stockton, CA, 1985.

[174] K. Paranjape, É. Bédard, L. G. Whyte, J. Ronholm, M. Prévost, and S. P. Faucher, "Presence of legionella spp. in cooling towers: the role of microbial diversity, pseudomonas, and continuous chlorine application," *Water research*, vol. 169, p. 115252, 2020.

[175] P. J. Flory, *Principles of polymer chemistry*. Cornell university press, 1953.

[176] D. Zang, S. Tarafdar, Y. Y. Tarasevich, M. D. Choudhury, and T. Dutta, "Evaporation of a droplet: From physics to applications," *Physics Reports*, vol. 804, pp. 1–56, 2019.

[177] R. Bennacer and X. Ma, "Effect of temperature and surfactants on evaporation and contact line dynamics of sessile drops," *Heliyon*, vol. 8, no. 11, 2022.

[178] P. S. Epstein, "On the resistance experienced by spheres in their motion through gases," *Physical Review*, vol. 23, no. 6, p. 710, 1924.

[179] G. N. Lewis, M. Randall, K. S. Pitzer, and L. Brewer, *Thermodynamics*. Courier Dover Publications, 2020.

[180] S. Kumar, "Insight on the evaporation dynamics in reducing the covid-19 infection triggered by respiratory droplets," *Physics of Fluids*, vol. 33, no. 7, p. 072004, 2021.

[181] E. Choi, Z. Tan, and W. A. Anderson, "Formation of secondary organic aerosols by germicidal ultraviolet light," *Environments*, vol. 6, no. 2, p. 17, 2019.

[182] J. Koehling and V. Wagner, "High speed picoliter droplet top-view analysis for advancing and receding contact angles, boiling regimes and droplet-droplet interaction," *International Journal of Heat and Mass Transfer*, vol. 169, p. 120939, 2021.

[183] D. Hardy, J. Archer, P. Lemaitre, R. Vehring, J. Reid, and J. Walker, "High time resolution measurements of droplet evaporation kinetics and particle crystallisation," *Physical Chemistry Chemical Physics*, vol. 23, no. 34, pp. 18 568–18 579, 2021.

[184] Y. Maruyama and K. Hasegawa, "Evaporation and drying kinetics of water-nacl droplets via acoustic levitation," *RSC advances*, vol. 10, no. 4, pp. 1870–1877, 2020.

[185] O. Gülcan, K. Günaydın, and A. Tamer, "The state of the art of material jetting—a critical review," *Polymers*, vol. 13, no. 16, p. 2829, 2021.

[186] S. Cheng and S. Chandra, "A pneumatic droplet-on-demand generator," *Experiments in fluids*, vol. 34, pp. 755–762, 2003.

[187] P. Zhu and L. Wang, "Passive and active droplet generation with microfluidics: a review," *Lab on a Chip*, vol. 17, no. 1, pp. 34–75, 2017.

[188] N. Ashgriz, *Handbook of atomization and sprays: theory and applications*. Springer Science & Business Media, 2011.

[189] K. Li, J.-k. Liu, W.-s. Chen, and L. Zhang, "Controllable printing droplets on demand by piezoelectric inkjet: applications and methods," *Microsystem technologies*, vol. 24, pp. 879–889, 2018.

[190] M. Singh, H. M. Haverinen, P. Dhagat, and G. E. Jabbour, "Inkjet printing—process and its applications," *Advanced materials*, vol. 22, no. 6, pp. 673–685, 2010.

[191] R. I. Haque, R. Vié, M. Germainy, L. Valbin, P. Benaben, and X. Boddaert, "Inkjet printing of high molecular weight pvdf-trfe for flexible electronics," *Flexible and Printed Electronics*, vol. 1, no. 1, p. 015001, 2015.

[192] R. Khoeini, H. Nosrati, A. Akbarzadeh, A. Eftekhari, T. Kavetskyy, R. Khalilov, E. Ahmadian, A. Nasibova, P. Datta, L. Roshangar *et al.*, "Natural and synthetic bioinks for 3d bioprinting," *Advanced NanoBiomed Research*, vol. 1, no. 8, p. 2000097, 2021.

[193] X. Lefebvre, A. Succar, E. Bédard, M. Prévost, and E. Robert, "Comparison of aerosol spectrometers: accounting for evaporation and sampling losses," *Measurement Science and Technology*, vol. 35, no. 4, p. 045301, 2024.

[194] X. Lefebvre, V. Ashok, D. Claveau-Mallet, E. Robert, and E. Bedard, "Data-driven cooling tower optimization: A comprehensive analysis of energy savings using microsand filtration," *arXiv preprint arXiv:2405.05346*, 2024.

[195] Y. Shah, J. W. Kurelek, S. D. Peterson, and S. Yarusevych, "Experimental investigation of indoor aerosol dispersion and accumulation in the context of covid-19: Effects of masks and ventilation," *Physics of Fluids*, vol. 33, no. 7, p. 073315, 2021. [Online]. Available: https://doi.org/10.1063/5.0057100

[196] R. Toossi and T. Novakov, "The lifetime of aerosols in ambient air: Consideration of the effects of surfactants and chemical reactions," *Atmospheric Environment (1967)*, vol. 19, no. 1, p. 127–133, 1985.

[197] H. Qian and X. Zheng, "Ventilation control for airborne transmission of human exhaled bio-aerosols in buildings," *Journal of Thoracic Disease*, vol. 10, no. 19, 2018. [Online]. Available: https://jtd.amegroups.com/article/view/18723

[198] T. C. Carvalho, J. I. Peters, and R. O. Williams, "Influence of particle size on regional lung deposition. what evidence is there?" *International Journal of Pharmaceutics*, vol. 406, no. 1, pp. 1–10, 2011. [Online]. Available: https://www.sciencedirect.com/science/article/pii/S0378517311000147

[199] M. Abuhegazy, K. Talaat, O. Anderoglu, and S. Poroseva, "Numerical investigation of aerosol transport in a classroom with relevance to covid-19," *Physics of Fluids*, vol. 32, 10 2020.

[200] A. Y. Gu, Y. Zhu, J. Li, and M. R. Hoffmann, "Speech-generated aerosol settling times and viral viability can improve covid-19 transmission prediction,"

Environ. Sci.: Atmos., vol. 2, pp. 34–45, 2022. [Online]. Available: http://dx.doi.org/10.1039/D1EA00013F

[201] J. Kangasluoma, R. Cai, J. Jiang, C. Deng, D. Stolzenburg, L. R. Ahonen, T. Chan, Y. Fu, C. Kim, T. M. Laurila, and et al., "Overview of measurements and current instrumentation for 1–10 nm aerosol particle number size distributions," *Journal of Aerosol Science*, vol. 148, p. 105584, 2020.

[202] G. Mainelis, "Bioaerosol sampling: Classical approaches, advances, and perspectives," *Aerosol Science and Technology*, vol. 54, no. 5, pp. 496–519, 2020. [Online]. Available: https://doi.org/10.1080/02786826.2019.1671950

[203] M. I. Guzman, "An overview of the effect of bioaerosol size in coronavirus disease 2019 transmission," *The International journal of health planning and management*, vol. 36, no. 2, pp. 257–266, 2021.

[204] N. Doggett, C.-W. Chow, and S. Mubareka, "Characterization of experimental and clinical bioaerosol generation during potential aerosol-generating procedures," *Chest*, vol. 158, no. 6, pp. 2467–2473, 2020.

[205] W. Griffiths and G. DeCosemo, "The assessment of bioaerosols: a critical review," *Journal of Aerosol Science*, vol. 25, no. 8, pp. 1425–1458, 1994.

[206] B. Y. H. Liu and K. W. Lee, "An aerosol generator of high stability." *American Industrial Hygiene Association journal*, vol. 36 12, pp. 861–5, 1975.

[207] I. von Deschwanden, F.-K. Benra, H. J. Dohmen, and D. Brillert, *PDA Measurements in Spray Generated by Twin-Jet-Nozzles*, ser. Fluids Engineering Division Summer Meeting, 07 2017, vol. Volume 1B, Symposia: Fluid Measurement and Instrumentation; Fluid Dynamics of Wind Energy; Renewable and Sustainable Energy Conversion; Energy and Process Engineering; Microfluidics and Nanofluidics; Development and Applications in Computational Fluid Dynamics; DNS/LES and Hybrid RANS/LES Methods, v01BT06A001. [Online]. Available: https://doi.org/10.1115/FEDSM2017-69003

[208] P. Rouhiainen and J. Stachiewicz, "On the deposition of small particles from turbulent streams," 1970.

[209] C. Haig, W. Mackay, J. Walker, and C. Williams, "Bioaerosol sampling: sampling mechanisms, bioefficiency and field studies," *Journal of Hospital Infection*, vol. 93,

no. 3, pp. 242–255, 2016.

[210] D. Massabò, S. G. Danelli, P. Brotto, A. Comite, C. Costa, A. Di Cesare, J. F. Doussin, F. Ferraro, P. Formenti, E. Gatta *et al.*, "Chambre: a new atmospheric simulation chamber for aerosol modelling and bio-aerosol research," *Atmospheric Measurement Techniques*, vol. 11, no. 10, pp. 5885–5900, 2018.

[211] Z. Xu, K. Wei, Y. Wu, F. Shen, Q. Chen, M. Li, and M. Yao, "Enhancing bioaerosol sampling by andersen impactors using mineral-oil-spread agar plate," *PLoS One*, vol. 8, no. 2, p. e56896, 2013.

[212] S. C. Wang and R. C. Flagan, "Scanning electrical mobility spectrometer," *Aerosol Science and Technology*, vol. 13, no. 2, pp. 230–240, 1990.

[213] J. G. Watson, J. C. Chow, D. A. Sodeman, D. H. Lowenthal, M.-C. O. Chang, K. Park, and X. Wang, "Comparison of four scanning mobility particle sizers at the fresno supersite," *Particuology*, vol. 9, no. 3, pp. 204–209, 2011.

[214] J. Smolik and V. Zdimal, "Condensation of supersaturated vapors. homogeneous nucleation of bis (2-ethyl-hexyl) sebacate (dehs)," *Journal of aerosol science*, vol. 24, no. 5, pp. 589–596, 1993.

[215] R. P. Nguyen, "Études sur les jets à contre-courant," Montréal, QC, Canada, 2018.

[216] N. Froessling, "On the evaporation of falling drops," ARMY BIOLOGICAL LABS FREDERICK MD, Tech. Rep., 1968.

[217] M. F. Trujillo and A. E. Parkhill, "A local lagrangian analysis of passive particle advection in a gas flow field," *International journal of multiphase flow*, vol. 37, no. 9, pp. 1201–1208, 2011.

[218] G. N. Lewis and M. Randall, *Thermodynamics*. Krishna Prakashan Media, 1963, no. 44.

[219] K. A. Hamilton, M. H. Weir, and C. N. Haas, "Dose response models and a quantitative microbial risk assessment framework for the mycobacterium avium complex that account for recent developments in molecular biology, taxonomy, and epidemiology," *Water research*, vol. 109, pp. 310–326, 2017.

[220] P. Biswas, C. L. Jones, and R. C. Flagan, "Distortion of size distributions by condensation and evaporation in aerosol instruments," *Aerosol Science and Technology*, vol. 7,

no. 2, pp. 231–246, 1987.

[221] A. J. Prussin, Z. Cheng, W. Leng, S. China, and L. C. Marr, "Size-resolved elemental composition of respiratory particles in three healthy subjects," *Environmental Science & Technology Letters*, vol. 10, no. 4, pp. 356–362, 2023.

[222] G. Cossali, M. Ratcliffe, E. Routledge, T. Karayiannis, and J. Fielder, "The cost of Legionellosis and technical ways forward," *CIBSE*, 2013.

[223] F. F. Graham and M. G. Baker, "Epidemiology and direct health care costs of hospitalised legionellosis in New Zealand, 2000–2020," *Infection, Disease & Health*, vol. 28, no. 1, pp. 27–38, 2023.

[224] B. A. Cunha, A. Burillo, and E. Bouza, "Legionnaires' disease," *The Lancet*, vol. 387, no. 10016, pp. 376–385, 2016.

[225] CDC, "Legionellosis — United States, 2000–2009," 2011, publisher: Center for Disease Control and Prevention (CDC). [Online]. Available: https://www.cdc.gov/mmwr/preview/mmwrhtml/mm6032a3.htm

[226] A. Prussin II, D. Schwake, and L. Marr, "Ten questions concerning the aerosolization and transmission of *Legionella* in the built environment," *Building and Environment*, vol. 123, 06 2017.

[227] E. Kussell, R. Kishony, N. Q. Balaban, and S. Leibler, "Bacterial persistence: a model of survival in changing environments," *Genetics*, vol. 169, no. 4, pp. 1807–1814, 2005.

[228] L. Trudel, M. Veillette, L. Bonifait, and C. S. Duchaine, "Management of the 2012 *Legionella* crisis in quebec city: need for a better communication between resources and knowledge transfer," *Frontiers in Microbiology*, vol. 5, 2014.

[229] A. Sidor, J. Ślączka, D. Rylska-Malita, K. Rajzer, A. Sierakowska, and U. Mikulska, "Outbreak of Legionnaires'disease in Rzeszów in 2023." *Epidemiological Review/Przegląd Epidemiologiczny*, vol. 78, no. 1, 2024.

[230] N. V. Grossmann, "Large community outbreak of Legionnaires disease potentially associated with a cooling tower—Napa County, California, 2022," *MMWR. Morbidity and Mortality Weekly Report*, vol. 72, 2023.

[231] C. Young, D. Smith, T. Wafer, and B. Crook, "Rapid testing and interventions to control *Legionella* proliferation following a Legionnaires' disease outbreak associated

with cooling towers," *Microorganisms*, vol. 9, no. 3, p. 615, 2021.

[232] L. T. Orkis, L. H. Harrison, K. J. Mertz, M. M. Brooks, K. J. Bibby, and J. E. Stout, "Environmental sources of community-acquired *Legionnaires'* disease: A review," *International journal of hygiene and environmental health*, vol. 221, no. 5, pp. 764–774, 2018.

[233] L. Vermeulen, P. Brandsema, J. Van De Kassteele, B. Bom, H. Sterk, F. Sauter, H. van den Berg, and A. de Roda Husman, "Atmospheric dispersion and transmission of legionella from wastewater treatment plants: A 6-year case-control study," *International Journal of Hygiene and Environmental Health*, vol. 237, p. 113811, 2021.

[234] E. Van Heijnsbergen, J. A. Schalk, S. M. Euser, P. S. Brandsema, J. W. den Boer, and A. M. de Roda Husman, "Confirmed and potential sources of *Legionella* reviewed," *Environmental science & technology*, vol. 49, no. 8, pp. 4797–4815, 2015.

[235] H. Trigui, S. Matthews, E. Bedard, D. Charron, S. Chea, C. Fleury, J. F. G. Maldonado, M. Rivard, S. P. Faucher, and M. Prévost, "Assessment of monitoring approaches to control legionella pneumophila within a complex cooling tower system," *Science of The Total Environment*, vol. 950, p. 175136, 2024.

[236] P. Dennis, D. Green, and B. Jones, "A note on the temperature tolerance of *Legionella*," *Journal of Applied Bacteriology*, vol. 56, no. 2, pp. 349–350, 1984.

[237] I. Pinel, D. Moed, J. S. Vrouwenvelder, and M. Van Loosdrecht, "Bacterial community dynamics and disinfection impact in cooling water systems," *Water research*, vol. 172, p. 115505, 2020.

[238] J. Ruiz, C. Cutillas, A. Kaiser, B. Zamora, H. Sadafi, and M. Lucas, "Experimental study on pressure loss and collection efficiency of drift eliminators," *Applied Thermal Engineering*, vol. 149, pp. 94–104, 2019. [Online]. Available: https://www.sciencedirect.com/science/article/pii/S1359431118355388

[239] E. Sylvestre, D. Charron, X. Lefebvre, E. Bedard, and M. Prevost, "Leveraging regulatory monitoring data for quantitative microbial risk assessment of legionella pneumophila in cooling towers," *medRxiv*, pp. 2024–05, 2024.

[240] R. Bentham and H. Whiley, "Quantitative microbial risk assessment and opportunist waterborne infections–are there too many gaps to fill?" *International journal of environmental research and public health*, vol. 15, no. 6, p. 1150, 2018.

[241] L. Tang, W. J. Rhoads, A. Eichelberg, K. A. Hamilton, and T. R. Julian, "Applications of quantitative microbial risk assessment to respiratory pathogens and implications for uptake in policy: A state-of-the-science review," *Environmental Health Perspectives*, vol. 132, no. 5, p. 056001, 2024.

[242] K. O. Bøifot, J. Gohli, G. Skogan, and M. Dybwad, "Performance evaluation of high-volume electret filter air samplers in aerosol microbiome research," *Environmental Microbiome*, vol. 15, pp. 1–16, 2020.

[243] W. Hennessy, "Chapter 10 - flow and level sensors," in *Sensor Technology Handbook*, J. S. Wilson, Ed. Burlington: Newnes, 2005, pp. 237–254.

[244] E. Brown, M. W. Skougstad, and M. J. Fishman, "Methods for collection and analysis of water samples for dissolved minerals and gases," 1970.

[245] A. F. Rusydi, "Correlation between conductivity and total dissolved solid in various type of water: A review," in *IOP conference series: earth and environmental science*, vol. 118, no. 1. IOP Publishing, 2018, p. 012019.

[246] M. Grimard-Conea, E. Deshommes, E. Doré, and M. Prévost, "Impact of recommissioning flushing on legionella pneumophila in a large building during the covid-19 pandemic," *Frontiers in Water*, vol. 4, p. 959689, 2022.

[247] F. Hammes, H.-U. Weilenmann, M. Vital, J. Helbing, U. Bosshart, P. Huber, R. Odermatt, and B. Sonnleitner, "Development and laboratory-scale testing of a fully automated online flow cytometer for drinking water analysis," *Cytometry. Part A : the journal of the International Society for Analytical Cytology*, vol. 81, pp. 508–16, 04 2012.

[248] R. Germerdonk, "Droplet separation. von a. bürkholz. vch, weinheim–new york–basel–cambridge 1989. xvii, 229 s., zahlr. abb. u. tab., geb., dm 164," 1990.

[249] R. Signor and N. Ashbolt, "Comparing probabilistic microbial risk assessments for drinking water against daily rather than annualised infection probability targets," *Journal of water and health*, vol. 7, no. 4, pp. 535–543, 2009.

[250] J. P. Glennon, *Estimating microorganism densities in aerosols from spray irrigation of wastewater*. US Environmental Protection Agency, 1982, vol. 82, no. 3.

[251] K. W. Peterson and B. PE, "Open cooling tower design considerations," *ASHRAE J*, vol. 58, pp. 50–54, 2016.

[252] ASHRAE, *Legionellosis: risk management for building water systems.* ASHRAE, 2018.

[253] P. Perrott, N. Turgeon, L. Gauthier-Levesque, and C. Duchaine, "Preferential aerosolization of bacteria in bioaerosols generated in vitro," *Journal of Applied Microbiology*, vol. 123, no. 3, pp. 688–697, 2017.

[254] B. Scharfman, A. Techet, J. Bush, and L. Bourouiba, "Visualization of sneeze ejecta: steps of fluid fragmentation leading to respiratory droplets," *Experiments in Fluids*, vol. 57, pp. 1–9, 2016.

[255] Y. Wang, R. Dandekar, N. Bustos, S. Poulain, and L. Bourouiba, "Universal rim thickness in unsteady sheet fragmentation," *Physical review letters*, vol. 120, no. 20, p. 204503, 2018.

[256] M. J. Donohue, S. Vesper, J. Mistry, and J. M. Donohue, "Impact of chlorine and chloramine on the detection and quantification of *Legionella pneumophila* and Mycobacterium species," *Applied and environmental microbiology*, vol. 85, no. 24, pp. e01 942–19, 2019.

[257] G. A. Cangelosi and J. S. Meschke, "Dead or alive: molecular assessment of microbial viability," *Applied and environmental microbiology*, vol. 80, no. 19, pp. 5884–5891, 2014.

[258] L. Li, T. Qin, Y. Li, H. Zhou, H. Song, H. Ren, L. Li, Y. Li, and D. Zhao, "Prevalence and molecular characteristics of waterborne pathogen *Legionella* in industrial cooling tower environments," *International Journal of Environmental Research and Public Health*, vol. 12, no. 10, pp. 12 605–12 617, 2015.

[259] S. Lee and J. Lee, "Outbreak investigations and identification of *Legionella* in contaminated water," *Legionella: Methods and Protocols*, pp. 87–118, 2013.

[260] W. H. Organization *et al.*, "Global health estimates technical paper who," *Department of Information*, pp. 2010–2019, 2013.

[261] L. Haan and A. Ferreira, *Extreme value theory: an introduction.* Springer, 2006, vol. 3.

[262] F. Wong and J. J. Collins, "Evidence that coronavirus superspreading is fat-tailed," *Proceedings of the National Academy of Sciences*, vol. 117, no. 47, pp. 29 416–29 418, 2020.

[263] J. Chen, X. Lei, L. Zhang, and B. Peng, "Using extreme value theory approaches to

forecast the probability of outbreak of highly pathogenic influenza in zhejiang, china," *PloS one*, vol. 10, no. 2, p. e0118521, 2015.

[264] A. Daouia, G. Stupfler, and A. Usseglio-Carleve, "Extreme value modelling of sars-cov-2 community transmission using discrete generalized pareto distributions," *Royal Society Open Science*, vol. 10, no. 3, p. 220977, 2023.

[265] L. Bourouiba, "A sneeze," *New England Journal of Medicine*, vol. 375, no. 8, p. e15, 2016.

[266] I. G. Goncalves, H. S. Fernandes, A. Melo, S. F. Sousa, L. C. Simoes, and M. Simoes, "Legionelladb–a database on legionella outbreaks," *Trends in Microbiology*, vol. 29, no. 10, pp. 863–866, 2021.

[267] M. Palusińska-Szysz and M. Simões, "Legionella pneumophila-transmission, pathogenesis, host-pathogen interaction, prevention and treatment," p. 1364620, 2024.

[268] M. Cavazzuti and P. Tartarini, "Transport and evaporation of exhaled respiratory droplets: an analytical model," *Physics of Fluids*, vol. 35, no. 10, 2023.

[269] J. M. Straka, *Cloud and precipitation microphysics: principles and parameterizations*. Cambridge University Press, 2009.

[270] G. A. Perchetti, M.-L. Huang, V. Peddu, K. R. Jerome, and A. L. Greninger, "Stability of sars-cov-2 in phosphate-buffered saline for molecular detection," *Journal of Clinical Microbiology*, vol. 58, no. 8, pp. 10–1128, 2020.

[271] P. Gonzalez-Tello, F. Camacho, and G. Blazquez, "Density and viscosity of concentrated aqueous solutions of polyethylene glycol," *Journal of Chemical and Engineering Data*, vol. 39, no. 3, pp. 611–614, 1994.

[272] R. N. Berglund and B. Y. Liu, "Generation of monodisperse aerosol standards," *Environmental Science & Technology*, vol. 7, no. 2, pp. 147–153, 1973.

[273] B. Y. Liu, R. N. Berglund, and J. K. Agarwal, "Experimental studies of optical particle counters," *Atmospheric Environment (1967)*, vol. 8, no. 7, pp. 717–732, 1974.

[274] R. M. Sayer, R. D. Gatherer, R. J. Gilham, and J. P. Reid, "Determination and validation of water droplet size distributions probed by cavity enhanced raman scattering," *Physical Chemistry Chemical Physics*, vol. 5, no. 17, pp. 3732–3739, 2003.

[275] H.-E. Albrecht, N. Damaschke, M. Borys, and C. Tropea, *Laser Doppler and phase Doppler measurement techniques*. Springer Science & Business Media, 2013.

[276] I. von Deschwanden, F.-K. Benra, H. J. Dohmen, and D. Brillert, "Pda measurements in spray generated by twin-jet-nozzles," in *Fluids Engineering Division Summer Meeting*, vol. 58059. American Society of Mechanical Engineers, 2017, p. V01BT06A001.

[277] C. Duchaine and C. J. Roy, "Bioaerosols and airborne transmission: Integrating biological complexity into our perspective," *Science of The Total Environment*, vol. 825, p. 154117, 2022.

[278] M. Grimard-Conea and M. Prévost, "Controlling legionella pneumophila in showerheads: Combination of remedial intervention and preventative flushing," *Microorganisms*, vol. 11, no. 6, p. 1361, 2023.

[279] Z.-L. Zhou, C. Cao, L.-D. Cao, L. Zheng, J. Xu, F.-M. Li, and Q.-L. Huang, "Evaporation kinetics of surfactant solution droplets on rice (oryza sativa) leaves," *PLoS One*, vol. 12, no. 5, p. e0176870, 2017.

[280] M. J. Rosen and J. T. Kunjappu, *Surfactants and interfacial phenomena*. John Wiley & Sons, 2012.

[281] P. A. Sadd, *Effect of surfactants on heat and mass transfer to water drops in air*. University of Surrey (United Kingdom), 1987.

[282] J. M. Smith, "Introduction to chemical engineering thermodynamics," 1950.

[283] M. R. R. Niño and J. R. Patino, "Surface tension of bovine serum albumin and tween 20 at the air-aqueous interface," *Journal of the American Oil Chemists' Society*, vol. 75, pp. 1241–1248, 1998.

[284] L. S. Blachechen, J. O. Silva, L. R. Barbosa, R. Itri, and D. F. Petri, "Hofmeister effects on the colloidal stability of poly (ethylene glycol)-decorated nanoparticles," *Colloid and Polymer Science*, vol. 290, pp. 1537–1546, 2012.

[285] A. Ghasemi, B. Ahmet Tuna, and X. Li, "Inverse cascade of the vortical structures near the contact line of evaporating sessile droplets," *Scientific Reports*, vol. 9, no. 1, p. 6784, 2019.

[286] T.-S. Wang and W.-Y. Shi, "Transition of marangoni convection instability patterns during evaporation of sessile droplet at constant contact line mode," *International*

Journal of Heat and Mass Transfer, vol. 148, p. 119138, 2020.

[287] B. D. MacDonald and C. Ward, "Onset of marangoni convection for evaporating sessile droplets," *Journal of colloid and interface science*, vol. 383, no. 1, pp. 198–207, 2012.

[288] M. Grimard-Conea, E. Bédard, and M. Prévost, "Can free chlorine residuals entering building plumbing systems really be maintained to prevent microbial growth?" *Science of The Total Environment*, vol. 939, p. 173651, 2024.

[289] R. Picknett and R. Bexon, "The evaporation of sessile or pendant drops in still air," *Journal of colloid and Interface Science*, vol. 61, no. 2, pp. 336–350, 1977.

[290] R. D. Deegan, "Pattern formation in drying drops," *Physical review E*, vol. 61, no. 1, p. 475, 2000.

[291] R. B. Bird, W. Stewart, and E. Lightfoot, "Transport phenomena.(4thedn)," 2006.

[292] R. H. Ewell and H. Eyring, "Theory of the viscosity of liquids as a function of temperature and pressure," *The Journal of Chemical Physics*, vol. 5, no. 9, pp. 726–736, 1937.

[293] S. Chapman and T. G. Cowling, *The mathematical theory of non-uniform gases: an account of the kinetic theory of viscosity, thermal conduction and diffusion in gases*. Cambridge university press, 1990.

[294] S. Arrhenius, "Über die reaktionsgeschwindigkeit bei der inversion von rohrzucker durch säuren," *Zeitschrift für physikalische Chemie*, vol. 4, no. 1, pp. 226–248, 1889.

[295] H. Inoue, K. Ono, W. Masuda, T. Inagaki, M. Yokota, and K. Inenaga, "Rheological properties of human saliva and salivary mucins," *Journal of Oral Biosciences*, vol. 50, no. 2, pp. 134–141, 2008.

[296] H. Li, Y. Zheng, D. Akin, and R. Bashir, "Characterization and modeling of a microfluidic dielectrophoresis filter for biological species," *Journal of microelectromechanical systems*, vol. 14, no. 1, pp. 103–112, 2005.

[297] D. Issadore, H. Shao, J. Chung, A. Newton, M. Pittet, R. Weissleder, and H. Lee, "Self-assembled magnetic filter for highly efficient immunomagnetic separation," *Lab on a Chip*, vol. 11, no. 1, pp. 147–151, 2011.

[298] S. Allegra, L. Leclerc, P. A. Massard, F. Girardot, S. Riffard, and J. Pourchez, "Char-

acterization of aerosols containing legionella generated upon nebulization," *Scientific reports*, vol. 6, no. 1, p. 33998, 2016.

[299] S.-N. Li, D. A. Lundgren, and D. Rovell-Rixx, "Evaluation of six inhalable aerosol samplers," *AIHAJ-American Industrial Hygiene Association*, vol. 61, no. 4, pp. 506–516, 2000.

[300] M. Ouriemi and G. Homsy, "Experimental study of the effect of surface-absorbed hydrophobic particles on the landau-levich law," *Physics of Fluids*, vol. 25, no. 8, 2013.

[301] H. N. Dixit and G. Homsy, "The elastocapillary landau–levich problem," *Journal of fluid mechanics*, vol. 735, pp. 1–28, 2013.

[302] F. Macedonio, M. Frappa, A. Brunetti, G. Barbieri, and E. Drioli, "Recovery of water and contaminants from cooling tower plume," *Environmental Engineering Research*, vol. 25, no. 2, pp. 222–229, 2020.

[303] J. Bronsted, "Studies on solubility. i. the solubility of salts in salt solutions." *Journal of the American Chemical Society*, vol. 42, no. 4, pp. 761–786, 1920.

[304] W. C. Winn Jr and R. L. Myerowitz, "The pathology of the legionella pneumonias: a review of 74 cases and the literature," *Human pathology*, vol. 12, no. 5, pp. 401–422, 1981.

[305] L. A. Dombrovsky, A. A. Fedorets, V. Y. Levashov, A. P. Kryukov, E. Bormashenko, and M. Nosonovsky, "Modeling evaporation of water droplets as applied to survival of airborne viruses," *Atmosphere*, vol. 11, no. 9, p. 965, 2020.

[306] J. P. Crimaldi, A. C. True, K. G. Linden, M. T. Hernandez, L. T. Larson, and A. K. Pauls, "Commercial toilets emit energetic and rapidly spreading aerosol plumes," *Scientific Reports*, vol. 12, no. 1, p. 20493, 2022.

[307] S. Hatte, K. Pandey, K. Pandey, S. Chakraborty, and S. Basu, "Universal evaporation dynamics of ordered arrays of sessile droplets," *Journal of Fluid Mechanics*, vol. 866, pp. 61–81, 2019.

[308] M. A. Shah, D.-G. Lee, B.-Y. Lee, and S. Hur, "Classifications and applications of inkjet printing technology: A review," *IEEE Access*, vol. 9, pp. 140 079–140 102, 2021.

[309] XAAR, "Xaar xj128 guide to operation," 2001. [Online]. Available: https://pedagogy-vestnik.ksu.kz/apart/2021-104-4/13.pdf

[310] C. Wootton and C. Wootton, "Serial peripheral interface (spi)," *Samsung ARTIK Reference: The Definitive Developers Guide*, pp. 335–349, 2016.

[311] A. Tinklenberg, M. Guala, and F. Coletti, "Turbulence effect on disk settling dynamics," *Journal of Fluid Mechanics*, vol. 992, p. A4, 2024.

[312] R. D. Boehm, P. R. Miller, J. Daniels, S. Stafslien, and R. J. Narayan, "Inkjet printing for pharmaceutical applications," *Materials Today*, vol. 17, no. 5, pp. 247–252, 2014.

[313] R. E. Saunders and B. Derby, "Inkjet printing biomaterials for tissue engineering: bioprinting," *International Materials Reviews*, vol. 59, no. 8, pp. 430–448, 2014.

[314] V. Beedasy and P. J. Smith, "Printed electronics as prepared by inkjet printing," *Materials*, vol. 13, no. 3, p. 704, 2020.

[315] H. Sirringhaus and T. Shimoda, "Inkjet printing of functional materials," *MRS bulletin*, vol. 28, no. 11, pp. 802–806, 2003.

[316] X. Luo, Z. Zeng, X. Wang, J. Xiao, Z. Gan, H. Wu, and Z. Hu, "Preparing two-dimensional nano-catalytic combustion patterns using direct inkjet printing," *Journal of Power Sources*, vol. 271, pp. 174–179, 2014.

[317] H.-C. Flemming and J. Wingender, "The biofilm matrix," *Nature reviews microbiology*, vol. 8, no. 9, pp. 623–633, 2010.

[318] T. Jagadeesh and K. Reddy, "Performance analysis of the natural draft cooling tower in different seasons," *IOSR-Journal Mech Civ Eng*, vol. 7, pp. 19–23, 01 2013.

[319] D. R. B.-H. A. SHRYOCK and H. A. Baker, "A comprehensive approach to the analysis of cooling tower performance," *J. Heat Transfer*, vol. 83, no. 3, pp. 339–349, 1961.

[320] M. A. Bernier, "Cooling tower performance: theory and experiments," American Society of Heating, Refrigerating and Air-Conditioning Engineers . . . , Tech. Rep., 1994.

[321] J. Song, Y. Chen, X. Wu, S. Ruan, and Z. Zhang, "A novel approach for energy efficiency prediction of various natural draft wet cooling towers using ann," *Journal of Thermal Science*, vol. 30, pp. 859–868, 2021.

[322] A. Silverwood, M. Bosisio, and F. Bordeleau, "Cross-flow microsand filtration for membrane pre-treatment," *Desalination and Water Treatment*, vol. 57, no. 55, pp. 26 548–26 551, 2016.

[323] D. C. Wang, C. F. Qian, S. X. Cao, Y. Liu, and J. W. Sun, "Effect of different biofouling characteristics on heat transfer of the heat exchanger," *Advanced Materials Research*, vol. 724, pp. 1282–1288, 2013.

[324] Y. Zhou, Q. Li, Z. Wang, S. Li, F. Wei, J. Liu, and D. Yu, "Thermal performance model of cooling towers for operational optimization: An equivalent temperature difference coefficient-based approach," *Applied Thermal Engineering*, p. 123595, 2024.

[325] J. Wang and T. Zhao, "Medium spatiotemporal characteristics based global optimization method for energy efficiency trade-off issue in variable flow rate hvac system," *Applied Thermal Engineering*, vol. 247, p. 123132, 2024.

[326] Y.-D. Yu, Z. Yang, and Y.-Y. Duan, "Sludge components and their fouling properties in a submerged micro-membrane filtration system," *Applied Thermal Engineering*, vol. 88, pp. 211–216, 2015.

[327] P. Navarro, J. Serrano, L. Roca, P. Palenzuela, M. Lucas, and J. Ruiz, "A comparative study on predicting wet cooling tower performance in combined cooling systems for heat rejection in csp plants," *Applied Thermal Engineering*, p. 123718, 2024.

[328] Y. Li, Y. Wu, Y. Zhong, and S. Zhang, "Numerical study on heat and mass transfer performance of a natural draft wet cooling tower based on baffle optimization," *Applied Thermal Engineering*, vol. 245, p. 122738, 2024.

[329] P. Services and P. Canada, "Cooling towers and evaporative condensers - mechanical design," Canada.ca, 2013, https://www.tpsgc-pwgsc.gc.ca/legionella-towers. [Online]. Available: https://www.tpsgc-pwgsc.gc.ca/legionella-towers

[330] H. Quebec, "Comparison of electricity prices in major north american cities," Technical Report, Canada, Tech. Rep., 2023.

[331] "Historical Climate Data - Climate - Environment and Climate Change Canada." [Online]. Available: https://climate.weather.gc.ca/index_e.html

[332] C. Heald, *Cameron hydraulic data: A Handy reference on the subject of hydraulics, and steam.* Ingersoll-Rand, 1988.

[333] J. Bezanson, A. Edelman, S. Karpinski, and V. B. Shah, "Julia: A fresh approach to numerical computing," *SIAM review*, vol. 59, no. 1, pp. 65–98, 2017.

[334] G. Biau and E. Scornet, "A random forest guided tour," *Test*, vol. 25, pp. 197–227, 2016.

[335] P. Joshi, *Artificial intelligence with python*. Packt Publishing Ltd, 2017.

[336] T. Susnjak, D. Kerry, A. Barczak, N. Reyes, and Y. Gal, "Wisdom of crowds: an empirical study of ensemble-based feature selection strategies," in *AI 2015: Advances in Artificial Intelligence: 28th Australasian Joint Conference, Canberra, ACT, Australia, November 30–December 4, 2015, Proceedings 28*. Springer, 2015, pp. 526–538.

[337] T. Jayalakshmi and A. Santhakumaran, "Statistical normalization and back propagation for classification," *International Journal of Computer Theory and Engineering*, vol. 3, no. 1, pp. 1793–8201, 2011.

[338] S. Riffat and X. Ma, "Improving the coefficient of performance of thermoelectric cooling systems: a review," *International journal of energy research*, vol. 28, no. 9, pp. 753–768, 2004.

[339] J. C. Chen, "Correlation for boiling heat transfer to saturated fluids in convective flow," *Industrial & engineering chemistry process design and development*, vol. 5, no. 3, pp. 322–329, 1966.

[340] F. P. Incropera, D. P. DeWitt, T. L. Bergman, A. S. Lavine *et al.*, *Fundamentals of heat and mass transfer*. Wiley New York, 1996, vol. 6.

[341] M. S. Al-Homoud, "Optimum thermal design of office buildings," *International Journal of Energy Research*, vol. 21, no. 10, pp. 941–957, 1997.

[342] C. Balaras, "The role of thermal mass on the cooling load of buildings. an overview of computational methods," *Energy and buildings*, vol. 24, no. 1, pp. 1–10, 1996.

[343] F. Zheng, S. Hu, J. Ma, L. Wang, K. Li, B. Wu, Q. Bao, J. Peng, C. Li, H. Zong *et al.*, "Will the globe encounter the warmest winter after the hottest summer in 2023?" 2023.

[344] V. Ashok, F. Absalan, A. Silverwood, E. Robert, D. Claveau-Mallet, and E. Bédard, "Crossflow microsand filtration in cooling tower systems: A sustainable approach to control fouling in heat exchanger devices," *Journal of Building Engineering*, 2024, accepted with revisions, JBE-D-24-03903.

[345] M. Fumagalli, M. Sironi, U. Pozzoli, A. Ferrer-Admettla, L. Pattini, and R. Nielsen, "Signatures of environmental genetic adaptation pinpoint pathogens as the main se-

lective pressure through human evolution," *PLoS genetics*, vol. 7, no. 11, p. e1002355, 2011.

[346] E. K. Karlsson, D. P. Kwiatkowski, and P. C. Sabeti, "Natural selection and infectious disease in human populations," *Nature Reviews Genetics*, vol. 15, no. 6, pp. 379–393, 2014.

[347] M. L. Cohen, "Changing patterns of infectious disease," *Nature*, vol. 406, no. 6797, pp. 762–767, 2000.

[348] M. M. Marta, "A brief history of the evolution of the medical research article," *Clujul Medical*, vol. 88, no. 4, p. 567, 2015.

[349] N. H. Leung, "Transmissibility and transmission of respiratory viruses," *Nature Reviews Microbiology*, vol. 19, no. 8, pp. 528–545, 2021.

[350] R. M. Ferry, W. F. Brown, and E. B. Damon, "Studies of the loss of viability of stored bacterial aerosols*. ii. death rates of several non-pathogenic organisms in relation to biological and structural characteristics," *Epidemiology & Infection*, vol. 56, no. 1, pp. 125–150, 1958.

[351] X. Chen, D. Kumari, and V. Achal, "A review on airborne microbes: the characteristics of sources, pathogenicity and geography," *Atmosphere*, vol. 11, no. 9, p. 919, 2020.

[352] N. Castano, S. C. Cordts, M. Kurosu Jalil, K. S. Zhang, S. Koppaka, A. D. Bick, R. Paul, and S. K. Tang, "Fomite transmission, physicochemical origin of virus–surface interactions, and disinfection strategies for enveloped viruses with applications to sars-cov-2," *ACS omega*, vol. 6, no. 10, pp. 6509–6527, 2021.

[353] G. R. Johnson and L. Morawska, "The mechanism of breath aerosol formation," *Journal of aerosol medicine and pulmonary drug delivery*, vol. 22, no. 3, pp. 229–237, 2009.

[354] P. Hoeksma, A. J. A. Aarnink, and N. Ogink, "Effect of temperature and relative humidity on the survival of airborne bacteria= effect van temperatuur en relatieve luchtvochtig-heid op de overleving van bacteriën in de lucht," Wageningen UR Livestock Research, Tech. Rep., 2015.

[355] S. Webb, "Factors affecting the viability of air-borne bacteria: I. bacteria aerosolized from distilled water," *Canadian Journal of Microbiology*, vol. 5, no. 6, pp. 649–669, 1959.

[356] S. Dutil, M. Veillette, A. Mériaux, L. Lazure, J. Barbeau, and C. Duchaine, "Aerosolization of mycobacteria and legionellae during dental treatment: low exposure despite dental unit contamination," *Environmental microbiology*, vol. 9, no. 11, pp. 2836–2843, 2007.

[357] G. S. Dias, D. A. Machado, J. C. de Andrade, and F. de Souza Costa, "Enc-2020-0193 hydrous ethanol atomization by impinging jets."

[358] J. Boulton-Stone and J. Blake, "Gas bubbles bursting at a free surface," *Journal of Fluid Mechanics*, vol. 254, pp. 437–466, 1993.

[359] S. A. McBride, "Contaminated bubble bursting," *Nature Physics*, pp. 1–2, 2023.

[360] B. Lighthart and J. Kim, "Simulation of airborne microbial droplet transport," *Applied and Environmental Microbiology*, vol. 55, no. 9, pp. 2349–2355, 1989.

[361] M. Alsved, S. Holm, S. Christiansen, M. Smidt, B. Rosati, M. Ling, T. Boesen, K. Finster, M. Bilde, J. Löndahl *et al.*, "Effect of aerosolization and drying on the viability of pseudomonas syringae cells," *Frontiers in microbiology*, vol. 9, p. 3086, 2018.

[362] M. K. Ijaz, B. Zargar, K. E. Wright, J. R. Rubino, and S. A. Sattar, "Generic aspects of the airborne spread of human pathogens indoors and emerging air decontamination technologies," *American Journal of Infection Control*, vol. 44, no. 9, pp. S109–S120, 2016.

[363] C. C. Wang, K. A. Prather, J. Sznitman, J. L. Jimenez, S. S. Lakdawala, Z. Tufekci, and L. C. Marr, "Airborne transmission of respiratory viruses," *Science*, vol. 373, no. 6558, p. eabd9149, 2021.

[364] J. W. Tang, "The effect of environmental parameters on the survival of airborne infectious agents," *Journal of the Royal Society Interface*, vol. 6, no. suppl_6, pp. S737–S746, 2009.

[365] I. Boppe, E. Bedard, C. Taillandier, D. Lecellier, M.-A. Nantel-Gauvin, M. Villion, C. Laferrière, and M. Prévost, "Investigative approach to improve hot water system hydraulics through temperature monitoring to reduce building environmental quality hazard associated to legionella," *Building and Environment*, vol. 108, pp. 230–239, 2016.

[366] H. Wang, E. Bedard, M. Prevost, A. K. Camper, V. R. Hill, and A. Pruden, "Methodological approaches for monitoring opportunistic pathogens in premise plumbing: A

review," *Water research*, vol. 117, pp. 68–86, 2017.

[367] D. Verreault, M. Marcoux-Voiselle, N. Turgeon, S. Moineau, and C. Duchaine, "Resistance of aerosolized bacterial viruses to relative humidity and temperature," *Applied and environmental microbiology*, vol. 81, no. 20, pp. 7305–7311, 2015.

[368] A. Adhikari, E. M. Kettleson, S. Vesper, S. Kumar, D. L. Popham, C. Schaffer, R. Indugula, K. Chatterjee, K. K. Allam, S. A. Grinshpun *et al.*, "Dustborne and airborne gram-positive and gram-negative bacteria in high versus low ermi homes," *Science of the Total Environment*, vol. 482, pp. 92–99, 2014.

[369] E. Caron, G. Chevrefils Jr, B. Barbeau, P. Payment, and M. Prévost, "Impact of microparticles on uv disinfection of indigenous aerobic spores," *Water Research*, vol. 41, no. 19, pp. 4546–4556, 2007.

[370] B. Lighthart, "Survival of airborne bacteria in a high urban concentration of carbon monoxide," *Applied microbiology*, vol. 25, no. 1, pp. 86–91, 1973.

[371] H. Rüden, E. Thofern, P. Fischer, and U. Mihm, "Airborne microorganisms: Their occurrence, distribution and dependence on environmental factors—especially on organic compounds of air-pollution," *pure and applied geophysics*, vol. 116, pp. 335–350, 1978.

[372] H. S. Xu, N. Roberts, F. Singleton, R. Attwell, D. J. Grimes, and R. Colwell, "Survival and viability of nonculturable escherichia coli and vibrio cholerae in the estuarine and marine environment," *Microbial ecology*, vol. 8, pp. 313–323, 1982.

[373] L. Stetzenbach, "Airborne infectious microorganisms," *Encyclopedia of Microbiology*, p. 175, 2009.

[374] C. Xu, H. Chen, Z. Liu, G. Sui, D. Li, H. Kan, Z. Zhao, W. Hu, and J. Chen, "The decay of airborne bacteria and fungi in a constant temperature and humidity test chamber," *Environment International*, vol. 157, p. 106816, 2021.

[375] L. Jiang, M. Li, J. Tang, X. Zhao, J. Zhang, H. Zhu, X. Yu, Y. Li, T. Feng, and X. Zhang, "Effect of different disinfectants on bacterial aerosol diversity in poultry houses," *Frontiers in microbiology*, vol. 9, p. 2113, 2018.

[376] V. F. McNeill, "Airborne transmission of sars-cov-2: evidence and implications for engineering controls," *Annual Review of Chemical and Biomolecular Engineering*, vol. 13, pp. 123–140, 2022.

[377] T. J. Robinson and A. E. Ouellet, "Filters and filtration," *ASHRAE journal*, vol. 41, pp. 65–70, 1999.

[378] M. S. Rawat and A. R. Ferro, "Respiratory virus deposition and resuspension from indoor surfaces," in *Studies to Combat COVID-19 using Science and Engineering*. Springer, 2022, pp. 107–118.

[379] X. Xie, Y. Li, T. Zhang, and H. H. Fang, "Bacterial survival in evaporating deposited droplets on a teflon-coated surface," *Applied microbiology and biotechnology*, vol. 73, pp. 703–712, 2006.

[380] M. Nikfar, R. Paul, K. Islam, M. Razizadeh, A. Jagota, and Y. Liu, "Respiratory droplet resuspension near surfaces: Modeling and analysis," *Journal of Applied Physics*, vol. 130, no. 2, p. 024702, 2021.

[381] C. Costantini, E. Nunzi, and L. Romani, "From the nose to the lungs: the intricate journey of airborne pathogens amid commensal bacteria," *American Journal of Physiology-Cell Physiology*, vol. 323, no. 4, pp. C1036–C1043, 2022.

[382] M. Mohamadzadeh, L. Chen, and A. L. Schmaljohn, "How ebola and marburg viruses battle the immune system," *Nature Reviews Immunology*, vol. 7, no. 7, pp. 556–567, 2007.

[383] P. Dettmer, *Immune: A Journey Into the Mysterious System that Keeps You Alive*. Random House, 2021.

[384] D. I. Meiron, G. R. Baker, and S. A. Orszag, "Analytic structure of vortex sheet dynamics. part 1. kelvin–helmholtz instability," *Journal of Fluid Mechanics*, vol. 114, pp. 283–298, 1982.

[385] D. H. Sharp, "An overview of rayleigh-taylor instability," *Physica D: Nonlinear Phenomena*, vol. 12, no. 1-3, pp. 3–18, 1984.

[386] A. Ilinca, E. McCarthy, J.-L. Chaumel, and J.-L. Rétiveau, "Wind potential assessment of quebec province," *Renewable energy*, vol. 28, no. 12, pp. 1881–1897, 2003.

[387] V. Charitatos and S. Kumar, "Droplet evaporation on soft solid substrates," *Soft Matter*, vol. 17, no. 41, pp. 9339–9352, 2021.

[388] W. Roger and P. Haines, *HVAC systems design handbook*. McGraw-Hill, New York, 2010.

[389] D. A. McQuarrie and J. D. Simon, *Physical chemistry: a molecular approach*. University science books Sausalito, CA, 1997, vol. 1.

[390] O. L. Brown, "The clausius-clapeyron equation," *Journal of Chemical Education*, vol. 28, no. 8, p. 428, 1951.

[391] P. W. Atkins, J. De Paula, and J. Keeler, *Atkins' physical chemistry*. Oxford university press, 2023.

[392] H. Siegrist and W. Gujer, "Mass transfer mechanisms in a heterotrophic biofilm," *Water Research*, vol. 19, no. 11, pp. 1369–1378, 1985.

APPENDIX A FACTORS AFFECTING THE VIABILITY OF PATHOGENS TRANSMITTED VIA THE AIRBORNE ROUTE

A review By
Xavier Lefebvre

Introduction

Infectious diseases are probably among the strongest selective pressures on human populations [345]. As humans evolved and societies developed, population densities have expanded and the frequency of the exposition to dangerous pathogens has increased [346]. Infectious diseases have always been part of human history and are still influencing our fate, with the COVID-19 pandemic as a prime example [2]. These illnesses are caused by pathogenic microorganisms such as bacteria, viruses, fungi or parasites (Figure A.1), which can be transmitted either through direct contact, fomites (objects which are likely to carry infection) or the airborne route [347].

These pathogens have been studied extensively as a result of the detrimental effects of infectious diseases. Although there is still ongoing research, most applications of infectious diseases that pertain to pathogen host invasion, infectious disease pathogenesis and immunology have been thoroughly investigated, with scientific literature dating back to 1677 [348]. However, until recently, one research area had been largely neglected: the transmission phase, especially of airborne-mediated pathogens. This has forced the field of infectious diseases to transition from solely health related to the inclusion of fluid mechanics concepts, which govern the generation of pathogen-laden droplets, as well as their airborne transmission, and even the viability of the pathogens they carry [3].

The underlying mechanisms of airborne transmission involve complex multiphase flows in which pathogen-laden droplets play a prominent role. However, the transmission of pathogens from one host to another is simply a necessary step in their life cycle [3]. Thus, to persist, pathogens have to adapt to and survive this unavoidable process. The propensity for respiratory diseases to be transmitted is therefore affected by their ability to remain viable under environmental stress [349].

The viability of microorganisms is defined as their capacity to replicate, which involves the integrity of the envelope of the pathogen, as well as its internal proteins and genetic material

enabling the replication (Figure A.1) [257]. As the viability of pathogens is binary (either dead or alive), the viability rate is often used as a metric to evaluate the infection risks from the ratio of viable pathogens from a population present in a fluid. Studying the effect of external factors on the viability of airborne pathogens is a complex task because multiple variables have tangible effects on the integrity of microorganisms. Despite this challenge, the loss of viability, called inactivation, of aerosolized pathogens has been described in two stages. The first stage is a rapid loss in viability upon aerosolization due to direct effects on the pathogens. The second is the first-order exponential decay model, described as a relatively slower loss in viability over a prolonged period of time due to the effects of ambient conditions on the pathogens (Equation A.1) [350].

$$N(t) = N_0 e^{-kt} \tag{A.1}$$

where:

- $N(t)$ is the number of viable bacteria at time t
- N_0 is the initial number of viable bacteria
- k is the decay constant, which determines the rate of decay

These stages of inactivation highlight the broad range of conditions that airborne pathogens must face to achieve infection in a new host. Environmental factors that affect their viability include temperature, relative humidity, ultraviolet radiation, as well as the composition of the air and the fluid forming the droplet. The conditions in the atmosphere are often unfavorable to microorganisms as they need to tolerate harsh environmental conditions. However, protected by the aqueous layer of the droplet surrounding them, a considerable fraction of airborne pathogens can remain viable for extended periods of time [351].

In the context of infectious diseases, fundamental questions revolve around the viability of airborne pathogens. How do specific pathogens lose their viability in the transport process? How are they able to adapt to harsh conditions? Can the inactivation of airborne pathogens be used as a mitigation strategy? What are the most effective decontamination procedures? These questions apply to all pathogenic microorganisms. Similar prevention, epidemiology and mitigation questions can be asked for agricultural, waterborne, animal or specific human infectious diseases [3]. Improvement in our understanding of how pathogens are transmitted via the airborne route can help with adequate risk assessment for specific infectious diseases, as well as the adoption of efficient mitigation strategies.

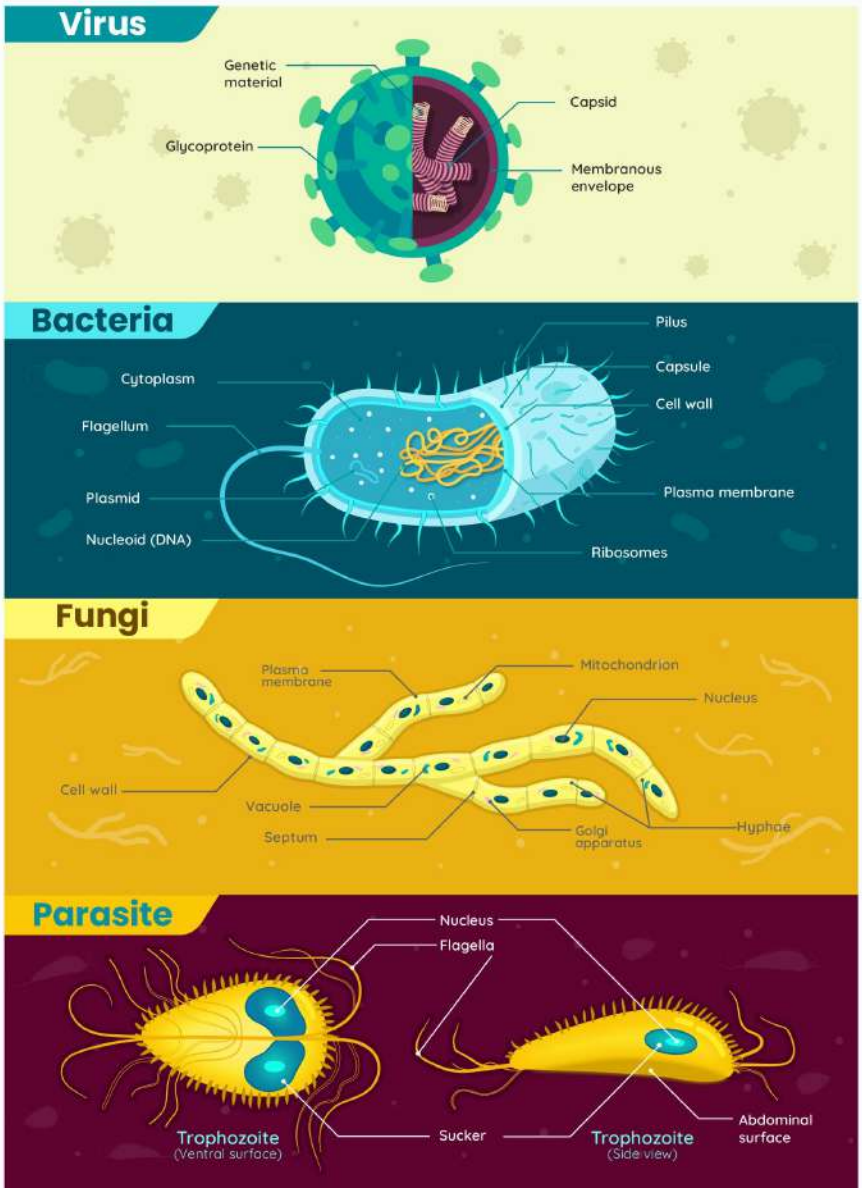

Figure A.1 Infectious diseases are caused by pathogenic microorganisms such as bacteria, viruses, fungi or parasites. These microorganisms all have different shapes, and sizes, as well as chemical and biological compositions, but their goal, as with any organism is to replicate. Cell replication involves various components such as cell wall, internal proteins and genetic material, of which the integrity must be preserved to remain viable [346].

Framework for the viability of airborne pathogens

Airborne transmission can be achieved in several ways. The source of the pathogen-laden droplets can be from a human cough, sneeze, breath or from engineered systems such as toilets, faucets or cooling towers [3]. The droplets can be transported in air with varying characteristics. The pathogens transported via the airborne route can either be viruses, bacteria or fungi and they can reach the host at a still virulent state or they can be dormant in a viable but non culturable (VBNC) state [10]. Nevertheless, the airborne transmission of pathogen-laden droplets follows the same pattern: **From the source, through the air, via surfaces, into the lungs** (Figure A.2) [352]. Bacterial loss of viability can occur at either of these steps in the airborne transmission process. To make sense of the complexity surrounding the viability of pathogen transported via the airborne route, following the chronological order of the infection process is well suited. We therefore propose a framework based on these distinct phases in the airborne transmission process.

In this review, the factors affecting the viability of pathogens transported via the airborne route are discussed in the different phases of airborne transmission with a fluid dynamics perspective. The aerosolization process is first covered (Section 3), followed by the airborne transport phenomena (Section 4). Then, the possible deposition and resuspension of pathogens is discussed (Section 5) before we cover the factors that can affect the viability of bacteria inhaled by a new host (Section 6). Finally, we conclude with a summary of the current knowledge gaps and the opportunities for future research in this important and emerging field at the crossway between fluid and health (Section 7).

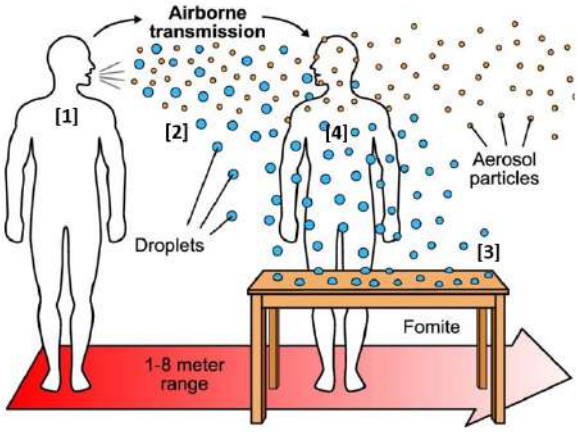

Figure A.2 Respiratory droplets and aerosol particles produced by an infected host, the source (1), during coughing/sneezing, talking, or exhaling are transported through the air (2) and can infect fomites via surfaces (3). The transmission process leads to the infection of a new host (4) [352].

From the source : Aerosolization

The journey of pathogens from the source to a new host begins with aerosolization (also called droplet generation), the process from which the fluid harboring pathogens is converted into small droplets [353]. During this process, pathogens can be trapped inside the generated droplets and transported via the airborne route. However, during the aerosolization, these droplets are subjected to strong shearing forces which could lead to the loss of viability of the pathogens present in the fluid [354].

Aerosol droplets can be generated through multiple processes, including atomization often observed in coughing and sneezing [265], impaction through raindrops falling on the ground [26], as well as disintegration and bubble bursting while breathing, talking, signing [3]. A combination of these mechanisms is usually responsible for most aerosolization processes, including from engineered systems such as toilets, faucets, spray irrigation or cooling towers [81]. The characteristics of the droplets generated, such as size distribution and velocity, are highly dependent upon the specific aerosolization mechanism which can also affect the viability of aerosolized pathogens.

However, regardless of the aerosol generation mechanism, the fluid dynamics governing the formation of pathogen-laden droplets can be divided into two categories: Steady and unsteady fragmentation. Steady fragmentation describes the generation of spray particles, where a liquid jet is disintegrated into droplets in surrounding gas, as well as flow focusing droplet generation, mostly used in microfluidics. Steady fragmentation depends on fluid inertia, surface tension and shear forces, but the droplet generation is usually uniform because the conditions are forced through the velocity of the jet. In most configurations, the significant forces applied on the fluid during the steady fragmentation process inactivate the majority of the pathogens [355] [356].

Conversely to the uniformity of steady fragmentation, interfacial instabilities play a crucial role in the unsteady fragmentation process of droplet formation. It is hypothesized that the destabilization of the surfaces where the pathogen-laden fluid and surrounding airflow interact is caused by a combination of Kelvin-Helmholtz and Rayleigh-Taylor instabilities (see Appendix) [254]. As droplets are generated, these instabilities cause the fluid to deform and break into smaller fragments [3]. Unsteady fragmentation is influenced by various factors, such as viscous and aerodynamic forces, surface tension, and flow rate. The magnitude of these factors varies at different points in the configuration and determines the viability rate of the aerosolized pathogens [254].

This process of aerosolization through unsteady fragmentation has been well described in the context of coughing and sneezing (Figure A.3) [254]. In general, when a liquid volume is exposed to an airflow, it experiences differential aerodynamic pressure that causes it to deform into a flattened sheet. This sheet then transforms into a bag-like structure that expands and thins until it becomes unstable and ruptures. Then, as the holes in the sheet grow and the destabilization of the fluid increases, ligaments perpendicular to the surface are formed and stretched until they eventually break into droplets. However, it is noteworthy that this process can vary depending on the specific aerosolization method used for particular applications. As illustrated in Figure A.4, the fluid sheet can rupture in a variety of ways [357].

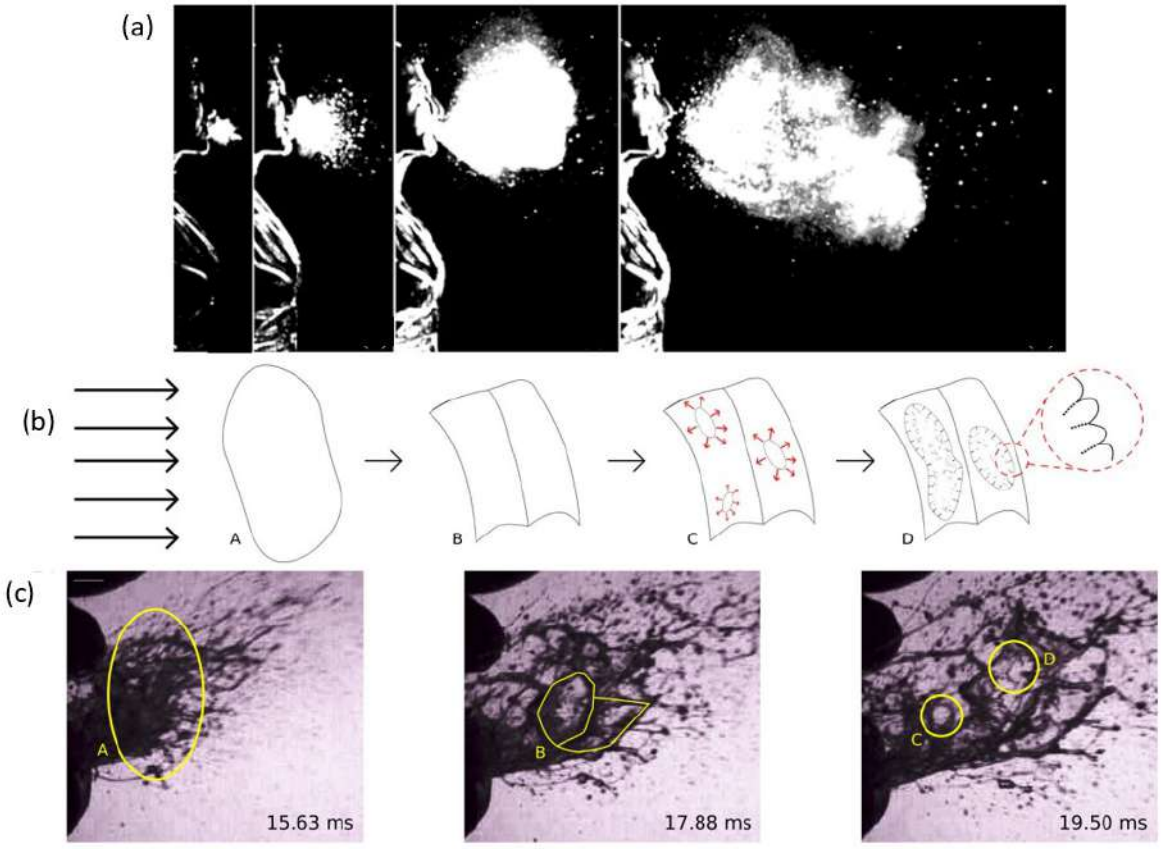

Figure A.3 a) Steps in the generation of pathogen-laden aerosols from a human sneeze [3]. b) Schematic of the fragmentation process of a liquid volume in response to applied aerodynamic forces. c) photographs of the aerosolization process from a sneeze. The initial liquid volume (A) is flattened into a sheet (B), followed by hole formation (C) and subsequent destabilization into ligaments, and, finally, droplets (D) [254]. Reprinted with written permission from Springer Nature.

Essentially, both steady and unsteady fragmentation yield significant shear forces to the fluid

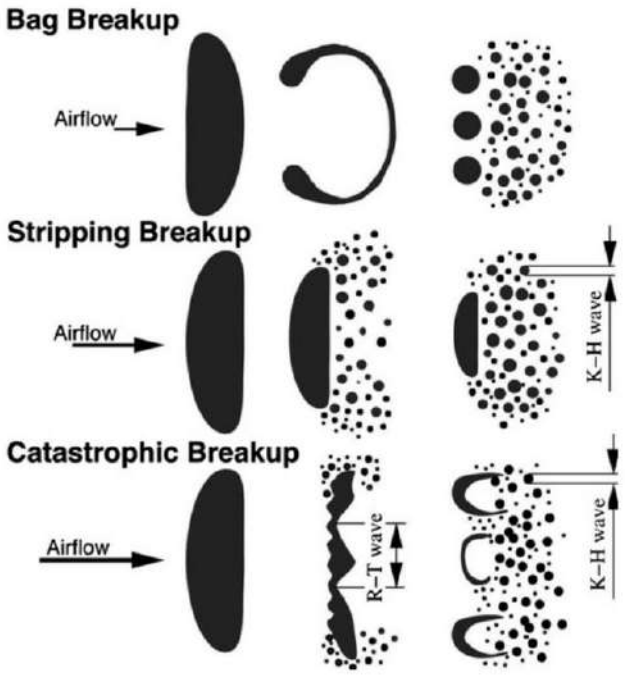

Figure A.4 Schematic of different modes of droplet formation through the rupture of the fluid sheet [357]. Reprinted with written permission from CCA

through instabilities. The deformation and breakup of the fluid can inactivate pathogens by damaging either their cell wall or their genetic material. The same consequences were observed in the aerosolization through the bursting of bubble [358] or through impaction [26] [359]. The somewhat violent rupture of the fluid that generates the pathogen-laden droplets is therefore also responsible for inactivating other pathogens present in the fluid.

During the aerosolization process, the mechanisms with the largest shear stresses have been associated with the lowest viability rates after the droplet generation. For instance, in a comparative study, atomization has yielded a higher viability rate than flow focusing aerosolization [360]. In turn, the viability rate is higher during bubble bursting than during atomization. However, cellular damage can usually be observed on most inactivated pathogens and even on viable ones, suggesting that the shear forces upon aerosolization are significant. Depending on the specific pathogen and the configuration, between 25 and 75 % of pathogens can be damaged [361] after the aerosolization process.

Aerosol droplets are usually generated within milliseconds to seconds, depending on the generation mechanism. However, it was shown that the largest loss of viability occurs in the first 30 seconds upon aerosolization [354], which relates to the first stage of the loss of viability of airborne pathogens described earlier. The viability rate is also significantly lower

for pathogens trapped in smaller droplets as the thinner aqueous layer is weaker against shear forces induced by the aerosolization process. Essentially, the shear forces induced in the aerosolization process is an important factor for the viability of pathogen aerosolized before being transported via the airborne route.

Through the air : Airborne transport

Once bioaerosols have been generated and the pathogens have remained viable through the significant induced forces of the aerosolization process, the second step of airborne transmission is the transport phenomenon. The viability of airborne pathogens depends on multiple elements. Psychrometric factors such as temperature and relative humidity yield physical changes to the pathogen-laden droplet as well as metabolic changes inside pathogens. Ultraviolet radiation also has detrimental effects on their integrity. The composition and dynamics of the surrounding air can influence the viability of pathogens as well. Finally, even the composition of the bulk fluid forming the droplet can have an impact on the viability of the transported microorganisms [362]. This section covers the effects of environmental factors on viruses, bacteria and fungi.

Temperature

Temperature is critical in mediating the survival of airborne pathogens, likely by affecting the stability of proteins, lipids, and genetic material [363]. From a thermodynamic point of view, temperature can also influence the evaporation process which can contribute to the dehydration of the trapped pathogen and make it more vulnerable to other environmental conditions [10].

Virus and temperature

Temperature is one of the most important factors affecting virus viability as it can affect its genome as well the state of important proteins. Generally, as temperature rises, virus viability decreases. Maintaining temperatures above 60 °C for more than 60 minutes is generally sufficient to inactivate most airborne viruses, but higher temperatures for shorter time periods can be just as effective at inactivating viruses [364].

Bacteria and temperature

Temperatures above 24 °C are universally linked with a decrease in the viability of airborne bacteria. This concept is true for almost all bacteria, regardless of their structure, and especially if other environmental factors are also considered [364]. However, to inactivate most bacteria, temperatures must be above 50 to 60 °C [365]. In effect, some bacteria will revert to a dormant viable but non culturable (VBNC) state with rising temperature and are able to remain viable through harsher conditions [366].

Relative humidity

Relative humidity is also a very important factor affecting the viability of airborne pathogens. By modulating the evaporation rate and equilibrium size of aerosols, relative humidity affects their transport and the viability of pathogens they carry. However, the relationship between relative humidity and pathogen viability is not well understood [364].

Virus and relative humidity

Generally, most respiratory viruses survive longer at lower relative humidity as it affects their level of hydration and these organisms thrive when less moisture is available [362]. The seasonality of viruses that cause common colds have been partially attributed to relative humidity. In effect, relative humidity is lower during winter than during the summer which entails that viruses remains viable longer during the winter [364]. However, the literature available is limited regarding the effect of relative humidity on specific viruses [367].

Bacteria and relative humidity

The ability of bacteria to remain viable under different levels of relative humidities is related to the organism's surface biochemistry. Bacteria cell wall structure is divided into two categories : gram positive and gram negative, which are related to the cell-wall characteristics of the microorganisms [368]. In general, it has been reported that most gram-negative bacteria associated with aerosols tend to survive longer periods at mid-level relative humidity and the opposite has been observed for gram positive bacteria [362]. It is unclear why this dichotomy occurs for different bacteria. Some researchers have hypothesized that gram positive bacteria support better conditions over dehydration and over-hydration whereas gram negative bacteria quickly lose their viability in these contexts. What is clear however is that the correlation between relative humidity and the bacterial loss of viability is significant [364].

Ultraviolet radiation

Irradiation with ultraviolet light has long been established as an effective approach to inactivate airborne pathogens as it damages their genetic material [364]. However, multiple studies showed an increase in viability rate in the presence of ultraviolet radiation at higher relative humidity due to the protective effect of a thicker aqueous layer [363]. Therefore, ultraviolet radiation is not considered as an effective decontamination strategy unless combined with other disinfection procedures [369].

Air composition

The chemical composition of the air also influences the viability of airborne pathogens. It was shown that the presence of 85 ppm of carbon monoxide (CO) in the surrounding air enhances pathogen death rate of a factor between 4 and 7 [370]. However, over long distances (km range), common chemical components found in the atmosphere have shown to provide suitable micro-environments for airborne pathogens [351], but particulate air pollution has a negative impact on their airborne viability [371]. These studies entail that surrounding air composition can have significant effects on the viability of airborne pathogens, but further investigations are needed to understand the specific mechanisms governing their impact.

Turbulence

Recent studies in the field of the fluid mechanics of disease transmission have yielded a model that depict the behavior of airborne pathogen-laden droplets, which suggests that the spread of pathogen via the aerosol route is accurately represented by a turbulent multiphase cloud that carries particles through the air (Figure A.5) [3]. This configuration explains how pathogen-laden particles can travel far from the source while remaining viable. However, not much information is available on the effect of turbulence on the viability of pathogens transported via the airborne route.

Reynolds numbers of approximately 10^4 were observed in these multiphase clouds [23]. The higher the Reynolds number, the higher the speed of the flow, the higher the probability of collisions between particles and the higher the shear forces induced by turbulence which can affect the integrity of the pathogens. The primary forces involved in a turbulent flow are inertia, as well as viscous and pressure forces. Also, according to Bernouilli's principle, pressure gradients induced by turbulence can influence the stability of droplets by changing their shape dynamically which could damage the carried pathogens [20]. In any case, higher Reynolds numbers are associated with lower viability rate for pathogens, but the effects of turbulence are usually exceeded by other environmental factors [372].

Bulk liquid composition

The role of the composition of the bulk liquid making up the droplet in the viability of airborne pathogens is that it can provide nutrients for the trapped pathogens [373]. In certain conditions, a solid crust can form on the surface of droplets which can further protect the pathogens from the environmental conditions [3]. Depending on the bulk liquid properties, it also evaporates at varying rates, which influences the state of the pathogens. Overall, the composition of the bulk liquid is not a dominant factor for the viability of airborne pathogens.

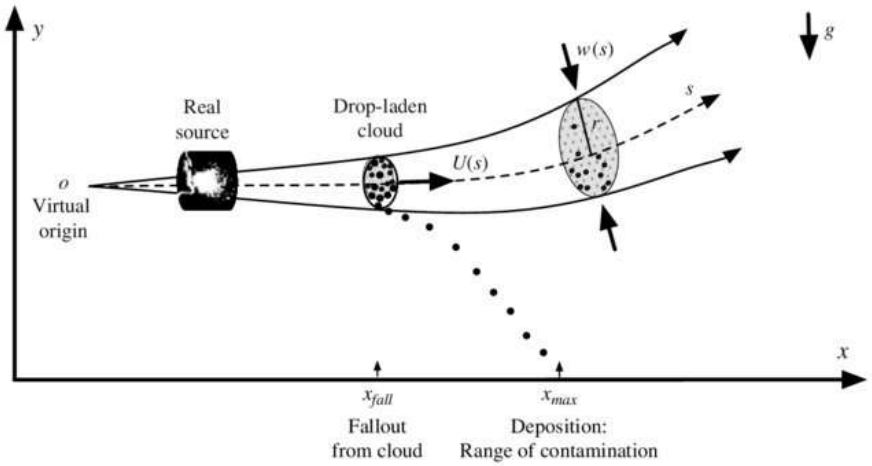

Figure A.5 Physical picture of the evolution of a cough or sneeze cloud emitted horizontally. Larger suspended droplets are circulated within the cloud until they settle out (at a horizontal distance x_{fall}) and reach a final position x_{max} , corresponding to the range of contamination. The virtual origin is shown behind the sneezer source and is extrapolated from the measured trajectory of the cloud. The cloud climbs in response to its increasing buoyancy as larger droplets fall out [23]. Reprinted with written permission from Cambridge University Press.

The case of fungi

Relatively few laboratory experiments have been conducted on the viability of airborne fungi. Most data relating temperature and relative humidity to airborne fungi viability have been obtained from the environments were the organisms are naturally found. These studies show a seasonal variation owing to temperature, relative humidity, and turbulence of the surrounding air. Generally, fungi are more resistant to environmental conditions than viruses and bacteria, especially as it pertains to UV radiation and the composition of the surrounding atmosphere. Additionally, a rise of temperature and relative humidity is usually correlated with higher airborne fungi viability [364].

Viability and environmental factors

The transport step in the airborne transmission process can vary from seconds to hours and therefore contributes to the second stage of the loss of viability described earlier [367]. In the last section, we individually described the effects of different environmental factors on the viability of several pathogens, which are summarized in Figure A.6. Essentially, some general trends can be extracted from the literature, but there are always outliers and these effects vary individually for pathogens, which highlights the complexity of these microorganisms. Additionally, in the context of airborne transmission, these environmental factors all act simultaneously on the transported pathogen-laden droplet, which affects the viability

of the carried pathogens differently. Sudden, drastic changes in these parameters tend to exacerbate their respective effects on airborne pathogens [362]. Therefore, the intricacy of the combinatory effect of environmental factors makes it challenging to accurately assess the viability of airborne pathogen, which is highly related to the contamination risks.

Environmental factor	Viruses	Bacteria	Fungi
Temperature	• As temperature increases, survival decreases • DNA viruses are more stable than RNA viruses at higher temperatures	• Temperatures >24°C decrease survival	• Highest fungal counts occur in the summer, at higher temperatures
RH*	• Enveloped viruses (most respiratory viruses, influenza) survive longer at lower RH (20%-30%) • Nonenveloped viruses (adenovirus, rhinovirus, and polio virus) survive longer in higher RH (70%-90%) • Exceptionally, nonenveloped rotaviruses survive best at medium RH	• Most gram-negative bacteria survive best in high RH and low temperature, except *Klebsiella pneumoniae*, which is stable at RH 60% • Gram-positive bacteria have the highest death rates at intermediate RH • Sudden changes in RH reduce survival	• Dehydration and rehydration of fungi particles provide conflicting results • Spore concentrations seem higher at higher RH
Atmospheric gases	• Ozone inactivates airborne viruses to a greater degree than bacteria or fungi	• CO decreased survival at low RH (<25%), but protected bacteria at high RH (90%)	• Oxygen supports growth
Light and irradiation	• UV light is harmful (RH-dependent)	• UV light is harmful but may be mitigated by higher RH (water coat protects aerosolized particles)	• More resilient to the effects of UV light than viruses or bacteria
Surrounding organic material (eg, saliva, mucus)	• Protects viruses from environmental changes	• May affect survival based on RH	• Decomposition of organic waste (food remains) may act as a source of fungal spores

CO, carbon monoxide; *RH*, relative humidity; *UV*, ultraviolet.
*RH is a measure of the amount of water vapor in the air at a specific temperature; therefore, temperature and RH always interact to affect survival.

Figure A.6 Environmental factors associated with survival of airborne infectious agents [362]. Reprinted with written permission from Elsevier.

Via surfaces : Deposition

Although not essential to the airborne transmission process, pathogen-laden droplets are occasionally deviated from their trajectory between the source and a new host. Particles can be deposited on surfaces through gravitational settling, especially if the droplets are large ($> 10\mu m$) [152]. They can also be captured in masks or filters either as an obstacle in their chaotic airborne transport or through a ventilation process altering their path. During this inhibition in their journey to find a new host and replicate, particles can lose their viability through time, usually linked to the second stage of airborne pathogens inactivation described previously.

Gravitational settling

Once deposited on a surface, the survival of pathogens is usually dependent on the evaporation of their protective aqueous layer as they are submitted to the same environmental factors discussed in the previous section. The effect of these environmental conditions expedites the loss of viability of the pathogens. In effect, without the input of the peripheral environment, the viability of aerosolized pathogens can remain high for approximately 20 days [374]. However, in standard ambient conditions, the viability rate of most deposited airborne pathogens is usually still extensive after several hours with between 44 and 77 % of pathogens still viable on average after two hours, a reminder that the process of pathogen inactivation is not immediate [21]. Surface cleaning mitigates transmission risks by altering their cell membrane, inactivating the pathogens quicker than through the naturally induced environmental factors [375].

Filtration

The filtration of airborne particles captured in masks or filters is achieved through multiple mechanisms: inertial impaction, interception of the particle streamlines by the fiber and the diffusion of very small particles due to Brownian motion [24]. As a result of these mechanisms, filters can be effective at capturing particles smaller that the pore size of the weave. The captured pathogens lose their viability when moisture is eliminated, which starves the pathogens or damages their structure from the shear forces induced by the airflow going through the filter [376]. ASHRAE standards on filters involve capture efficiencies of 85% for particles smaller than 1 μm and over 90 % for larger particles. Paired ventilation and filtration were shown to reduce airborne viral loads in a controlled chamber [377].

Resuspension

Once deposited, the airborne transmission process is halted and the fate of the pathogen leads to its loss of viability unless it is resuspended. Resuspension is therefore essential in the airborne transmission process if deposition occurs. It can happen to particles that have deposited on surfaces or haven been captured in filters or masks [378]. Subtle movements can induce resuspension. Walking, opening the door, hand gestures, and even airflow dynamics induced by ventilation systems can cause the resuspension of pathogen-laden droplets. Turbulence in the airflow caused by these movements can transmit forces that naturally transport particles back into the airborne flow. During resuspension, the droplets are usually not subjected to shear stress as potent as during the aerosolization process, so the extended loss of viability associated with resuspension is less common. Therefore, the longer the pathogens in the deposited droplets remain viable, the higher the associated risks of airborne transmission from secondary suspension (Figure A.7) [379].

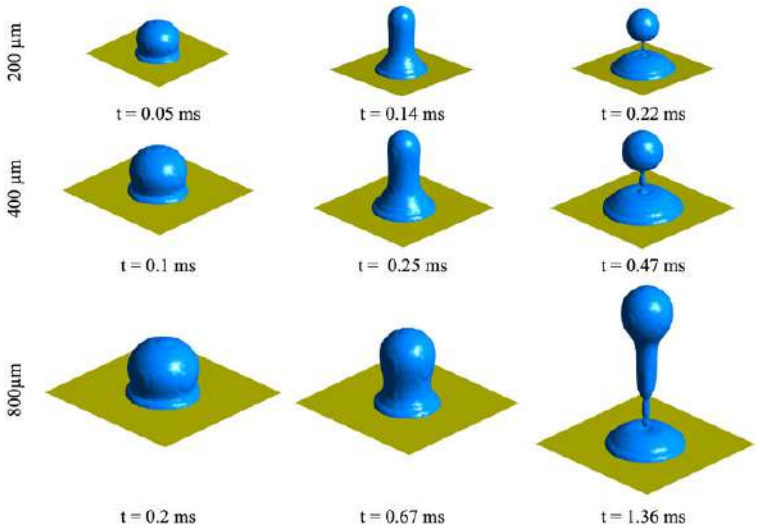

Figure A.7 Droplet detachment process near the surface for droplets of different sizes [380]. Reprinted with written permission from AIP.

Into the lungs : In the host

The last step in the airborne transmission process is the infection of the host. Even if the pathogen trapped inside a droplet has remained viable through the aerosolization process, the transport process, as well as the possible deposition and resuspension, it must survive the transport through the respiratory system and the immune response of the host [381]. After the inhalation and as soon as the pathogens deposit in the respiratory tract, they start replicating which initiates the infection process. Upon infection, the immune response is activated to combat the invading pathogen. The ensuing interaction between the pathogens and host immune system is often described as a battle, as the pathogens and the immune cells engage in a conflict, with only one emerging victorious [382]. The role of the immune system is therefore critical in the mitigation of airborne transmission risks [383].

Through the droplet transport in the respiratory system during the inhalation process of the host, nasal hair, the mucus layer of the respiratory tract and follicles from epithelial cells in the lungs act as physical barriers which involve complex fluid mechanics (Figure A.8). These body components act as filters and can trap bacteria through the different mechanisms which we expanded on in the previous section. Once trapped, they eventually lose their viability and are cleared from the body of the host through the mucus layer. Depending on the size of the particle and on the properties of the inhaled flow, pathogens can deposit anywhere between the nasal cavities and deep in the lungs' alveoli, which provide different environmental conditions that can affect the viability and the infectivity of the pathogens [383].

If the pathogen overcomes the hostile environment of the host respiratory tract it must then face the immune system through a chaotic struggle [363]. In a coordinated dance, macrophages, neutrophils, the complement system and natural killer cells will serve as the first line of defense, commonly called the innate immune system (Figure A.9). Although somewhat effective at inactivating the invading pathogens trying to replicate, the innate immune system is simply a temporary solution to the infection. The acquisition of immunity against specific pathogens through the adaptive immune system is a more efficient and permanent solution. During this process, dendritic cells deliver valuable information about the invading pathogens to the adaptive immune system and coordinate a complex inflammatory process with T cells and B cells which will generate antibodies able to inactivate the remaining viable pathogens in the body and provide long-term immunity [383].

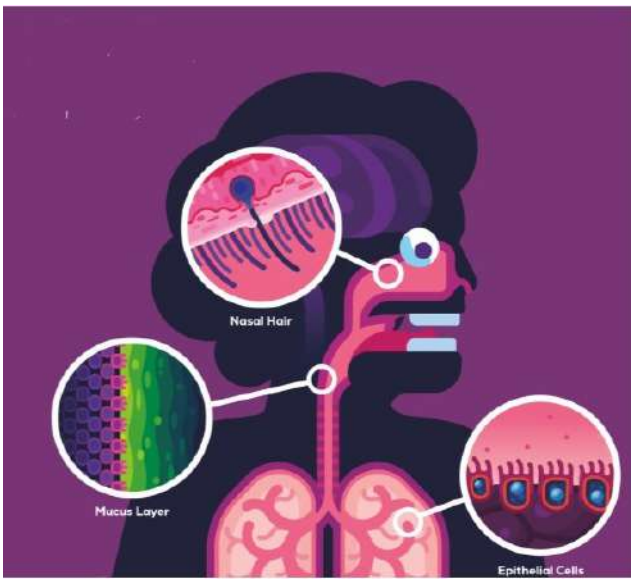

Figure A.8 Illustration of the physical barriers of the immune system against the invasion of pathogens [383].

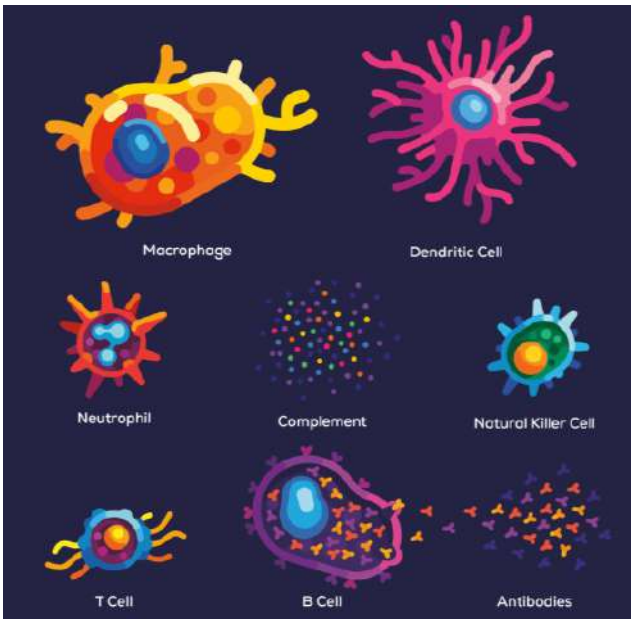

Figure A.9 Overview of the important organisms involved in the adaptive and innate immune system [383].

Discussion and perspective

Airborne transmission has lately been highlighted as an important research field with dire implications on the quality of life for individuals [2]. The various stages involved in airborne transmission begin from the aerosolization of pathogen-laden droplets at the source, through their transport in the ambient air, via potential deposition on surfaces or filters, and into the lungs of a new host. The impact of these steps on pathogen viability is governed by fluid dynamics phenomena that reveal the complexity of the process. Through this framework, we have scoured the literature and presented the factors which influence the viability of pathogens transported via the airborne route. The importance of fluid dynamics principles related to each step of the airborne transmission process, as well as external factors such as temperature, relative humidity and ultraviolet radiation have been highlighted.

In recent years, research on infectious diseases has transitioned from solely focused on microbiology and immunology to multidisciplinary, including the principles of fluid mechanics in our understanding of the transport of pathogens. This paradigm shift has led to important breakthroughs, but also lead to the emergence of new important questions regarding the behavior of pathogen-laden droplets and how the viability of pathogens is affected.

Effectively, the microbiological principles related to the viability of specific pathogens are highly documented and the mechanisms that influence their state are thoroughly discussed. Additionally, the fluid dynamics which govern the formation of droplets and the airborne transport of particles are well known. Although the understanding of the subject is still in its early stages, multiple fundamental phenomena that pertain to the behavior of airborne droplets can be retrieved from other applications of fluid dynamics and multiphase flow. Nevertheless, there is still a need for comprehensive research that integrates both microbiology and fluid dynamics.

In effect, multiple aerosolization mechanisms are characterized with a fluid dynamics perspective, but there is a research need to improve our understanding of how pathogens are entrapped inside the generated droplets and to quantitatively assess the effects of shear forces on the viability of specific pathogens through these different mechanisms. Also, the effects of environmental conditions on pathogens are complex and are still the object of thorough investigations. However, the airborne transport of these pathogens must be considered to accurately assess the infection risks. Turbulence in the airflow in relation to the viability of pathogens must be further investigated as well. Finally, the deposition and resuspension of droplets have been highlighted as significant infection risks during the COVID-19 pandemic [2]. Nonetheless, the fluid dynamics principles of resuspension are not fully under-

stood. As much as this review has highlighted the significance of combining health-related research with fluid dynamics concepts, it has also shown that it is still in an embryonic state and that much is left to do. The combination of both fields will lead to the newly acquired knowledge of infectious risks and the possibility of mitigation as it relates to the viability of pathogens.

This exciting prospective command new opportunities for the development of analytical, experimental and numerical tools to unfold the mysteries related to the viability of pathogens transported via the airborne route, at the intersection of fluid and health. As this technological contingency progresses, authors have indicated that it is crucial to implement well-established fluid dynamics methodologies given their demonstrated effectiveness in reducing errors in domains such as aeronautics and astronautics, where lives are also at stake [3].

This call for scientific improvement is analog to the survival of microorganisms responsible for infectious diseases. In the context of airborne transmission and risk mitigation, it must be taken into consideration that pathogens adapt and develop immunities against the harsh environmental conditions they are subjected to. In the evolutionary process of pathogens, only the ones that can remain viable through the airborne transmission process replicate. Therefore, just as bacteria become immune to antibiotics, over time, pathogens might be building immunity to the airborne transmission process, which means that we are engaged in a race to adopt effective risk mitigation strategies.

Investigations on the viability of pathogens through airborne transmission are a reminder that the infection of a new host is a necessary step in the lifecycle of pathogens. Through complex phenomena involving fluid dynamics, microbiology and immunology, the transmission of infectious diseases via the airborne route is merely another successful example of evolutionary adaptation where the behavior of pathogens is dictated by their genetic code adjusted for survival. The study of the viability of such pathogens is essential to the mitigation of the risks for humans in an aspiration to eventually thrive in a world rid of infectious diseases.

Fluid instabilities

Kelvin–Helmholtz instability

The Kelvin–Helmholtz instability (after Lord Kelvin and Hermann von Helmholtz) is a fluid instability that occurs when there is velocity shear in a single continuous fluid or a velocity difference across the interface between two fluids [384].

If the density and velocity vary continuously in space, the dynamics of the Kelvin-Helmholtz instability is described by the following equation :

$$\frac{\partial}{\partial t}\left(\rho_1 \mathbf{u}_1 + \rho_2 \mathbf{u}_2\right) + \nabla \cdot \left(\rho_1 \mathbf{u}_1 \mathbf{u}_1 + \rho_2 \mathbf{u}_2 \mathbf{u}_2 + p\mathbf{I}\right) = \mathbf{f} \tag{A.2}$$

where ρ_1 and ρ_2 are the densities of the two fluids, $\mathbf{u}_1$ and $\mathbf{u}_2$ are the velocities of the two fluids, p is the pressure, $\mathbf{I}$ is the identity matrix, and $\mathbf{f}$ is an external force.

Rayleigh–Taylor instability

The Rayleigh–Taylor instability (after Lord Rayleigh and G. I. Taylor), is an instability of an interface between two fluids of different densities which occurs when the lighter fluid is pushing the heavier fluid [385].

Assuming that the fluids are incompressible and that there is no viscosity, the dynamics of the Rayleigh-Taylor instabilities is described by the following equation :

$$\frac{\partial^2 \xi}{\partial t^2} = g\frac{\rho_2 - \rho_1}{\rho_1 + \rho_2}\xi + \frac{1}{\rho_1}\nabla \cdot \left(\rho_1 h \nabla \xi\right), \tag{A.3}$$

where ξ is the displacement of the interface between the two fluids, g is the acceleration due to gravity, ρ_1 and ρ_2 are the densities of the two fluids, and h is the height of the interface.

APPENDIX B SUPPLEMENTARY MATERIAL OF ARTICLE 1

Settings for the PDA

The settings (Table 1), were selected to ensure that the maximum number of particles were measured by the PDA, without saturating the detectors. Lasers were set to the maximum power of 300 mW and the gain was set to 20 dB for both detectors. The sensitivity of the detectors, which is adjusted with voltage, was the driving factor in the number of particles measured. The detector voltage was set to 1300 V when using DEHS aerosols and to 900 V when using the larger water-based aerosols. When salt was added and the particles dried to their nuclei, the sensitivity was set to 1100V. Repetitive measurements were taken every 60 seconds for 5 minutes and averaged in a single size distribution profile.

Table B.1 Settings used on the PDA system

Receiver focal length	300 mm
Scattering angle	30 deg
Aperture mask	Mask A for DEHS and Mask B for water-based
Particle refractive index	1.454 for DEHS and 1.334 for water

Comparative table

The results demonstrate the challenges and opportunities of combining aerosol size distributions obtained from different instruments. In the context of airborne transmission, the critical, potentially dangerous, size range for transmission can be characterized by combining multiple instruments. Table B.2 compares multiple characteristics of the size distribution measurement instruments as well as their advantages and limitations.

Table B.2 Comparison of measurement size range, measurement time, sampling volume rate, evaporation coefficients, advantages and limitations of the size distribution measurement instruments

	Size range (mu m)	Measurement time (s)	Sampling volume rate (L/min)	Advantages	Limitations
PDA	0.5 - 8000	300	N/A	- No sampling line - Large measurement range - Punctual measurement - High resolution	- Calculated number concentrations - Loss of precision under 0.5 mu m
OAS	0.25 - 32	6	1.2	- Portable - High measurement frequency	- Losses in sampling line - Limited precision in submicron range
SMPS	0.022 - 0.671	76	1.2	- Gold standard in submicron range - High measurement frequency	- Limited size range
Cascade impactor	0.16 - 10	1800	10	- Portable - Allows for microbial analysis	- Mass-based measurement - Losses in sampling line - Limited resolution

APPENDIX C SUPPLEMENTARY MATERIAL OF ARTICLE 2

Cooling towers

Types of cooling towers

One of the most common types is counterflow cooling towers, where the air enters the bottom of the cooling towers and flows vertically upwards counter to the flow of falling water, while pressurized nozzles spray water downwards. Alternatively for crossflow cooling towers, water flows downwards vertically, while the air flows horizontally across the falling water. Finally, forced-draft cooling towers use a blower type fan placed at the air intake, instead of a fan at the air outlet, to force air into the cooling tower which creates high entering and low exiting air velocities [39]. As the different type of cooling towers work on different principles, the aerosol generation can differ. The type of cooling tower and drift eliminator for each sampling site were thus recorded (Table C.1).

Capacity

Cooling tower capacity refers to the amount of heat a cooling tower can remove from a system, typically measured in tons of refrigeration (Tons) or megawatts (MW). It is determined by the rate at which the tower cools water, often calculated using the mass flow rate of the water, the specific heat capacity of water, and the temperature difference between the inlet and outlet water. Mathematically, the cooling tower capacity, Q, can be expressed as:

$$Q = \dot{m} \cdot c_p \cdot \Delta T$$

where $\dot{m}$ is the mass flow rate of water (kg/s), c_p is the specific heat capacity of water (kJ/kg°C), and ΔT is the temperature difference between the water entering and exiting the cooling tower (°C). This equation provides the heat removal rate in kilowatts, which can then be converted to tons of refrigeration or other units as needed. The capacities of the investigated cooling towers are shown in Table C.2.

Monitoring sampling cooling towers

The behavior of the three cooling towers monitored weekly was also influenced by their specific characteristics. Cooling tower S1 is a counterflow model fitted with a blade type drift eliminator. The outlet diameter is 4.24 m. The tower was functioning at a normal rate,

pumping water at 137 L/s with the 30 HP fan turned on. Cooling tower S5 is a crossflow model fitted with cellular type drift eliminators. The outlet diameter is 2.57 m and the fan is 15 HP at full capacity. The tower and the fan were operating at 100% capacity during measurement. Cooling tower S11-L is a counterflow model significantly smaller than cooling tower S1, and fitted with a cellular-type drift eliminator. The outlet diameter is 2.73 m. The tower was usually operating at full capacity, with the 20 HP fan at full speed, unless the outside temperature was below 18 °C in which case the pump and the fan were at 80%.

Table C.1 Types of cooling towers and drift eliminators sampled during the sampling campaign

Cooling tower / Drift eliminator	Crossflow	Counterflow	Induced draft
Cellular type	S11P, S21, S22_1, S2	S1, S6A	
Blade type	S5, S22_2	S11, S16, S20, S12, S24	S6B, S23

Table C.2 Capacity ranges of the cooling towers sampled during the campaign. The range refers to specific cooling towers rather than the whole system (often composed of more than one cooling tower).

Capacity range	Cooling towers (L_w/s)
50 Tons (Small-size)	S6A, S6B, S12
500 Tons (Medium-size)	S1, S2, S5, S11, S11P, S20, S21, S22_1, S22_2, S24
5000 Tons (Large-size)	S16, S23

Table C.3 *L.spp.*, *L.p.*, and *L.p. SG1* qPCR results of the concentration in water inside the basin for each cooling tower during the blitz. ND refers to non-detected.

	S1	S2	S5	S6A	S6B	S11	S11P	S12
L.spp. (UG/L)	4.46×10^3	9.54×10^3	2.47×10^3	ND	ND	ND	3.52×10^2	ND
L.p. (UG/L)	6.00×10^2	ND	ND	ND	5.13×10^5	ND	4.46×10^3	2.27×10^3
L.p. SG1 (UG/L)	ND	ND	ND	ND	5.93×10^5	ND	2.42×10^3	1.56×10^3

	S16	S20	S21	S22_1	S22_2	S23	S24
L.spp. (UG/L)	2.79×10^4	ND	2.90×10^4	ND	5.69×10^2	5.13×10^5	2.27×10^3
L.p. (UG/L)	6.10×10^2	5.70×10^2	ND	1.04×10^4	ND	2.79×10^4	2.79×10^4
L.p. SG1 (UG/L)	5.90×10^2	5.50×10^2	ND	6.00×10^2	ND	2.69×10^4	2.69×10^4

Sampling calendar

Table C.4 Calendar of the longitudinal monitoring sampling campaign with information on temperature, relative humidity, and cooling tower operating rate.

Date	26/05/2022	31/05/2022	02/06/2022	07/06/2022	09/06/2022
Site	S11	S11	S11	S1	S11
Temperature	15	14	14	17	14
Humidity rate	82%	79%	79%	84%	91%
Operating rate	80%	80%	100%	66%	80%
Rain					

Date	14/06/2022	16/06/2022	05/07/2022	07/07/2022
Site	S11	S1 - S5	S11	S1 - S5
Temperature	19	21	20	17
Humidity rate	73%	76%	69%	65%
Operating rate	100%	44% - 100%	100%	66% - 100%
Rain				

Table C.5

Date	12/07/2022	14/07/2022	02/08/2022	04/08/2022	09/08/2022
Site	S11	S1 - S5	S11	S1 - S5	S1 - S5
Temperature	20	20	22	23	15
Humidity rate	93%	74%	88%	85%	92%
Operating rate	100%	100% - 100%	100%	100% - 100%	15% - 100%
Rain	X		X	X	X

Date	11/08/2022	16/08/2022	18/08/2022
Site	S11	S11	S1 - S5
Temperature	19	19	19
Humidity rate	82%	72%	78%
Operating rate	100%	100%	70% - 100%
Rain			

Table C.6 Calendar of the sampling blitz with information on temperature, relative humidity, and cooling tower operating rate.

Date	29/08/2022	30/08/2022	31/08/2022	01/09/2022
Site	S11P - S11	S6	S20, S21	S1, S5
Temperature	22	24	19	14
Humidity rate	85%	83%	85%	74%
Operating rate	100%-100%			15% - 100%
Rain				

Date	06/09/2022	07/09/2022	08/09/2022	09/09/2022	13/09/2022
Site	S16	S22	S2, S12	S23	S24
Temperature	14	16	17	18	21
Humidity rate	83%	91%	89%	90%	83%
Operating rate					
Rain					

QMRA Analysis

The QMRA methodology was adapted from Hamilton et. al [81, 108]. It assumes that *Legionella pneumophila* exposure risks are based on : the emission of potentially contaminated bioaerosols from a cooling tower, the atmospheric dispersion of the generated particles, the inhalation and deposition of the particles depending on their size, and finally the pathogenic dose-response specific to each individual. Table C.7 describes the parameters used for the obtained results.

The emission rate is dependant upon the propensity of the bacteria to be transferred from the bulk water in the basin of the cooling tower, to the aerosol being discharged in the environment. The fractions of *Legionella pneumophila* transferred in aerosol particles of size 1-10 μm (partitioning) used for the different investigated scenarios was measured. Spatial parameters specific to the cooling tower configuration, such as the critical height of the system pertaining to the height difference between the outlet of the cooling tower and the mouth of the inhaling subject, at 10m on average, and the critical distance from the source of the aerosol, which represents the maximal concentration downwind from the source (approximately 110 m), were chosen to be representative of the investigated cooling tower configurations. The mouth of the subject was assumed to be at a heigh of 1.5 m. The parameters for the atmospheric dispersion model represented standard north american conditions with an average wind speed of 4.5 m/s based on results obtained at 66 meteorological stations in Quebec [386]. Total absorption of the droplets deposited on the ground was also assumed for the dispersion model.

Table C.7 QMRA parameters for the proposed model and the Hamilton model

	Proposed model	**Hamilton model (2018)**
Flowrate of air inhaled (m^3/min)	0.015	0.015
Exposition time per day (min)	60	60
Number of days of exposition	365	365
Emission model		
Bacteria concentration in water (#/L)	Cooling tower dependant	Cooling tower dependant
Ratio of accuracy for the detection method R	0.7	0.7
Water flow rate Q_w (L/s)	Not applicable	1000
Drift eliminator capture efficiency E	Not applicable	0.00003
Mass fraction of droplets size 1-10 q μm	Not applicable	0.17
Atmospheric dispersion model		
Wind speed (m/s)	4.5	4.5
Ry	0.233	0.233
ry	0.855	0.855
sigma_y (m)	7.94	7.94
Rz	0.076	0.076
rz	0.879	0.879
sigma_z (m)	4.268	4.268
x (m)	110	110
y (m)	0	0
z (m)	1.5	1.5
H_e (m)	10	10
alpha	-1	-1
Inhalation model : Partitioning		
1 μm	Cooling tower dependant	0.175
2 μm	Cooling tower dependant	0.1639
3 μm	Cooling tower dependant	0.1556
4 μm	Cooling tower dependant	0.0667
5 μm	Cooling tower dependant	0.0389
6 μm	Cooling tower dependant	0.025
7 μm	Cooling tower dependant	0.0278
8 μm	Cooling tower dependant	0.05
9 μm	Cooling tower dependant	0.0528
10 μm	Cooling tower dependant	0.0389
Inhalation model : Deposition		
1 μm	0.25	0.25
2 μm	0.53	0.53
3 μm	0.62	0.62
4 μm	0.61	0.61
5 μm	0.52	0.52
6 μm	0.40	0.40
7 μm	0.29	0.29
8 μm	0.19	0.19
9 μm	0.12	0.12
10 μm	0.06	0.06

QMRA Results

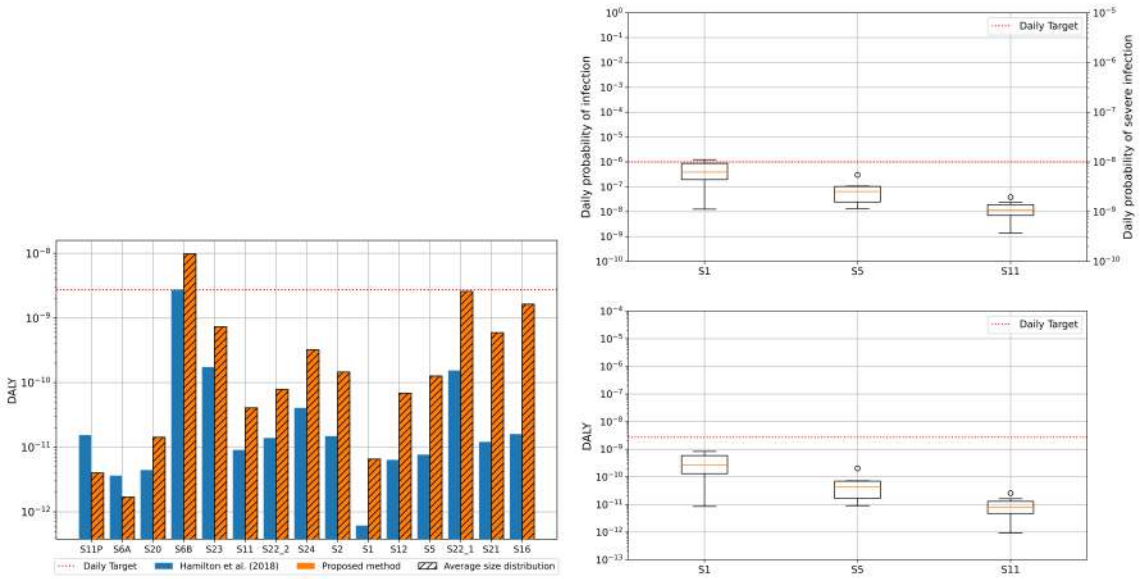

(a) (b)

Figure C.1 a) Daily QMRA results (DALY) comparing the proposed method with the Hamilton method for the blitz-sampled CTs, sorted by the difference between methods. The proposed method's DALY, using individual droplet size distributions, is compared to results using the average distribution. b) Daily QMRA results of the monitored cooling towers S1, S5 and S11 obtained using the Hamilton method for the emission model. The daily risks are presented and are compared to daily targets for the annual probability of infection and the DALY.

APPENDIX D SUPPLEMENTARY MATERIAL OF ARTICLE 3

Settings for the PDA

The settings (Table D.1), were selected to ensure that the maximum number of particles were measured by the PDA, without saturating the detectors. Lasers were set to the maximum power of 300 mW, the gain was set to 20 dB for both detectors and the current saturation limit was set to 2000 μA. The sensitivity of the detectors, which is adjusted with voltage, was the driving factor in the number of particles measured. The detector sensitivity voltage was set to 600 V at the beginning of the scan, but was gradually increased up to 1200 V to allow for a better detection when the droplets were evaporating.

Effect of surface tension on the Balachandar et. al model

The Balachandar et al. model indirectly accounted for the effect of surface tension on the evaporation process. It is given by the following equation :

$$-\frac{dm}{dt} = \pi d D \rho_p Nu \ln(1 + B_m) \tag{D.1}$$

The variables in the equation are defined as follows: m (kg) is the mass of a droplet with diameter d (m), D (m^2/s) is the diffusion coefficient of the vapor in the surrounding air, and ρ_{p} (kg/m^3) is the density of puff air. The dimensionless Spalding mass number B_m (-) is given by $B_m = \frac{Y_d - Y_p}{1 - Y_s}$, where Y_d (-) is the mass fraction of water vapor at the droplet surface, and Y_p (-) is the mass fraction of water vapor in the surrounding puff. Nu (-) is the dimensionless Nusselt number. The Nusselt number is calculated from the Reynolds number, Re, and the Prandtl number, Pr, according to the following equations:

$$Nu = 2 + 0.4 Re^{1/2} Pr^{1/3} \tag{D.2}$$

Table D.1 Settings used on the PDA system

Receiver focal length	300 mm
Scattering angle	30 deg
Aperture mask	Mask C
Particle refractive index	1.334 for all solutions

$$Re = \frac{d_s \rho_p v}{\mu} \tag{D.3}$$

$$Pr = \frac{\mu}{\rho_p D} \tag{D.4}$$

Assuming that Nu and B_m remain nearly constant for small droplets, equation 2 can be integrated to derive the following relationship for the evolution of the droplet, defined as the squared law of evaporation [158]:

$$d(t) = \sqrt{d_e^2 - k't} \tag{D.5}$$

Where

$$k' = 4DNu \ln(1 + B_m) \tag{D.6}$$

In these equations, d_e (m) is the initial diameter of the droplet, and k' represents an effective evaporative diffusivity with units of m^2/s.

The only variable that is expected to change with the presence of surfactants is the Spalding number B_m. Indeed, the concentration of water molecules at the droplet-air interface Y_d which are available for diffusion is reduced by the presence of surfactants, which in turn reduces the evaporation rate of the droplet [282]. The reduction in Y_d is directly proportional to the surface density of the surfactant, allowing to quantify this reduction in surface tension [176]. Y'_d (-), the mass fraction of water vapor at the droplet surface in the presence of surfactants, can be expressed as a function of the surface of the droplet S_d (m^2), the number of surfactant molecules n_{surf} and the surface density of surfactants Γ (molecules/m^2) [280]:

$$Y'_d = Y_d * (1 - \frac{n_{surf}}{S_d \Gamma}) \tag{D.7}$$

The surface of a 60 μm droplet is $S_d = 1.13 \times 10^{-8}$ (m^2). The number of surfactant molecules $n_{surf} = 4.91 \times 10^5$, and the surface density of surfactants $\Gamma = 1.5 \times 10^{12}$ (molecules/m^2) [280]. Thus, for a droplet of 60 μm in diameter with 0.05% m/m of surfactants, the mass fraction of water vapor at the droplet surface is reduced by 20%. This reduction in Y_d will reduce the Spalding number B_m and the evaporation rate of the droplet from 0.0104 in PBS droplets to approximately 0.0100 with 0.05% m/m of surfactants.

Ratio of the droplet surface occupied by microbeads

Since the microbeads behave like bacteria, they can be assumed to be dispersed pseudo-randomly in the bulk solution [239]. Thus, contrary to surfactants where most of the concentration was eventually located at the droplet-air interface during the evaporation process, the number of microbeads located at the air-droplet interface at any point during the evaporation process and thus impede the evaporation process is stochastic. By comparing the size and concentration of the microbeads C_{micro} (microbeads/m^3) to the surface of the droplet S_d (m^2), knowing the volume of the droplets V_d (m^3) and the projected surface of the microbeads S_{proj} (m^2/microbead), the average ratio of the surface occupied by the microbeads r_S (-) can be calculated with the following equation:

$$r_S = \frac{C_{micro} V_d S_{proj}}{S_d} \tag{D.8}$$

Where

$$S_{proj} = \pi r_{micro}^2 \tag{D.9}$$

APPENDIX E SUPPLEMENTARY MATERIAL OF ARTICLE 5

Sliding window algorithm

The sliding window approach is a standard algorithm used in time series analysis and other sequential data processing tasks. It involves moving a fixed-size window across the data, one step at a time, and performing calculations or extracting features within each window.

For example, let's compare the average for two datasets of 5 values each:

- Dataset A: [3, 5, 2, 8, 7]
- Dataset B: [4, 6, 1, 9, 5]

If we use a sliding window of size 3, we calculate the average of the first 3 values for both datasets:

- For Dataset A: $(3 + 5 + 2)/3 = 3.33$
- For Dataset B: $(4 + 6 + 1)/3 = 3.67$

Next, we slide the window one step forward and calculate the average for the next 3 values:

- For Dataset A: $(5 + 2 + 8)/3 = 5.00$
- For Dataset B: $(6 + 1 + 9)/3 = 5.33$

We continue this process until we reach the end of the datasets. This method allows us to compare the datasets in a step-by-step manner and observe how the local patterns or trends evolve over time. In the article, we used the sliding window algorithm to compare all the possible time series combinations for the two configurations (Vortisand ON and OFF).

Random Forest machine learning model

The random forest regressor model, a versatile machine learning technique, is a powerful tool for regression tasks. Comprising an ensemble of decision trees, it leverages the wisdom of crowds, in which the collective judgment or decision-making of a group of individuals is often more accurate and insightful than the judgment of any single member within the group, to enhance predictive accuracy [336]. A random forest is essentially an ensemble of decision trees, where each internal node corresponds to a decision based on a feature,

each branch represents the outcome of that decision, and each leaf node denotes the final prediction. Each decision tree in the forest independently processes a subset of the training data, and their outputs are aggregated to produce a robust and generalizable prediction. This ensemble approach mitigates overfitting and improves model performance, making it particularly effective for complex datasets. Implementation of the random forest regressor is favored for its ability to handle non-linear relationships and capture intricate patterns in the data [334].

Convergence analysis

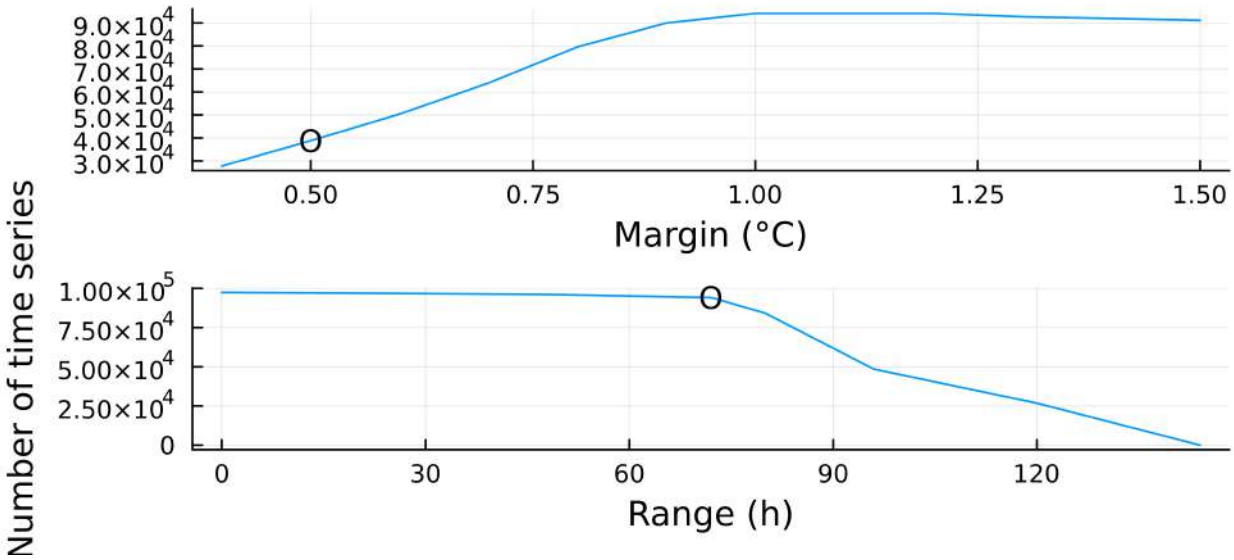

Figure E.1 Convergence analysis for the *margin*, *range* and *inertia* parameters respectively, displaying the number of time series according to the value of each parameter individually. The circled datapoints represent the selected value for each of the parameters.

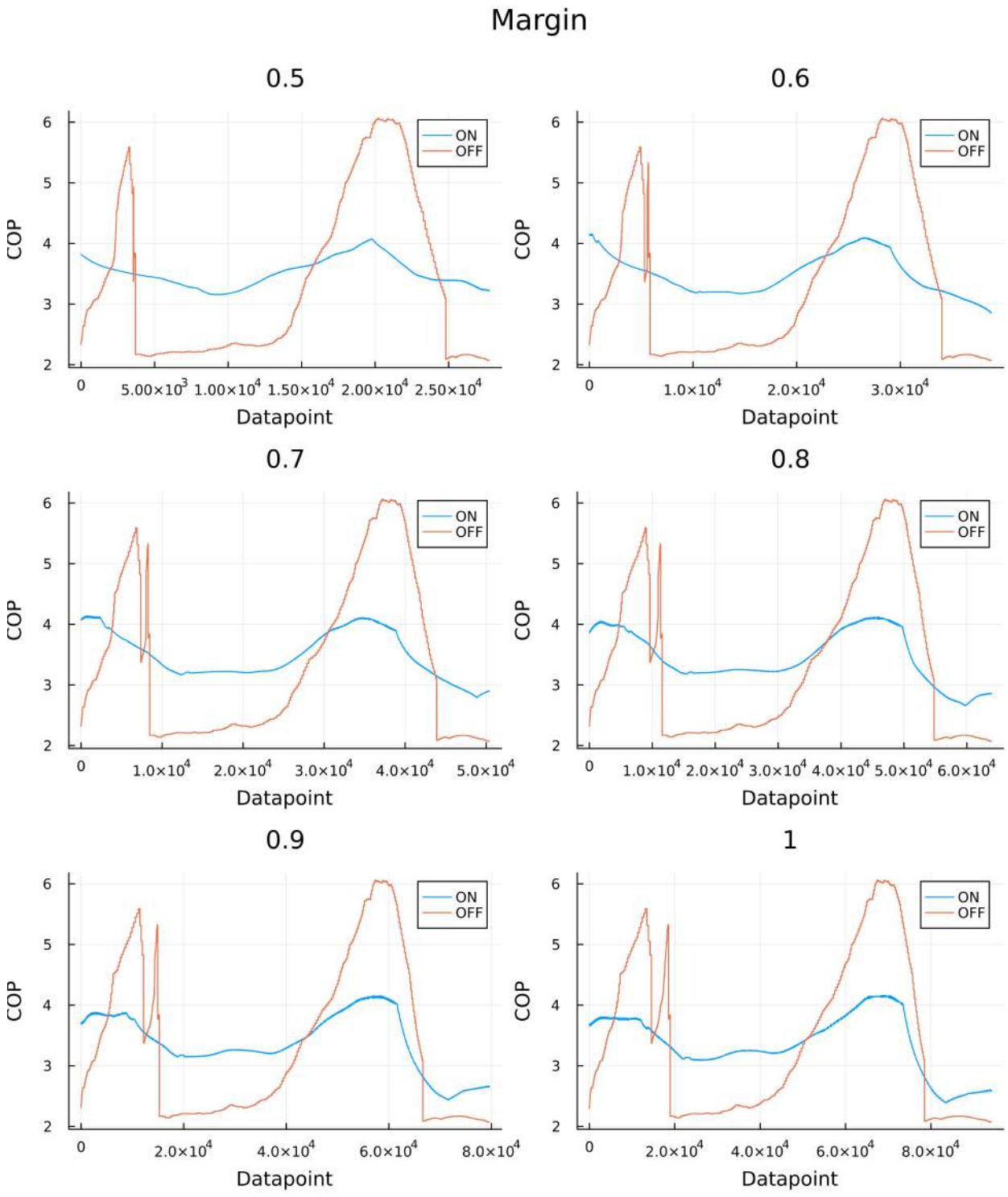

Figure E.2 Coefficient of performance according to the *margin* parameter. *range* and *inertia* parameters were set at 6h. Outliers were cleaned up from the dataset.

Effect of the wet-bulb temperature on the coefficient of performance

The high-resolution dataset collected in this study can provide critical information on the effect of environmental conditions on the performance of the system. As the peaks of the coefficient of performance when the filter was not operating indicated that the system was sometimes more efficient energetically without the filter, it was therefore essential to investigate on the sepcific conditions that caused this behavior.

An increase in the ambient wet-bulb temperature does not affect the electric consumed energy ($\dot{E}_{co}$) directly. Rather, it decreases the potential for evaporation cooling and as such, the energy that can be exchanged within the system ($\dot{E}_{ex}$). The effect of the wet-bulb temperature on the coefficient of performance can therefore be assumed to be equivalent to its effect on the evaporation cooling inside the system and thus, on the evaporation rate. The equations of Maxwell for evaporation link the wet-bulb temperature to the evaporation rate [162]. These equations consider the simplified case of quasistationary evaporation of a spherical droplet, but can also be applied to the investigated system in terms of the effects of the environmental conditions [387]. In the case of cooling towers, the evaporation rate I (kg/s) is dependent upon the characteristic length of the gas-liquid interface L (m), the mass diffusivity D (m^2/s), the concentration of vapor at the gas-liquid interface c_0 and in the ambient air, at a significant distance from the cooling tower c_∞ (kg/m^3):

$$I = LD\,(c_0 - c_\infty) \tag{E.1}$$

The higher the evaporation rate, the higher the potential for evaporative cooling and the higher the energy exchanged within the system. An increase in wet-bulb temperature can affect two parameters associated with the evaporation rate: The mass diffusivity D, influenced mostly by the atmospheric temperature, and the concentration of vapor of the ambient air c_∞ linked to both atmospheric temperature and relative humidity. The mass diffusivity at the gas-liquid interface D (m^2/s) is dependent upon the temperature of the process water T_0 and of the air T_∞ (K), as well as the mass diffusivity of the environment D_∞ and a correlation factor μ based on the two fluids interacting, equal to 2 in the case of air and water [154]:

$$D = D_\infty \left(\frac{T_0}{T_\infty}\right)^\mu \tag{E.2}$$

Thus, the larger the change in the atmospheric temperature, the larger the effect on the mass diffusivity at the gas-liquid interface. However, the temperature difference between the inside and the outside of cooling towers, called approach temperature, typically ranges

between 3 and 10 °C for the type of cooling tower system investigated [388]. For instance, the higher range of 10°C would only make a 6% difference in the diffusivity between air and water, considering typical cooling season conditions. Conversely, the same wet-bulb temperature difference could yield up to a 70% increase in the water vapor concentration of the atmosphere according to the Clausius-Clapeyron equation, which links vapor pressure and atmospheric temperature [389, 390]. This emphasizes the dominant role of ambient vapor concentration over mass diffusivity in modulating evaporation rates. In the context of evaporative cooling, the effect of the wet-bulb temperature on the diffusion coefficient is small enough to be neglected. As such, when the wet-bulb temperature increases, the concentration of vapor in the environment increases, which linearly decreases the evaporation rate and thus, the coefficient of performance. The negative linear relationship between the coefficient of performance and the wet-bulb temperature was therefore due to the increased concentration of water vapor in the environment associated with increased wet-bulb temperature.

According to the literature, the investigated filter can induce a significant difference on the concentration of suspended solids in the cooling tower process water, as well as in the presence of biofilm [122, 123]. For analogous environmental conditions, more impurities in the water imply fewer water molecules per unit volume [154]. Thus, the concentration of vapor at the gas-liquid interface c_0 is likely to decrease [389, 391]. Furthermore, with the presence of sufficient biofilm throughout the system, the mass diffusivity D would likely decrease by 50 to 80% [392]. Therefore, the combinatory effect of these factors might explain the steeper slope of the coefficient of performance with increasing wet-bulb temperature when the filter was not operating.